

厚生労働科学研究費補助金
食品の安全確保推進研究事業

非定型 BSE（牛海綿状脳症）に対する安全対策等に関する研究

平成 26～28 年度 総合研究報告書

平成 29 年 3 月

研究代表者

堀内 基広

（北海道大学大学院獣医学研究科）

厚生労働科学研究費補助金
食品の安全確保推進研究事業

非定型 BSE（牛海綿状脳症）に対する安全対策等に関する研究

平成 26～28 年度 総合研究報告書

平成 29 年 3 月

研究代表者

堀内 基広

（北海道大学大学院獣医学研究科）

食品の安全確保推進研究事業
「非定型 BSE（牛海綿状脳症）に対する安全対策等に関する研究」班
班員名簿

堀内 基広	北海道大学 大学院獣医学研究科 獣医衛生学教室	教授
新 竜一郎	宮崎大学 医学部 感染症学講座（平成28年3月～）	教授
	長崎大学 大学院医歯薬学総合研究科 感染分子解析学分野（平成28年2月まで）	准教授
柴田 宏昭	自治医科大学 先端医療技術開発センター 共同利用コーディネート部門（平成28年7月～）	講師
	独立行政法人医薬基盤研究所 霊長類医科学研究センター（平成28年6月まで）	プロジェクト研究院
飛梅 実	国立感染症研究所 感染病理部	主任研究官
萩原 健一	国立感染症研究所 細胞生化学部	第1室室長
長谷部 理絵	北海道大学 大学院獣医学研究科 獣医衛生学教室	講師
福田 茂夫	北海道総合研究機構 畜産試験場 基盤研究部 畜産工学グループ	研究主任
室井 喜景	帯広畜産大学 畜産学部 基礎獣医学研究部門	准教授
岩丸 祥史	国立研究開発法人 農業・食品産業技術総合研究機構 動物衛生研究部門	上級研究員
	独立行政法人農業・食品産業技術総合研究機構農研機構 動物衛生研究所	主任研究員

目次

I.	総合研究報告書（平成 26～28 年度）	
	非定型 BSE（牛海綿状脳症）に対する安全対策等に関する研究	1
	研究代表者：堀内 基広（北海道大学・大学院獣医学研究科）	
II.	研究成果に関する刊行一覧表	1 1
III.	研究成果の刊行物・別刷	1 6

厚生労働科学研究費補助金（食品の安全確保推進研究事業）
非定型 BSE（牛海綿状脳症）に対する安全対策等に関する研究
（H26-食品-一般-004）

総合研究報告書

研究代表者 堀内 基広 北海道大学大学院獣医学研究科

研究要旨

英国で発生して世界各地に広がった BSE（定型 BSE, C-BSE）は大きな社会問題となったが、飼料規制などの管理措置が機能した結果、その発生は制御下にある。しかし、能動サーベイランスの結果、C-BSE とは性質が異なる BSE（非定型 BSE, L-BSE および H-BSE）が、主に高齢牛で発見され、ヒトへの感染リスクや C-BSE の原因となる可能性が指摘されている。本研究では、食品を介する非定型 BSE の感染拡大を防ぐための安全対策等に貢献することを目標として、これまでに培った技術・経験および科学的知見を活用して、1) 非定型 BSE 感染動物における感染病態機序の解明に資する研究、2) 非定型 BSE のヒトへのリスクの推定に資する研究、3) 潜在的な非定型 BSE の存在リスクの推定、非定型 BSE が C-BSE の起源となる可能性の推定、に資する研究を進め、以下に述べる研究成果が得られた。

L-BSE 脳内接種牛の臨床症状と PrP^{Sc} 検出時期を調べた結果、臨床症状が出現する 6ヶ月前、病末期の約 11ヶ月前には PrP^{Sc} が検出されることを明らかにした。L-BSE の脳内分布の解析から、原因不明の死亡牛の検査部位として嗅脚などが適していることを示した。BSE 解析用のモデルとして、C-BSE モルモット馴化株、L-BSE ハムスター馴化株を作出した。C-BSE の PrP^{Sc} が熱処理により PrP^{Sc} の分子サイズが変化するという、これまで報告がない生化学的特徴を見出した。プリオン感染動物脳からプリオン感染神経細胞を同定・分離する方法を世界で初めて確立した。C-, L-, および H-BSE プリオン感染 TgBovPrP の比較から、3種の BSE プリオンに共通した宿主応答、およびそれぞれの BSE プリオンに特徴的な宿主応答があることを明らかにした。

カニクイザルを用いた L-BSE の経口感染試験から、L-BSE は経口的にヒトに感染するリスクがあることを明らかにした。ヒト PrP 過発現マウス (TgHuPrP) マを用いた伝達試験の結果から、ヒトの BSE プリオンの感受性は、L-BSE > C-BSE > H-BSE と推測され、L-BSE は C-BSE よりもヒトで増殖しやすく、H-BSE のヒトへの感染リスクは低いと考えられた。L-BSE 感染牛の骨格筋（上腕三頭筋、半腱様筋、大腰筋、最長筋）に脳の 1/10,000 程度の感染価が存在することを明らかにした。BSE 検査に使用されている市販キットが、L-, および H-BSE ウシの摘発に有効であることを確認した。

rCerPrP を用いることで、C-BSE と L-BSE プリオンの高感度検出および鑑別を一回の反応で実施可能な実用的な RT-QuIC 法を確立した。rMoPrP と rHaPrP に対する C-BSE と L-BSE の反応性の差を利用して、両者を高精度に鑑別する方法を確立した。しかし、C-, L-, および H-BSE を 1度で検出・鑑別する方法の確立には至らなかった。L-BSE プリオンが、単純な加熱や酸・アルカリ等の物理・化学的処理によって C-BSE 様のプリオンに変化する可能性は低いと考えられた。

研究分担者

新 竜一郎（宮崎大学 医学部 感染症学講座教授）

柴田 宏昭（自治医科大学 先端医療技術開発センター 共同利用コーディネーター部門 講師）

飛梅 実（国立感染症研究所 感染病理部 主任研究官）

萩原 健一（国立感染症研究所 細胞生化学部 第1室室長）

長谷部 理絵（北海道大学 大学院獣医学研究科 獣医衛生学教室 講師）

福田 茂夫（北海道総合研究機構 畜産試験場 基盤研究部 畜産工学グループ 研究主任）

室井 喜景（帯広畜産大学 畜産学部 基礎獣医学研究部門 准教授）

岩丸 祥史（国立研究開発法人 農業・食品産業技術総合研究機構 動物衛生研究部門 上級研究員）

A．研究目的

英国で発生して世界各地に広がった BSE（定型 BSE, C-BSE）は大きな社会問題となったが、飼料規制などの管理措置が機能した結果、その発生は制御下にある。しかし、能動サーベイランスの結果、C-BSE とは性質が異なる BSE（非定型 BSE, L-BSE, H-BSE）が、主に高齢牛で発見され、ヒトへの感染リスクや C-BSE の原因となる可能性が指摘されている。非定型 BSE は自然発生する疾病の可能性があり、実験的に牛やヒト PrP 遺伝子発現マウスに伝達することから、牛を飼養する国と地域の共通の問題として、グローバルなレベルで、感染拡大リスクを考慮した長期的な対策が必要である。しかし、リスク評価および適切な管理措置の策定に必要な科学的知見が乏しいのが現状である。

先の食品の安心・安全確保推進研究事業（平成 20-22 年度、平成 23-25 年度）の実績から、サル、

ウシおよび各種モデル動物を用いる感染実験によるプリオン病の病態解析手法、異常型プリオンタンパク質（PrP^{Sc}）の高感度検出法などの技術が格段に向上している。本研究では、食品を介する非定型 BSE の感染拡大を防ぐための安全対策等に貢献することを目標として、これまでに培った技術・経験および科学的知見を活用して、項目 1) 非定型 BSE 感染動物における感染病態機序の解明に資する研究、項目 2) 非定型 BSE のヒトへのリスクの推定に資する研究、項目 3) 潜在的な非定型 BSE の存在リスクの推定、非定型 BSE が C-BSE の起源となる可能性の推定、に資する研究を進める。

本研究で取り組む、非定型 BSE 感染牛の中樞神経系における PrP^{Sc} の出現部位と時期の解析、牛可食部位における感染価の解析（項目 1）、霊長類を用いた非定型 BSE の感染実験（項目 2）、潜在的な非定型 BSE の調査（項目 3）から得られる成果は、非定型 BSE のヒトへの感染リスクを考慮した BSE 管理措置の策定に必要な科学的知見であり、食品健康影響評価および食品衛生行政に貢献する。さらに、得られる研究リソースおよび技術は、プリオン病の診断・治療法の開発、プリオンの検出法に応用可能であり、広く保健医療に貢献する。また、非定型 BSE の病態解明は、難解かつ不明な点が多いことが最大の不安要因であるプリオン病に対する、消費者の不安・懸念の払拭にも役立つ。

B．研究方法

1) 非定型 BSE 感染動物における感染病態機序の解明に資する研究

- ・ L-および H-BSE 脳内接種牛における PrP^{Sc} の脳内出現部位を経時的に解析して、発症前に PrP^{Sc} が検出される時期や部位を明らかにする。
- ・ C-BSE, L-BSE の病態解析モデル系として、遺伝子組換え動物以外に、野生型動物を用いる病態解析系の確立を目指す。
- ・ C-BSE および非定型 BSE 由来 PrP^{Sc} の蛋白化学的な解析により両者の相違に関する知見を集積する。
- ・ 組織切片上での PrP^{Sc} 特異染色法(食品の安全性確保推進研究事業[平成 23-25 年実施])

で確立)を用いて、C-, L-, および H-BSE 感染牛および感染動物の神経病変を詳細に解析して、非定型 BSE の神経病変の特徴を明らかにする。

- ・ プリオン病の新規病態解析技術として、PrP^{Sc} 特異染色法を応用して、プリオン感染動物の中枢神経系組織からプリオン感染神経細胞を分取する方法を確立する。
- ・ C-, L-, および H-BSE プリオン感染ウシ PrP 過発現マウス (TgBovPrP) の中枢神経系組織の網羅的遺伝子発現解析により、各々の病原体により引き起こされる病態の相違を明らかにする。

2) 非定型 BSE のヒトへのリスクの推定に資する研究

- ・ 先の食品の安全性確保推進研究事業 (平成 23-25 年実施) で開始した、L-BSE 経口接種カニクイザルの、臨床経過の観察、運動機能試験、脳波測定による神経機能解析を継続する。L-BSE の実験モデル化のために実施中の脳内接種連続継代中のサルについても、同様に実施する。
- ・ H-BSE のヒトへのリスクの推定のために、カニクイザルの経口接種および脳内接種試験を新規に開始して (2-4 頭使用予定) 経過観察、血液および脳脊髄液の採取を行う。
- ・ 先の食品の安全性確保推進研究事業 (平成 23-25 年実施) から継続している、C-BSE 経口接種カニクイザル、および輸血による C-BSE の伝播リスクを検証するために C-BSE 感染カニクイザルの血液を輸血したカニクイザルの、臨床経過の観察、運動機能試験、脳波測定による神経機能解析を継続する。
- ・ ヒト PrP 過発現マウス (TgHuPrP) を新たに作製し、C-, L-, および H-BSE を脳内接種して伝達性を調べることで、ヒトが非定型 BSE に感受性であるかを推測する。
- ・ 市販 BSE 検査キットの非定型 BSE の検出精度を精査する。
- ・ L-および H-BSE 実験感染牛の発症牛の可食部位に、検出する PrP^{Sc} およびプリオン感染価が存在するか否かを、免疫組織化学および TgBovPrP を用いるバイオアッセイに

より調べる。

3) 潜在的な非定型 BSE の存在リスクの推定、非定型 BSE が C-BSE の起源となる可能性の推定

- ・ C-BSE と非定型 BSE を一回の反応で、検出感度を損なわずに検出でき、かつ鑑別可能な、実用レベルの RT-QuIC 法を構築する。
- ・ 非定型 BSE 試料の熱処理や化学処理が C-BSE を誘発する可能性を検討する。
- ・ L-BSE や C-BSE の病原学的性状が異種動物伝達により変化するかについて検討する。

(倫理面への配慮)

各々の研究分担者が所属する機関での動物実験委員会等で審査を受けた動物実験プロトコル等に従い、実験動物の福祉および動物実験倫理に十分配慮して動物実験を実施した。感染症病原体等の取り扱いは、各々の機関の病原微生物等安全管理委員会あるいはバイオセーフティ委員会などの承認を得て実施した。

C. 研究結果

1) 非定型 BSE 感染動物における感染病態機序の解明

1-1) L-BSE 感染牛の病態解析

L-BSE を脳内接種した牛を接種後 4.7 ヶ月で病理解剖し、中枢神経系組織における PrP^{Sc} の蓄積を調べた結果、中脳、橋および延髄にわずかな PrP^{Sc} の蓄積を確認した。接種後 1.7 および 4.2 ヶ月で安楽殺した各一頭の牛の脳内では明瞭な PrP^{Sc} の蓄積は検出されなかったが、接種後 7.5 および 9.1 ヶ月では、脳幹部の他、小脳、視床に PrP^{Sc} が検出された。脳内接種による L-BSE 感染牛の臨床症状は接種後 11 ヶ月頃から確認されることから、臨床症状が出現する 6 ヶ月前頃には PrP^{Sc} が検出されるようになることが示唆された。

C-および L-BSE 感染牛の脳組織における PrP^{Sc} の出現部位と時期を比較したところ、延髄および中脳では、L-BSE は接種後 5 ヶ月で、C-BSE は 10 か月で PrP^{Sc} が検出され、L-BSE

が5ヶ月早く PrP^{Sc} が検出された。小脳皮質、大脳皮質前頭部ではL-BSEで接種後11ヶ月に対しC-BSEで接種後18ヶ月、19ヶ月に検出され、それぞれL-BSEが早く蓄積した。嗅脚では、L-BSEは接種後7ヶ月、C-BSEでは接種後19ヶ月で検出され、線条体では、L-BSEは9ヶ月、C-BSEは16ヶ月で検出された。L-BSEではC-BSEよりも早くから、かつ脳の広範囲にわたりPrP^{Sc}が検出されることが判明した。

H-BSE感染牛の解析は、平成28年度8-9月に道東で発生した台風被害により研究期間内での実施が困難となった。

1-2) L-BSEの病態解析モデルの確立と病態の解析

C-BSEはモルモットへ伝達したが、ハムスターへは伝達しなかった。逆に、L-BSEはハムスターに伝達したが、モルモットへは伝達しなかった。その結果、C-BSEモルモット馴化株(C-BSE/gu)、L-BSEハムスター馴化株(L-BSE/ham)が作出できた。そこで、これらの病理学的解析を行った。L-BSE/ham接種ハムスターでは末梢組織でPrP^{Sc}の蓄積が認められず、中枢神経系組織で血管周囲や脳室周囲器官でPrP^{Sc}の蓄積が認められることから、脳脊髄液を介して、あるいは血行性に中枢神経系組織内で蓄積部位が拡大することが示唆された。

C-BSEモルモット馴化株(C-BSE/gu)、L-BSEハムスター馴化株(L-BSE/ham)を用いて、C-BSE/guをハムスターに、L-BSE/hamをモルモットに接種して、異種間伝達に伴うプリオンの性状変化を解析した。C-BSE/gu感染モルモットでは、顆粒細胞の減数と分子層の菲薄化による小脳皮質の萎縮が顕著であった。また、脳全体にPrP^{Sc}の沈着が認められ、プラーク状沈着が特徴的であった。L-BSE/ham感染ハムスターでは脳全体にび慢性のPrP^{Sc}の沈着が認められ、微細顆粒状や血管周囲への小斑状の沈着が特徴的であった。異種間伝播モデルであるC-BSE/gu感染ハムスターでは、脳全体にPrP^{Sc}の沈着が認められ、海馬、間脳、大脳へのび慢性、放射状沈着が主であった。C-BSE/gu感染ハムスターでは、C-BSE/gu感染モルモットでみられる特徴的な小脳病変は形成されず、L-BSE/ham感染ハムスターでみられる特徴的な沈着分布や沈着パターンの多くがみられた。従って、C-BSE/L-BSEの実験的異種間伝播に

おける病理学的特徴は、動物種とプリオン株の両方の影響を受けるものと考えられる。

1-3) BSE由来PrP^{Sc}のタンパク質化学性状の解析

PrP^{Sc}の温度およびpH処理に対する性状変化を調べた。C-BSE由来PrP^{Sc}は今回調べた範囲のpH・温度ではプロテアーゼへの抵抗性を維持していたが、通常の消化条件(37°C)と比較して、高温消化条件では、プロテアーゼ抵抗性のPrP^{Sc}断片の分離量が大きくなることを見出した。この変化はC-BSE感染ウシ脳組織では確認できるが、C-BSEプリオンを異種動物(カニクイザルやマウス)へ伝播・馴化させると認められなくなることから、これまで報告がない生化学性状であるが、C-BSEプリオン株に特徴的な生化学マーカーとして使用できる可能性がある興味深い知見である。

1-4) 病態解析ツールとしてのPrP^{Sc}特異抗体mAb8D5とmAb132の有用性の検討

異なるエピトープを認識する2種の抗PrP抗体、mAb8D5と132を用いたPrP^{Sc}特異的免疫染色法の応用性を検討するために、牛およびTgBovPrPの脳組織における両抗体の反応性を検討した。mAb8D5は、非感染牛脳組織でも、橋、視床および視床下部の少数の細胞の細胞質にもシグナルが検出されたことから、牛脳組織の特定の領域ではPrP^CとPrP^{Sc}の区別が困難である可能性が示唆された。mAb132は非感染牛脳組織でシグナルが検出されなかったことから、ウシ脳組織におけるPrP^{Sc}の検出に有用であると考えられる。mAb132はPrP^Cの局所の濃度が高いとPrP^Cと反応する。非感染TgBovPrPの脳では嗅球の一部に、感染マウスとは区別できないmAb132の強いシグナルが認められたが、嗅球以外の部位では、PrP^Cの過発現の影響を受けずにPrP^{Sc}の検出が可能と思われた。

1-5) プリオン病の新規病態解析技術の確立

プリオン感染マウスから、神経細胞マーカーとPrP^{Sc}の二重染色により、フローサイトメーターを用いて、プリオン感染神経細胞を同定する方法を確立した。この方法は世界で初めての報告であり、セルソーターを用いて、プリオン感染動物の脳組織からプリオンに感染した神経細胞を分離することが可能となった。

1-6) C-, L- および H-BSE プリオン感染 TgBovPrP の中枢神経系組織のトランスクリプトーム

まず、宿主応答が明らかに認められる時期として、遺伝子発現パターンが、陰性対照の非感染マウスと比較して異なるクラスターに分離できる日を評価の目安とした。そうすると、L-BSE では、接種後 167 日、C-BSE では接種後 204 日、H-BSE では接種後 253 日までは、非感染マウスと区別できなかったことから、明瞭な宿主応答が生じるのは、これらの時点より後になると考えられた。

K-mean クラスタリングにより分類されたクラスターのうち、クラスター C-1 は、C-, L-, および H-BSE プリオン感染 TgBovPrP ともに病末期に遺伝子発現が上昇する遺伝子群であった (184 遺伝子)。共通して発現が上昇する遺伝子群には、ミクログリアで発現が上昇する自然免疫系に関連する遺伝子が多く含まれていた。これに対し、C-2 (212 遺伝子)、C-3 (179 遺伝子)、および C-4 (200 遺伝子) はそれぞれ、L-BSE, C-BSE, あるいは H-BSE プリオン感染 TgBovPrP でのみ発現が上昇する傾向にある遺伝子から構成されるグループであり、各々の病態が異なることも明らかとなった。

2) 非定型 BSE のヒトへのリスクの推定

2-1) L-BSE 感染サル の病態解析

L-BSE (非定型 BSE JP/24 佐世保) では初代接種より、短い潜伏期間で発症が認められ、C-BSE に比べて、発症後の神経症状進行は緩徐であった。ほぼ同様の臨床症状ステージで解剖した安楽死後の MRI 画像では C-BSE 接種サルに比べて、L-BSE 接種サルの脳室拡張が顕著で、脳萎縮が進行していた。

PMCA 法の増幅条件を検討し、L-BSE 感染サル由来 PrP^{Sc} の超高感度検出が可能になった。発症前の L-BSE 脳内接種サルの脳脊髄液、尿や唾液中にも、PrP^{Sc} が検出されることから、PMCA 法を用いて、経口接種サルの体液を経時的に検査することで、感染成立の有無を調べる事が可能となった。

平成 27 年度、投与後約 3.5 年目の唾液から PrP^{Sc} が検出されたが、同一個体ではその後採

材した唾液からは PrP^{Sc} は検出されなかった。また、平成 28 年度、投与後 3.7 年の個体の血漿から一過性に PrP^{Sc} を検出した。投与後 5.5 年を経過した現時点で臨床症状は認められていないが、経口投与した 2 頭のサルともに体液から PrP^{Sc} が検出されたこと、および、L-BSE を脳内接種したカニクイザルでも発症前の尿、唾液、脳脊髄液から PrP^{Sc} が検出できることから、L-BSE は経口的にヒトに感染するリスクがあると判断すべきである。

この 2 頭については、平成 28 年度末に安楽死を行い、組織・臓器からの PrP^{Sc} 検出を行い、ヒトに近い真猿類での L-BSE 経口感染リスクを評価する。

2-2) H-BSE 感染サル の病態解析

H-BSE のサルへの伝播を確認するための脳内接種と食を通じてのヒトへの感染リスクを評価するための経口投与の実験を開始した。いずれも接種してから 1.4 年を経過したが、現在まで、臨床的に異常はない。潜伏期を考慮すると、平成 29 年度以降の実験継続が必要である。

2-3) C-BSE の経口および輸血による伝播リスクの評価

C-BSE 感染牛脳乳剤のカニクイザルへの経口投与、および C-BSE 感染牛脳乳剤を脳内接種されて感染したカニクイザルの血液をカニクイザルに輸血する輸血実験を行い経過観察を継続してきた。途中、未発症の 2 頭を安楽死したが、残りのサルは発症が確認できないまま、それぞれ 13.5 年目、10.4 年目に安楽死した。経口接種群では、定期的に採材していた体液類からは PrP^{Sc} は検出されなかった。安楽死直後の脳 MRI 像では、脳室拡張に伴う脳萎縮は見られなかった。また輸血実験群のサルの神経及び末梢組織を高感度検出系で検査したが、調べた組織からは PrP^{Sc} は検出されなかった。

2-4) ヒト PrP 過発現マウス (TgHuPrP) を用いたヒトの非定型 BSE 感受性の推定

ヒト型 PrP 遺伝子(コドン 129 番目メチオニン)を過剰発現する TgHuPrP を 4 系統(#21、#38、#51、#07)作製した。すべての系統は内因性のマウス PrP 遺伝子をノックアウト化した。ヒト 129M PrP^C の脳での発現量は、野生型マウスと比べて、#21 で 4 倍、#38 で 4 倍、#51

で1.5倍、#07で1倍であった。

これらのTgHuPrPに、C-, L-, およびH-BSEプリオンを脳内接種した。L-BSEはTgHuPrPを高発現するTgマウスにはattack rate 100%で伝達したが、低発現するTgマウスへは伝達したがattack rateは低かった。C-BSEはHuPrPを高発現するTgマウスにattack rateが低いながら伝達が認められた。しかしH-BSEはいずれのTgにも伝達しなかった。

従って、L-BSEはヒトへの伝達効率がC-BSEよりも高いことが示唆された。

2-5) 食肉衛生検査所等でのBSEスクリーニングに使用されている迅速検査キットの性能評価

当該の検査キットがL-, およびH-BSE罹患ウシを適切に摘発できることを示した。欧州の評価基準に照らしてもBSE罹患ウシの摘発に有効と判断される結果となった。

2-6) L-およびH-BSE 実験感染牛の発症牛の可食部位におけるPrP^{Sc}およびプリオン感染価の解析

L-BSE臨床症状期の牛の筋組織を抗プリオンタンパク質抗体(F99/97.6.1:VMRD, Pullman, WA, USA)の免疫組織化学染色で解析すると、筋組織の筋紡錘でPrP^{Sc}陽性となった。L-BSE感染牛の可食部(骨格筋:上腕三頭筋、半腱様筋、大腰筋、最長筋)の乳剤をTgBovPrPに接種したところ、全ての試料でマウスの発症が認められた。平成26年度に作成したL-BSEの感染価-潜伏期標準曲線から、感染価を推定した結果、これらの可食部には、脳の1/10,000程度の感染価が存在することが判明した。本実験で調べた3頭のL-BSE実験感染牛で同様の結果が得られた。

また、H-BSEの感染価を測定するための感染価-潜伏期標準曲線を作成した。これにより、H-BSE感染牛の可食部の感染価の定量解析が可能となった。

3) 潜在的な非定型BSEの存在リスクの推定、非定型BSEがC-BSEの起源となる可能性の推定

3-1) C-BSEと非定型BSEを一回の反応で、検

出感・鑑別可能なRT-QuIC法の構築

rCerPrPを基質として用いた場合、C-BSEおよびL-BSEともに、被検試料の脳乳剤濃度が最高となる 10^{-3} 希釈でも陽性となり、L-BSEおよびC-BSEともに 10^{-7} 希釈まで再現性良く陽性となることから、rCerPrPを用いたRT-QuIC法は、ELISAやWBよりも10,000以上検出感度が高く、TgBovPrPを用いたバイオアッセイよりも10倍程度感度が高いことが確認できた。H-BSEプリオンも 10^{-3} ~ 10^{-8} 希釈で検出可能であった。

この反応系に、終濃度0.1%となるように非感染牛脳乳剤を加えると、L-BSEの検出限界は 10^{-8} と1段階上昇したが、C-BSEの検出限界は 10^{-3} までと著しく低下した。従って、rCerPrPを用いたRT-QuIC反応を、非感染牛脳乳剤存在/非存在下で行うことで、一回のRT-QuIC法で、C-BSEとL-BSEの高感度検出と鑑別が可能となった。しかし、C-, L-, およびH-BSEの3種を鑑別可能な方法の確立には至らなかった。

rCerPrP以外に、マウス、ハムスター、ウシ、およびハタネズミの組換えPrPを使用したが、被検試料の脳乳剤濃度が最高となる 10^{-3} 希釈でも安定して陽性となり、かつ 10^{-7} 希釈まで再現性良く陽性となるのはrCerPrPを基質としたRT-QuICであった。

3-2) L-BSEとC-BSEのRT-QuIC法におけるrMoPrP、rHaPrPへのシード活性の違い

rMoPrPとrHaPrPを反応基質として用い、L-, C-BSEをそれぞれシードとしてRT-QuIC法を実施すると、L-BSEはrMoPrP、rHaPrPの両者に対してシード活性を示したのに対してC-BSEはrHaPrPに全く活性を示さなかった。さらにL-BSE、C-BSEをシードとしたRT-QuIC法の継代を継続(最初の反応をRound-1とし、その反応液の希釈液の一部を次の反応[Round-2]のシードとしてRT-QuIC法を実施)したところ、Round-2においてもrHaPrPはC-BSEに反応しなかった。それに対してrMoPrPおよびrHaPrPはL-BSEに高い反応を示した。しかし、C-BSEのrPrP種特異性は、RT-QuICを4~5回連続することで消失した。従って、Round-2まで含めたrMoPrPとrHaPrPの反応性の違いを利用すれば、RT-QuIC法によってL-BSEとC-BSEの鑑別が可能となる。

また、ステンレススチールワイヤーに付着したプリオンの活性を2日間程度で評価できるWire-QuIC法を開発した。この方法により、RT-QuIC法の適用範囲の拡大が期待できる。

3-3) 非定型 BSE 試料の熱処理や化学処理が C-BSE を誘発する可能性の検討

熱処理により L-BSE 由来 PrP^{Sc} が C-BSE 由来 PrP^{Sc} 様の性状を獲得するかを調べるために、L-BSE 感染脳乳剤を加熱処理した。70°C では白濁した状態を維持していたが、100°C 以上で固形分の凝集が見られた。135°C 以上では液状部分が透明となり、150°C では黄褐色に変色した。WB では、70°C から 110°C まで明瞭な PrP^{Sc} のバンドが確認され、分子量およびバンドパターンに変化はなかった。加熱処理した L-BSE 感染脳を、C-BSE の PrP^{Sc} を増幅する PMCA 法により PrP^{Sc} 増幅を試みたが、C-BSE 様の PrP^{Sc} は検出されなかった。

化学処理により L-BSE 由来 PrP^{Sc} が C-BSE 由来 PrP^{Sc} 様の性状を獲得するかを調べるために、10% L-BSE 感染脳乳剤を、2 規定 (N) から 2 倍階段希釈 (2 ~ 1/16N) した等量の塩酸または水酸化ナトリウムで処理した後、C-BSE の PrP^{Sc} を増幅する PMCA 法により PrP^{Sc} 増幅を試みた。いずれの処理条件でも、C-BSE 様の PrP^{Sc} は検出されなかった。

3-4) カニクイザルで増殖した C-, L-BSE プリオンの特性変化の検証

C-BSE プリオンや L-BSE プリオンが、ウシから異種動物へ伝播した場合に、そのウイルス学的特徴に変化が起こるのかという点を検討することは、プリオン株の起源や新たなプリオン株の出現を考察・予測する上で意義深い。霊長類モデルであるカニクイザルへ伝播した C-, L-BSE プリオンの病原性の変化の有無を、近交系マウスに対する病原性を比較することで調べた。その結果、カニクイザルで増殖した C-, L-BSE プリオンの病原学的特性は、ウシ脳の C-, L-BSE プリオンと大差なかったことから、仮に L-BSE がヒトに感染したとしても、すぐに vCJD のような病態を呈することはないことが示唆される。

D. 考察

1) 非定型 BSE 感染動物における感染病態機序の解明

接種後 4.7 ヶ月の脳内接種 L-BSE 感染牛 2 頭に蓄積する PrP^{Sc} は、脳幹部に局限し、蓄積量もわずかであった。これより前の段階では PrP^{Sc} は検出されなかった。接種後 7.5 月では脳内の PrP^{Sc} 蓄積部位が広がっていた。脳内接種による L-BSE 感染牛の臨床症状が接種後 11 ヶ月頃から確認されることから、臨床症状が出現する約 6 ヶ月前、あるいは病末期の約 11 ヶ月前に PrP^{Sc} を検出できることが示唆された。また、嗅脚は L-BSE の PrP^{Sc} が蓄積しやすい部位の一つであることから、原因不明の死亡牛の検査では、この部位を採材することで、確実に L-BSE を摘発できると思われる。

本研究で作出した、C-BSE モルモット馴化株 (C-BSE/gu)、L-BSE ハムスター馴化株 (L-BSE/ham) は、BSE の起源の推定を含めて、今後の研究の有用なツールとなる。特に C-BSE/gu は世界初の例であり、特徴的な小脳病変を示すことから、BSE のみならずヒトプリオン病の病態モデルとしても有用と思われる。L-BSE ハムスター馴化モデルでは脳内で増幅した PrP^{Sc} が神経性あるいは血行性に脊髄へ伝播することは示唆された。末梢神経や血液を介した末梢組織への遠心性伝播は確認されなかった。L-BSE の末梢神経、他臓器への親和性を欠くことは L-BSE 起源を考える上で重要と思われる。

C-BSE 由来 PrP^{Sc} の見かけ上の分子量が、高温消化条件で大きくなる現象を見出した。このメカニズムは不明であるが、本現象は C-BSE プリオンの判別法として有用と思われる。ただし、新たに生じた PrP^{Sc} 断片と、通常の消化条件で得られる PrP^{Sc} 断片との感染性や病原性を検討して C-BSE の生物性状を維持しているか確認する必要はある。

PrP^{Sc} 特異抗体 mAb8D5 と mAb132 はプリオン病の神経病態解析用のツールとして可能性を秘めている。しかし、mAb8D5 は非感染牛の脳組織の特定の部位でシグナルが認められたことから、残念ながら牛の脳組織の解析には応用が難しい。抗 PrP 抗体 mAb132 はエピトープの密度が高くなると反応性が向上するため、PrP を過発現するマウスでは PrP^C 由来のシグナルを検出する可能性

が予想されたが、嗅球を除いては TgBovPrP の脳組織における PrP^{Sc} の解析に使用可能であると思われる。

mAb132 を用いる PrP^{Sc} 特異検出法と、フローサイトメトリーの解析法を工夫することで、プリオン感染動物の脳からプリオンに感染した神経細胞を検出することが可能になった。世界で初めての技術であり、今後、セルソーターを用いて、プリオン感染神経細胞を分取し、プロテオームやトランスクリプトームを行うことで、プリオンに感染した神経細胞で生じる変化をより特異的に解析することが可能となる。また、mAb 132 のエピトープはほ乳類から鳥類まで保存されていることから、本法はマウスのみならず、多くの動物種に応用可能と考えられる。

C-, L-, および H-BSE プリオン感染 TgBovPrP の脳幹のトランスクリプトームでは、3 種の BSE プリオン感染で共通して発現が上昇するのは、主にミクログリアで発現が上昇する遺伝子群であった。つまり、ミクログリアの活性化は BSE プリオンの種類を問わず共通の現象であることが示された。一方で、C-, L- あるいは H-BSE プリオンの感染に対して特異的に発現が上昇する遺伝子群の存在を明らかにした。ミクログリアが同じように活性化する一方で、C-, L-, および H-BSE プリオンの感染に対する宿主の反応の違いは、プリオン病の神経変性機構を考える上で非常に興味深い現象である。

2) 非定型 BSE のヒトへのリスクの推定

L-BSE を経口接種して 3 年を過ぎた時点で、カニクイザル 2 頭の体液から、一過性であるが PrP^{Sc} が検出されたことは、L-BSE は経口的にヒトに感染するリスクがあることを示していることから、管理措置の継続等、適切な対応が望まれる。

L-BSE の臨床症状期の牛の筋組織（筋紡錘）における PrP^{Sc} の分布を明らかにした。この事実は、L-BSE の臨床症状期の牛の筋組織（上腕三頭筋、半腱様筋、大腰筋、最長筋）にプリオン感染性が検出されたことと矛盾しない。筋組織は脳と比べて 1/10,000 程度の感染価を有していると推定できた。これまでにイタリアでの自然発生例でも、筋組織に感染性が分布することが報告されている。

感染価は低い、L-BSE は経口ルートでヒトへ感染するリスクがあることから、特定部位以外にも L-BSE プリオンが存在し得るという前提で、慎重な対応が必要と思われる。

新たに作製した TgHuPrP を用いた、C-, L-, および H-BSE の接種試験では、ヒトの感受性は L-BSE, C-BSE, H-BSE の順に低下することが示唆された。接種に用いた L-BSE や H-BSE の感染価は 10^{0.3} 倍の僅かな差しかないにもかかわらず、L-BSE は TgHuPrP に感染したが H-BSE は感染しなかったことから、H-BSE プリオンのヒトへの感染リスクは低いと考えられる。しかし、現在進行中のカニクイザルを用いた H-BSE 感染実験の結果と合わせて判断する必要がある。

3) 潜在的な非定型 BSE の存在リスクの推定、非定型 BSE が C-BSE の起源となる可能性の推定

rCerPrP を基質に用いて、RT-QuIC の反応系に非感染牛脳乳剤を添加することで、一回の RT-QuIC 反応で、検出感度を損なうことなく、C-BSE と L-BSE を鑑別可能となった。rCerPrP 以外に、マウス、ハムスター、ウシ、およびハタネズミの組換え PrP を使用したが、被検試料の脳乳剤濃度が最高となる 10⁻³ 希釈でも安定して陽性となり、かつ 10⁻⁷ 希釈まで再現性良く陽性となるのは rCerPrP を基質とした RT-QuIC であった。これまで rCerPrP を基質とした BSE 検出系は報告されていないが、rCerPrP は BSE プリオンの増殖に有効であると考えられる。

最近アメリカの研究グループが種々の rPrP (Bank vole や Sheep) を用いた RT-QuIC 法において、反応性の違いから C-, L-, および H-BSE を鑑別可能であることを報告している (Masujin et al., 2016)。この方法は、高濃度の組織乳剤存在下での検討は行われておらず、高感度検出と鑑別の両方を備えた実用的な方法には至っていない。

非定型 BSE のプリオンに何らかの変化が生じて C-BSE プリオンが生じる可能性を探るため、本研究では、熱処理、および酸・アルカリ処理により L-BSE 由来 PrP^{Sc} が、C-BSE 様の PrP^{Sc} に変化する可能性を調べた。この際、C-BSE 由来 PrP^{Sc} を選択的に増幅する PMCA 法を応用して、僅かに生じるかもしれない C-BSE 様 PrP^{Sc} の検出を試みたが、L-BSE プリオンが C-BSE 様のプリオンに変化

する現象を再現することが出来なかった。従って、L-BSE が単純な加熱や酸・アルカリ等の物理・化学的処理によって C-BSE 様のプリオンに変化する可能性は低いと考えられた。

本研究では、L-BSE プリオンが、vCJD のようなヒトプリオン病の原因となり得るかを推測するために、カニクイザルに伝達した C-BSE と L-BSE プリオンの病原学的性状を調べたが、ウシ脳の C-, L-BSE プリオンと大差なかったことから、仮に L-BSE がヒトに感染したとしても、vCJD のような病態を呈する可能性は低いと思われる。

E . 結論

1) 非定型 BSE 感染動物における感染病態機序の解明

- ・ 非定型 L 型 BSE 感染牛の臨床症状が確認される約 6 ヶ月前頃から PrP^{Sc} が検出されることが明らかとなった。
- ・ L-BSE 感染牛における PrP^{Sc} の脳内分布が改めて確認できた。嗅脚で早期から PrP^{Sc} が検出されることから、原因不明の死亡牛の検査では、嗅脚などを採材することで、確実な摘発が可能になるとと思われる。
- ・ BSE 解析用のモデルとして、C-BSE モルモット馴化株 (C-BSE/gu)、L-BSE ハムスター馴化株 (L-BSE/ham) を作出した。
- ・ L-BSE は末梢組織への親和性が低いこと、血行性あるいは血管周囲器官を介して中枢神経系組織内で拡散する可能性が示唆された。
- ・ C-BSE の PrP^{Sc} が熱処理により PrP^{Sc} の分子サイズが変化するという、これまでに報告がない生化学的特徴を見出した。
- ・ プリオン感染動物脳から、プリオン感染神経細胞を同定・分離する方法を世界で初めて確立した。
- ・ C-, L-, および H-BSE プリオン感染 TgBovPrP の比較から、3 種の BSE プリオンに共通した宿主応答、およびそれぞれの BSE プリオンに特長的な宿主応答があることを明らかにした。

2) 非定型 BSE のヒトへのリスクの推定に資する研究

- ・ L-BSE を経口接種したカニクイザルの 2 頭ともが、接種後 3 年経過した時点で、一過性ではあるが体液から PrP^{Sc} が検出された。L-BSE は経口的にヒトに感染するリスクがあることを示唆する重要な結果である。
- ・ TgHuPrP マウスへの伝達試験の結果から、ヒトの BSE プリオンの感受性は、L-BSE > C-BSE > H-BSE と推測され、H-BSE のヒトへの感染リスクは低いと考えられた。
- ・ L-BSE 感染牛の可食部 (骨格筋：上腕三頭筋、半腱様筋、大腰筋、最長筋) に脳の 1/10,000 程度の感染価が存在することを明らかにした。
- ・ BSE スクリーニング検査に使用されている市販キットが、H-BSE ウシの摘発に有効であることを確認した。

3) 潜在的な非定型 BSE の存在リスクの推定、非定型 BSE が C-BSE の起源となる可能性の推定

- ・ rCerPrP を用いることで、C-BSE と L-BSE プリオンの高感度検出および鑑別を一回の反応で実施可能な RT-QuIC 法を確立した。C-, L-, および H-BSE を 1 度で検出・鑑別する方法の確立には至らなかった。
- ・ rMoPrP と rHaPrP に対する C-BSE と L-BSE の反応性の差を利用して、両者を高精度に鑑別する方法を確立した。
- ・ L-BSE プリオンが、単純な加熱や酸・アルカリ等の物理・化学的処理によって C-BSE 様のプリオンに変化する可能性は低いと考えられた。

F . 健康危険情報 該当なし

G . 研究発表

1 . 論文発表

- II. 研究成果に刊行物一覧を、また、代表的な論文を選択して掲載した。

2.学会発表

- 件数が多いため割愛した。各年度の総括・分担研究報告書に記載した通りである。

該当なし

H. 知的財産権の出願・登録状況

1. 特許取得
該当なし

2. 実用新案登録

研究成果の刊行に関する一覧表

書籍

著者氏名	論文タイトル名	書籍全体の編集者名	書 籍 名	出版社名	出版地	出版年	ページ
*堀内基広	牛海綿状脳症、変異クロイツフェルト・ヤコブ病	木村哲、喜田宏	人獣共通感染症改訂3版	医薬ジャーナル社	東京	2015	184-189

雑誌

発表者氏名	論文タイトル名	発表誌名	巻号	ページ	出版年
*Yamasaki T, Baron GS, Suzuki A, Hasebe R, Horiuchi M.	Characterization of intracellular dynamics of inoculated PrP-res and newly generated PrPSc during early stage prion infection in Neuro2a cells.	Virology	450-451C	324-335	2014
Yamasaki T, Suzuki A, Hasebe R, Horiuchi M.	Comparison of anti-prion mechanism of four different anti-prion compounds, anti-PrP monoclonal antibody 44B1, Pentosan polysulfate, chlorpromazine and U18666A, in prion-infected mouse neuroblastoma cells.	PLoS One	9	e106516	2014
Hasebe R, Suzuki A, Yamasaki T, Horiuchi M.	Temporary upregulation of anti-inflammatory cytokine IL-13 expression in the brains of CD14 deficient mice in the early stage of prion infection.	Biochem. Biophys. Res. Commun.	454	125-130	2014
Uchida L, Heriyanto A, Thongchai C, Hanh TT, Horiuchi M, Ishihara K, Tamura Y, Muramatsu Y.	Genetic diversity in the prion protein gene (PRNP) of domestic cattle and water buffaloes in Vietnam, Indonesia and Thailand.	J. Vet. Med. Sci.	76	1001-1008	2014
Akasaka K, Maeno A, Murayama T, Tachibana H, Fujita Y, Yamanaka H, Nishida N, Atarashi R.	Pressure-assisted dissociation and degradation of "proteinase K-resistant" fibrils prepared by seeding with scrapie-infected hamster prion protein.	Prion	8	314-318	2014
Homma T, Ishibashi D, Nakagaki T, Fuse T, Sano K, Satoh K,	Persistent prion infection disturbs the function of Oct-1, resulting in the	Sci. Rep.	4	6006	2014

Atarashi R, Nishida N.	down-regulation of murine interferon regulatory factor-3.				
*Sano K, Atarashi R, Ishibashi D, Nakagaki T, Satoh K, Nishida N.	Conformational properties of prion strains can be transmitted to recombinant prion protein fibrils in real-time quaking-induced conversion.	J. Virol.	88	11791-11801	2014
Qina T, Sanjo N, Hizume M, Higuma M, Tomita M, Atarashi R, Satoh K, Nozaki I, Hamaguchi T, Nakamura Y, Kobayashi A, Kitamoto T, Murayama S, Murai H, Yamada M, Mizusawa H.	Clinical features of genetic Creutzfeldt-Jakob disease with V180I mutation in the prion protein gene.	BMJ Open	4	e004968	2014
Homma T, Ishibashi D, Nakagaki T, Satoh K, Sano K, Atarashi R, Nishida N.	Increased expression of p62/SQSTM1 in prion diseases and its association with pathogenic prion protein.	Sci. Rep.	4	4504	2014
*Murayama Y, Masujin K, Imamura M, Ono F, Shibata H, Tobiume M, Yamamura T, Shimozaki N, Terao K, Yamakawa Y, Sata T.	Ultrasensitive detection of PrPSc in the cerebrospinal fluid and blood of macaques infected with bovine spongiform encephalopathy prion.	J. Gen. Virol.	95	2576-2588	2014
Langeveld JPM, Jacobs JG, Erkens JHF, Baron T, Andréoletti O, Yokoyama T, Keulen LJM, Zijderveld FG, Davidse A, Hope J, Tang Y, Bossers A.	Sheep prions with molecular properties intermediate between classical scrapie, BSE and CH1641-scrapie.	Prion	8	296-305	2014
Okada H, Miyazawa K, Fukuda S, Iwamaru Y, Imamura M, Masujin K, Matsuura Y, Fujii T, Fujii K, Kageyama S, Yoshioka M, Murayama Y, Yokoyama T.	The presence of disease-associated prion protein in skeletal muscle of cattle infected with classical bovine spongiform encephalopathy.	J. Vet. Med. Sci.	76	103-107	2014
*堀内 基広	BSE の発生とその対策を振り返って	日本獣医師会雑誌	67	345-353	2014
Nagasawa Y, Takahashi Y, Itani W, Watanabe H,	Prion protein binds to aldolase A of bovine intestinal M cells.	Open J Vet Med	05	43-60	2015

Hidaka Y, Morita S, Watanabe K, Ohwada S, Kitazawa H, Imamura M, Yokoyama T, Horiuchi M, Sakaguchi S, Mohri S, Rose M, Nochi T, Aso H.					
Fuchigami T, Yamashita Y, Kawasaki M, Ogawa A, Haratake M, Atarashi R, Sano K, Nakagaki T, Ubagai K, Ono M, Yoshida S, Nishida N, Nakayama M.	Characterisation of radioiodinated flavonoid derivatives for SPECT imaging of cerebral prion deposits.	Sci Rep.	5	18440	2015
Ishibashi D, Homma T, Nakagaki T, Fuse T, Sano K, Takatsuki H, Atarashi R, Nishida N.	Strain-Dependent Effect of Macroautophagy on Abnormally Folded Prion Protein Degradation in Infected Neuronal Cells.	PLoS One	10	e0137958	2015
Sano K, Atarashi R, Nishida N.	Structural conservation of prion strain specificities in recombinant prion protein fibrils in real-time quaking-induced conversion.	Prion	9	237-243	2015
Takatsuki H, Satoh K, Sano K, Fuse T, Nakagaki T, Mori T, Ishibashi D, Mihara B, Takao M, Iwasaki Y, Yoshida M, Atarashi R, Nishida N.	Rapid and Quantitative Assay of Amyloid-Seeding Activity in Human Brains Affected with Prion Diseases.	PLoS One	10	e0126930	2015
Homma T, Ishibashi D, Nakagaki T, Fuse T, Mori T, Satoh K, Atarashi R, Nishida N.	Ubiquitin-specific protease 14 modulates degradation of cellular prion protein.	Sci Rep	5	11028	2015
福田 茂夫	脳内接種による BSE 感染牛の異常プリオンタンパク質の分布	北海道獣医師会雑誌	59	98-103	2015
*福田 茂夫	道総研畜産試験場における非定型 BSE に関する研究	北海道獣医師会雑誌	59	260-265	2015
*Murayama, Y., Ono,	L-Arginine ethylester	Biochem Biophys	470	563-568	2016

F., Shimozaki, N. and Shibata, H.	enhances in vitro amplification of PrPSc in macaques with atypical L-type bovine spongiform encephalopathy and enables presymptomatic detection of PrPSc in the bodily fluids.	Res Commun.			
*Mori T, Atarashi R, Furukawa K, Takatsuki H, Satoh K, Sano K, Nakagaki T, Ishibashi D, Ichimiya K, Hamada M, Nakayama T, Nishida N.	A direct assessment of human prion adhered to steel wire using real-time quaking-induced conversion.	Sci. Rep.	6	24993	2016
McGuire LI, Poggioli A, Poggiolini I, Suardi S, Grznarova K, Shi S, de Vil B, Sarros S, Satoh K, Cheng K, Cramm M, Fairfoul G, Schmitz M, Zerr I, Cras P, Equestre M, Tagliavini F, Atarashi R, Knox D, Collins S, Haik S, Parchi P, Pocchiari M, Green A.	Cerebrospinal fluid real-time quaking-induced conversion is a robust and reliable test for sporadic creutzfeldt-jakob disease: An international study.	Ann. Neurol.	80(1)	160-165	2016
Ishibashi D, Nakagaki T, Ishikawa T, Atarashi R, Watanabe K, Cruz FA, Hamada T, Nishida N.	Structure-Based Drug Discovery for Prion Disease Using a Novel Binding Simulation.	EBioMedicine	9	238-249	2016
Schmitz M, Cramm M, Llorens F, Müller-Cramm D, Collins S, Atarashi R, Satoh K, Orrù CD, Groveman BR, Zafar S, Schulz-Schaeffer WJ, Caughey B, Zerr I.	The real-time quaking-induced conversion assay for detection of human prion disease and study of other protein misfolding diseases.	Nat. Protoc.	11(11)	2233-2242	2016
Takatsuki H, Fuse T, Nakagaki T, Mori T, Mihara B, Takao M, Iwasaki Y, Yoshida M, Murayama S, Atarashi R, Nishida N, Satoh K.	Prion-Seeding Activity Is widely Distributed in Tissues of Sporadic Creutzfeldt-Jakob Disease Patients.	EBioMedicine	12	150-155	2016
Murayama Y, Ono F, Shimozaki N, and Shibata H.	L-Arginine ethylester enhances in vitro amplification of PrPSc in macaques with atypical	Biochem. Biophys. Res. Commun.	470	563-568	2016

	L-type bovine spongiform encephalopathy and enables presymptomatic detection of PrPSc in the bodily fluids.				
Saijo E, Hughson AG, Raymond GJ, Suzuki A, Horiuchi M, and Caughey B.	PrPSc-Specific Antibody Reveals C-Terminal Conformational Differences between Prion Strains.	J. Virol.	90	4905-4913	2016
Hasebe R, Tanaka M, Suzuki A, Yamasaki T, and Horiuchi M.	Complement factors alter the amount of PrP(Sc) in primary-cultured mouse cortical neurons associated with increased membrane permeability.	Virology	496	9-20	2016
*Tanaka M, Fujiwara A, Suzuki A, Yamasaki T, Hasebe R, Masujin K, and Horiuchi M.	Comparison of abnormal isoform of prion protein in prion-infected cell lines and primary-cultured neurons by PrPSc-specific immunostaining.	J. Gen. Virol.	97	2030-2042	2016
*Shan Z, Yamasaki T, Suzuki A, Hasebe R, and Horiuchi M.	Establishment of a simple cell-based ELISA for the direct detection of abnormal isoform of prion protein from prion-infected cells without cell lysis and proteinase K treatment.	Prion	10	305-318	2016
Hagiwara K, Iwamaru Y, Tabeta N, Yokoyama T, and Tobiume M.	Evaluation of rapid post-mortem test kits for bovine spongiform encephalopathy (BSE) screening in Japan: Their analytical sensitivity to atypical BSE prions.	Prion			in press
堀内 基広	プリオン病治療実験モデル系確立の試み -免疫療法と細胞治療の可能性-	臨床評価	44	712-718	2017

*代表的成果として、「III. 研究成果の刊行物・別刷」の項に掲載した。

牛海綿状脳症, 変異クロイツフェルト・ヤコブ病



- ▶ 感染因子“プリオン”の感染により生じる致死性神経変性疾患。
- ▶ BSE (牛海綿状脳症) がヒトに感染して vCJD (変異クロイツフェルト・ヤコブ病) が発生した。
- ▶ vCJD は輸血により伝播する。
- ▶ 管理措置が有効に機能し、世界的に BSE の発生は収束している。

1 病名

牛海綿状脳症 (bovine spongiform encephalopathy: BSE), 変異クロイツフェルト・ヤコブ病 (variant Creutzfeldt-Jakob disease: vCJD)。

2 定義

BSE はウシのプリオン病で、BSE プリオンの感染により生じる、神経細胞および神経網の空胞化、アストログリオシス、およびミクログリアの増生を特徴とする致死性神経変性疾患。食を介して BSE プリオンがヒトに感染した結果、それまで知られていたヒトのプリオン病である、孤発性あるいは家族性のクロイツフェルト・ヤコブ病 (Creutzfeldt-Jakob disease: CJD) とは病型の異なる vCJD が発生した。

3 概要

プリオン病は、その原因により、感染性、遺伝性、特発性 (原因不明)、の 3 種に分類される (表 1)。ヒトのプリオン病には獲得性 (感染性)、遺伝性、および特発性の 3 種がある。このうち、特発性に分類される孤発性 CJD (sporadic CJD: sCJD) が 85% を占める。

BSE は 1980 年代半ばに英国で出現し、大流行した。その後、欧州、北米およびアジアへ拡散した。1996 年に、BSE がヒトに感染した結果発生したと考えられる vCJD の存在が報告された¹⁾。BSE の起源は、ヒツジのスクレイピーが原因であるとする説と、元来ウシに存在していた病気とする説があるが結論は出ていない。

い。図 1 に BSE 出現後の動物種を越えた感染拡大を示す。

BSE は 1985 年頃から英国で発生し、発生数は 1992 年にピークに達した (図 2)。英国では 1988 年 7 月に、反芻動物由来の肉骨粉を反芻動物に与えることを禁止する飼料規制を導入した。6 年が経過した 1994 年以降、BSE の発生は減少に転じた。欧州諸国では 2000 年以降 BSE 牛の数が著しく増加したが、2003 ~ 2004 年をピークに BSE の発生数は減少している (図 2)。わが国でも 2002 年 2 月以降に生まれたウシで BSE 牛は捕獲されていない。

vCJD はこれまで英国で 177 例、英国以外で 52 例の報告がある (表 2)。英国での発生は 2000 年をピークに減少している (図 2)。わが国でも欧州滞在歴がある症例が 1 例報告されている。

4 病因

プリオン病の病原体“プリオン”は、蛋白質から構成され、病原体ゲノムとなる核酸はない。一個の感染粒子の形態も不明である。プリオンの主要構成要素である異常型プリオン蛋白質 (PrP^{Sc}) は、宿主遺伝子 PrP にコードされる正常型プリオン蛋白質 (PrP^C) の構造異性体であり、アミノ酸配列は PrP^C と同じである。“Sc”は scrapie (スクレイピー) に、“C”は細胞の cellular に由来する。

PrP^C は中枢神経系組織で発現が高いが、生命維持に必須ではない。プリオン病に罹患したヒトや動物の脳組織には PrP^{Sc} が蓄積する。PrP^{Sc} は PrP^C と高次構造

表1 動物とヒトのプリオン病

動物のプリオン病	動物種	原因など
スクレイピー	ヒツジ、ヤギ	感染(自然状態)
慢性消耗病(CWD)	シカ、エルク	感染(自然状態)
牛海綿状脳症(BSE)	ウシ	感染(汚染飼料)
伝達性ミンク脳症(TME)	ミンク	感染(汚染飼料)
猫海綿状脳症(FSE)	猫科動物	感染(汚染飼料)
ヒトのプリオン病	分類	原因など
クロイツフェルト・ヤコブ病(CJD)		
孤発性 CJD (sCJD)	特発	偶発的(宿命)
家族性 CJD (fCJD)	遺伝	PrP 遺伝子の変異
医原性 CJD (iCJD)	感染(獲得性)	汚染硬膜移植等
変異 CJD (vCJD)	感染(獲得性)	BSE
ゲルストマン・ストライスラー症候群(GSS)	遺伝	PrP 遺伝子の変異
致死性家族性不眠症(FFI)	遺伝	PrP 遺伝子の変異
クールー(Kuru)	感染(獲得性)	宗教的食人儀式

プリオン病は、その原因により感染性、遺伝性、および特発性に分類される。動物のプリオン病はすべて感染が原因と考えられている。ヒトのプリオン病には3種の原因のものが存在する。

CWD : chronic wasting disease, BSE : bovine spongiform encephalopathy, TME : transmissible mink encephalopathy, FSE : feline spongiform encephalopathy, CJD : Creutzfeldt-Jakob disease, sCJD : sporadic CJD, fCJD : familial CJD, iCJD : iatrogenic CJD, vCJD : variant CJD, GSS : Gerstmann Sträussler syndrome, FFI : fatal familial insomnia
(筆者作成)

が異なる。PrP^cが α ヘリックスの割合が高いのに対し、PrP^{sc}は β ストランドの割合が高い。そのためPrP^{sc}は凝集体を形成し、蛋白分解酵素(proteinase K:PK)抵抗性(図3)や不溶性となる。実際には、PrP^{sc}にはPKに感受性と抵抗性の画分があり、凝集体も、小さなオリゴマーから大きな凝集体までを含むヘテロな集団である。

図4に、PrP^{sc}の細胞内産生機構を示す。プリオン感染細胞では、細胞内膜輸送に関わる細胞内小器官でPrP^{sc}が検出される³⁾。PrP^{sc}は主に細胞膜上およびendocytic-recycling経路にある細胞内小器官で産生される。特に、エンドソーマルリサイクリングコンパートメントはPrP^{sc}産生に関わる主要な細胞内小器官の一つと考えられる。

5 動物の感染症

BSEの潜伏期は平均4~8年である。英国におけるBSEの大流行は、1980年頃にレンダリング工程(肉骨

粉の製造工程)がバッチ方式から連続方式に代わったことによりプリオンが完全に不活化されず肉骨粉に残存し、そのような肉骨粉を代用乳・人工乳に添加して給餌したことに起因する。

経口ルートで侵入したプリオンは、消化管からパイエル氏板などの消化管付随リンパ濾胞の上皮に存在するM細胞から体内に取り込まれる。体内に取り込まれたプリオンは、末梢神経へと移行し、副交感神経系(迷走神経)を経て延髄に至る経路と、交感神経系(内臓神経)を経て脊髄胸腰部に至る経路で、中枢神経系に侵入する。BSEの最少感染量は、BSE感染牛脳1mg以下と非常に少ない³⁾。

BSE病原体の体内分布は神経系組織に限局している。中枢神経系組織、背根神経節、三叉神経節、座骨神経などの末梢神経、および回腸遠位部などで感染性が確認されている。自然状態でウシ間の水平感染は起こらない。

BSEの初期症状としては音に対する異常反応、不安

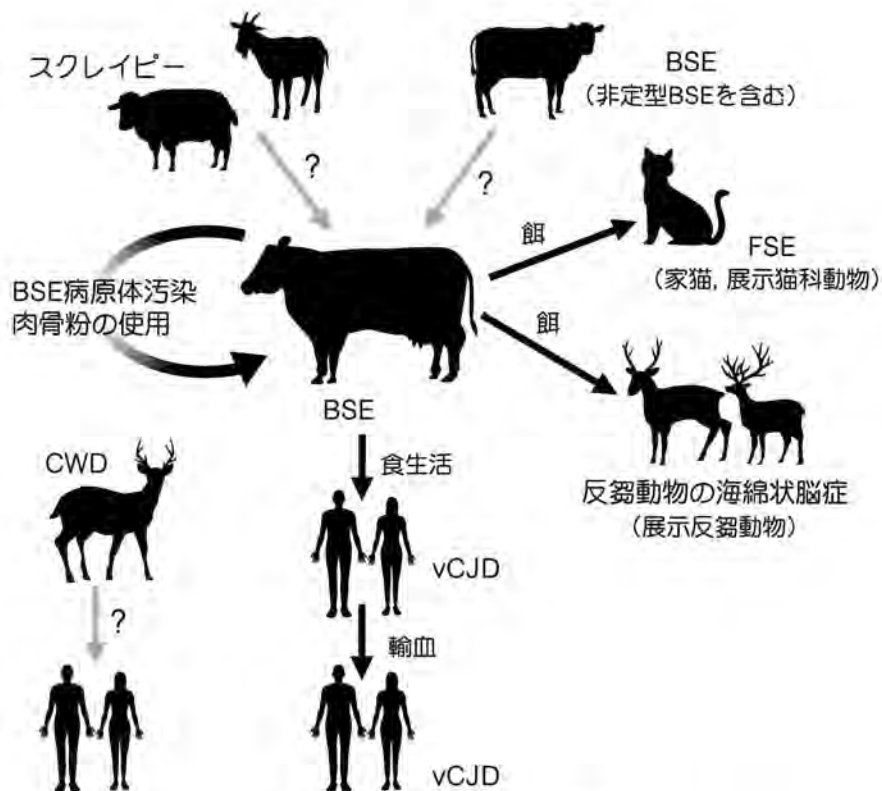


図1 種を越えた感染拡大と感染経路

BSEの起源は不明であるが、BSEの感染拡大はBSE病原体に汚染された肉骨粉の使用が原因である。BSEは猫科動物、展示反芻動物に感染が拡大した。ヒトにも感染が拡大してvCJDが発生した。CWDがヒトに伝播するかは明らかでない。

(筆者作成)

動作、持続的に鼻をなめる、などの行動異常が観察される。その後、起立時の後肢開脚、ふらつき歩行などの運動失調を経て、起立不能へと症状が進行し、死に至る。神経病理組織学的検査による神経細胞および神経網の空胞化とアストログリオシスの確認、ELISA、ウェスタンブロット、あるいは免疫組織化学によるPrP^{Sc}の検出により確定診断する(図5, 6)。

英国で発生して欧州、北米、日本に感染が広がったBSEを“定型BSE”と呼ぶ。一方、2004年以降、定型BSEとは病原体の性状が異なる、“非定型BSE”が、欧州、北南米、および日本で、主に8歳以上の高齢牛で見つかっている。非定型BSEは、ヒトの孤発性CJDのように、高齢牛で自然発生するBSEの可能性が指摘されている。

6 ヒトの感染症

プリオン病は長い潜伏期の後発症し、一度発症すると、亜急性に進行して死に至る致死性の神経変性疾患で有効な治療法はない。英国でのvCJDの発生は一つのピークを過ぎた(図2)。これらの患者はPrPのコドン129がMet/Metのホモであり、vCJDに感受性が高い集団である。今後PrPコドン129がMet/Val、あるいはVal/Valを持つヒトでvCJDが発生するかどうか注視する必要がある。

sCJDと異なり、vCJDでは中枢神経系以外に扁桃や盲腸の粘膜下リンパ濾胞など末梢のリンパ系組織でもPrP^{Sc}が検出される。英国における盲腸PrP^{Sc}検出の週及研究では、数千人から数万人のvCJDキャリアが存

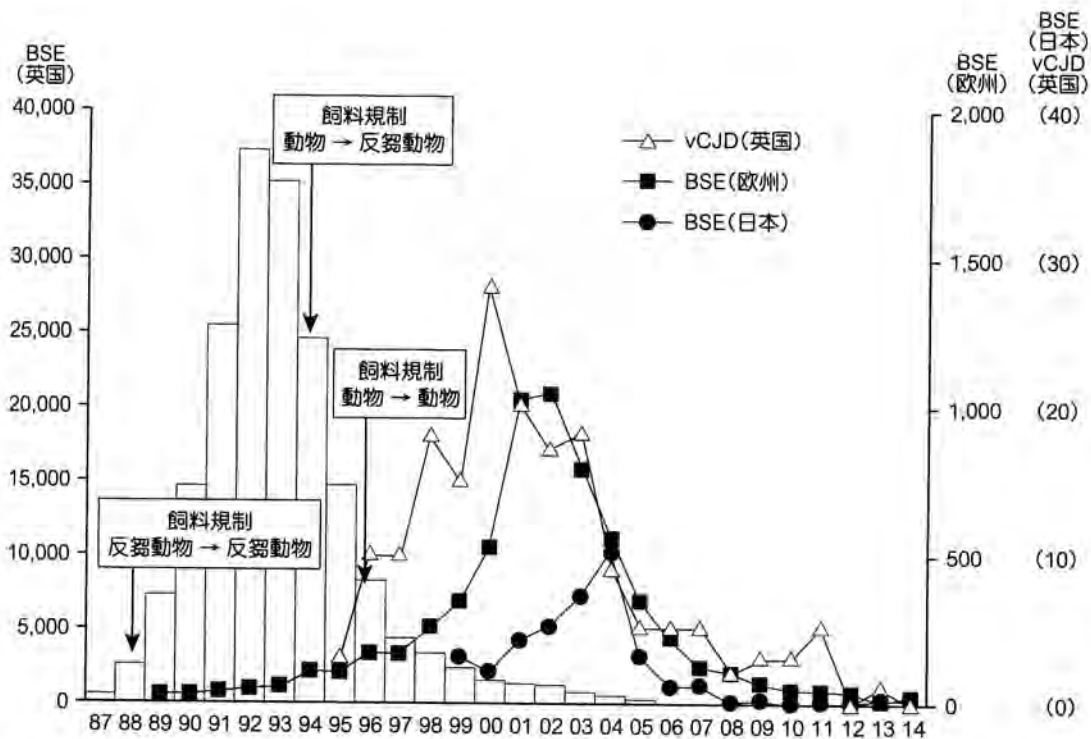


図2 英国，欧州，および日本におけるBSE発生数の経時変化と英国におけるvCJD患者数の変化

棒グラフは英国におけるBSE発生数，△は英国におけるvCJD発生数，■は欧州におけるBSE発生数，●は日本におけるBSE発生数を示す。
(筆者作成)

表2 vCJD患者数

国	患者数(人)
イギリス	177
フランス	27
アイルランド	4
イタリア	2
アメリカ	4
カナダ	2
サウジアラビア	1
日本	1
オランダ	3
ポルトガル	2
スペイン	5
台湾	1

vCJDの発生はBSEが大流行した英国で最も多く、これまでに英国で177例、次いでフランスで27例の報告がある。英国以外では計52例の報告がある。わが国でも欧州滞在歴がある症例が1例確認されている。

(www.cjd.ed.ac.uk [2015年2月13日]を基に筆者作成)

在するとの推測もある¹⁾。vCJDは輸血により伝播する(図1)。

vCJDの発症年齢(12～74歳[平均26歳])はsCJD(日本:32～94歳[平均68歳])に比べると若く、発症後の経過も6～39カ月(平均13.0カ月)と、sCJDと比較して緩徐である。初発症状は抑うつ、無気力、不安などの精神症状であり、神経症状としては上下肢の疼痛性感覚異常が認められる²⁾。末期には興奮、偏執、方向感覚の喪失などの精神症状が出現する。sCJDで高率に認められる周期性同期性放電は、vCJDの有症期後期にまれにみられるのみである。神経病理学的特徴として、vCJDの患者の脳では、florid plaqueと呼ばれる、花卉状のPrPブランクが認められる。PrP^{Sc}は、Parchiらの分類による2b型³⁾(Collingeらの分類による4型)を示す。MRIはvCJDの診断に有効で、FLAIR画像やT2強調画像で、pulvinar signと呼ばれ

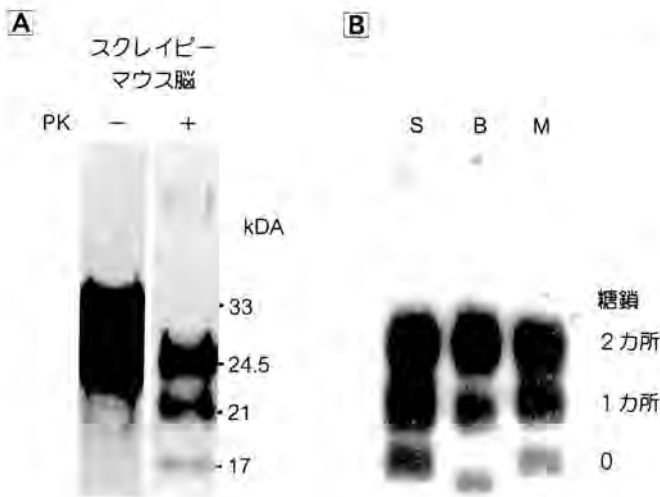


図3 プリオン蛋白 (PrP^{Sc}) の SDS ポリアクリルアミドゲル電気泳動

A: スクレイビー感染マウス脳を proteinase K (PK) 消化前 (-) と後 (+) を SDS- ポリアクリルアミドゲル (12%) で電気泳動し, 抗プリオン蛋白抗体 B103 を用いたウエスタンブロット法により検出した。消化前は 33 kDa 以下の不明瞭なスメア状のバンドが, 消化後は 24.5 kDa 以下, 糖鎖の結合数の違いにより明瞭な 3本のバンドとなる。

B: スクレイビー感染羊 (S), BSE 感染牛 (B) およびスクレイビー感染マウス (M) の脳を PK 消化後泳動し, A と同様に異常プリオン蛋白を検出した。種による分子量の差がいくらか認められるが, いずれも 3本のバンドを形成する。

(筆者提供)

(カラー図譜 21 頁)

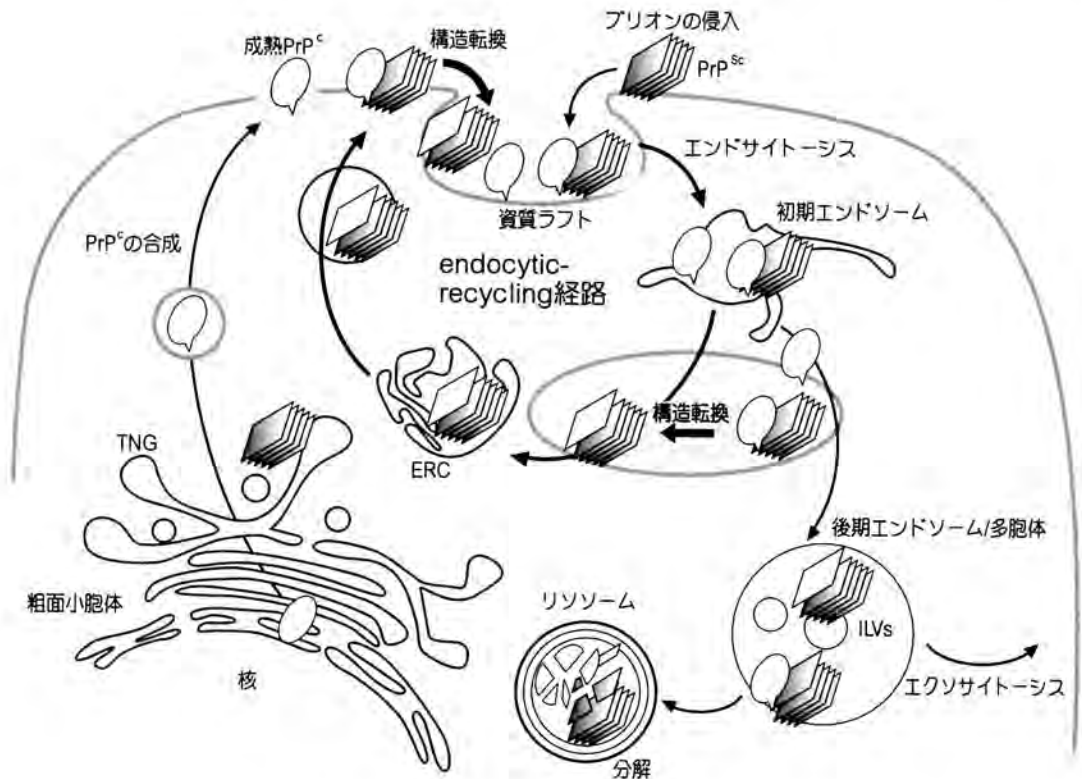


図4 PrP^{Sc} の細胞内産生機構

PrP^{Sc} は細胞内小胞輸送に関わる細胞内小器官に存在する。PrP^{Sc} は主に, 細胞膜上および endocytic-recycling 経路にある細胞内小器官で産生される。

ERC: エンドソームリサイクリングコンパートメント, TGN: トランスゴルジネットワーク

(筆者作成)

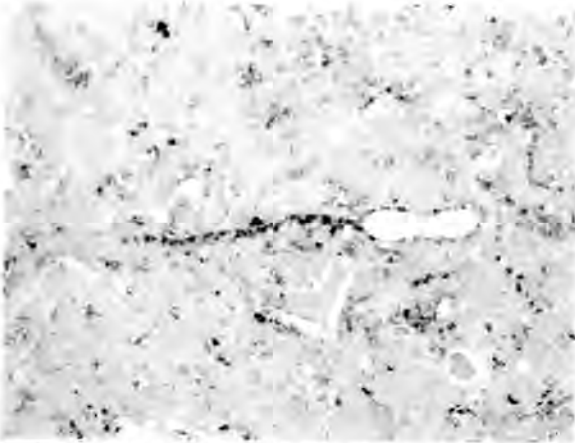


図5 抗プリオン蛋白抗体を用いた BSE の免疫組織化学
(中脳の空胞辺縁および神経網の陽性反応)
ニューロピルの空胞変性とその空胞辺縁および神経網に、
プリオンの蓄積が免疫反応陽性として証明される。
(帯広畜産大学家畜病理学教室 古岡博士提供)
(カラー図譜 21 頁)

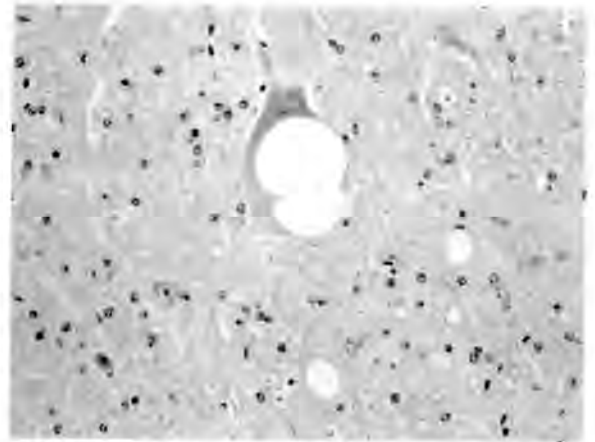


図6 BSE の病変 (ヘマトキシリン・エオシン染色)
中脳にみられた神経細胞細胞質およびニューロピルの空
胞変性。
(帯広畜産大学家畜病理学教室 古岡博士提供)
(カラー図譜 21 頁)

る視床枕での両側性の高信号が認められる。

vCJD 以外の獲得性プリオン病として、クールーと
医原性 CJD がある。わが国では、プリオン汚染脳硬
膜の使用による医原性 CJD が大きな薬害問題となり、
症例は 140 例を超えた。当該脳硬膜が使用されていた
のは 1991 年までであるが、20 年以上を経過した今日
でも、まれに発生がある。パプアニューギニアのフォ
ア族で発生していたクールーは宗教的な食人儀式的廃
止により発生は減少したが、潜伏期は長い例で 50 年
を超える可能性もある。

7 教訓

BSE 対策は、食の安全・安心の担保、治療法のない
致死性疾患であること、病原体の不活化が難しいこと
などから、実際リスクに比して厳しい管理措置がと
られてきた。定型 BSE の発生は収束し、管理措置が緩
和されている。非定型 BSE、ヒツジのスクレイピーは
存在することから、BSE 再興の悪夢を阻止するには、
適切な管理措置の維持が必須である。

(堀内 基広)

【文 献】

- 1) Will RG, Ironside JW, Zeidler M, et al: A new variant of Creutzfeldt-Jakob disease in the UK. *Lancet* 347 : 921-925, 1996.
- 2) Yamasaki T, Suzuki A, Shimizu T, et al : Characterization of intracellular localization of PrPSc in prion-infected cells using a mAb that recognizes the region consisting of aa 119-127 of mouse PrP. *J Gen Virol* 93 : 668-680, 2012.
- 3) Wells GA, Konold T, Arnold ME, et al: Bovine spongiform encephalopathy: the effect of oral exposure dose on attack rate and incubation period in cattle. *J Gen Virol* 88 : 1363-1373, 2007.
- 4) Gill ON, Spencer Y, Richard-Loendt A, et al : Prevalent abnormal prion protein in human appendixes after bovine spongiform encephalopathy epizootic : large scale survey. *BMJ* 347 : f5675, 2013.
- 5) Spencer MD, Knight RS, Will RG : First hundred cases of variant Creutzfeldt-Jakob disease : retrospective case note review of early psychiatric and neurological features. *BMJ* 24 : 1479-1482, 2002.
- 6) Parchi P, Capellari S, Chen SG, et al : Typing prion isoforms. *Nature* 386 : 232-234, 1997.



Characterization of intracellular dynamics of inoculated PrP^{res} and newly generated PrP^{Sc} during early stage prion infection in Neuro2a cells



Takeshi Yamasaki^a, Gerald S. Baron^b, Akio Suzuki^a, Rie Hasebe^a, Motohiro Horiuchi^{a,*}

^a Laboratory of Veterinary Hygiene, Graduate School of Veterinary Medicine, Hokkaido University, Kita 18, Nishi 9, Kita-ku, Sapporo 060-0818, Japan

^b Laboratory of Persistent Viral Diseases, Rocky Mountain Laboratories, National Institute of Allergy and Infectious Diseases, National Institutes of Health, Hamilton, MT, USA

ARTICLE INFO

Article history:

Received 16 September 2013

Returned to author for revisions

15 October 2013

Accepted 4 November 2013

Keywords:

Prions

Membrane trafficking

Endosomes

Neurodegenerative diseases

Rab proteins

ABSTRACT

To clarify the cellular mechanisms for the establishment of prion infection, we analyzed the intracellular dynamics of inoculated and newly generated abnormal isoform of prion protein (PrP^{Sc}) in Neuro2a cells. Within 24 h after inoculation, the newly generated PrP^{Sc} was evident at the plasma membrane, in early endosomes, and in late endosomes, but this PrP^{Sc} was barely evident in lysosomes; in contrast, the majority of the inoculated PrP^{Sc} was evident in late endosomes and lysosomes. However, during the subsequent 48 h, the newly generated PrP^{Sc} increased remarkably in early endosomes and recycling endosomes. Overexpression of wild-type and mutant Rab proteins showed that membrane trafficking along not only the endocytic-recycling pathway but also the endo-lysosomal pathway is involved in *de novo* PrP^{Sc} generation. These results suggest that the trafficking of exogenously introduced PrP^{Sc} from the endo-lysosomal pathway to the endocytic-recycling pathway is important for the establishment of prion infection.

© 2013 Elsevier Inc. All rights reserved.

Introduction

Prions are causative agents of transmissible spongiform encephalopathies (TSEs), neurodegenerative disorders that are characterized by accumulation of an abnormal isoform of prion protein (PrP^{Sc}) in the central nervous system (CNS). PrP^{Sc} is the only known proteinaceous component of prions, and infectivity of prions is thought to be associated with PrP^{Sc} oligomers (Silveira et al., 2005; Wang et al., 2010). PrP^{Sc} is a conformational isomer of a cellular prion protein (PrP^C) and is rich in β -sheet; PrP^{Sc} is generated from PrP^C, a protein that is expressed on the surface of host cells (Prusiner, 1998). Conversion of PrP^C to PrP^{Sc} is thought to be triggered by direct contact between “seed” PrP^{Sc} and “substrate” PrP^C.

The intracellular dynamics of PrP^{Sc} immediately following exposure of the cells to prions have been analyzed to understand the mechanisms by which a prion infection becomes established. Although PrP^C is not necessary for the internalization of PrP^{Sc} (Greil et al., 2008; Hijazi et al., 2005; Jen et al., 2010; Magalhaes et al., 2005; Paquet et al., 2007), some candidates such as laminin receptor, heparan sulfate, or low-density lipoprotein receptor-related protein 1 (LRP1) have been reported to act as receptors

that mediate internalization of exogenously inoculated PrP^{Sc} (Gauczynski et al., 2006; Horonchik et al., 2005; Jen et al., 2010).

During the early stage after inoculation of PrP^{Sc}, internalized PrP^{Sc} has been reported to be directed to late endosomes/lysosomes via the endo-lysosomal pathway (Jen et al., 2010; Magalhaes et al., 2005). In cells persistently infected with prions, a number of studies have shown that PrP^{Sc} localizes throughout the endocytic compartments—specifically the plasma membrane, early endosomes, recycling endosomes, late endosomes, secondary lysosomes, and the peri-nuclear Golgi region (Marijanovic et al., 2009; McKinley et al., 1991; Pimpinelli et al., 2005; Taraboulos et al., 1990; Veith et al., 2009; Vey et al., 1996; Yamasaki et al., 2012). Earlier studies suggested that the generation of PrP^{Sc} occurs on the cell surface or within the endocytic pathway (Borchelt et al., 1992; Caughey and Raymond, 1991; Taraboulos et al., 1992). Marijanovic et al. reported that the endocytic recycling compartment (ERC) may be the site where the conversion of PrP^C to PrP^{Sc} occurs (Marijanovic et al., 2009). In a very early stage of prion infection where new PrP^{Sc} formation was measured within minutes after initiation of infection, Gould et al. recently reported that the plasma membrane is a primary site of conversion (Gould et al., 2011).

In spite of the efforts described above, the events required for the establishment of prion infection in cells, especially those that occur in the early stage after introduction of the infectious prions,

* Corresponding author. Tel./fax: +81 11 706 5293.

E-mail address: horichi@vetmed.hokudai.ac.jp (M. Horiuchi).

are poorly understood. Simultaneous analysis of inoculated PrP^{Sc} and newly generated PrP^{Sc} in a short period after challenge with prions is important for understanding the early events of prion infection. However, such analysis is limited due to the technical difficulties in the distinction of PrP^{Sc} from PrP^C and also in the distinction of newly generated PrP^{Sc} from inoculated PrP^{Sc}. For example, antibody epitope-tagging has been used to specifically detect host cell-derived PrP or input PrP^{Sc} (Greil et al., 2008; Vorberg et al., 2004) but not both. Specific labeling of PrP^{Sc} with anti-PrP antibody via pre-treatment of cells with chaotropic agents such as guanidinium salt has been widely used to detect PrP^{Sc} in cells (Marijanovic et al., 2009; Pimpinelli et al., 2005; Taraboulos et al., 1990). However, this method is limited because weak PrP^{Sc} signals such as newly generated PrP^{Sc} may be lost or obscured because the detector gain or exposure times need to be adjusted to

a level at which signals from endogenous PrP^C are below the detection limit.

We recently reported that mAb 132, an anti-PrP monoclonal antibody that recognizes an epitope consisting of amino acids 119–127 of mouse PrP, allowed us to visualize PrP^{Sc} in prion-infected cells by indirect immunofluorescence assay (IFA) without specific manipulation of threshold setting to diminish PrP^C signals (Yamasaki et al., 2012). Here, we established a method in which inoculated PrP^{Sc} and newly generated PrP^{Sc} can be distinguished by combining the use of fluorescent-dye-labeled purified proteinase K (PK)-resistant PrP^{Sc} (PrP-res) as inoculum with PrP^{Sc}-specific staining with mAb 132. By using this method, in the present study, we extensively analyzed the fate of the inoculated PrP-res and the appearance of newly generated PrP^{Sc} in Neuro2a cells during the early stages of prion infection.

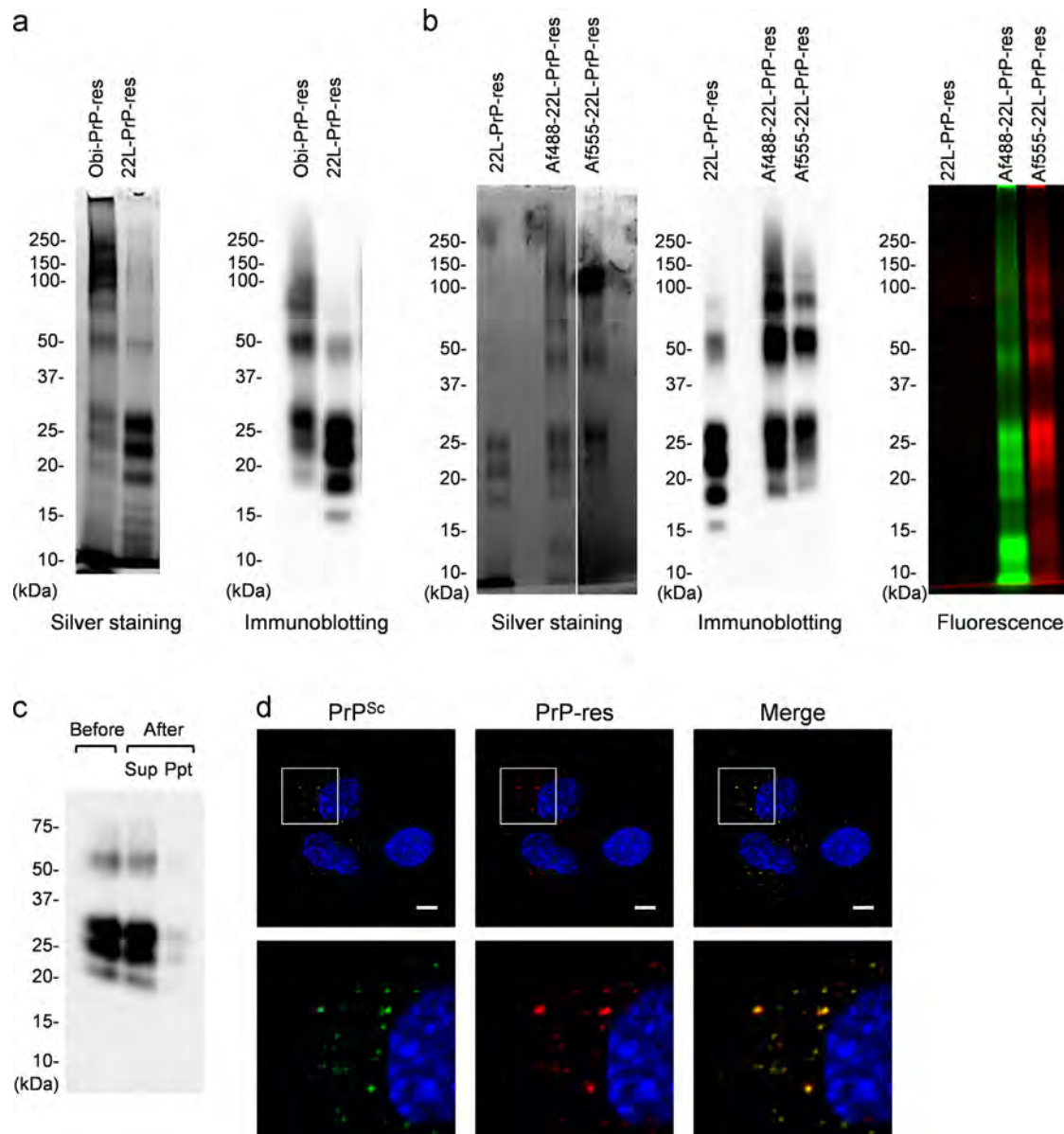


Fig. 1. Characterization of purified PrP-res. (a) Purity of the PrP-res preparation. Purified PrP-res fractions from the brains of mice infected with the Obihiro strain (Obi-PrP-res) and the 22-L strain (22-L-PrP-res) were subjected to SDS-PAGE followed by silver staining and immunoblotting with mAb 31C6. (b) Purity of fluorescent-dye-labeled PrP-res. The purified 22-L-PrP-res was labeled with Alexa Fluor 488 (Af488-22-L-PrP-res) or Alexa Fluor 555 (Af555-22-L-PrP-res). Purity and fluorescent-dye-labeling were analyzed with silver staining, immunoblotting with mAb 31C6, and fluorescence imaging. (c) Influence of sonication on purified PrP-res. Purified 22-L-PrP-res was sonicated and then before and after centrifugation at $10,000 \times g$ for 10 min [supernatant (Sup), precipitate (Ppt)] the PrP-res was subjected to immunoblotting with mAb 31C6. (d) PrP^{Sc}-specific staining of cells inoculated with PrP-res. N2a-3 cells were incubated with Af555-22-L-PrP-res for 6 h at 37 °C, and then subjected to PrP^{Sc}-specific staining. The top panel shows the images of PrP^{Sc} detected with mAb 132 (green, left) and Af555-22-L-PrP-res (red, center), and their merged image (right). The bottom panel shows the corresponding high-magnification images of the boxed regions. Cells were counterstained with DAPI (blue). Scale bar: 10 μm.

Results

Purification and labeling of PrP-res

To monitor the intracellular dynamics of PrP-res after inoculation, PrP-res was purified from the brains of mice infected with the 22-L or Obihiro scrapie strain and the purified PrP-res was labeled with Alexa Fluor 488 or Alexa Fluor 555 succinimidyl ester. Silver staining and immunoblotting of the labeled and unlabeled preparations showed the expected three major bands ranging from 35 to 20 kDa corresponding to the three PrP glycoforms, demonstrating purity of the PrP-res fraction (Fig. 1a and b). However, both preparations contained bands less than mol wt 15 kDa that did not react with mAb 31C6 (Fig. 1a). Fluorescence imaging, as well as silver staining and immunoblotting of Alexa Fluor 488- or 555-labeled purified PrP-res (Af488-22-L-PrP-res or Af555-22-L-PrP-res, respectively), revealed that the purity was satisfactory for the analysis of intracellular trafficking of 22-L-PrP-res by fluorescent microscopy (Fig. 1b). The size of PrP^{Sc} aggregates influences the uptake of PrP^{Sc} into cells (Greil et al., 2008; Jen et al., 2010; Magalhaes et al., 2005); therefore, the 22-L-PrP-res was extensively sonicated and large aggregates were removed by centrifugation. The PrP-res that largely remained in the supernatant (Fig. 1c) was used as the inoculum for N2a-3 cells, a Neuro2a clone which is susceptible to prion infection (Uryu et al., 2007). As was the case in previous studies (Jen et al., 2010; Magalhaes et al., 2005), the Af555-22-L-PrP-res that was internalized by cells was dynamically moving throughout the cells at 6 h after inoculation (Supplementary video 1). Most of the Af555-22-L-PrP-res particles were co-localized with PrP^{Sc} signals by immuno-staining with mAb 132 (Fig. 1d), which demonstrated the utility of detection of Alexa Fluor 555 signals for monitoring the trafficking of inoculated PrP-res by fluorescence microscopy.

Supplementary material related to this article can be found online at <http://dx.doi.org/10.1016/j.virol.2013.11.007>.

Intracellular localization of inoculated PrP-res

To analyze the intracellular trafficking of the inoculated PrP-res, particularly in the very early stages after internalization, trafficking of the Af555-22-L-PrP-res was monitored in cells that transiently express enhanced green fluorescent protein (EGFP)-tagged wild-type Rab4a, 5a, 7, 9, 11a, or 22a as markers of distinct endocytic compartments as follows: Rab4a, early endosomes including rapid endocytic recycling endosomes; Rab5a, early endosomes; Rab7, late endosomes; Rab9, late endosomes involved in retrograde transport to the *trans*-Golgi network (TGN); Rab11a, recycling endosomes; Rab22a, early endosomes involved in transport to recycling endosomes and TGN (Stenmark, 2009). To reduce the possibility of observing ectopically targeted Rab GTPase-EGFP fusion proteins, cells showing relatively weak EGFP signals were selected for these observations. Within 2 h after the initiation of incubation with Af555-22-L-PrP-res, we observed particles of Af555-22-L-PrP-res that were incorporated into the EGFP-positive vesicles and thereafter, PrP-res particles moved together with the EGFP-positive vesicles throughout the cells. These dynamics were observed in cells that expressed any type of Rab GTPase-EGFP fusion protein (Fig. 2, arrows). These observations indicated that exogenously introduced PrP-res was most likely transported throughout endocytic compartments within a short period after internalization.

Transferrin (Tfn) binds to the Tfn receptor, which is internalized from the cell surface by clathrin-coated pits, transported to early endosomes and then recycled back to the plasma membrane via the ERC (Maxfield and McGraw, 2004). In contrast, low-density lipoprotein (LDL) binds to the LDL receptor, which is also

internalized from the cell surface via clathrin-coated pits; however, after dissociation from the LDL receptor in early endosomes, LDL is transported to late endosomes for degradation (Ikonen, 2008). Herein we define the pathway by which the Tfn receptor is recycled between the plasma membrane and the ERC as “endocytic-recycling pathway” and the pathway by which LDL is directed to late endosomes or lysosomes for degradation as “endo-lysosomal pathway”. To analyze the trafficking of PrP-res immediately after internalization, Af555-22-L-PrP-res and Alexa Fluor 488-conjugated Tfn (Af488-Tfn) or Alexa Fluor 488-conjugated LDL (Af488-LDL) were inoculated simultaneously into N2a-3 cells. Time-lapse imaging showed that within 2 h after the initiation of incubation with PrP-res, a particle of Af555-22-L-PrP-res on the cell surface was internalized and merged with Af488-Tfn signals (Fig. 3a, between 1 min 40 s and 4 min 30 s) during transport to a peri-nuclear region, and thereafter, Af555-PrP-res and Af488-Tfn moved together back to a peripheral region of the cell (e.g., 10 min 20 s). We also observed internalization of an Af555-22-L-PrP-res particle from the cell surface that subsequently merged with an Af488-LDL-positive vesicle (Fig. 3b, between 7 min 50 s and 9 min 5 s), and thereafter, Af555-PrP-res and Af488-LDL moved together (e.g., 10 min 5 s).

To clarify the trafficking pathway of the inoculated PrP-res, cells incubated with Af555-22-L-PrP-res for 6 h were subsequently cultured for up to 30 h. Six hours after the incubation with PrP-res, some of the Af555-22-L-PrP-res signals co-localized with the Af488-Tfn signal not at the center of the cluster of the Af488-Tfn signal, but at a region around the cluster (Fig. 3c, Tfn, 0 h). On the other hand, a large portion of the Af555-22-L-PrP-res appeared to co-localize with Af488-LDL throughout the cells (Fig. 3c, LDL, 0 h). Quantitative analysis of the co-localization revealed that Af555-22-L-PrP-res co-localized more with Af488-LDL (53%) than Af488-Tfn (26%). The co-localization of Af555-22-L-PrP-res with Af488-LDL was still obvious (49%) 30 h after the inoculation, whereas, the co-localization of Af555-22-L-PrP-res with Af488-Tfn had apparently decreased (4%) (Fig. 3c, LDL and Tfn, 30 h). These results suggested that internalized PrP-res entered both the endocytic-recycling pathway and the endo-lysosomal pathway immediately following internalization, but a large portion of the inoculated PrP-res was eventually directed to the endo-lysosomal pathway.

The kinetics of inoculated PrP-res metabolism and generation of PrP^{Sc}

To determine the fate of the inoculated PrP-res and detect *de novo* generation of PrP^{Sc}, the PrP-res level in cells inoculated with Af488-22-L-PrP-res was analyzed with immunoblotting. The level of inoculated Af488-22-L-PrP-res, which was detected with an anti-Alexa Fluor 488 antibody, was drastically decreased within 24 h post inoculation (hpi) (Fig. 4a). In contrast, the total PrP-res level, which was detected with an anti-PrP antibody reactive to both the inoculated PrP-res and newly generated PrP^{Sc}, was unchanged at 24 hpi but increased thereafter (Fig. 4a). The decrease in the inoculated PrP-res was also consistent with the decrease in the PrP-res signal observed by live-cell imaging of Af555-22-L-PrP-res over the same time period (Fig. 4b). The increase of the mono-glycosylated PrP-res on immunoblots of total PrP-res at 24 hpi suggested that the *de novo* generation of PrP^{Sc} takes place within 24 hpi (Fig. 4a, arrowhead). Therefore, we analyzed the inoculated PrP-res and newly generated PrP^{Sc} simultaneously in individual cells by IFA. We used Af555-22-L-PrP-res in combination with mAb 132-mediated specific detection of PrP^{Sc} to distinguish *de novo* PrP^{Sc}, which could be detected only with mAb 132 (Fig. 4c, arrows), from exogenous PrP-res, which was labeled with both Alexa Fluor 555 and mAb 132 (Fig. 4c, arrowheads). Signals from newly generated PrP^{Sc} became detectable at 24 hpi, especially at a peri-nuclear region of the cells (arrows), and the

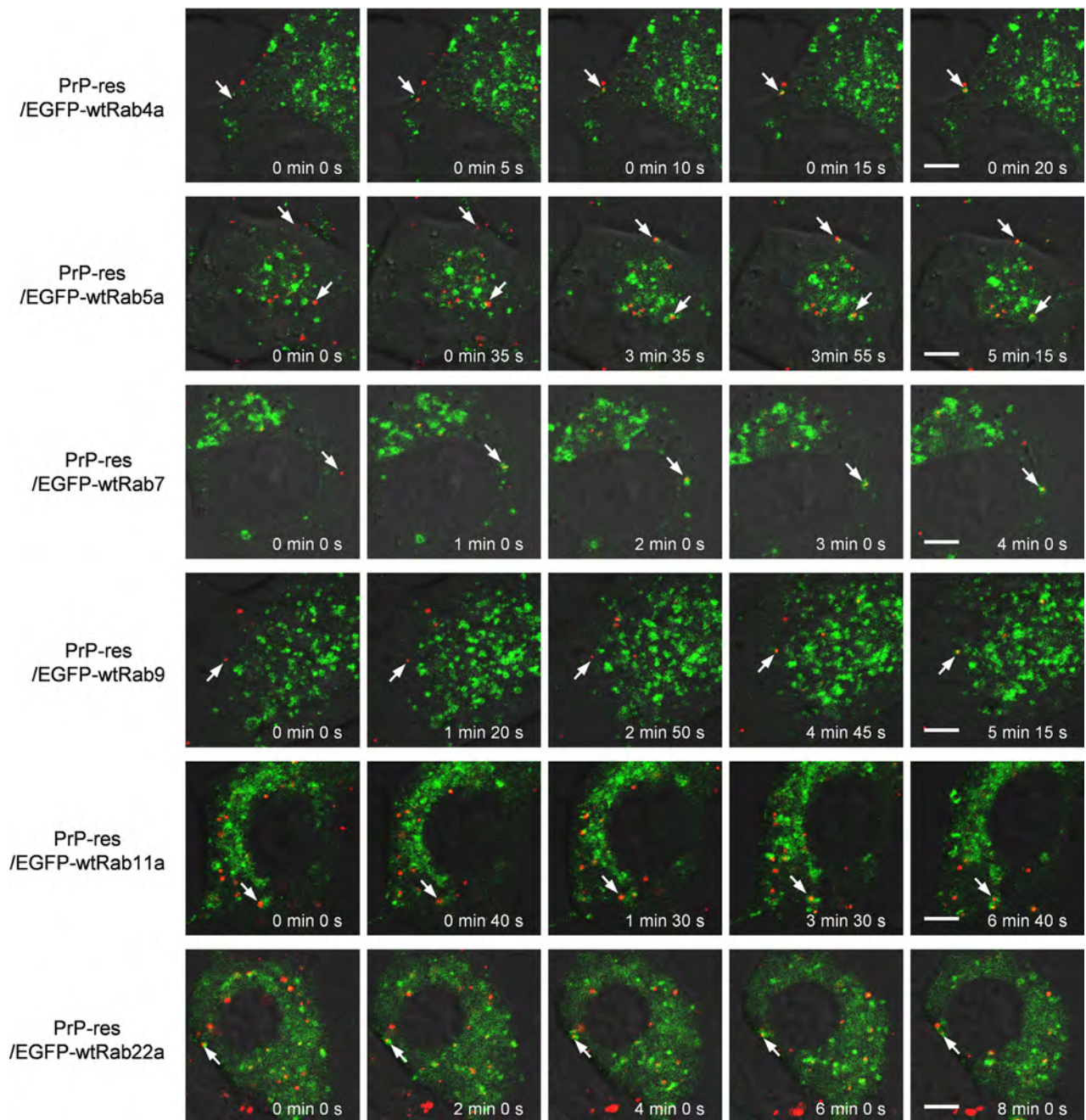


Fig. 2. Intracellular localization of fluorescent-dye-labeled, purified-PrP-res. N2a-3 cells grown on chambered coverglass were transfected with expression plasmids of EGFP-tagged wild-type of Rab4a, 5a, 7, 9, 11a or 22a. Medium (200 μl) containing 10 ng of Af555-22-L-PrP-res was added to cells 72 h after transfection. Time series of images were acquired any of 15 min-duration (images were acquired every 5 s within 2 h after the initiation of incubation with Af555-22-L-PrP-res. Each image in a row shows a merged image of Af555-22-L-PrP-res (red) and EGFP-Rab GTPase (green) with differential interference contrast (DIC) at the indicated time point. Arrows indicate examples of Af555-22-L-PrP-res that became co-localized with EGFP-Rab GTPases during the period of observation. Scale bar: 5 μm.

number of newly generated PrP^{Sc} granules and their fluorescent intensities increased thereafter. In contrast to the increase of newly generated PrP^{Sc}, the inoculated PrP-res decreased with time (Fig. 4c, arrowheads).

Intracellular localization of inoculated PrP-res and newly generated PrP^{Sc}

To identify the site of *de novo* generation of PrP^{Sc}, we next analyzed the intracellular localization of inoculated Af555-22-L-PrP-res and newly generated PrP^{Sc} with markers for endocytic compartments. At 24 hpi, some fluorescent signals from the newly generated PrP^{Sc} co-localized well with EEA1 (early endosomes)

and Rab7 (late endosomes), but were poorly co-localized with Rab11a (recycling endosomes) or cathepsin D (lysosomes) (Fig. 5). Furthermore, faint signals from newly generated PrP^{Sc} could be detected at the cell surface at 24 hpi. The intensities of these PrP^{Sc} signals increased with time after inoculation (Fig. 5, from 24 to 72 hpi). In order to clarify the kinetics of distribution of the inoculated PrP-res and newly generated PrP^{Sc}, we quantitatively analyzed co-localization ratios of the inoculated PrP-res and newly generated PrP^{Sc} co-localized with markers (Fig. 6). Consistent with the data from the live-cell imaging (Fig. 3), a large proportion of the inoculated PrP-res localized to late endosomes (40%) while a smaller portion was detected at the cell surface (22%) at 0 hpi. The exogenous PrP-res at the cell surface almost disappeared

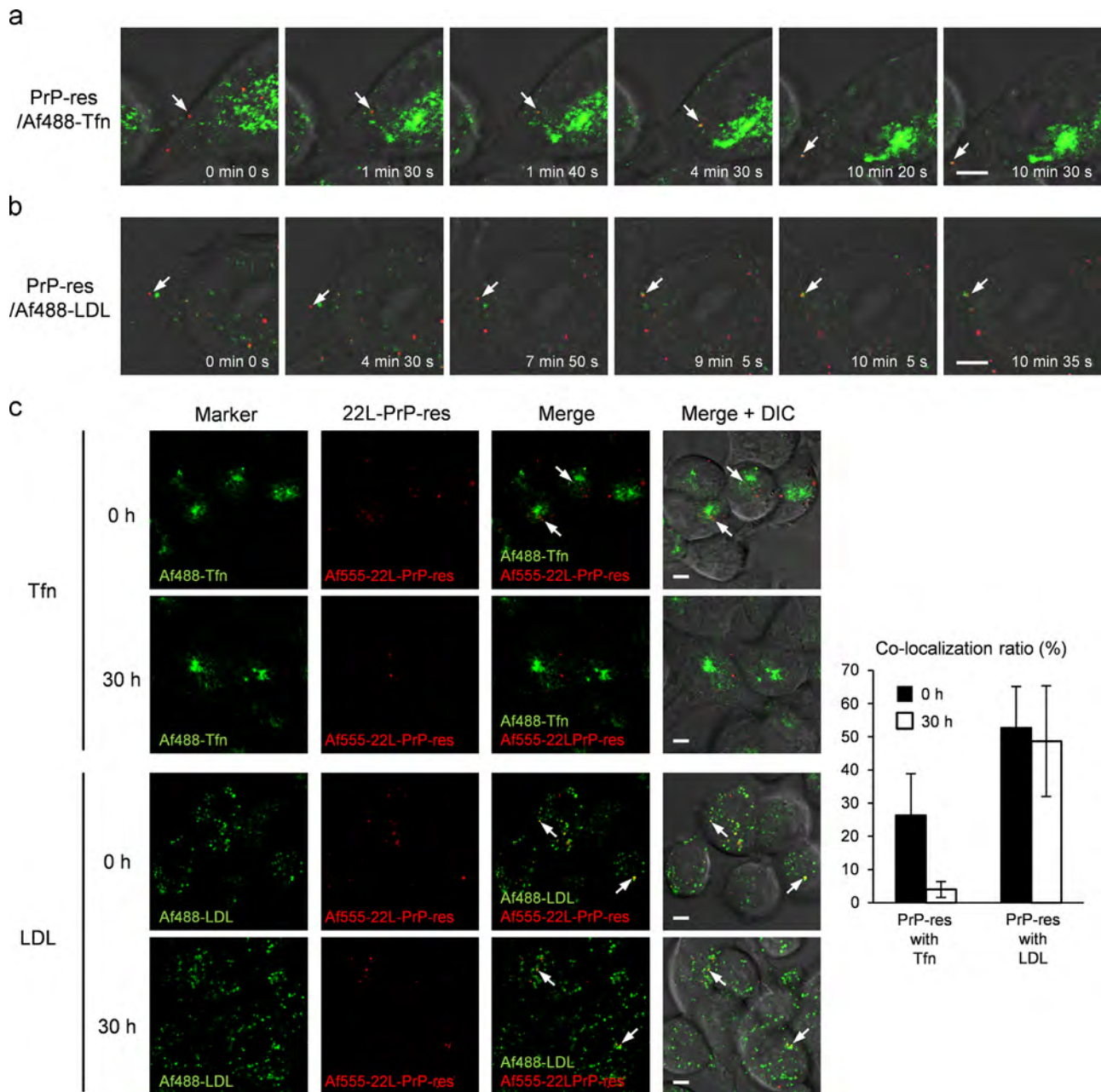


Fig. 3. Co-localization of Af555-22-L-PrP-res with Tf or LDL. Time-lapse imaging of inoculated PrP-res and Af488-Tfn (a) or Af488-LDL (b). N2a-3 cells grown on chambered coverglass were incubated with Af555-22-L-PrP-res (red) and 10 μ g/ml of Af488-Tfn (green) as a marker of the endocytic-recycling pathway (a) or 4 μ g/ml of Af488-LDL (green) as a marker of the endo-lysosomal pathway (b). Time-lapse images were acquired every 5 s within 2 h after the initiation of incubation with PrP-res. Each image within a row shows a merged image of Af555-22-L-PrP-res (red) and Af488-Tfn or Af488-LDL (green) with the DIC at the indicated time point. Arrows indicate examples of Af555-22-L-PrP-res that became co-localized with Af488-Tfn (a) or Af488-LDL (b) in the period of observation. (c) Co-localization of Af555-22-L-PrP-res with Af488-Tfn or Af488-LDL. N2a-3 cells were incubated with Af555-22-L-PrP-res and Af488-Tfn or Af488-LDL for 6 h at 37 $^{\circ}$ C. After the removal of excess Af555-22-L-PrP-res, the cells were subjected to live-cell imaging (0 h). To monitor co-localization of PrP-res one day after inoculation, N2a-3 cells were incubated with Af555-22-L-PrP-res for 6 h. After the removal of excess Af555-22-L-PrP-res, the cells were further incubated for 24 h at 37 $^{\circ}$ C. The cells were then incubated for an additional 6 h in the presence of Af488-Tfn or Af488-LDL before imaging (30 h). The right-most column shows the merged images of Af488-Tfn (green) or Af488-LDL (green), Af555-22-L-PrP-res (red), and DIC. Arrows indicate examples of Af555-22-L-PrP-res co-localized with Af488-Tfn or Af488-LDL. Scale bar: 5 μ m. The graph on the right shows ratios of Af555-22-L-PrP-res signals co-localized with Af488-Tfn or Af488-LDL signals relative to sum of the Af555-22-L-PrP-res signals (methods for the calculation of the co-localization ratio are described in the Supplementary information). Mean and SD of the values acquired from 15 fields of view are depicted. Total numbers of foci and cells used for co-localization statistics from the 15 view fields were listed in Table S4.

during the subsequent 48 h and the remaining PrP-res localized to late endosomes (from 16% to 14%) and lysosomes (from 11% to 9%). In contrast, at 24 hpi newly generated PrP^{Sc} localized mainly at the cell surface (27%), in early endosomes (15%), and late endosomes (30%), but a minor portion localized to lysosomes (3%). Interestingly, the proportion of newly generated PrP^{Sc} localized to early endosomes or recycling endosomes increased (from 15% to 30%

and from 5% to 33%, respectively); in contrast, the amount of PrP^{Sc} at the cell surface decreased from 27% to 3% with time after inoculation. These data suggested that even though newly generated PrP^{Sc} was detected in late endosomes and lysosomes at 24 hpi, newly generated PrP^{Sc} remarkably appeared in the intracellular organelles on the endocytic-recycling pathway thereafter.

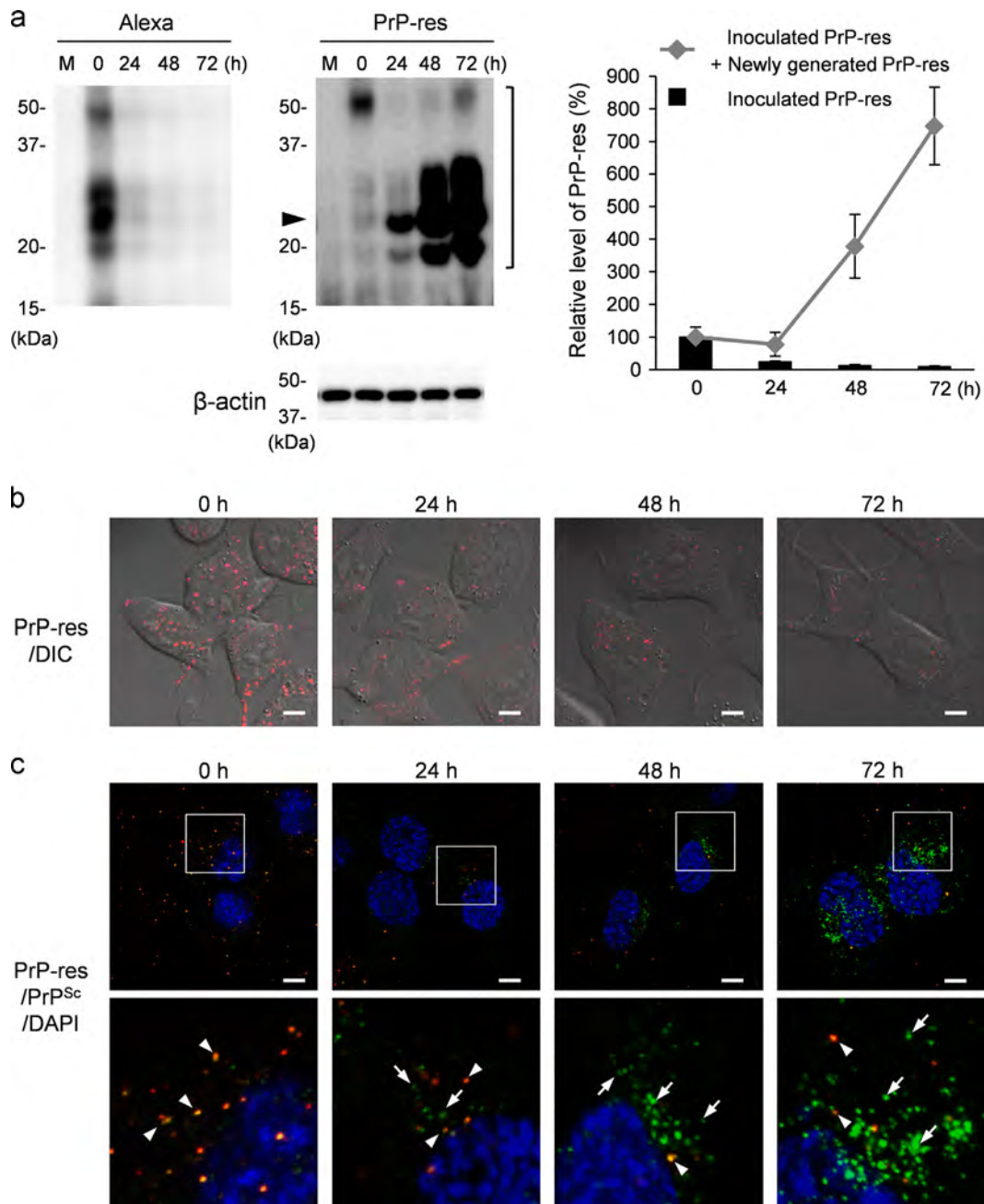


Fig. 4. Kinetics of inoculated PrP-res and *de novo* generation of PrP^{Sc}. (a) The levels of inoculated PrP-res and total PrP-res. N2a-3 cells grown on 12-well plates were inoculated with Af488-22-L-PrP-res. After the inoculation, the cells were cultured for the indicated period and then subjected to immunoblotting. As a control for detection of PrP-res, mock-infected cells were prepared (M). PK-untreated samples equivalent to 100 μ g of total protein per lane were loaded to detect Af488-22-L-PrP-res with anti-Alexa Fluor 488 antibody (Alexa), while PK-digested samples equivalent to 100 μ g of total protein were also loaded to monitor total PrP-res, which contained inoculated PrP-res and newly generated PrP-res with anti-PrP mAb 31C6 (PrP-res). β -actin was used as an internal control. Bands corresponding to monomeric and dimeric PrP^{Sc} (indicated by the square bracket) were quantified. The arrowhead indicates the mono-glycosylated form of PrP-res. The graph on the right shows the result of a quantitative analysis. Black bars indicate the inoculated PrP-res levels relative to that at 0 h and gray line indicates the total PrP-res levels relative to that at 0 h. Mean and SD of 3 independent experiments are shown. (b) Live-cell image of Af555-22-L-PrP-res. N2a-3 cells grown on chambered coverglass were inoculated with Af555-22-L-PrP-res and then cultured for the indicated time. Merged images containing Af555-22-L-PrP-res (red) and DIC are shown. (c) Discrimination of newly generated PrP^{Sc} from inoculated PrP-res in a single cell. The top panel shows the merged images of signals of Af555-22-L-PrP-res (red), PrP^{Sc} (green) and DAPI-stained nuclei (blue). The bottom panel shows the corresponding high-magnification images of the boxed region. Arrowheads indicate examples of inoculated PrP-res that was detected via both Alexa Fluor 555 (red, directly coupled to purified 22-L-PrP-res) and mAb 132 (green, indirect immuno-staining with Alexa Fluor 488-conjugated secondary antibody). As a result, inoculated PrP-res can be detected as yellow. Arrows indicate examples of newly generated PrP^{Sc} that was detected only with mAb 132 (green). Scale bar: 5 μ m.

Influence of the impairment of intracellular transport on *de novo* generation of PrP^{Sc}

To determine which pathway of intracellular transport is involved in *de novo* generation of PrP^{Sc}, we analyzed the levels of newly generated PrP^{Sc} in cells in which trafficking between the endocytic compartments was selectively impaired by the

overexpression of wild-type or dominant-negative mutants of Rab GTPase proteins (Fig. 7). The impairment of the endocytic-recycling pathway by overexpression of wild-type Rab22a or a dominant-negative mutant of Rab11a, which are known to affect the transport from early endosomes to recycling endosomes (Magadan et al., 2006) or the transport from recycling endosomes to plasma membrane (Ren et al., 1998), respectively, reduced the

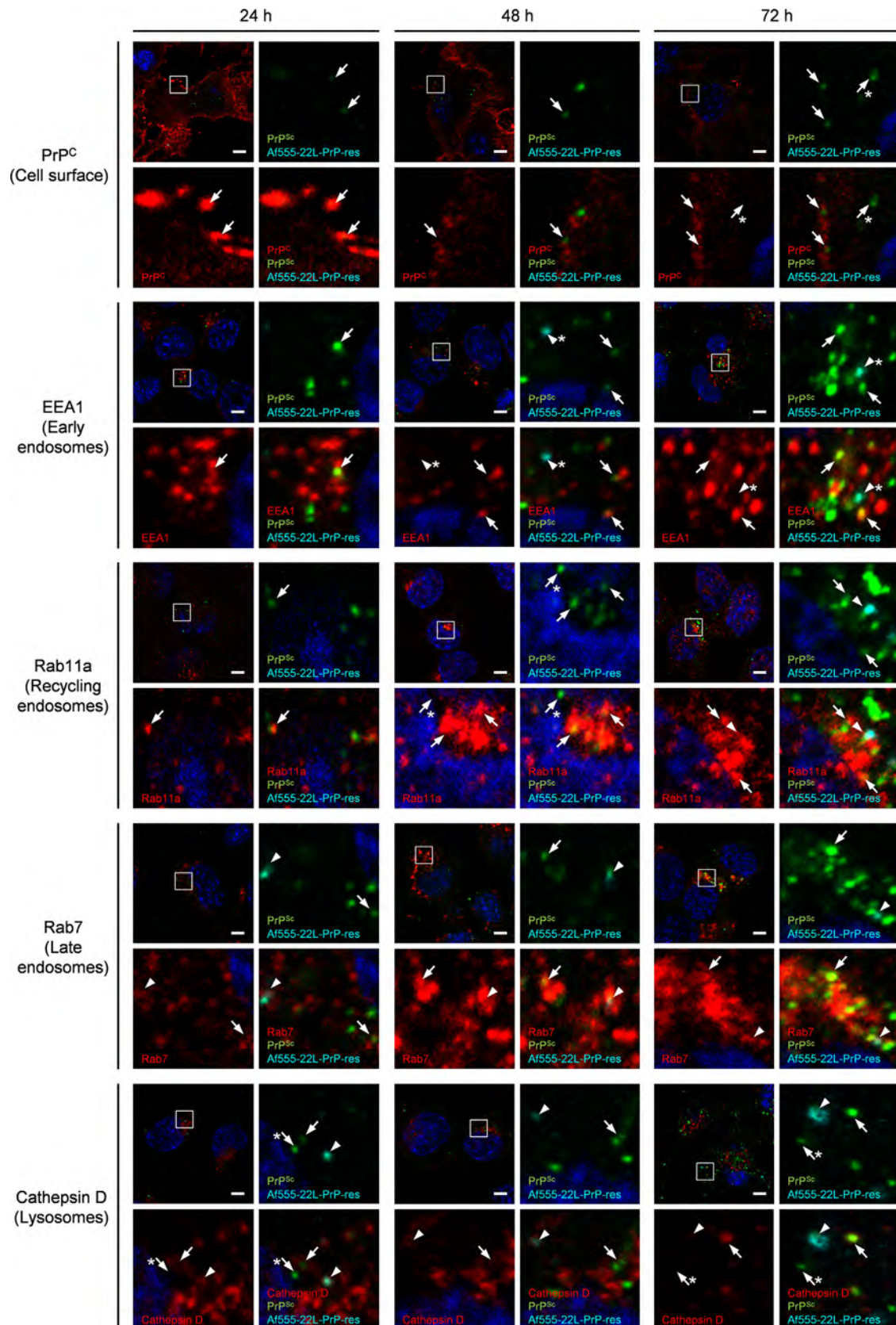


Fig. 5. Kinetics of the intracellular localization of inoculated PrP-res and newly generated PrP^{Sc}. N2a-3 cells inoculated with Af555-22-L-PrP-res were cultured for the indicated time and subjected to double-staining of PrP^{Sc} with mAb 132 and an organelle marker molecule as indicated. For staining of PrP^c at cell surface, cells were incubated with B103 antiserum prior to the fixation for PrP^{Sc}-specific detection. Alexa Fluor 647-conjugated secondary antibody was used to stain the marker molecules. The cell nuclei were counterstained with DAPI. The upper left image in each panel consists of four images showing a lower magnification view of a merged image of organelle marker molecule (red), PrP^{Sc} (green), Af555-22-L-PrP-res (cyan), and nuclei (blue). The other three images are the corresponding high-magnification image of the boxed region for the merged image of organelle marker and nuclei (bottom left), for the merged image of PrP^{Sc}, Af555-22-L-PrP-res and nuclei (upper right), and for the merged images of the organelle marker, PrP^{Sc}, Af555-22-L-PrP-res and nuclei (bottom right). Arrowheads indicate representative co-localization of Af555-22-L-PrP-res with organelle marker molecules, while arrows indicate that of newly generated PrP^{Sc} with organelle marker molecules. Arrowheads with asterisks indicate Af555-22-L-PrP-res that was not co-localized with organelle marker molecules, while arrows with asterisks indicate newly generated PrP^{Sc} that was not co-localized with organelle marker molecules. Co-localization areas were defined as pixels that were positive for both PrP^{Sc} and organelle marker signals, or that were positive for both Af555-22-L-PrP-res and organelle marker signals. Scale bars: 5 μ m.

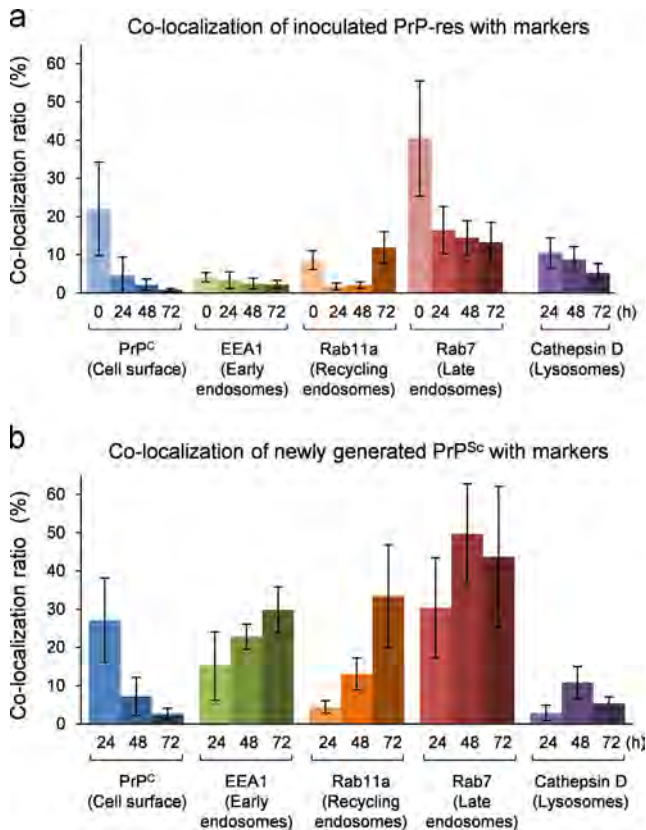


Fig. 6. Co-localization statistics. Co-localization analysis of the images shown in Fig. 5 was carried out as described in the Supplementary materials. (a) Ratio of the Af555-22-L-PrP-res signals co-localized with each marker to the sum of the Af555-22-L-PrP-res signals. (b) Ratio of the newly generated PrP^{Sc} signals co-localized with each marker to the sum of newly generated PrP^{Sc} signals. Mean and SD of the value acquired in 5 fields of view are shown. Total numbers of foci and cells used for co-localization statistics from the 5 view fields were listed in Table S5.

amount of *de novo* generated PrP^{Sc} at 48 hpi by 62% or 69% of the control (Fig. 7). Additionally, the impairment of the endo-lysosomal pathway by the overexpression of a dominant-negative mutant of Rab7, which is known to affect the transport from early endosomes to late endosomes and/or lysosomes (Bucci et al., 2000; Feng et al., 1995), also reduced the amount of *de novo* generated PrP^{Sc} at 48 hpi by 60% of the control (Fig. 7). A wild-type Rab9 is reported to be involved in the transport from late endosomes to TGN (Riederer et al., 1994). The overexpression of wild-type Rab9 reduced the amount of *de novo* generated PrP^{Sc} by 71% of the control; however, it was not clear which intracellular transport pathway was actually influenced (Fig. 7). The level of endogenous PrP^C in cells and cell-surface expression of PrP^C were not altered by overexpression of wild-type Rab9, wild-type Rab22a, a dominant-negative Rab7 mutant, or a dominant-negative Rab11a (Supplementary Fig. 1). Taken together, these results indicated that the inhibition of *de novo* generation of PrP^{Sc} was not caused by a change in the expression of PrP^C. These data suggested that intracellular transport along the endocytic-recycling pathway as well as the endo-lysosomal pathway is involved in the *de novo* generation of PrP^{Sc} after the inoculation of PrP-res.

Discussion

The lack of a method that can distinguish newly generated PrP^{Sc} from endogenous PrP^C and from inoculum-derived PrP^{Sc} was one of the obstacles to the investigation of the cellular events that mediate the *de novo* generation of PrP^{Sc} in the early stage of prion infection. Therefore, the analysis of intracellular dynamics of PrP^{Sc} just after inoculation of prions has been limited to inoculum-derived PrP^{Sc} as described previously (Jen et al., 2010; Magalhaes et al., 2005). Here, we solved this problem with a combination of the fluorescent-dye-labeled purified PrP-res and PrP^{Sc}-specific staining with mAb 132. This technique allowed us to distinguish

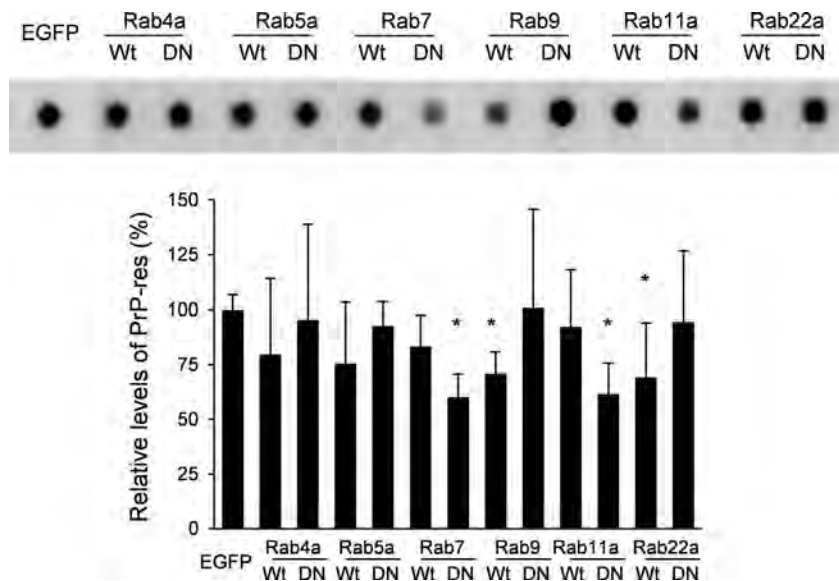


Fig. 7. Effect of overexpression of Rab GTPases on the *de novo* generation of PrP^{Sc}. N2a-3 cells grown in a 24-well plate were inoculated with unlabeled 22-L-PrP-res and were incubated for 6 h. After washing the cells, an expression plasmid encoding an EGFP-tagged wild-type (Wt) Rab GTPase, Rab4a, Rab5a, Rab7, Rab9, Rab11a or Rab22a, or an EGFP-tagged dominant-negative mutant (DN) of a Rab GTPases, Rab4aS22N (Roberts et al., 2001), Rab5aS34N (Stenmark et al., 1994), Rab7T22N (Feng et al., 1995), Rab9S21N (Riederer et al., 1994), Rab11aS25N (Ren et al., 1998) or Rab22aS19N (Weigert et al., 2004), was introduced. The expression vector pEGFP-C1 (Clontech) was used as a control. At 48 h after transfection, the cells were processed for dot-blotting to monitor PrP-res. A representative image of a dot-blot is shown on the top, and the graph below shows the levels of PrP-res relative to that of control plasmid-transfected cells (EGFP). Mean and SD of 4 independent experiments are depicted. Asterisks indicate a significant decrease compared to the control (Student's *t*-test, *p* < 0.05).

newly generated PrP^{Sc} from the inoculated PrP-res within individual cells.

Considering that the inoculated PrP-res was mainly detected in late endosomes and lysosomes (Figs. 5 and 6) and that its levels decreased from 24 to 72 h after the inoculation (Fig. 4), the PrP-res directed to the endo-lysosomal pathway appeared to be degraded in late endosomes and/or lysosomes. Previous studies showed that inoculated PrP-res is transported to late endosomes/lysosomes after being taken up by SN56 cells or primary sensory neurons (Jen et al., 2010; Magalhaes et al., 2005). Purified PrP-res of the Obihiro strain, which cannot establish a persistent infection in N2a-3 cells, was also transported to late endosomes and lysosomes; the intracellular distribution of Alexa Fluor-labeled Obihiro strain-derived PrP-res was indistinguishable from that of the 22-L strain-derived PrP-res and the inoculated PrP-res of Obihiro strain was degraded similarly to 22-L strain-derived PrP-res (data not shown). Amyloid fibrils of the A β 1-42 peptide were also reported to be transported via the endo-lysosomal pathway in SN56 cells (Magalhaes et al., 2005). Taken together, the trafficking of PrP-res via the endo-lysosomal pathway appears to be a general pathway for degradation of exogenously introduced macromolecules, rather than a pathway specific to PrP^{Sc} and the propagation of prions (Saftig and Klumperman, 2009).

Recently, Goold et al. reported that the plasma membrane is one of the sites for conversion based on the results from experiments using PK-1 cells that express PrP^C tagged with Myc-epitope at the C-terminus (Goold et al., 2011). In this report, PrP^{Sc} was primarily generated at the plasma membrane within 2 min after prion challenge. Contrary to this report, we found no evidence that *de novo* generation of PrP^{Sc} primarily occurred at plasma membrane (Figs. 4–6). This discrepancy may be due to multiple factors, one of which includes clonal differences between these cell lines. For example, the former study showed that newly generated PrP^{Sc} attained steady levels by 2 h after inoculation of prions and approximately 20% of PK-1 cells in the cultures became PrP^{Sc}-positive. However, in the N2a-3 cells used in our study, the levels of newly generated PrP^{Sc} in the cells increased at least up to 72 hpi (Fig. 4), and most of the cells in the culture eventually became PrP^{Sc}-positive (data not shown). In addition, Goold et al. reported that PrP^{Sc} was detected at the cell membrane of prion-infected PK-1 cells; however, PrP^{Sc} was only weakly detected at the plasma membrane of N2a-3 cells persistently infected with prions, even when formic acid pre-treatment that was used for PrP^{Sc}-specific detection by Goold et al. was employed (data not shown). Finally, the differences between the two studies might be accounted for the different inocula (purified PrP-res vs. brain homogenate) used to initiate infection.

Most PrP^C is known to cycle between a peri-nuclear region of the cell and the plasma membrane via the endocytic-recycling pathway after being trafficked to the cell surface, but some portion of PrP^C is also delivered to late endosomes and lysosomes (Morris et al., 2006; Peters et al., 2003; Shyng et al., 1993). Considering that the newly generated PrP^{Sc} appeared in late endosomes, but was rarely observed in lysosomes at 24 hpi, at which time a large portion of the inoculated PrP-res was localized in late endosomes (Figs. 5 and 6), the initial conversion of PrP^C to PrP^{Sc} may occur in late endosomes, at least when purified PrP-res is used as an inoculum. This idea is consistent with the finding that overexpression of the dominant-negative mutant of Rab7, which inhibits transport from early endosomes to late endosomes and/or lysosomes (Bucci et al., 2000; Feng et al., 1995), partly inhibited the generation of PrP^{Sc} after the inoculation of PrP-res (reduced to 60% of the control, Fig. 7). This finding raises the possibility that although most of the inoculated PrP-res was transported to and degraded in late endosomes/lysosomes, smaller PrP-res oligomers might be generated in late endosomes during the degradation

process. Such smaller PrP-res oligomers may initiate PrP^C conversion because smaller oligomers have greater seeding activity for the conversion of PrP^C and higher infectivity than larger PrP-res aggregates (Silveira et al., 2005).

Earlier studies suggested that in cells persistently infected with prions, PrP^{Sc} is formed either on the plasma membrane or during endocytic trafficking (Borchelt et al., 1992; Caughey and Raymond, 1991; Taraboulos et al., 1992). In later years, Béranger et al. and Marijanovic et al. reported that overexpression of dominant-negative mutants of Rab4a or Rab11a, which are known to impair the transport from early endosomes to the plasma membrane (Roberts et al., 2001) or from recycling endosomes to the plasma membrane (Ren et al., 1998), respectively, raised the PrP^{Sc} level (Beranger et al., 2002; Marijanovic et al., 2009). On the other hand, overexpression of wild-type Rab22a, which inhibits the transport from early endosomes to recycling endosomes (Magadan et al., 2006), reduced the PrP^{Sc} level in cells persistently infected with prions (Marijanovic et al., 2009). Based on these findings, one of the sites for PrP^{Sc} formation in cells persistently infected with prions is thought to be in the transport pathway from early endosomes to recycling endosomes. Also in the early stage of prion infection, we confirmed the inhibition of *de novo* generation of PrP^{Sc} by overexpression of a wild-type Rab22a (reduced to 69% of the control, Fig. 7), consistent with the results of Marijanovic et al. in persistently prion-infected cells (Marijanovic et al., 2009). However, unlike the findings in cells persistently infected with prions, the generation of PrP^{Sc} after the inoculation of PrP-res was partly inhibited by overexpression of a dominant-negative Rab11a mutant (reduced to 62% of the control, Fig. 7). These observations suggested that the initiation of PrP^{Sc} generation shortly after PrP-res inoculation required the recycling pathway between recycling endosomes and the plasma membrane. Further studies will be required to explain the apparent inconsistency between these results. However, the newly generated PrP^{Sc} appeared at the plasma membrane and in early endosomes where the inoculated PrP-res was rarely detected at 24 hpi (Figs. 5 and 6), suggesting the involvement of the recycling pathway; therefore, either the exogenous PrP-res degraded to an undetectable level or PrP^{Sc} newly generated in late endosomes was recycled back to the plasma membrane and acted as a “seed” for conversion. Moreover, the marked increase in the newly generated PrP^{Sc} at early and recycling endosomes during the following 48 h (Figs. 5 and 6) suggested that efficient generation of PrP^{Sc} occurred once the PrP^{Sc} was transferred to the endocytic-recycling pathway.

The results in this study suggest that the transfer of the inoculated PrP-res and/or newly generated PrP^{Sc} from the endo-lysosomal pathway to the endocytic-recycling pathway is important for efficient PrP^{Sc} formation after prion inoculation. One possible route of such transfer is the trafficking from the late endosomes to the plasma membrane through the TGN, a route by which cation-independent mannose-6-phosphate receptor (CIMPR) is transported (Maxfield and McGraw, 2004). CIMPR delivers hydrolase precursors from the Golgi apparatus to the endosomes and releases hydrolases into compartments in the process of late endosome formation; CIMPR is then recycled back from late endosomes to the TGN by retrograde transport. CIMPR in the TGN is also delivered to the plasma membrane (Ghosh et al., 2003). The overexpression of Rab9, which is involved in this retrograde transport of CIMPR (Riederer et al., 1994), was reported to decrease the levels of PrP^{Sc} in cells persistently infected with prions (Gilch et al., 2009) as well as inhibit the generation of PrP^{Sc} after prion inoculation (this study), suggesting that the trafficking from late endosomes to the TGN may be involved in the generation of PrP^{Sc}.

Direct transport from late endosomes to the plasma membrane might be an alternative route. This atypical transport was reported

in the trafficking of class II molecules of the major histocompatibility complex (MHC) and CD1 family molecules in antigen-presenting cells (Gelin et al., 2009; Neeffjes et al., 2011). Furthermore, MHC class II molecules are also known to be transported in the process of exosomes release (Berger and Roche, 2009; Von Bartheld and Altick, 2011). Considering the fact that PrP^C is present on the membranes of both multivesicular bodies and intraluminal vesicles and that PrP^{Sc} as well as PrP^C are released from cells with exosomes (Fevrier et al., 2004), the inoculated PrP-res and/or newly generated PrP^{Sc} in late endosomes may be recycled back to the plasma membrane through multivesicular bodies via a pathway similar to the MHC class II molecules. This idea is consistent with the finding that *de novo* generation of PrP^{Sc} was inhibited by the overexpression of the dominant-negative Rab11a mutant, which also inhibits the release of exosomes (Savina et al., 2002). The PrP^{Sc} recycled to the plasma membrane via these mechanisms may, in turn, contribute to *de novo* generation of PrP^{Sc} in the compartments on the endocytic-recycling pathway.

The intracellular dynamics of PrP^{Sc} in CNS neurons in the early stages after prion infection is largely unknown. It was reported that PrP^{Sc} could be detected in endosomal and lysosomal fractions prior to the detection of PrP^{Sc} in the plasma membrane fraction after intracerebral inoculation of prions (Dearmond and Bajsarowicz, 2010), and that protease-sensitive PrP^{Sc} could be detected in early and recycling endosomes in neurons in the hippocampus during the preclinical stage of infected mice (Godsave et al., 2008). These facts suggest that there are similarities in prion propagation in neuroblastoma cells and neurons in CNS.

In this study, we showed the intracellular dynamics of inoculated PrP-res in prion-susceptible neuroblastoma cells. Our data suggest that transfer of inoculated PrP-res from the endo-lysosomal pathway to the endocytic-recycling pathway is involved in the initiation of efficient *de novo* generation of PrP^{Sc} in the early stage of infection (Fig. 8). However, further analyses are required for understanding the mechanisms of prion propagation in neurons in CNS. Experiments are underway to clarify the intracellular

site for PrP^{Sc} generation in neurons in CNS using PrP^{Sc}-specific staining with mAb 132.

Materials and methods

Antibodies, expression plasmids, and reagents

Anti-PrP mouse mAbs 31C6 and 132 and a rabbit polyclonal antibody B103 were used (Horiuchi et al., 1995; Kim et al., 2004). The other commercially available primary and secondary antibodies that were used for immunoblotting and IFA are listed in Table S1. Alexa Fluor 488- and 555-conjugated Tfn and Alexa Fluor 488-conjugated LDL (Life Technologies) were used as markers for the endocytic pathway. Expression plasmids encoding EGFP-tagged Rab GTPases were prepared as described in Supplemental materials according to methods described elsewhere (Table S2 and S3) (Fukuda, 2003).

Cell culture

N2a-3 cells, a subclone of the mouse neuroblastoma cell line Neuro2a, were cultured as described previously (Uryu et al., 2007).

Purification of PrP-res

PrP-res was prepared from detergent-resistant membranes as described previously (Baron et al., 2011) with slight modifications (Supplementary materials). The purification procedure included a PK treatment, so from this point forward we use the term “PrP-res” to indicate the purified, PK-treated PrP^{Sc}.

Fluorescent-dye-labeling of PrP-res

PrP-res in PBS (10 µg in 50 µl) containing 0.5% Zwittergent 3-14 was sonicated with a Cross Ultrasonic Protein Auto Activating Instrument, ELSTEIN NP070-GOT (Nepa Gene), by 4 cycles of

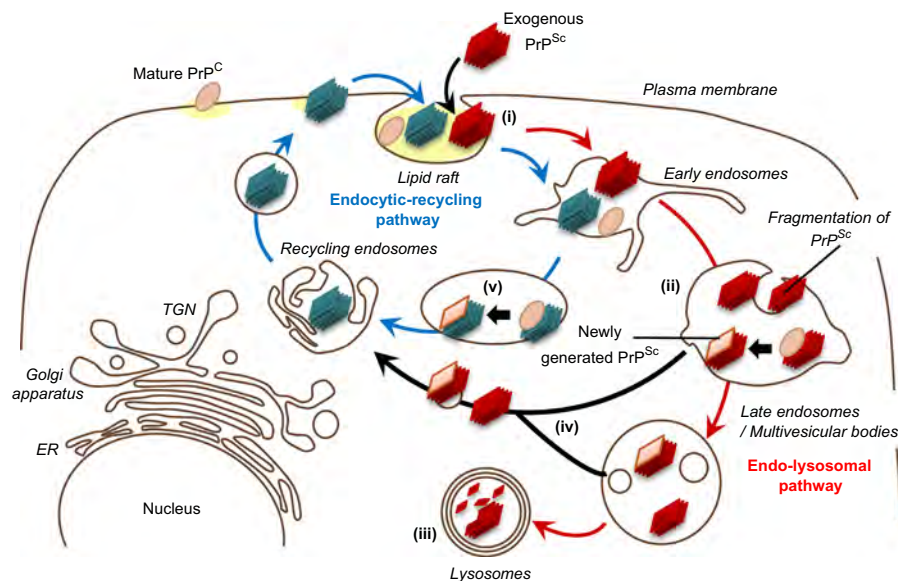


Fig. 8. Summary of intracellular dynamics of inoculated PrP^{Sc} and *de novo* generation of PrP^{Sc} in early stage of prion infection. Exogenously introduced PrP^{Sc} (red parallelograms) is internalized into a cell (i). Although inoculated PrP^{Sc} is transported throughout endocytic compartment immediately after internalization, most of the inoculated PrP^{Sc} eventually directed to endo-lysosomal pathway (indicated as red arrows) and is delivered to lysosomes and degraded (iii). Conversion of PrP^C (pink ellipse) to PrP^{Sc} (pink parallelogram) may be initiated by fragmented inoculated PrP^{Sc} (a smaller PrP^{Sc} oligomer) that is generated during the transport on the endo-lysosomal pathway (ii). A smaller PrP^{Sc} oligomer generated by fragmentation of inoculated PrP^{Sc} and/or newly generated PrP^{Sc} is transferred from the endo-lysosomal pathway to the endocytic-recycling pathway (iv). Once PrP^{Sc} that is capable of inducing conversion (blue parallelograms) is transferred to endocytic-recycling pathway (indicated as blue arrows) initiates efficient PrP^{Sc} formation that leads to the establishment of prion infection. The sites where efficient conversion occurs are thought to be early endosomes and recycling endosomes (v).

15 min-sonication followed by 5 min-incubation at 4 °C prior to fluorescent-dye labeling. The PrP-res was then mixed with 200 µg of Alexa Fluor 488 succinimidyl ester or Alexa Fluor 555 succinimidyl ester (Life Technologies) dissolved in 5 µl of anhydrous dimethyl sulfoxide (Sigma). Fluorescent-dye labeling was performed under 16 cycles of 15 min-sonication followed by 30 min-incubation at 4 °C. To quench the excess reactive dye, 3 ml of 50 mM glycine in PBS was mixed with the PrP-res and the sample was centrifuged at 45,000 rpm for 30 min at 4 °C in a S80AT3 rotor (Hitachi). The pellet was washed twice with 50 mM glycine in PBS and each wash was followed by centrifugation; the final pellet was resuspended in 100 µl of PBS with sonication. The fluorescent-dye-labeled PrP-res or unlabeled PrP-res was subjected to SDS-PAGE followed by fluorescent imaging with Typhoon FLA 9000 (GE Healthcare) or by silver-staining with 2D-SILVER STAIN-II (Cosmo bio CO.), respectively.

Inoculation of PrP-res

Purified PrP-res or fluorescent-dye-labeled PrP-res was diluted with Opti-MEM (Life technologies), sonicated with an ELSTEIN NP070-GOT sonicator for 5 min, and centrifuged at 10,000 × g for 10 min to remove large PrP-res aggregates. The supernatant was diluted with Opti-MEM at 10 ng PrP-res/200 µl or 20 ng PrP-res/250 µl or 35 ng PrP-res/500 µl for use on 8-well Lab-Tek II chambered coverglass (Thermo Scientific) or 24- or 12-well plates, respectively. The culture medium for the N2a-3 cells grown on a chambered coverglass or in the multi-well plates was replaced with Opti-MEM containing PrP-res, and the cells were then incubated for 2 or 6 h at 37 °C. After incubation, the cells were washed three times with pre-warmed PBS and then cultured in Opti-MEM containing 10% fetal bovine serum (FBS), 1% non-essential amino acids (NEAA; Gibco), and 1X penicillin-streptomycin solution (100 U/ml–100 µg/ml, PS; Gibco).

Immunofluorescence assay (IFA)

IFA, including PrP^{Sc}-specific staining, was carried out as described previously (Yamasaki et al., 2012) with some modifications. Cells were grown on an 8-well Lab-Tek II chambered coverglass and all the staining procedures were carried out without the removal of the media chamber. For double staining of cell surface PrP^C and PrP^{Sc}, living cells were incubated with B103 (5 µg/ml) in Opti-MEM for 15 min at 37 °C. The cells were then immediately fixed with pre-warmed 4% paraformaldehyde with 4% sucrose in PBS for 10 min and blocked with 5% FBS in PBS. Cells were then incubated with secondary antibody, and the cells were fixed again with 4% paraformaldehyde in PBS for 10 min and were subjected to the PrP^{Sc}-specific staining. To counterstain cell nuclei, cells were incubated with 5 µg/ml of 4', 6-diamidino-2-phenylindole, dilactate (DAPI; Invitrogen) in PBS at room temperature (rt) for 30 min. Finally, the media chamber was filled with PBS and confocal fluorescent images were acquired with a 63 × objective lens on a Zeiss LSM700 inverted microscope and the ZEN 2009 software. Z-series of the images were taken at every 0.8 µm steps from the top to bottom of the cells in the area.

Transfection

N2a-3 cells seeded onto 8-well chambered coverglass or 24-well plates at 1:5 ratio were cultured in Dulbecco's modified Eagle's medium (DMEM; ICN Biomedicals) for 2 days prior to the inoculation of PrP-res and transfection. The cells were transfected with 2.8% Lipofectamine 2000 (Invitrogen) and 2 µg/ml expression plasmid in 250 µl (8-well chamber) or 500 µl (24-well plate) of Opti-MEM that contained 8% FBS, 0.8% NEAA, and 0.8X PS. After

transfection (24 h), the medium was replaced with fresh Opti-MEM containing 10% FBS, 1% NEAA and 1X PS and cultured until used for immunoblots or IFA.

Immunoblotting and dot-blotting

Immunoblotting and dot-blotting were performed to monitor PrP and other molecules as described elsewhere (Nakamitsu et al., 2010; Uryu et al., 2007). To monitor PrP-res via immunoblotting, the protein concentration of cell lysate was adjusted to 1 mg/ml and the samples were then treated with 1 µg/ml of PK for 20 min at 37 °C. Meanwhile, to monitor Alexa Fluor 488-labeled PrP-res, PK treatment was omitted. The cell lysates were incubated with 50 µg/ml of DNase I (Roche) for 15 min at rt. Proteins were concentrated by incubating the samples with 0.3% phosphotungstic acid for 20 min at rt; this incubation was followed by centrifugation at 20,500g for 20 min at 4 °C.

To monitor PrP-res via dot-blotting, cell lysate equivalent to 40 µg of total protein per well was transferred onto a polyvinylidene difluoride (PVDF) membrane by a dot-blotter (Bio-Rad). The PVDF membrane was treated with 20 µg/ml of PK for 1 h at 37 °C and then incubated with 1 mM Pefabloc SC for 15 min at 4 °C. The membrane was treated with 50 µg/ml of DNase I for 15 min at rt and then incubated in 3 M GdnSCN for 30 min at rt. Samples on each membrane were then subjected to immuno-detection with mAb 31C6 and HRP-conjugated secondary antibody. ECL Western Blotting Detection Reagents (GE Healthcare) and a LAS-3000 chemiluminescence image analyzer (Fuji Film) were used to visualize the immunoreactive proteins.

Acknowledgments

T.Y. is supported by a Grant-in-Aid for JSPS Fellows (No. 22·4181). This work was supported by a Grant-in-Aid for Science Research (A) (Grant no. 23248050), a Grant from the Global COE Program (F-001) and the Program for Leading Graduate Schools (F01), and the Japan Initiative for Global Research Network on Infectious Diseases (J-GRID), from the Ministry of Education, Culture, Sports, Science, and Technology, Japan. This work was also supported by grants for TSE research (H23-Shokuhin-Ippan-005) and Research on Measures for Intractable Diseases from the Ministry of Health, Labour and Welfare of Japan and in part by the Intramural Research Program, National Institute of Allergy and Infectious Diseases, National Institutes of Health. We also thank Zensho Co. Ltd. for BSL3 facility.

Appendix A. Supporting information

Supplementary data associated with this article can be found in the online version at <http://dx.doi.org/10.1016/j.virol.2013.11.007>.

References

- Baron, G.S., Hughson, A.G., Raymond, G.J., Offerdahl, D.K., Barton, K.A., Raymond, L.D., Dorward, D.W., Caughey, B., 2011. Effect of glycans and the glycoposphatidylinositol anchor on strain dependent conformations of scrapie prion protein: improved purifications and infrared spectra. *Biochemistry* 50, 4479–4490.
- Beranger, F., Mange, A., Goud, B., Lehmann, S., 2002. Stimulation of PrP (C) retrograde transport toward the endoplasmic reticulum increases accumulation of PrP(Sc) in prion-infected cells. *J. Biol. Chem.* 277, 38972–38977.
- Berger, A.C., Roche, P.A., 2009. MHC class II transport at a glance. *J. Cell Sci.* 122, 1–4.
- Borchelt, D.R., Taraboulos, A., Prusiner, S.B., 1992. Evidence for synthesis of scrapie prion proteins in the endocytic pathway. *J. Biol. Chem.* 267, 16188–16199.
- Bucci, C., Thomsen, P., Nicoziani, P., McCarthy, J., van Deurs, B., 2000. Rab7: a key to lysosome biogenesis. *Mol. Biol. Cell* 11, 467–480.

- Caughy, B., Raymond, G.J., 1991. The scrapie-associated form of PrP is made from a cell surface precursor that is both protease- and phospholipase-sensitive. *J. Biol. Chem.* 266, 18217–18223.
- Dearmond, S.J., Bajsarowicz, K., 2010. PrPSc accumulation in neuronal plasma membranes links Notch-1 activation to dendritic degeneration in prion diseases. *Mol. Neurodegener.* 5, 6.
- Feng, Y., Press, B., Wandinger-Ness, A., 1995. Rab 7: an important regulator of late endocytic membrane traffic. *J. Cell Biol.* 131, 1435–1452.
- Fevrier, B., Vilette, D., Archer, F., Loew, D., Faigle, W., Vidal, M., Laude, H., Raposo, G., 2004. Cells release prions in association with exosomes. *Proc. Natl. Acad. Sci. U.S.A.* 101, 9683–9688.
- Fukuda, M., 2003. Distinct Rab binding specificity of Rim1, Rim2, rabphilin, and Noc2. Identification of a critical determinant of Rab3A/Rab27A recognition by Rim2. *J. Biol. Chem.* 278, 15373–15380.
- Gauczynski, S., Nikles, D., El-Gogo, S., Papy-Garcia, D., Rey, C., Alban, S., Barritault, D., Lasmezas, C.I., Weiss, S., 2006. The 37-kDa/67-kDa laminin receptor acts as a receptor for infectious prions and is inhibited by polysulfated glycanes. *J. Infect. Dis.* 194, 702–709.
- Gelin, C., Sloma, I., Charron, D., Mooney, N., 2009. Regulation of MHC II and CD1 antigen presentation: from ubiquity to security. *J. Leukoc. Biol.* 85, 215–224.
- Ghosh, P., Dahms, N.M., Kornfeld, S., 2003. Mannose 6-phosphate receptors: new twists in the tale. *Nat. Rev. Mol. Cell Biol.* 4, 202–212.
- Gilch, S., Bach, C., Lutzny, G., Vorberg, I., Schatzl, H.M., 2009. Inhibition of cholesterol recycling impairs cellular PrP(Sc) propagation. *Cell. Mol. Life Sci.* 66, 3979–3991.
- Godsave, S.F., Wille, H., Kujala, P., Latawiec, D., DeArmond, S.J., Serban, A., Prusiner, S.B., Peters, P.J., 2008. Cryo-immunogold electron microscopy for prions: toward identification of a conversion site. *J. Neurosci.* 28, 12489–12499.
- Goold, R., Rabbanian, S., Sutton, L., Andre, R., Arora, P., Moonga, J., Clarke, A.R., Schiavo, G., Jat, P., Collinge, J., Tabrizi, S.J., 2011. Rapid cell-surface prion protein conversion revealed using a novel cell system. *Nat. Commun.* 2, 281.
- Greil, C.S., Vorberg, I.M., Ward, A.E., Meade-White, K.D., Harris, D.A., Priola, S.A., 2008. Acute cellular uptake of abnormal prion protein is cell type and scrapie-strain independent. *Virology* 379, 284–293.
- Hijazi, N., Kariv-Inbal, Z., Gasset, M., Gabizon, R., 2005. PrPSc incorporation to cells requires endogenous glycosaminoglycan expression. *J. Biol. Chem.* 280, 17057–17061.
- Horiuchi, M., Yamazaki, N., Ikeda, T., Ishiguro, N., Shinagawa, M., 1995. A cellular form of prion protein (PrP^C) exists in many non-neuronal tissues of sheep. *J. Gen. Virol.* 76 (Pt 10), 2583–2587.
- Horonchik, L., Tzaban, S., Ben-Zaken, O., Yedidia, Y., Rouvinski, A., Papy-Garcia, D., Barritault, D., Vlodaysky, I., Taraboulos, A., 2005. Heparan sulfate is a cellular receptor for purified infectious prions. *J. Biol. Chem.* 280, 17062–17067.
- Ikonen, E., 2008. Cellular cholesterol trafficking and compartmentalization. *Nat. Rev. Mol. Cell Biol.* 9, 125–138.
- Jen, A., Parkyn, C.J., Mootosamy, R.C., Ford, M.J., Warley, A., Liu, Q., Bu, G., Baskakov, I.V., Moestrup, S., McGuinness, L., Emptage, N., Morris, R.J., 2010. Neuronal low-density lipoprotein receptor-related protein 1 binds and endocytoses prion fibrils via receptor cluster 4. *J. Cell Sci.* 123, 246–255.
- Kim, C.L., Umetani, A., Matsui, T., Ishiguro, N., Shinagawa, M., Horiuchi, M., 2004. Antigenic characterization of an abnormal isoform of prion protein using a new diverse panel of monoclonal antibodies. *Virology* 320, 40–51.
- Magadan, J.G., Barbieri, M.A., Mesa, R., Stahl, P.D., Mayorga, L.S., 2006. Rab22a regulates the sorting of transferrin to recycling endosomes. *Mol. Cell Biol.* 26, 2595–2614.
- Magalhaes, A.C., Baron, G.S., Lee, K.S., Steele-Mortimer, O., Dorward, D., Prado, M.A., Caughy, B., 2005. Uptake and neuritic transport of scrapie prion protein coincident with infection of neuronal cells. *J. Neurosci.* 25, 5207–5216.
- Marijanovic, Z., Caputo, A., Campana, V., Zurzolo, C., 2009. Identification of an intracellular site of prion conversion. *PLoS Pathog.* 5, e1000426.
- Maxfield, F.R., McGraw, T.E., 2004. Endocytic recycling. *Nat. Rev. Mol. Cell Biol.* 5, 121–132.
- McKinley, M.P., Taraboulos, A., Kenaga, L., Serban, D., Stieber, A., DeArmond, S.J., Prusiner, S.B., Gonas, N., 1991. Ultrastructural localization of scrapie prion proteins in cytoplasmic vesicles of infected cultured cells. *Lab. Invest.* 65, 622–630.
- Morris, R.J., Parkyn, C.J., Jen, A., 2006. Traffic of prion protein between different compartments on the neuronal surface, and the propagation of prion disease. *FEBS Lett.* 580, 5565–5571.
- Nakamitsu, S., Kurokawa, A., Yamasaki, T., Uryu, M., Hasebe, R., Horiuchi, M., 2010. Cell density-dependent increase in the level of protease-resistant prion protein in prion-infected Neuro2a mouse neuroblastoma cells. *J. Gen. Virol.* 91, 563–569.
- Neefjes, J., Jongstra, M.L., Paul, P., Bakke, O., 2011. Towards a systems understanding of MHC class I and MHC class II antigen presentation. *Nat. Rev. Immunol.* 11, 823–836.
- Paquet, S., Daude, N., Courageot, M.P., Chapuis, J., Laude, H., Vilette, D., 2007. PrP^C does not mediate internalization of PrP^{Sc} but is required at an early stage for de novo prion infection of Rov cells. *J. Virol.* 81, 10786–10791.
- Peters, P.J., Mironov Jr., A., Peretz, D., van Donselaar, E., Leclerc, E., Erpel, S., DeArmond, S.J., Burton, D.R., Williamson, R.A., Vey, M., Prusiner, S.B., 2003. Trafficking of prion proteins through a caveolae-mediated endosomal pathway. *J. Cell Biol.* 162, 703–717.
- Pimpinelli, F., Lehmann, S., Maridonneau-Parini, I., 2005. The scrapie prion protein is present in flotillin-1-positive vesicles in central- but not peripheral-derived neuronal cell lines 21, 2063–2072. *Eur. J. Neurosci.* 21, 2063–2072.
- Prusiner, S.B., 1998. Prions. *Proc. Natl. Acad. Sci. U.S.A.* 95, 13363–13383.
- Ren, M., Xu, G., Zeng, J., De Lemos-Chiarandini, C., Adesnik, M., Sabatini, D.D., 1998. Hydrolysis of GTP on rab11 is required for the direct delivery of transferrin from the pericentriolar recycling compartment to the cell surface but not from sorting endosomes. *Proc. Natl. Acad. Sci. U.S.A.* 95, 6187–6192.
- Riederer, M.A., Soldati, T., Shapiro, A.D., Lin, J., Pfeffer, S.R., 1994. Lysosome biogenesis requires Rab9 function and receptor recycling from endosomes to the trans-Golgi network. *J. Cell Biol.* 125, 573–582.
- Roberts, M., Barry, S., Woods, A., van der Sluijs, P., Norman, J., 2001. PDGF-regulated rab4-dependent recycling of alphavbeta3 integrin from early endosomes is necessary for cell adhesion and spreading. *Curr. Biol.* 11, 1392–1402.
- Saftig, P., Klumperman, J., 2009. Lysosome biogenesis and lysosomal membrane proteins: trafficking meets function. *Nat. Rev. Mol. Cell Biol.* 10, 623–635.
- Savina, A., Vidal, M., Colombo, M.I., 2002. The exosome pathway in K562 cells is regulated by Rab11. *J. Cell Sci.* 115, 2505–2515.
- Shyng, S.L., Huber, M.T., Harris, D.A., 1993. A prion protein cycles between the cell surface and an endocytic compartment in cultured neuroblastoma cells. *J. Biol. Chem.* 268, 15922–15928.
- Silveira, J.R., Raymond, G.J., Hughson, A.G., Race, R.E., Sim, V.L., Hayes, S.F., Caughy, B., 2005. The most infectious prion protein particles. *Nature* 437, 257–261.
- Stenmark, H., 2009. Rab GTPases as coordinators of vesicle traffic. *Nat. Rev. Mol. Cell Biol.* 10, 513–525.
- Stenmark, H., Parton, R.G., Steele-Mortimer, O., Lutcke, A., Gruenberg, J., Zerial, M., 1994. Inhibition of rab5 GTPase activity stimulates membrane fusion in endocytosis. *EMBO J.* 13, 1287–1296.
- Taraboulos, A., Raeber, A.J., Borchelt, D.R., Serban, D., Prusiner, S.B., 1992. Synthesis and trafficking of prion proteins in cultured cells. *Mol. Biol. Cell* 3, 851–863.
- Taraboulos, A., Serban, D., Prusiner, S.B., 1990. Scrapie prion proteins accumulate in the cytoplasm of persistently infected cultured cells. *J. Cell Biol.* 110, 2117–2132.
- Uryu, M., Karino, A., Kamihara, Y., Horiuchi, M., 2007. Characterization of prion susceptibility in Neuro2a mouse neuroblastoma cell subclones. *Microbiol. Immunol.* 51, 661–669.
- Veith, N.M., Plattner, H., Stuermer, C.A., Schulz-Schaeffer, W.J., Burkle, A., 2009. Immunolocalisation of PrP^{Sc} in scrapie-infected N2a mouse neuroblastoma cells by light and electron microscopy. *Eur. J. Cell Biol.* 88, 45–63.
- Vey, M., Pilkuhn, S., Wille, H., Nixon, R., DeArmond, S.J., Smart, E.J., Anderson, R.G., Taraboulos, A., Prusiner, S.B., 1996. Subcellular colocalization of the cellular and scrapie prion proteins in caveolae-like membranous domains. *Proc. Natl. Acad. Sci. U.S.A.* 93, 14945–14949.
- Von Bartheld, C.S., Altick, A.L., 2011. Multivesicular bodies in neurons: distribution, protein content, and trafficking functions. *Prog. Neurobiol.* 93, 313–340.
- Vorberg, I., Raines, A., Priola, S.A., 2004. Acute formation of protease-resistant prion protein does not always lead to persistent scrapie infection in vitro. *J. Biol. Chem.* 279, 29218–29225.
- Wang, F., Wang, X., Yuan, C.G., Ma, J., 2010. Generating a prion with bacterially expressed recombinant prion protein. *Science* 327, 1132–1135.
- Weigert, R., Yeung, A.C., Li, J., Donaldson, J.G., 2004. Rab22a regulates the recycling of membrane proteins internalized independently of clathrin. *Mol. Biol. Cell* 15, 3758–3770.
- Yamasaki, T., Suzuki, A., Shimizu, T., Watarai, M., Hasebe, R., Horiuchi, M., 2012. Characterization of intracellular localization of PrP(Sc) in prion-infected cells using a mAb that recognizes the region consisting of aa 119–127 of mouse PrP. *J. Gen. Virol.* 93, 668–680.

Conformational Properties of Prion Strains Can Be Transmitted to Recombinant Prion Protein Fibrils in Real-Time Quaking-Induced Conversion

Kazunori Sano, Ryuichiro Atarashi, Daisuke Ishibashi,
Takehiro Nakagaki, Katsuya Satoh and Noriyuki Nishida
J. Virol. 2014, 88(20):11791. DOI: 10.1128/JVI.00585-14.
Published Ahead of Print 30 July 2014.

Updated information and services can be found at:
<http://jvi.asm.org/content/88/20/11791>

REFERENCES

These include:

This article cites 53 articles, 26 of which can be accessed free
at: <http://jvi.asm.org/content/88/20/11791#ref-list-1>

CONTENT ALERTS

Receive: RSS Feeds, eTOCs, free email alerts (when new
articles cite this article), [more»](#)

Information about commercial reprint orders: <http://journals.asm.org/site/misc/reprints.xhtml>
To subscribe to to another ASM Journal go to: <http://journals.asm.org/site/subscriptions/>

Conformational Properties of Prion Strains Can Be Transmitted to Recombinant Prion Protein Fibrils in Real-Time Quaking-Induced Conversion

Kazunori Sano,^a Ryuichiro Atarashi,^{a,b} Daisuke Ishibashi,^a Takehiro Nakagaki,^a Katsuya Satoh,^a Noriyuki Nishida^a

Department of Molecular Microbiology and Immunology, Nagasaki University Graduate School of Biomedical Sciences, Nagasaki, Japan^a; Research Centre for Genomic Instability and Carcinogenesis, Nagasaki University, Nagasaki, Japan^b

ABSTRACT

The phenomenon of prion strains with distinct biological characteristics has been hypothesized to be involved in the structural diversity of abnormal prion protein (PrP^{Sc}). However, the molecular basis of the transmission of strain properties remains poorly understood. Real-time quaking-induced conversion (RT-QUIC) is a cell-free system that uses *Escherichia coli*-derived recombinant PrP (rPrP) for the sensitive detection of PrP^{Sc}. To investigate whether the properties of various prion strains can be transmitted to amyloid fibrils consisting of rPrP (rPrP fibrils) using RT-QUIC, we examined the secondary structure, conformational stability, and infectivity of rPrP fibrils seeded with PrP^{Sc} derived from either the Chandler or the 22L strain. In the first round of the reaction, there were differences in the secondary structures, especially in bands attributed to β -sheets, as determined by infrared spectroscopy, and conformational stability between Chandler-seeded (1st-rPrP-fib^{Ch}) and 22L-seeded (1st-rPrP-fib^{22L}) rPrP fibrils. Of note, specific identifying characteristics of the two rPrP fibril types seen in the β -sheets resembled those of the original PrP^{Sc}. Furthermore, the conformational stability of 1st-rPrP-fib^{Ch} was significantly higher than that of 1st-rPrP-fib^{22L}, as with Chandler and 22L PrP^{Sc}. The survival periods of mice inoculated with 1st-rPrP-fib^{Ch} or 1st-rPrP-fib^{22L} were significantly shorter than those of mice inoculated with mixtures from the mock 1st-round RT-QUIC procedure. In contrast, these biochemical characteristics were no longer evident in subsequent rounds, suggesting that nonspecific uninfected rPrP fibrils became predominant probably because of their high growth rate. Together, these findings show that at least some strain-specific conformational properties can be transmitted to rPrP fibrils and unknown cofactors or environmental conditions may be required for further conservation.

IMPORTANCE

The phenomenon of prion strains with distinct biological characteristics is assumed to result from the conformational variations in the abnormal prion protein (PrP^{Sc}). However, important questions remain about the mechanistic relationship between the conformational differences and the strain diversity, including how strain-specific conformations are transmitted. In this study, we investigated whether the properties of diverse prion strains can be transmitted to amyloid fibrils consisting of *E. coli*-derived recombinant PrP (rPrP) generated by real-time quaking-induced conversion (RT-QUIC), a recently developed *in vitro* PrP^{Sc} formation method. We demonstrate that at least some of the strain-specific conformational properties can be transmitted to rPrP fibrils in the first round of RT-QUIC by examining the secondary structure, conformational stability, and infectivity of rPrP fibrils seeded with PrP^{Sc} derived from either the Chandler or the 22L prion strain. We believe that these findings will advance our understanding of the conformational basis underlying prion strain diversity.

Prion diseases, or transmissible spongiform encephalopathies (TSEs), are infectious and fatal neurodegenerative disorders characterized by progressive spongiform changes and the accumulation of abnormal prion protein (PrP^{Sc}) in the central nervous system. Although the pathogenic mechanisms have not been fully elucidated, prion disease is thought to occur through autocatalytic conversion of normal prion protein (PrP^C) to PrP^{Sc} (1, 2), known as the protein-only hypothesis. Some biophysical properties are known to differ between PrP^C and PrP^{Sc}. PrP^C is monomeric, detergent soluble, and protease sensitive, while PrP^{Sc} is polymeric, detergent insoluble, and partially protease resistant (3). These differences are most likely due to the different conformations of the two isoforms. PrP^C is largely α -helical, whereas PrP^{Sc} is substantially enriched in β -sheets (4, 5), frequently resulting in amyloid fibril formation.

The existence of diverse prion strains in mammalian species manifesting as phenotypic differences is well-known. The strain-

specific characteristics are usually maintained upon serial passage in the same species and may be explained by conformational variations in PrP^{Sc}. Indeed, strain-dependent differences in β -sheet-rich structures of PrP^{Sc} have been demonstrated by infrared spectroscopy (6–9). In addition, the conformational stability of PrP^{Sc} differs among prion strains, as demonstrated by a guanidine hydrochloride (GdnHCl) denaturation assay followed by protease digestion (10, 11). However, the mechanistic relationship between

Received 26 February 2014 Accepted 26 July 2014

Published ahead of print 30 July 2014

Editor: B. W. Caughey

Address correspondence to Ryuichiro Atarashi, atarashi@nagasaki-u.ac.jp.

Copyright © 2014, American Society for Microbiology. All Rights Reserved.

doi:10.1128/JVI.00585-14

PrP^{Sc} conformational differences and the molecular basis of prion strains remains poorly understood.

Various *in vitro* PrP^{Sc} formation methods have been developed to elucidate the pathogenesis of prion diseases. One of these methods, protein misfolding cyclic amplification (PMCA), enabled the exponential amplification of PrP^{Sc} *in vitro* by sonication-induced fragmentation of large PrP^{Sc} polymers into smaller units (12). An increase in the infectivity of PrP^{Sc} amplified by PMCA was obtained by using brain homogenate (BH) from healthy mice (normal brain homogenate [NBH]) as a source of PrP^C substrates (BH-PMCA) (13). Furthermore, PrP^{Sc} generated by BH-PMCA from five different mouse prion strains retained the strain-specific properties (14). In addition, prion infectivity could be propagated when purified brain-derived PrP^C or baculovirus-derived PrP^C was used as the substrate in the presence of certain cofactors, such as nucleic acids and BH from PrP-deficient mice (15–17). These results provide strong evidence to support the protein-only hypothesis, but the structural basis of prion pathogenesis, including the tertiary structure of PrP^{Sc}, has not been fully clarified.

On the other hand, the use of *Escherichia coli*-derived purified recombinant PrP (rPrP) offers an advantage over the use of conformational analyses, which generally require target protein of high purity and a large quantity of the target protein. Spontaneously polymerized amyloid fibrils of rPrP have been reported to induce the accumulation of PrP^{Sc} in the brains of PrP-overexpressing transgenic (Tg) mice (18–20) and some wild-type hamsters (21); however, the incubation periods spanned no less than several hundred days, and none of the wild-type hamsters developed any neurological signs at first passage, indicating that the level of infectivity generated in these studies is very low. More recently, wild-type mice developed clinical disease typical of TSE at about 130 days after injection of proteinase K (PK)-resistant rPrP fibrils generated by unseeded PMCA in the presence of 1-palmitoyl-2-oleoylphosphatidylglycerol (POPG), a synthetic lipid molecule, and total liver RNA (22). Although these results were reproduced by the same group (23), others have reported that rPrP fibrils generated by the same method were unable to induce either neuropathological changes or the accumulation of PrP^{Sc} (24). Thus, the role of POPG and RNA in the *de novo* generation of infectious rPrP fibrils remains controversial.

Meanwhile, two different seeded PMCA reaction studies using rPrP as a substrate (rPrP-PMCA) have demonstrated the propagation of moderate levels of prion infectivity. One study showed that hamster rPrP can be converted to rPrP fibrils capable of inducing TSE in the presence of SDS, a synthetic anionic detergent, but there were great variations in the attack rate and the incubation period, which ranged from 119 to 401 days (25). Another study revealed that phosphatidylethanolamine (PE), a phospholipid found in biological membranes, enhances the conversion of mouse rPrP into rPrP fibrils capable of inducing TSE after about 400 days of incubation with a 100% attack rate (26, 27). Of note, three different strains used as a seed were converted into a single strain with unique properties during the serial rPrP-PMCA experiments (27). These studies suggest that a certain amphipathic molecule, such as PE, is a cofactor required for the propagation of prion infectivity *in vitro* but not for the transmission of strain-specific properties.

The recently developed real-time (RT) quaking-induced conversion (QUIC) is a sensitive prion detection method (28, 29) in which intermittent shaking enhances the conversion of soluble

rPrP into amyloid fibrils in the presence of PrP^{Sc}. The aim of the present research was to investigate whether properties of diverse prion strains can be transmitted to rPrP fibrils generated in the RT-QUIC system. We produced proteinase K-resistant rPrP fibrils seeded with minute quantities of mouse-adapted scrapie (Chandler or 22L strain) PrP^{Sc} and investigated the secondary structure, conformational stability, and infectivity.

MATERIALS AND METHODS

Mouse rPrP expression and purification. Recombinant PrP (rPrP) equivalent to residues 23 to 231 of the mouse PrP sequence was expressed, refolded into a soluble form, and purified essentially as previously described (30). The concentration of rPrP was determined by measuring the absorbance at 280 nm. The purity of the final protein preparations was $\geq 99\%$, as estimated by SDS-PAGE, immunoblotting, and liquid chromatography-mass spectrometry (data not shown). After purification, aliquots of the proteins were stored at -80°C in 10 mM phosphate buffer, pH 6.8, or distilled water.

Preparation of brain homogenates. Brain tissues were homogenized at 10% (wt/vol) in ice-cold phosphate-buffered saline (PBS) supplemented with a protease inhibitor mixture (Roche) using a multibead shaker (Yasui Kikai, Osaka, Japan). After centrifugation at $2,000 \times g$ for 2 min, supernatants were collected and frozen at -80°C until use. Total protein concentrations were determined by the bicinchoninic acid protein assay (Pierce). The PrP^{Sc} concentrations in the brain homogenates were estimated by dot blot analysis using a reference standard of rPrP, as previously described (31).

RT-QUIC experiments. We prepared reaction mixtures in a 96-well, optical, black-bottom plate (catalog number 265301; Nunc) to a final total volume of 100 μl . To avoid contamination, we prepared noninfectious materials inside a biological safety cabinet in a prion-free laboratory and used aerosol-resistant tips. The final concentrations of the reaction buffer components were 300 mM NaCl, 50 mM HEPES, pH 7.5, and 10 μM thioflavin T (ThT). The concentration of rPrP was 50 or 100 $\mu\text{g}/\text{ml}$, and only freshly thawed rPrP was used. Brain homogenate was diluted with reaction buffer prior to the reactions. The 96-well plate was covered with sealing tape (catalog number 236366; Nunc) and incubated at 40°C in a plate reader (Infinite M200 fluorescence plate reader; Tecan) with intermittent shaking consisting of 30 s of circular shaking at the highest speed and no shaking for 30 s and then with a 2-min pause to measure the fluorescence. The kinetics of amyloid formation was monitored by reading of the fluorescence intensity on the bottom of the plate every 10 min using monochromators with 440-nm excitation and 485-nm emission wavelengths.

RT-QUIC product analysis. For detection of protease-resistant rPrP, 10 μl of the QUIC samples (1 μg of rPrP) was diluted with 40 μl of buffer (300 mM NaCl, 50 mM HEPES, pH 7.5) and digested with 10 $\mu\text{g}/\text{ml}$ of PK at 37°C for 1 h. After adding 4-(2-aminoethyl)benzenesulfonyl fluoride hydrochloride (Pefabloc; Roche) at a final concentration of 4 mM and 20 μg of thyroglobulin, the proteins were precipitated with 4 volumes of methanol. The samples were heated in sample buffer (2% SDS, 5% β -mercaptoethanol, 5% sucrose, 0.005% bromophenol blue, 62.5 mM Tris-HCl, pH 6.8) at 95°C for 5 min and then loaded onto 10% bis-Tris NuPAGE gels (Invitrogen). Proteins were transferred onto polyvinylidene difluoride membranes (Millipore, Billerica, MA). The membranes were probed with polyclonal anti-PrP antibody R20 (the epitope located at mouse PrP amino acids 218 to 231) or ICSM35 (D-Gen, London, United Kingdom).

TEM. Negative staining was done on carbon supporting film grids, which were glow discharged before staining. The 10- μl samples were adsorbed to the grids for 3 min, and then the residual solution was absorbed by filter paper. The grids were stained with 20 μl of freshly filtered stain (2% uranyl acetate). Once they were dry, the samples were viewed in a transmission electron microscope (TEM; JEM-1200EX; JEOL, Japan).

FTIR. Fourier transform infrared spectroscopy (FTIR) spectra were measured with a Bruker Tensor 27 FTIR instrument (Bruker Optics) equipped with a mercuric cadmium telluride (MCT) detector cooled with liquid nitrogen. Three hundred microliters of each of the QUIC samples (30 μg of rPrP) was pelleted by centrifugation for 1 h at $77,000 \times g$ and resuspended in 20 μl buffer (300 mM NaCl, 50 mM HEPES, pH 7.5). The slurry was loaded into a BioATRCcell II attenuated total reflectance-type reflectance unit. PrP^{Sc} was purified from the brains of mice infected with the mouse-adapted Chandler and 22L prions using a combination of detergent solubilization, centrifugation at ultrahigh speeds, and PK digestion (4, 32), and 15 μl of purified PrP^{Sc} was directly loaded. One hundred twenty-eight scans at a 4-cm^{-1} resolution were collected for each sample under constant purging with nitrogen, corrected for water vapor, and the background spectra of the buffer were subtracted.

Conformational stability assay. Ten microliters of the QUIC products (equivalent to 1 μg of rPrP) and brain homogenates (80 μg of total proteins) was mixed with 22 μl of various concentrations of guanidine hydrochloride (GdnHCl) at final concentrations of 0 to 5 M and 0 to 3.5 M, respectively, and the mixed samples were incubated at 37°C for 1 h. After adjustment of the final GdnHCl concentration of the QUIC products to 1 M and the brain homogenates to 0.6 M, the samples were digested with PK (10 $\mu\text{g}/\text{ml}$) at 37°C for 1 h and analyzed by Western blotting following methanol precipitation. The bands were visualized using an Attophos AP fluorescent substrate system (Promega) and quantified using a Molecular Imager FX imager (Bio-Rad). The sigmoidal patterns of the denaturation curves were plotted using a Boltzmann curve fit. The concentration of GdnHCl required to denature 50% of PK-resistant fragments ($[\text{GdnHCl}]_{1/2}$) was estimated from the denaturation curves.

Bioassay. Four-week-old male ddY mice were intracerebrally inoculated with 40 μl of QUIC products (equivalent to 4 μg rPrP). As controls for rPrP fibrils, we performed a mock QUIC procedure using seed-only solutions that contained the same concentration of PrP^{Sc} as that from the 1st round of QUIC with the rPrP fibril (1st-rPrP-fibril; 1 $\text{pg}/\mu\text{l}$) or the 5th round of QUIC with the rPrP fibril (5th-rPrP-fibril; 1×10^{-8} $\text{pg}/\mu\text{l}$) and then added the same amount of rPrP and inoculated the mixtures into mice. Brain homogenates were serially diluted from 10^0 to 10^{-7} with PBS, and 20 μl of each dilution was intracerebrally inoculated. Mice were monitored weekly until the terminal stage of disease or sacrifice. Clinical onset was determined as the presence of 3 or more of the following signs: greasy and/or yellowish hair, hunchback, weight loss, yellow pubes, ataxic gait, and nonparallel hind limbs. The 50% lethal dose (LD_{50}) was determined according to the Behrens-Karber formula. Animals were cared for in accordance with the guidelines for animal experimentation of Nagasaki University.

Histopathology and lesion profiles. The brain tissue was fixed in 4% paraformaldehyde, and 5- μm paraffin sections were prepared on poly-L-lysine (PLL) coat slides using a microtome. After deparaffinization and rehydration, the tissue sections were stained with hematoxylin-eosin. The pattern of vacuolation was examined in 8 fields per slice from the hippocampus (HI), cerebral cortex, hypothalamus, pons, and cerebellum (CE). Spongiform degeneration was scored using the following scale: 0, no vacuoles; 1, a few vacuoles widely and unevenly distributed; 2, a few vacuoles evenly scattered; 3, moderate numbers of vacuoles evenly scattered; 4, many vacuoles with some confluences; and 5, dense vacuolation.

Statistical analysis. The fibril length or width determined by electron microscopy analysis was subjected to one-way analysis of variance (ANOVA) followed by the Tukey-Kramer test. Data from the conformational stability test were analyzed by one-way ANOVA followed by Student's *t* test. Analysis of the data for the survival times was evaluated by the log-rank test. The vacuolation scores were analyzed by Mann-Whitney's *U* test.

RESULTS

Conversion of the soluble form of mouse rPrP into amyloid fibrils by RT-QUIC.

We first tested whether formation of mouse

rPrP amyloid fibrils could be induced in the RT-QUIC by monitoring the levels of ThT fluorescence. We observed positive ThT fluorescence in the presence of diluted strain Chandler-seeded brain homogenate (BH) or strain 22L-seeded BH containing 100 pg of PrP^{Sc} (Fig. 1A), whereas negative-control reactions seeded with comparable dilutions of BH from healthy mice (normal brain homogenate [NBH]) or not seeded resulted in no increase in ThT fluorescence over 72 h (Fig. 1A). However, because an inverse correlation existed between the rate of fibril formation and the concentration of rPrP (28, 33), the spontaneous formation of rPrP fibrils (rPrP-fib^{sp^{on}}) was induced by decreasing the concentration of rPrP from 100 to 50 $\mu\text{g}/\text{ml}$ (Fig. 1A).

We next examined the PK resistance of rPrP fibrils by immunoblotting using anti-PrP antibody R20 directed toward C-terminal residues 218 to 231. Although the ThT-negative reactions seeded with NBH or not seeded produced no PK-resistant bands (Fig. 1B, middle), the Chandler-seeded rPrP fibrils (rPrP-fib^{Ch}) and 22L-seeded rPrP fibrils (rPrP-fib^{22L}) produced several (21-, 18-, 12-, 11-, and 10-kDa) PK-resistant fragments (Fig. 1B, left). In contrast, the PK digestion of rPrP-fib^{sp^{on}} generated only 10- to 12-kDa fragments. It should be noted that anti-PrP monoclonal antibody ICSM35 (directed toward an epitope consisting of residues 93 to 102) specifically recognized the 21- and 18-kDa fragments derived from PrP^{Sc}-seeded rPrP fibrils in the first round (1st-rPrP-fib^{Sc}), indicating that they contained mouse PrP from about residues 93 to 231 (Fig. 1B, right).

To further characterize the structure of 1st-rPrP-fib^{Sc} and rPrP-fib^{sp^{on}}, the samples were examined using a TEM with negative staining. The electron micrographs of samples of 1st-rPrP-fib^{Ch} and 1st-rPrP-fib^{22L} revealed bundles of irregularly rod-shaped and branched fibrils, while most samples of rPrP-fib^{sp^{on}} displayed smooth and nonbranched rod-shaped fibrils (Fig. 1C). Moreover, the lengths of 1st-rPrP-fib^{Ch} and 1st-rPrP-fib^{22L} were significantly longer than those of rPrP-fib^{sp^{on}} (Fig. 1D). Thus, the results of TEM analysis suggest that 1st-rPrP-fib^{Sc} are structurally distinct from spontaneous rPrP-fib^{sp^{on}}.

We next examined the morphology of PrP^{Sc}-seeded rPrP fibrils in the 2nd- and 5th-round reactions (2nd- and 5th-rPrP-fib^{Sc}, respectively) by TEM. In contrast to samples of 1st-rPrP-fib^{Sc}, samples of 2nd- and 5th-rPrP-fib^{Sc} displayed spindly and nonbranched fibrils or amorphous aggregates (Fig. 2). These data support the view that 1st-rPrP-fib^{Sc} are structurally distinct from 2nd- and 5th-rPrP fib^{Sc}.

Structural characterization of rPrP fibrils by FTIR. We next examined the secondary structure of rPrP fibrils and purified PrP^{Sc} from the brains of mice infected with Chandler or 22L scrapie by FTIR. A silver-stained SDS-polyacrylamide gel analysis revealed that Chandler and 22L PrP^{Sc} preparations were highly purified (Fig. 3A). Furthermore, TEM analysis demonstrated that the PrP^{Sc} preparations consisted exclusively of amyloid-like fibrils (Fig. 3B). FTIR analysis showed that Chandler PrP^{Sc} was characterized by a major band at $1,630\text{ cm}^{-1}$ in the β -sheet region of second-derivative spectra, while 22L PrP^{Sc} was characterized by two absorbance bands at $1,631$ and $1,616\text{ cm}^{-1}$ (Fig. 4A), indicating that there were conformational differences in the β -sheet structures between Chandler and 22L PrP^{Sc}, as previously reported (7). Consistent with previous reports (6–9), bands of about $1,656$ to $1,658\text{ cm}^{-1}$ were observed in both Chandler and 22L PrP^{Sc}. Although these bands were formerly attributed to an α -helix, recent studies using direct mass spectrometric analysis of hy-

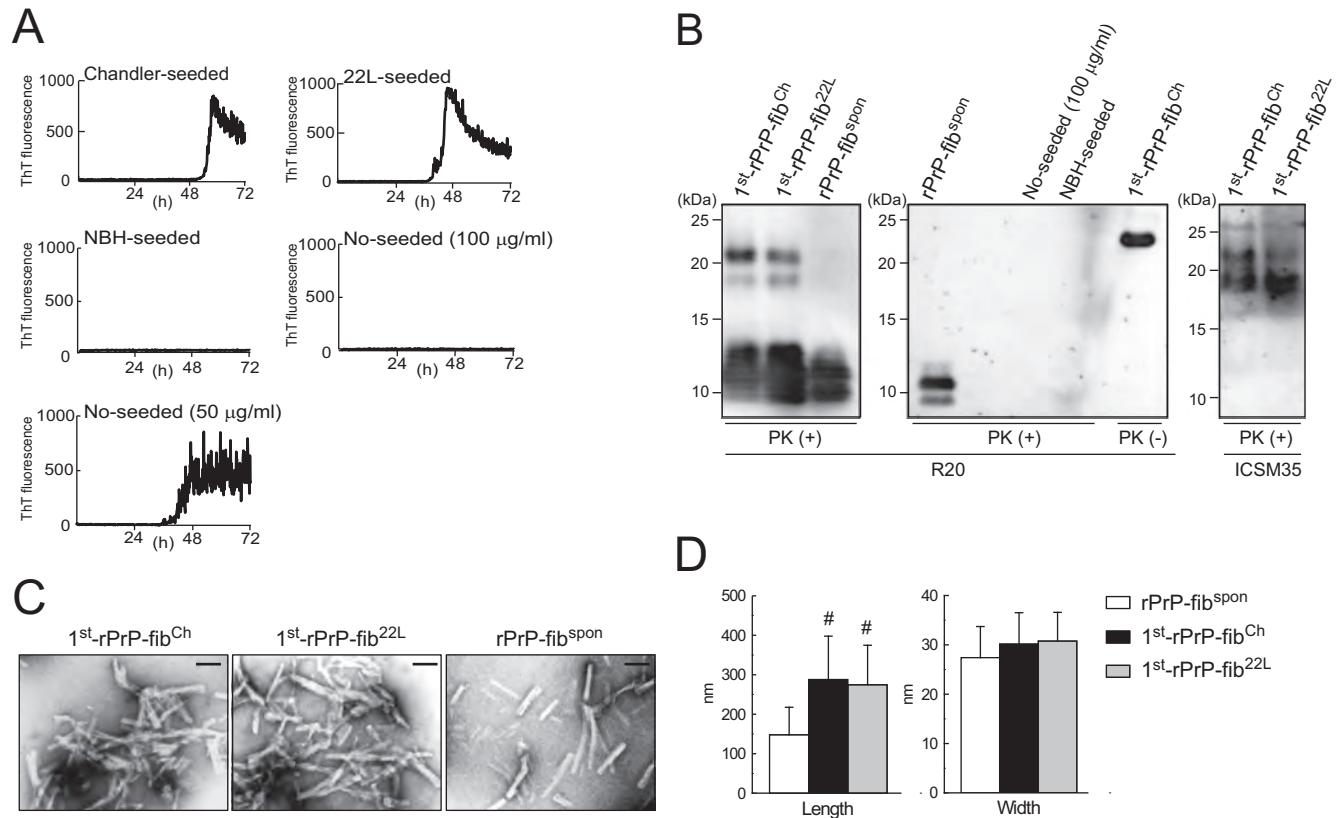


FIG 1 Formation of rPrP fibrils in RT-QUIC reactions. (A) The formation of rPrP fibrils in the presence of diluted Chandler or 22L BH containing 100 pg of PrP^{Sc} or a comparable amount of NBH or in the absence of seed (No-seeded) was monitored by measurement of ThT fluorescence. The graphs depict representative results of the RT-QUIC reactions. No-seed reactions were performed at two different concentrations (100 or 50 µg/ml) of rPrP. (B) The QUIC reaction mixtures were digested with PK and immunoblotted using polyclonal anti-PrP antibody R20 (specific for the epitope located at mouse PrP amino acids 218 to 231) or ICSM35 (specific for the epitope located at mouse PrP amino acids 93 to 102). For comparison, 1st-rPrP-fib^{Ch} (50 ng of total rPrP) without PK digestion [PK (-)] is shown. Molecular mass markers are indicated in kilodaltons (kDa) on the left side of each panel. (C) Samples (1st-rPrP-fib^{Ch}, 1st-rPrP-fib^{22L}, and rPrP-fib^{sp}) were examined by TEM. Bars, 100 nm. (D) The bar graph shows the length and width of rPrP-fib^{sp}, 1st-rPrP-fib^{Ch}, and 1st-rPrP-fib^{22L}. The results are the mean ± SD for 30 rPrP fibrils each. Statistical significance was determined using one-way ANOVA, followed by the Tukey-Kramer test. *, $P < 0.01$.

drogen-deuterium exchange and FTIR analysis have suggested that purified PrP^{Sc} has little α -helix content and the bands probably result from turns (9, 34). Native rPrP had a maximum absorbance at 1,653 cm^{-1} , which was congruent with that of prominent α -helical structures. In contrast, all rPrP fibrils displayed prominent bands at lower wave numbers (1,630 to 1,610 cm^{-1}), indicating a predominantly β -sheet content (Fig. 4A). The β -sheet spectra revealed conformational differences among rPrP-fib^{sp}, 1st-rPrP-fib^{Ch}, and 1st-rPrP-fib^{22L}. rPrP-fib^{sp} had a prominent band at 1,623 cm^{-1} and a modest band at 1,610 cm^{-1} . While the 1st-rPrP-fib^{Ch} were characterized by a single major band at 1,624 cm^{-1} , the 1st-rPrP-fib^{22L} had two major maxima at 1,629 and 1,617 cm^{-1} (Fig. 4A). Although 1st-rPrP-fib^{Sc} lacked the bands at about 1,656 to 1,658 cm^{-1} , the strain-specific shapes (one peak in Chandler versus two peaks in 22L) in the β -sheet spectrum of the purified PrP^{Sc} resembled those of 1st-rPrP-fib^{Sc}.

To test whether the strain-specific infrared spectra observed in 1st-rPrP-fib^{Ch} and 1st-rPrP-fib^{22L} are transmitted to sequential QUIC reactions, we performed 5 serial rounds of QUIC (Fig. 2A). There was little difference in the β -sheet spectra between 5th-rPrP-fib^{Ch} and 5th-rPrP-fib^{22L} (Fig. 3), suggesting that strain-specific conformations were lost in the 5th-rPrP-fib^{Sc}. Furthermore,

additional experiments revealed that the infrared spectra of rPrP fibrils produced in the presence of a small amount of PrP^{Sc} (1 pg) or under acidic conditions (pH 4) displayed few differences between strains (Fig. 4B).

Conformational stability analysis of rPrP fibrils and PrP^{Sc}. To examine the biochemical differences of rPrP fibrils and PrP^{Sc} in BH between strains, we performed a conformational stability assay, which combines GdnHCl denaturation with PK digestion. The [GdnHCl]_{1/2} values for Chandler and 22L PrP^{Sc} were 3.3 ± 0.4 and 1.7 ± 0.3 M, respectively (Fig. 5A and Table 1), indicating that the conformational stability of Chandler-PrP^{Sc} was significantly higher than that of 22L-PrP^{Sc}. Consistent with previous work (11), Chandler PrP^{Sc} bands treated with more than 1.5 M GdnHCl were approximately 5 kDa smaller than those treated with lower concentrations (Fig. 5A, top). The [GdnHCl]_{1/2} values of 1st-rPrP-fib^{Ch} and 1st-rPrP-fib^{22L} were 3.3 ± 0.1 and 2.3 ± 0.6 M, respectively (Fig. 5B and Table 1), showing that the stability of 1st-rPrP-fib^{Ch} was significantly higher than that of 1st-rPrP-fib^{22L}, as with Chandler and 22L PrP^{Sc}. Thus, the relationship between Chandler and 22L in terms of conformational stability was common to both the original PrP^{Sc} and 1st-rPrP-fib^{Sc}. In contrast, the [GdnHCl]_{1/2} of rPrP-fib^{sp} was more than 5 M,

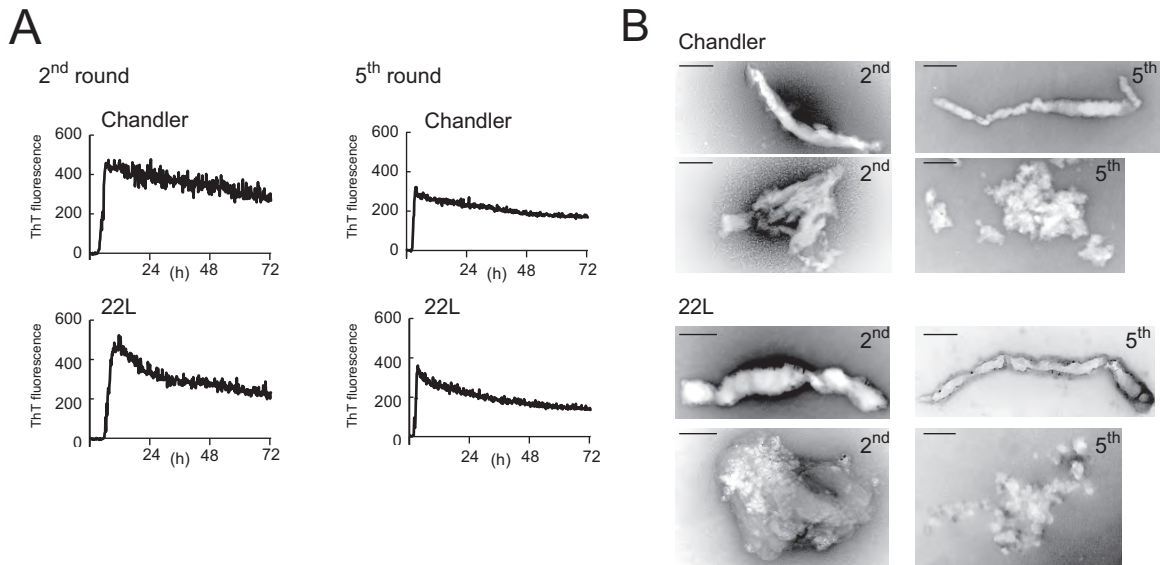


FIG 2 Formation of PrP^{Sc}-seeded rPrP fibrils in the 2nd round (2nd-rPrP-fib^{Sc}) and 5th round (5th-rPrP-fib^{Sc}) of RT-QUIC. (A) Between each round, the reaction mixtures from the previous reaction were diluted 100-fold into fresh rPrP. The reaction buffer contained 300 mM NaCl, 50 mM HEPES (pH 7.5), and 10 μ M ThT. The rPrP concentration was 100 μ g/ml. (B) TEM analysis of PrP^{Sc}-seeded rPrP fibrils generated in the second and fifth rounds of RT-QUIC. Bars, 100 nm.

which was markedly higher than that of 1st-rPrP-fib^{Sc} (Fig. 5B and Table 1). Additionally, we tested the conformational stability of 2nd- and 5th-rPrP-fib^{Sc} but found no significant differences between strains (Fig. 5C and D and Table 1).

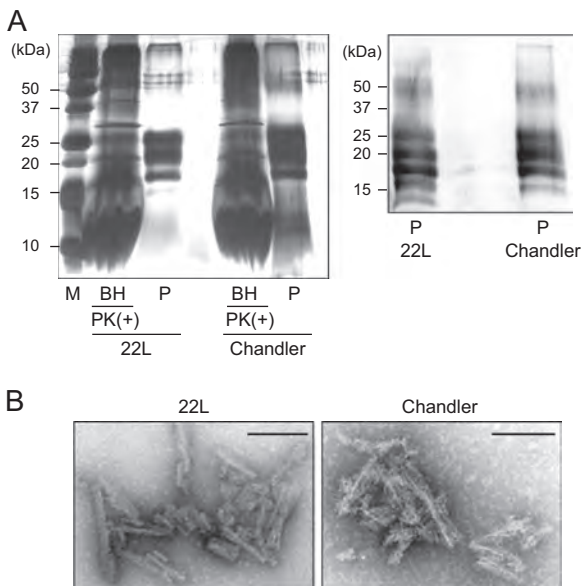


FIG 3 Silver staining and Western blot analysis of purified PrP^{Sc}. (A) The purified PrP^{Sc} samples (P) were examined by silver-stained SDS-polyacrylamide gel analysis (left). For comparison, the electrophoretic pattern of prion-infected BHs containing 100 μ g total protein digested with PK (20 μ g/ml, 37°C for 1 h) is shown (left). The purified PrP^{Sc} samples were immunoblotted with polyclonal anti-PrP antibody M20 (right). Molecular mass markers (lane M) are indicated in kilodaltons (kDa) on the left side of each panel. (B) Electron microscopy analysis of purified 22L PrP^{Sc} (left) and Chandler PrP^{Sc} (right). Bars, 100 nm.

Bioassay for rPrP fibrils generated in QUIC reactions. To determine whether the infectivity was transmitted to the rPrP fibrils, we performed a bioassay using wild-type mice. To prepare the control materials, seed-only solutions containing the same concentration of PrP^{Sc} as that in 1st- or 5th-rPrP-fib^{Sc} were subjected to a mock RT-QUIC procedure and then mixed with the same amount of soluble rPrP (Table 2). The survival periods of mice inoculated with 40- μ l aliquots containing rPrP fibrils were 185.5 ± 4.0 days postinoculation (dpi) for 1st-rPrP-fib^{Ch} and 213.0 ± 8.9 dpi for 1st-rPrP-fib^{22L} (Table 2). In contrast, the attack rate of these control mice was only 50% (2/4) for Chandler and 20% (1/5) for 22L. Moreover, the survival period of the affected mice was much longer than that of the mice inoculated with 1st-rPrP-fib^{Sc} (Table 2). For comparison with the 50% lethal dose (LD₅₀) of the original PrP^{Sc}, the LD₅₀ of 1st-rPrP-fib^{Sc} was determined from the linear regression relationship between infectious titers and survival periods. The infectious titers (per 40 μ l) of 1st-rPrP-fib^{Ch} and 1st-rPrP-fib^{22L} were estimated to be 407.2 ± 226.6 and $1,067.0 \pm 678.7$ LD₅₀s, respectively, whereas the titers of the Chandler and 22L prions were 20.2 and 28.9 LD₅₀ units/40 μ g of PrP^{Sc}, respectively. Because the QUIC reaction in the first round resulted in a 20- to 37-fold increase in the infectious titer, the seed contribution to infectivity is estimated to be about 3 to 5%. In contrast, none of the mice inoculated with 5th-rPrP-fib^{Sc} developed symptoms related to TSE (Table 2), suggesting that the 5th-rPrP-fib^{Sc} has no substantial infectivity.

We analyzed by Western blotting the levels of PrP^{Sc} in the brain tissues of mice in the terminal stage that had been inoculated with 1st-rPrP-fib^{Sc} or control materials (mock 1st QUIC) and found no apparent differences in the accumulation of PrP^{Sc} between them and mice inoculated with mock 1st QUIC (Fig. 6A). In addition, a conformational stability assay with GdnHCl revealed that the strain-specific digestion pattern was preserved in mice inoculated with 1st-rPrP-fib^{Sc} (Fig. 6B).

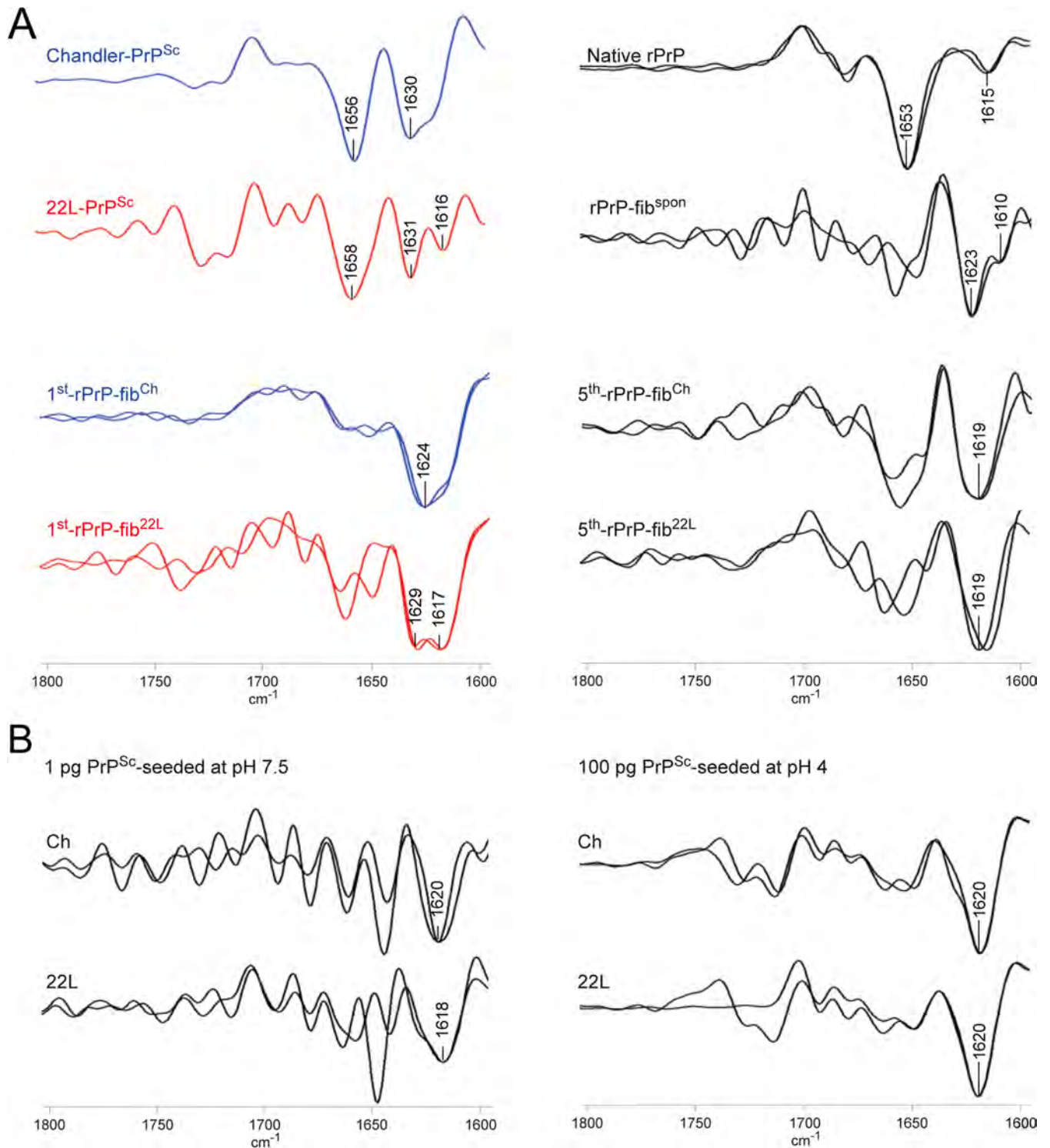


FIG 4 FTIR spectroscopic characterization of rPrP fibrils and purified PrP^{Sc}. (A) Second-derivative FTIR spectra are shown for purified PrP^{Sc}, 1st-rPrP-fib^{Sc}, 5th-rPrP-fib^{Sc}, spontaneously formed rPrP fibrils (rPrP-fib^{spont}), and native rPrP. Overlaid spectra are from independent preparations. (B) FTIR spectra of rPrP fibrils generated at pH 7.5 in the presence of a small amount (1 pg) of PrP^{Sc} and rPrP fibrils generated at pH 4 in the presence of 100 pg of PrP^{Sc}.

Next, the degree of vacuolation in brain sections, including the hippocampus (HI), cerebral cortex, thalamus, pons, and cerebellum (CE), from affected mice inoculated with 1st-rPrP-fib^{Sc} or mock 1st QUIC and those inoculated with the second passage of

1st-rPrP-fib^{Sc} was examined histologically (Fig. 6C and D). Of note, we found that the spongiform change in mice inoculated with 1st-rPrP-fib^{Sc} was less severe in the HI and CE than that in the HI and CE of mice inoculated with mock 1st QUIC strains (Fig. 6C

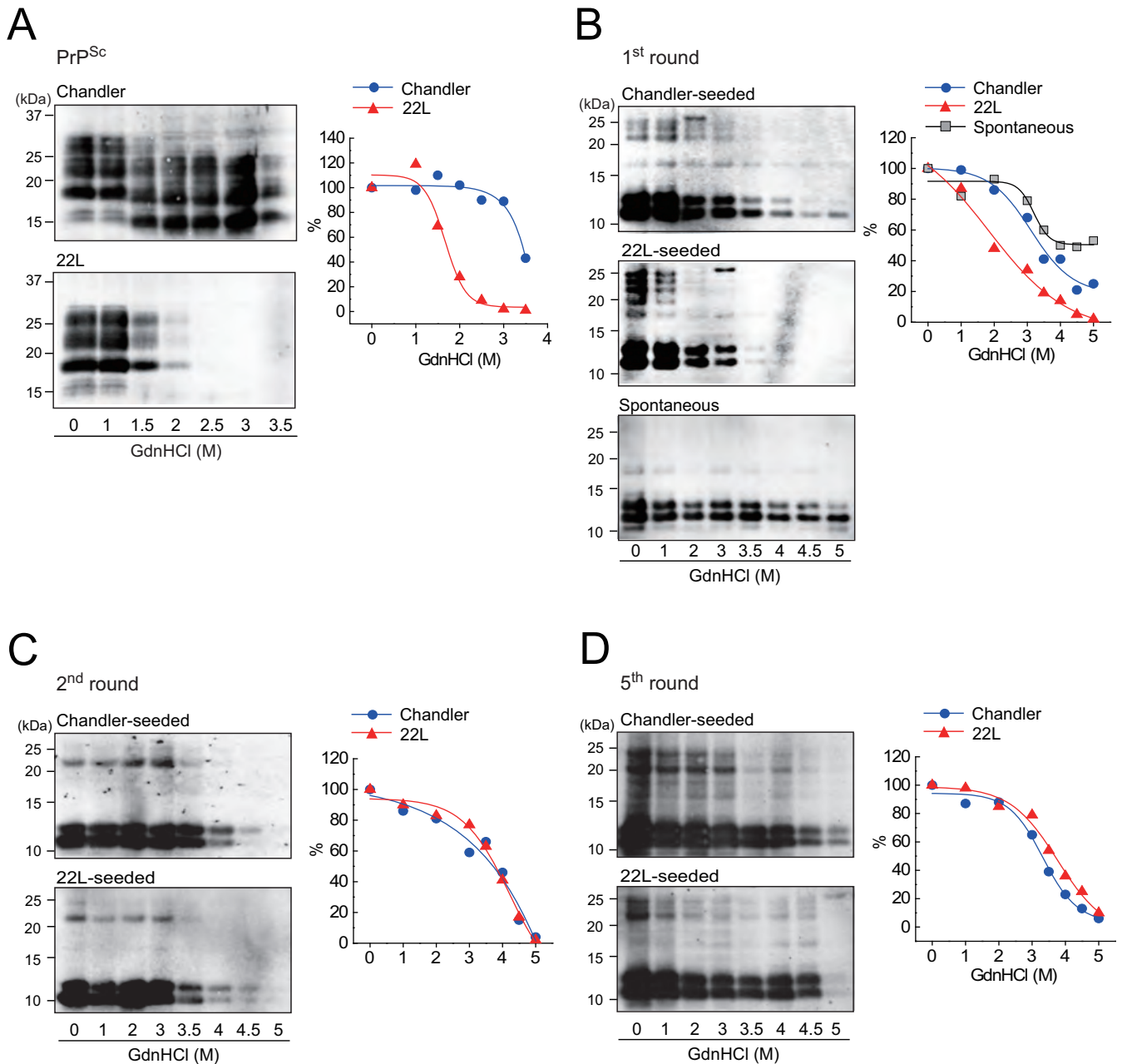


FIG 5 Conformational stability assay for PrP^{Sc} in BH and rPrP fibrils. (A) Chandler-infected (top left) or 22L-infected (bottom left) BHs were treated with 0 to 3.5 M GdnHCl and subjected to PK digestion. PrP^{Sc} was detected by R20 anti-PrP polyclonal antibody. The denaturation curves were plotted using Boltzmann curve fitting (right). (B to D) PK-digested 1st-rPrP-fib^{Sc} (generated as described in the legend to Fig. 1) and rPrP-fib^{spont} (B), 2nd-rPrP-fib^{Sc} (C), or 5th-rPrP-fib^{Sc} (D) were analyzed by Western blotting following GdnHCl treatment (0 to 5 M). The PK-resistant fragments of the rPrP fibrils were detected by antibody R20.

TABLE 1 Conformational stabilities of purified PrP^{Sc} and rPrP fibrils^a

Strain	[GdnHCl] _{1/2} (mol/liter)			
	Purified PrP ^{Sc}	rPrP fibrils		
		1st	2nd	5th
Chandler	3.3 ± 0.4**	3.3 ± 0.1*	3.7 ± 0.1	3.3 ± 0.3
22L	1.7 ± 0.3	2.3 ± 0.6	3.8 ± 0.2	3.5 ± 1.0
Spontaneous		>5		

^a The [GdnHCl]_{1/2} values (mol/liter) are means ± standard deviations from three independent experiments. Statistical significance was determined using one-way ANOVA, followed by Student's *t* test. **, *P* < 0.01 (compared with 22L); *, *P* < 0.05 (compared with 22L).

and D). Furthermore, these different lesion profiles observed in mice inoculated with 1st-rPrP-fib^{Sc} were preserved upon second passage (Fig. 6D), suggesting that the characters of 1st-rPrP-fib^{Sc} are partially distinct from those of the original strains. These findings support the notion that 1st-rPrP-fib^{Sc} provoke the emergence of a mutant strain beyond seed-derived infectivity.

DISCUSSION

Recent studies show that RT-QUIC assays are useful for the sensitive detection of PrP^{Sc} in most species and strains, including

TABLE 2 Bioassay for rPrP fibrils generated in QUIC reactions in wild-type mice^a

Inoculum	Concn of seed PrP ^{Sc} (pg/μl)	Survival period (dpi) ^b	Mortality (no. of dead mice/total no. tested)
1st-rPrP-fib ^{Ch}	1	185.5 ± 4.0 ^{*,d}	4/4
Mock 1st QUIC (Ch) ^c	1	201, 220 ^e	2/4
1st-rPrP-fib ^{22L}	1	213.0 ± 8.9 ^{**,d}	6/6
Mock 1st QUIC (22L) ^c	1	333 ^e	1/5
5th-rPrP-fib ^{Ch}	1 × 10 ⁻⁸	>660 ^f	0/4
Mock 5th QUIC (Ch) ^c	1 × 10 ⁻⁸	>660 ^f	0/4
5th-rPrP-fib ^{22L}	1 × 10 ⁻⁸	>660 ^f	0/6
Mock 5th QUIC (22L) ^c	1 × 10 ⁻⁸	>660 ^f	0/6
rPrP-fib ^{sp^{on}}	0	>660 ^f	0/6
Second passage of 1st-rPrP-fib ^{Ch}		152.0 ± 8.5 ^d	5/5
Second passage of mock 1st QUIC (Ch) ^g		148.4 ± 5.9 ^d	5/5
Second passage of 1st-rPrP-fib ^{22L}		153.5 ± 0.6 ^d	5/5
Second passage of mock 1st QUIC (22L) ^h		149.6 ± 10.4 ^d	4/4

^a Mice were intracerebrally inoculated with 40 μl of each inoculum. For the second passage, 10% BH was used.

^b Statistical significance was determined using the log rank test. **, $P < 0.01$ (compared with the controls); *, $P < 0.05$ (compared with the controls). dpi, days postinoculation.

^c After subjecting seed-only mixtures containing the same concentration of PrP^{Sc} as 1st- or 5th-rPrP-fib^{Sc} to a mock QUIC procedure, the same amount of rPrP was added. The solutions were inoculated into mice as controls for rPrP fibrils.

^d Data represent means ± standard deviations.

^e Data represent the survival periods of the TSE-positive mice. All nonsymptomatic mice were negative for PrP^{Sc} at 660 dpi.

^f Data represent the day postinoculation when the experiment was ended.

^g A sample from a mouse obtained at 201 dpi was used.

^h A sample from a mouse obtained at 333 dpi was used.

Creutzfeldt-Jakob disease (CJD) in humans (28, 35–37), scrapie in rodents (29, 38), and chronic wasting disease (CWD) in cervids (39). In the RT-QUIC reaction, soluble rPrP is converted to amyloid fibrils in a seed-dependent fashion in the presence of PrP^{Sc}. Previous studies using FTIR and hydrogen-deuterium exchange have shown that there are structural differences between PrP^{Sc}-seeded fibrils and spontaneous rPrP fibrils generated in rPrP amplified by PMCA (7, 40). We also found that the structural morphology (Fig. 1C), secondary structure (Fig. 3), and conformational stability (Fig. 4B and Table 1) distinguish 1st-rPrP-fib^{Sc} from rPrP-fib^{sp^{on}}. However, it has been unknown whether rPrP retains the conformational properties of the original PrP^{Sc} in the RT-QUIC. Consistent with previous reports (7, 11), we observed strain differences in the β-sheet structure and conformational stability of PrP^{Sc} between the Chandler and 22L strains. Likewise, the differences in the shape of the β-sheet spectrum between strains were common to both PrP^{Sc} and 1st-rPrP-fib^{Sc}. Furthermore, the conformational stability of 1st-rPrP-fib^{22L} was significantly lower than that of 1st-rPrP-fib^{Ch}, as was the case with Chandler and 22L PrP^{Sc}. Since the original PrP^{Sc} remaining in 1st-rPrP-fib^{Sc} was equivalent to only about 0.01 to 0.02% of the PK-resistant 1st-rPrP-fib^{Sc} (1 to 2 μg/10 μg of total PrP) in our estimation, the contribution to the FTIR spectra and the conformational stability

of 1st-rPrP-fib^{Sc} are considered to be negligible. Taken together, these studies demonstrate that at least some strain-specific conformational features, especially in the β-sheet region, are conserved between PrP^{Sc} and 1st-rPrP-fib^{Sc}. However, these unique structural features disappeared in subsequent rounds.

One of the reasons for the loss of strain specificity may be due to differences between *E. coli*-derived rPrP and brain-derived PrP^C. Studies using circular dichroism and ¹H nuclear magnetic resonance spectroscopy showed that the tertiary structure and the thermal stability of bovine rPrP from positions 23 to 230 are essentially identical to those of healthy calf brain-derived PrP^C (41). However, it should be noted that *E. coli*-derived rPrP lacks post-translational modifications of PrP^C, such as glycosylation and a glycosylphosphatidylinositol (GPI) anchor. PrP has two N-linked glycosylation sites at amino acids 180 and 196, resulting in di-, mono-, and unglycosylated forms. Mature PrP^C is rich in the diglycosylated form, whereas the glycoform ratio of PrP^{Sc} is known to vary among strains (42–44). Studies using PrP glycan-lacking Tg mice revealed that the strain-specific characteristics of strain 79A were affected by the glycosylation status of PrP^C, but those of strains ME7 and 301C were not (45). Meanwhile, enzymatic deglycosylation of PrP^C failed to affect strain-specific pathological changes in serial PMCA experiments seeded with two murine strains, RML and 301C (46). However, the same two strains were converted into a new single strain during serial rPrP-PMCA in the presence of synthetic PE (27). Similarly, the emergence of mutant strains whose lesion profiles differed from the lesion profile of the seed strain was also observed in a bioassay using hamster rPrP fibrils generated in seeded rPrP-PMCA (25) or 1st-rPrP-fib^{Sc} (Fig. 6C and D). These results raise the possibility that the lack of a GPI anchor in rPrP leads to alterations in strain-specific characteristics. Furthermore, the cell tropisms determined by the cell panel assay were altered in strains RML, 139A, 79A, and ME7 but not in strain 22L when the strains were propagated in Tg mice expressing PrP devoid of a GPI anchor (47). These studies demonstrate that glycosylation and a GPI anchor are not necessarily required for the propagation of prion infectivity but can influence the strain properties. Although the molecular basis of the emergence of mutant strains remains elusive, we can speculate that the posttranslational changes to PrP might affect the conformation of PrP^{Sc} or the interaction with some cofactor(s) in a strain-specific manner.

Another possible explanation is that nonspecific rPrP fibrils are generated during the serial RT-QUIC and replicate more rapidly than the fibrils with strain-specific conformations. The term “nonspecific rPrP fibrils” arises from our findings that there was little difference in the infrared spectra and conformational stability of 5th-rPrP-fib^{Sc} between strains. It has been reported that the propagation of prion strains in cells cultured under different environmental conditions often leads to the formation of quasispecies that are assumed to be composed of a variety of conformational variants (48, 49). Once generated, the competition among the variants is thought to occur during propagation. Indeed, two conformational variants of rPrP fibrils have been shown to be mutually exclusive and compete for monomeric rPrP as a substrate in fibril formation (30). Furthermore, competitive amplification of two prion strains was demonstrated by BH-PMCA (50). Similarly, nonspecific rPrP fibrils would be expected to become the majority if they had a selective growth advantage in the RT-QUIC. We found that the β-sheet spectra of rPrP fibrils generated in the presence of a small amount (1 pg) of PrP^{Sc} or rPrP fibrils

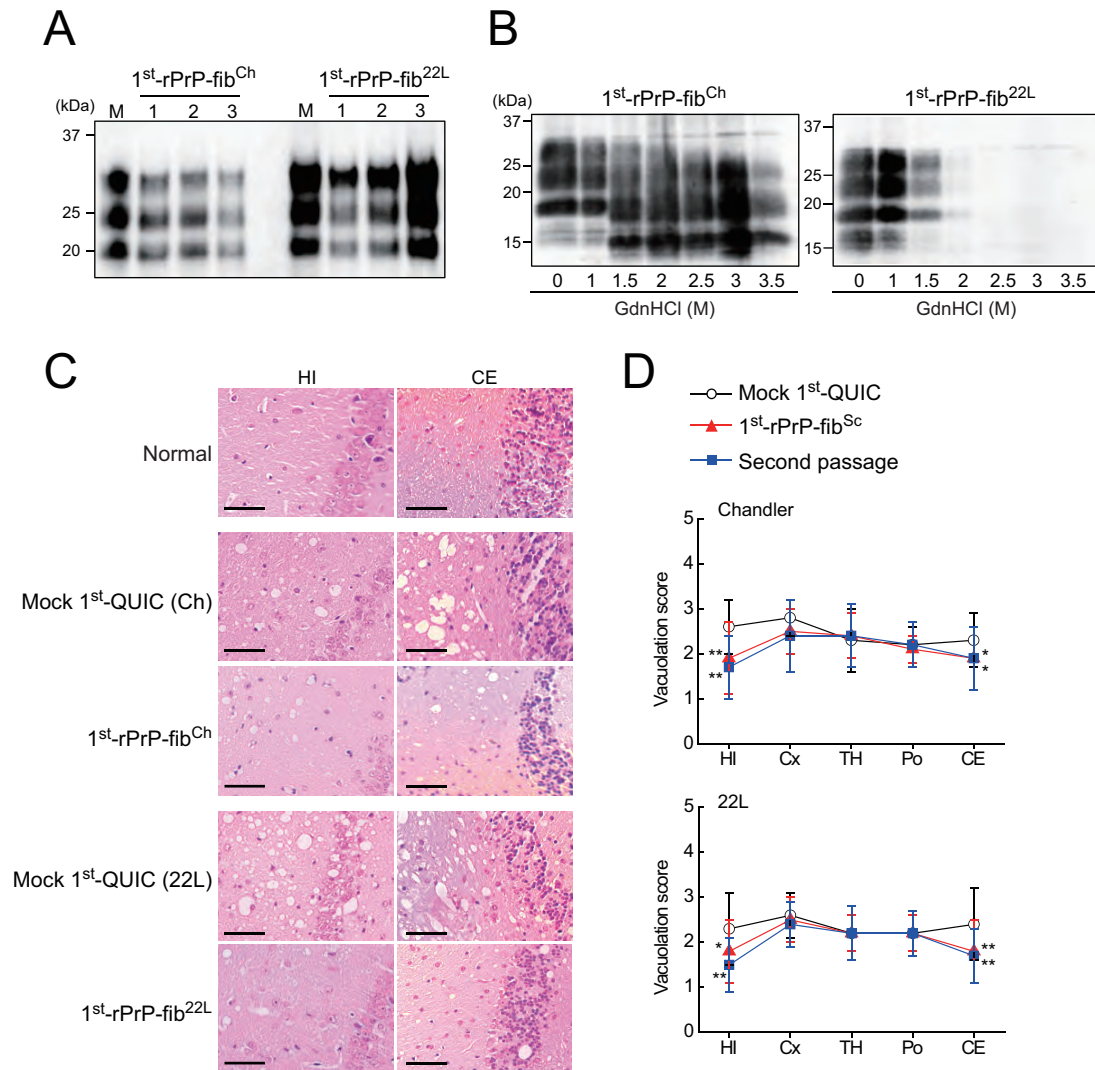


FIG 6 Bioassay of rPrP fibrils in mice. (A) PrP^{Sc} in the brains of prion-affected mice inoculated with 1st-rPrP-fib^{Ch} or 1st-rPrP-fib^{22L} was analyzed by Western blotting using anti-PrP antibody M20. Lanes M, mock 1st QUIC for strains Chandler and 22L. (B) The strain-specific properties of PrP^{Sc} in the brains of mice inoculated with 1st-rPrP-fib^{Sc} were examined by a conformational stability assay with GdnHCl (0 to 3.5 M). (C) Sections of the hippocampus (HI) and cerebellum (CE), stained with hematoxylin-eosin, from healthy mice, mice inoculated with 1st-rPrP-fib^{Sc}, and mock 1st QUIC-inoculated mice at terminal stages are shown. Bars, 50 μm. (D) Lesion profiles of spongiform changes in the hippocampus, cerebral cortex (Cx), thalamus (TH), pons (Po), and cerebellum were compared. Data are expressed as means ± SDs ($n = 3$). Statistical significance was determined using Mann-Whitney's U test. **, $P < 0.01$; *, $P < 0.05$.

generated at pH 4 in the first round were similar to those seen for 5th-rPrP-fib^{Sc} (Fig. 4B). These observations also support this hypothesis and suggest that the amplification of nonspecific rPrP fibrils is accelerated by certain conditions, such as an acidic environment. Further studies are needed to investigate whether unknown cofactors or environmental conditions are required to maintain the strain-specific conformations in subsequent rounds. On the other hand, this hypothesis also explains why prion infectivity was lost in the fifth round of RT-QUIC, as nonspecific rPrP fibrils generated during the serial RT-QUIC would be noninfectious. Although there remains the question as to what exactly the conformational differences between the noninfectious and infectious forms of rPrP fibrils are, the lack of cofactor molecules, such as SDS and synthetic PE, in the RT-QUIC might enhance the amplification of nonspecific rPrP fibrils lacking prion infectivity. Moreover, the fact that prion infectivity is sometimes too low to be

detected and, more frequently, the fact that prion infectivity declines in the serial rPrP-PMCA (24, 25) or BH-PMCA (51–53) are consistent with the hypothesis.

ACKNOWLEDGMENTS

We thank Takashi Suematsu for help with the electron microscopy study and Matsuo Atsuko and Ayumi Yamakawa for technical assistance.

This work was supported by a grant-in-aid for young scientists (B; grant no. 21790846) from the Ministry of Education, Culture, Sports, Science and Technology of Japan, a grant for BSE research, and a grant-in-aid from the Research Committee of Prion Disease and Slow Virus Infection from the Ministry of Health, Labor and Welfare of Japan.

REFERENCES

1. Prusiner SB. 1991. Molecular biology of prion diseases. *Science* 252: 1515–1522. <http://dx.doi.org/10.1126/science.1675487>.

2. Weissmann C, Enari M, Klohn PC, Rossi D, Flechsig E. 2002. Molecular biology of prions. *Acta Neurobiol. Exp. (Wars.)* 62:153–166.
3. Meyer RK, McKinley MP, Bowman KA, Braunfeld MB, Barry RA, Prusiner SB. 1986. Separation and properties of cellular and scrapie prion proteins. *Proc. Natl. Acad. Sci. U. S. A.* 83:2310–2314. <http://dx.doi.org/10.1073/pnas.83.8.2310>.
4. Caughey BW, Dong A, Bhat KS, Ernst D, Hayes SF, Caughey WS. 1991. Secondary structure analysis of the scrapie-associated protein PrP 27–30 in water by infrared spectroscopy. *Biochemistry* 30:7672–7680. <http://dx.doi.org/10.1021/bi00245a003>.
5. Pan KM, Baldwin M, Nguyen J, Gasset M, Serban A, Groth D, Mehlhorn I, Huang Z, Fletterick RJ, Cohen FE, Prusiner SB. 1993. Conversion of alpha-helices into beta-sheets features in the formation of the scrapie prion proteins. *Proc. Natl. Acad. Sci. U. S. A.* 90:10962–10966. <http://dx.doi.org/10.1073/pnas.90.23.10962>.
6. Caughey B, Raymond GJ, Bessen RA. 1998. Strain-dependent differences in beta-sheet conformations of abnormal prion protein. *J. Biol. Chem.* 273:32230–32235. <http://dx.doi.org/10.1074/jbc.273.48.32230>.
7. Atarashi R, Sim VL, Nishida N, Caughey B, Katamine S. 2006. Prion strain-dependent differences in conversion of mutant prion proteins in cell culture. *J. Virol.* 80:7854–7862. <http://dx.doi.org/10.1128/JVI.00424-06>.
8. Thomzig A, Spassov S, Friedrich M, Naumann D, Beekes M. 2004. Discriminating scrapie and bovine spongiform encephalopathy isolates by infrared spectroscopy of pathological prion protein. *J. Biol. Chem.* 279:33847–33854. <http://dx.doi.org/10.1074/jbc.M403730200>.
9. Baron GS, Hughson AG, Raymond GJ, Offerdahl DK, Barton KA, Raymond LD, Dorward DW, Caughey B. 2011. Effect of glycans and the glycoposphatidylinositol anchor on strain dependent conformations of scrapie prion protein: improved purifications and infrared spectra. *Biochemistry* 50:4479–4490. <http://dx.doi.org/10.1021/bi2003907>.
10. Peretz D, Scott MR, Groth D, Williamson RA, Burton DR, Cohen FE, Prusiner SB. 2001. Strain-specified relative conformational stability of the scrapie prion protein. *Protein Sci.* 10:854–863. <http://dx.doi.org/10.1110/ps.39201>.
11. Shindoh R, Kim CL, Song CH, Hasebe R, Horiuchi M. 2009. The region approximately between amino acids 81 and 137 of proteinase K-resistant PrP^{Sc} is critical for the infectivity of the Chandler prion strain. *J. Virol.* 83:3852–3860. <http://dx.doi.org/10.1128/JVI.01740-08>.
12. Saborio GP, Permanne B, Soto C. 2001. Sensitive detection of pathological prion protein by cyclic amplification of protein misfolding. *Nature* 411:810–813. <http://dx.doi.org/10.1038/35081095>.
13. Castilla J, Saa P, Hetz C, Soto C. 2005. In vitro generation of infectious scrapie prions. *Cell* 121:195–206. <http://dx.doi.org/10.1016/j.cell.2005.02.011>.
14. Castilla J, Morales R, Saa P, Barria M, Gambetti P, Soto C. 2008. Cell-free propagation of prion strains. *EMBO J.* 27:2557–2566. <http://dx.doi.org/10.1038/emboj.2008.181>.
15. Deleault NR, Harris BT, Rees JR, Supattapone S. 2007. Formation of native prions from minimal components in vitro. *Proc. Natl. Acad. Sci. U. S. A.* 104:9741–9746. <http://dx.doi.org/10.1073/pnas.0702662104>.
16. Imamura M, Kato N, Yoshioka M, Okada H, Iwamaru Y, Shimizu Y, Mohri S, Yokoyama T, Murayama Y. 2011. Glycosylphosphatidylinositol anchor-dependent stimulation pathway required for generation of baculovirus-derived recombinant scrapie prion protein. *J. Virol.* 85:2582–2588. <http://dx.doi.org/10.1128/JVI.02098-10>.
17. Imamura M, Kato N, Okada H, Yoshioka M, Iwamaru Y, Shimizu Y, Mohri S, Yokoyama T, Murayama Y. 2013. Insect cell-derived cofactors become fully functional after proteinase K and heat treatment for high-fidelity amplification of glycosylphosphatidylinositol-anchored recombinant scrapie and BSE prion proteins. *PLoS One* 8:e82538. <http://dx.doi.org/10.1371/journal.pone.0082538>.
18. Legname G, Baskakov IV, Nguyen HO, Riesner D, Cohen FE, DeArmond SJ, Prusiner SB. 2004. Synthetic mammalian prions. *Science* 305:673–676. <http://dx.doi.org/10.1126/science.1100195>.
19. Colby DW, Giles K, Legname G, Wille H, Baskakov IV, DeArmond SJ, Prusiner SB. 2009. Design and construction of diverse mammalian prion strains. *Proc. Natl. Acad. Sci. U. S. A.* 106:20417–20422. <http://dx.doi.org/10.1073/pnas.0910350106>.
20. Raymond GJ, Race B, Hollister JR, Offerdahl DK, Moore RA, Kodali R, Raymond LD, Hughson AG, Rosenke R, Long D, Dorward DW, Baron GS. 2012. Isolation of novel synthetic prion strains by amplification in transgenic mice coexpressing wild-type and anchorless prion proteins. *J. Virol.* 86:11763–11778. <http://dx.doi.org/10.1128/JVI.01353-12>.
21. Makarava N, Kovacs GG, Bocharova O, Savtchenko R, Alexeeva I, Budka H, Rohwer RG, Baskakov IV. 2010. Recombinant prion protein induces a new transmissible prion disease in wild-type animals. *Acta Neuropathol.* 119:177–187. <http://dx.doi.org/10.1007/s00401-009-0633-x>.
22. Wang F, Wang X, Yuan CG, Ma J. 2010. Generating a prion with bacterially expressed recombinant prion protein. *Science* 327:1132–1135. <http://dx.doi.org/10.1126/science.1183748>.
23. Zhang Z, Zhang Y, Wang F, Wang X, Xu Y, Yang H, Yu G, Yuan C, Ma J. 2013. De novo generation of infectious prions with bacterially expressed recombinant prion protein. *FASEB J.* 27:4768–4775. <http://dx.doi.org/10.1096/fj.13-233965>.
24. Timmes AG, Moore RA, Fischer ER, Priola SA. 2013. Recombinant prion protein refolded with lipid and RNA has the biochemical hallmarks of a prion but lacks in vivo infectivity. *PLoS One* 8:e71081. <http://dx.doi.org/10.1371/journal.pone.0071081>.
25. Kim JI, Cali I, Surewicz K, Kong Q, Raymond GJ, Atarashi R, Race B, Qing L, Gambetti P, Caughey B, Surewicz WK. 2010. Mammalian prions generated from bacterially expressed prion protein in the absence of any mammalian cofactors. *J. Biol. Chem.* 285:14083–14087. <http://dx.doi.org/10.1074/jbc.C110.113464>.
26. Deleault NR, Piro JR, Walsh DJ, Wang F, Ma J, Geoghegan JC, Supattapone S. 2012. Isolation of phosphatidylethanolamine as a solitary cofactor for prion formation in the absence of nucleic acids. *Proc. Natl. Acad. Sci. U. S. A.* 109:8546–8551. <http://dx.doi.org/10.1073/pnas.1204498109>.
27. Deleault NR, Walsh DJ, Piro JR, Wang F, Wang X, Ma J, Rees JR, Supattapone S. 2012. Cofactor molecules maintain infectious conformation and restrict strain properties in purified prions. *Proc. Natl. Acad. Sci. U. S. A.* 109:E1938–E1946. <http://dx.doi.org/10.1073/pnas.1206999109>.
28. Atarashi R, Satoh K, Sano K, Fuse T, Yamaguchi N, Ishibashi D, Matsubara T, Nakagaki T, Yamanaka H, Shirabe S, Yamada M, Mizusawa H, Kitamoto T, Klug G, McGlade A, Collins SJ, Nishida N. 2011. Ultrasensitive human prion detection in cerebrospinal fluid by real-time quaking-induced conversion. *Nat. Med.* 17:175–178. <http://dx.doi.org/10.1038/nm.2294>.
29. Wilham JM, Orru CD, Bessen RA, Atarashi R, Sano K, Race B, Meade-White KD, Taubner LM, Timmes A, Caughey B. 2010. Rapid end-point quantitation of prion seeding activity with sensitivity comparable to bioassays. *PLoS Pathog.* 6:e1001217. <http://dx.doi.org/10.1371/journal.ppat.1001217>.
30. Atarashi R, Moore RA, Sim VL, Hughson AG, Dorward DW, Onwubiko HA, Priola SA, Caughey B. 2007. Ultrasensitive detection of scrapie prion protein using seeded conversion of recombinant prion protein. *Nat. Methods* 4:645–650. <http://dx.doi.org/10.1038/nmeth1066>.
31. Fujihara A, Atarashi R, Fuse T, Ubagai K, Nakagaki T, Yamaguchi N, Ishibashi D, Katamine S, Nishida N. 2009. Hyperefficient PrP^{Sc} amplification of mouse-adapted BSE and scrapie strain by protein misfolding cyclic amplification technique. *FEBS J.* 276:2841–2848. <http://dx.doi.org/10.1111/j.1742-4658.2009.07007.x>.
32. Kocisko DA, Lansbury PT, Jr, Caughey B. 1996. Partial unfolding and refolding of scrapie-associated prion protein: evidence for a critical 16-kDa C-terminal domain. *Biochemistry* 35:13434–13442. <http://dx.doi.org/10.1021/bi9610562>.
33. Atarashi R, Sano K, Satoh K, Nishida N. 2011. Real-time quaking-induced conversion: a highly sensitive assay for prion detection. *Prion* 5:150–153. <http://dx.doi.org/10.4161/pri.5.3.16893>.
34. Smirnovas V, Baron GS, Offerdahl DK, Raymond GJ, Caughey B, Surewicz WK. 2011. Structural organization of brain-derived mammalian prions examined by hydrogen-deuterium exchange. *Nat. Struct. Mol. Biol.* 18:504–506. <http://dx.doi.org/10.1038/nsmb.2035>.
35. McGuire LI, Peden AH, Orru CD, Wilham JM, Appleford NE, Mallinson G, Andrews M, Head MW, Caughey B, Will RG, Knight RS, Green AJ. 2012. Real time quaking-induced conversion analysis of cerebrospinal fluid in sporadic Creutzfeldt-Jakob disease. *Ann. Neurol.* 72:278–285. <http://dx.doi.org/10.1002/ana.23589>.
36. Orru CD, Wilham JM, Raymond LD, Kuhn F, Schroeder B, Raeber AJ, Caughey B. 2011. Prion disease blood test using immunoprecipitation and improved quaking-induced conversion. *mBio* 2(3):e00078-00011. <http://dx.doi.org/10.1128/mBio.00078-11>.
37. Sano K, Satoh K, Atarashi R, Takashima H, Iwasaki Y, Yoshida M, Sanjo N, Murai H, Mizusawa H, Schmitz M, Zerr I, Kim YS, Nishida N.

2013. Early detection of abnormal prion protein in genetic human prion diseases now possible using real-time QuIC assay. *PLoS One* 8:e54915. <http://dx.doi.org/10.1371/journal.pone.0054915>.
38. Vascellari S, Orru CD, Hughson AG, King D, Barron R, Wilham JM, Baron GS, Race B, Pani A, Caughey B. 2012. Prion seeding activities of mouse scrapie strains with divergent PrP^{Sc} protease sensitivities and amyloid plaque content using RT-QuIC and eQuIC. *PLoS One* 7:e48969. <http://dx.doi.org/10.1371/journal.pone.0048969>.
 39. Henderson DM, Manca M, Haley NJ, Denkers ND, Nalls AV, Mathiason CK, Caughey B, Hoover EA. 2013. Rapid antemortem detection of CWD prions in deer saliva. *PLoS One* 8:e74377. <http://dx.doi.org/10.1371/journal.pone.0074377>.
 40. Smirnovas V, Kim JI, Lu X, Atarashi R, Caughey B, Surewicz WK. 2009. Distinct structures of scrapie prion protein (PrP^{Sc})-seeded versus spontaneous recombinant prion protein fibrils revealed by hydrogen/deuterium exchange. *J. Biol. Chem.* 284:24233–24241. <http://dx.doi.org/10.1074/jbc.M109.036558>.
 41. Hornemann S, Schorn C, Wuthrich K. 2004. NMR structure of the bovine prion protein isolated from healthy calf brains. *EMBO Rep.* 5:1159–1164. <http://dx.doi.org/10.1038/sj.embor.7400297>.
 42. Clarke AR, Jackson GS, Collinge J. 2001. The molecular biology of prion propagation. *Philos. Trans. R. Soc. Lond. B Biol. Sci.* 356:185–195. <http://dx.doi.org/10.1098/rstb.2000.0764>.
 43. Lawson VA, Collins SJ, Masters CL, Hill AF. 2005. Prion protein glycosylation. *J. Neurochem.* 93:793–801. <http://dx.doi.org/10.1111/j.1471-4159.2005.03104.x>.
 44. Aguzzi A, Heikenwalder M, Polymenidou M. 2007. Insights into prion strains and neurotoxicity. *Nat. Rev. Mol. Cell Biol.* 8:552–561. <http://dx.doi.org/10.1038/nrm2204>.
 45. Cancellotti E, Mahal SP, Somerville R, Diack A, Brown D, Piccardo P, Weissmann C, Manson JC. 2013. Post-translational changes to PrP alter transmissible spongiform encephalopathy strain properties. *EMBO J.* 32:756–769. <http://dx.doi.org/10.1038/embor.2013.6>.
 46. Piro JR, Harris BT, Nishina K, Soto C, Morales R, Rees JR, Supattapone S. 2009. Prion protein glycosylation is not required for strain-specific neurotropism. *J. Virol.* 83:5321–5328. <http://dx.doi.org/10.1128/JVI.02502-08>.
 47. Mahal SP, Jablonski J, Suponitsky-Kroyter I, Oelschlegel AM, Herva ME, Oldstone M, Weissmann C. 2012. Propagation of RML prions in mice expressing PrP devoid of GPI anchor leads to formation of a novel, stable prion strain. *PLoS Pathog.* 8:e1002746. <http://dx.doi.org/10.1371/journal.ppat.1002746>.
 48. Li J, Browning S, Mahal SP, Oelschlegel AM, Weissmann C. 2010. Darwinian evolution of prions in cell culture. *Science* 327:869–872. <http://dx.doi.org/10.1126/science.1183218>.
 49. Weissmann C, Li J, Mahal SP, Browning S. 2011. Prions on the move. *EMBO Rep.* 12:1109–1117. <http://dx.doi.org/10.1038/embor.2011.192>.
 50. Shikiya RA, Ayers JI, Schutt CR, Kincaid AE, Bartz JC. 2010. Coinfecting prion strains compete for a limiting cellular resource. *J. Virol.* 84:5706–5714. <http://dx.doi.org/10.1128/JVI.00243-10>.
 51. Bieschke J, Weber P, Sarafoff N, Beekes M, Giese A, Kretzschmar H. 2004. Autocatalytic self-propagation of misfolded prion protein. *Proc. Natl. Acad. Sci. U. S. A.* 101:12207–12211. <http://dx.doi.org/10.1073/pnas.0404650101>.
 52. Klingeborn M, Race B, Meade-White KD, Chesebro B. 2011. Lower specific infectivity of protease-resistant prion protein generated in cell-free reactions. *Proc. Natl. Acad. Sci. U. S. A.* 108:E1244–E1253. <http://dx.doi.org/10.1073/pnas.1111255108>.
 53. Gonzalez-Montalban N, Lee YJ, Makarava N, Savtchenko R, Baskakov IV. 2013. Changes in prion replication environment cause prion strain mutation. *FASEB J.* 27:3702–3710. <http://dx.doi.org/10.1096/fj.13-230466>.

Ultrasensitive detection of PrP^{Sc} in the cerebrospinal fluid and blood of macaques infected with bovine spongiform encephalopathy prion

Yuichi Murayama,¹ Kentaro Masujin,¹ Morikazu Imamura,¹ Fumiko Ono,² Hiroaki Shibata,³ Minoru Tobiume,⁴ Tomoaki Yamamura,¹ Noriko Shimozaki,¹ Keiji Terao,³ Yoshio Yamakawa⁵ and Tetsutaro Sata⁴

Correspondence
Yuichi Murayama
ymura@affrc.go.jp

¹Influenza and Prion Disease Research Center, National Institute of Animal Health, Tsukuba, Ibaraki, Japan

²Chiba Institute of Science Faculty of Risk and Crisis Management, Choshi, Chiba, Japan

³Tsukuba Primate Research Center, National Institute of Biomedical Innovation, Tsukuba, Ibaraki, Japan

⁴Department of Pathology, National Institute of Infectious Diseases, Tokyo, Japan

⁵Department of Biochemistry and Cell Biology, National Institute of Infectious Diseases, Tokyo, Japan

Prion diseases are characterized by the prominent accumulation of the misfolded form of a normal cellular protein (PrP^{Sc}) in the central nervous system. The pathological features and biochemical properties of PrP^{Sc} in macaque monkeys infected with the bovine spongiform encephalopathy (BSE) prion have been found to be similar to those of human subjects with variant Creutzfeldt–Jakob disease (vCJD). Non-human primate models are thus ideally suited for performing valid diagnostic tests and determining the efficacy of potential therapeutic agents. In the current study, we developed a highly efficient method for *in vitro* amplification of cynomolgus macaque BSE PrP^{Sc}. This method involves amplifying PrP^{Sc} by protein misfolding cyclic amplification (PMCA) using mouse brain homogenate as a PrP^C substrate in the presence of sulfated dextran compounds. This method is capable of amplifying very small amounts of PrP^{Sc} contained in the cerebrospinal fluid (CSF) and white blood cells (WBCs), as well as in the peripheral tissues of macaques that have been intracerebrally inoculated with the BSE prion. After clinical signs of the disease appeared in three macaques, we detected PrP^{Sc} in the CSF by serial PMCA, and the CSF levels of PrP^{Sc} tended to increase with disease progression. In addition, PrP^{Sc} was detectable in WBCs at the clinical phases of the disease in two of the three macaques. Thus, our highly sensitive, novel method may be useful for furthering the understanding of the tissue distribution of PrP^{Sc} in non-human primate models of CJD.

Received 24 March 2014

Accepted 10 July 2014

INTRODUCTION

Transmissible spongiform encephalopathies (TSEs), commonly known as prion diseases, are fatal neurodegenerative disorders that affect both animals and humans (Collinge, 2001). Prion diseases are characterized by the prominent accumulation of a misfolded prion protein, PrP^{Sc}, in the central nervous system (Prusiner, 1991, 1998). PrP^{Sc}, which is rich in beta-sheet structures and resistant to digestion by proteases and various inactivating treatments (Caughy *et al.*, 1991; Pan *et al.*, 1993), is considered to be the infectious agent for TSEs and appears to self-propagate

through post-translational modification of the normal prion protein PrP^C (Prusiner, 1998).

One type of human prion disease, Creutzfeldt–Jakob disease (CJD), can be aetiologically identified as sporadic, inherited or acquired by infection (Ironside, 1998; Belay, 1999; Glatzel *et al.*, 2002; Geissen *et al.*, 2007). In variant CJD (vCJD), which is a form of CJD caused by consumption of foods contaminated with bovine spongiform encephalopathy (BSE) prions (Will *et al.*, 1996; Hill *et al.*, 1997; Ironside, 2010), small amounts of PrP^{Sc} have been found in a broad range of peripheral tissues, including the lymph nodes, tonsils, spleen, kidneys, portions of the intestinal tract and skeletal muscle (Wadsworth *et al.*, 2001; Hilton *et al.*, 2004; Peden *et al.*, 2006; Notari *et al.*, 2010), as well as in the

Four figures and one table are available with the online version of this paper.

central nervous system. These observations have led to serious concerns that the disease could spread in humans via blood transfusions (Wroe *et al.*, 2006; Knight, 2010) and through the use of contaminated biological and surgical instruments. In order to effectively prevent the spread of this disease, it is important to be able to detect PrP^{Sc} as soon after infection as possible, and then, it is crucial to avoid PrP^{Sc} contamination in human-derived materials. As the concentration of PrP^{Sc} in the tissues or body fluids of infected subjects is predicted to be extremely low until marked clinical signs appear, development of both a sensitive method for detecting PrP^{Sc} and animal models to confirm its validity are necessary.

Several studies have used non-human primates to study the transmissibility of human prion diseases (Gajdusek *et al.*, 1966; Gibbs *et al.*, 1968), and the transmissibility of BSE has specifically been investigated using macaque monkeys (Lasmézas *et al.*, 1996, 2005; Comoy *et al.*, 2008; Ono *et al.*, 2011a, b). These studies have reported a number of advantages of using non-human primate models of prion disease. For example, the pathological feature of florid plaques in the brain tissue of BSE-infected macaques and the biochemical characteristics of the PrP^{Sc} glycoform profile in these macaques have been shown to be identical to those in human subjects with vCJD (Lasmézas *et al.*, 1996). In macaques inoculated with the BSE prion either intracerebrally or orally and in humans infected with vCJD, PrP^{Sc} has been found to be distributed in various peripheral tissues, such as the lymph nodes, spleen, tonsils and muscles. These findings strongly support the possibility that vCJD is caused by an exogenous infection of a BSE prion. Furthermore, BSE can be transmitted via intravenous inoculation (Lasmézas *et al.*, 2001), indicating that macaques can serve as model animals for suspected cases of secondary transmission (via blood transfusion) of vCJD in humans. Therefore, non-human primate models are ideally suited for assessing methods for diagnosis and treatment of prion diseases.

In scrapie-infected rodents (Brown *et al.*, 1998) and sheep (Houston *et al.*, 2008) as well as in deer with chronic wasting disease (CWD), bodily fluids such as the blood, urine, saliva and faeces have been reported to be infectious (Mathiason *et al.*, 2006; Haley *et al.*, 2009b; Mathiason *et al.*, 2010). By using the protein misfolding cyclic amplification (PMCA) technique, which amplifies PrP^{Sc} *in vitro* using normal brain homogenates as the PrP^C substrate, PrP^{Sc} has been detected in a variety of bodily fluids, including the blood, cerebrospinal fluid (CSF), urine, faeces, saliva and milk of prion-infected animals (Saborio *et al.*, 2001; Saá *et al.*, 2006; Murayama *et al.*, 2007, 2010; Thorne & Terry, 2008; Terry *et al.*, 2009; Maddison *et al.*, 2009, 2010; Haley *et al.*, 2009a, 2011; Tattum *et al.*, 2010; Gough *et al.*, 2012). Furthermore, several reports have described the successful detection of PrP^{Sc} in bodily fluids of humans with CJD (Orrú *et al.*, 2009; Atarashi *et al.*, 2011; Edgeworth *et al.*, 2011; Peden *et al.*, 2012; Rubenstein & Chang, 2013). For example, PrP^{Sc} in the CSF of patients with sporadic CJD (sCJD) and vCJD has been detected using the

quaking-induced conversion technique (Atarashi *et al.*, 2007), which detects PrP^{Sc}-triggered formation of amyloid fibrils of recombinant prion proteins. Similarly, PrP^{Sc} has been detected in the CSF of patients with sCJD using PMCA followed by a sensitive immunoassay termed SOFIA (Rubenstein & Chang, 2013), and bead-captured ELISA has been used to detect blood PrP^{Sc} in patients with vCJD (Edgeworth *et al.*, 2011). Therefore, bodily fluids may have high utility as diagnostic materials for CJD. However, the quantitative changes of PrP^{Sc} in bodily fluids of non-human primate models of CJD has not yet been determined due to a lack of sensitive methods for assessing very small amounts of prions in these animal models.

In the present study, we have developed a highly efficient PMCA method suitable for cynomolgus macaque BSE PrP^{Sc} amplification. This method, which involves amplifying PrP^{Sc} using xenogeneic (mouse) PrP^C substrate in the presence of sulfated dextran compounds, is capable of amplifying a very small amount of PrP^{Sc} from the CSF, blood, and peripheral tissue of BSE-infected macaques. We further investigated CSF and blood PrP^{Sc} levels during the period from the latent to terminal stages of the disease and compared PrP^{Sc} dynamics in macaques.

RESULTS

Amplification of cynomolgus macaque BSE PrP^{Sc} by PMCA

We first examined the amplification efficiency of PMCA, using the brain homogenate of BSE-infected cynomolgus macaque no. 7 as the PrP^{Sc} seed. Before amplification, distinct signals of protease-resistant PrP (PrP^{res}) were detected in brain homogenates diluted up to 10⁻² by Western blot analysis (Fig. 1a). In the absence of potassium dextran sulfate (DSP), brain homogenates derived from the squirrel monkey and cynomolgus macaque were not suitable for amplification of cynomolgus PrP^{Sc} (Fig. 1b, upper panel). Similarly, no significant amplification was observed using cow, TgBoPrP and PrP^{0/0} mice (Fig. 1b, middle panel), or hamster brain homogenates (Fig. 1b, lower panel) as PrP^C substrates. On the other hand, amplification of PrP^{Sc} was achieved in samples diluted to 10⁻³ and 10⁻⁴ when the WT mouse brain homogenate was used as the PrP^C substrate (Fig. 1b, lower panel). Furthermore, amplification efficiency of mouse PrP^{Sc} for PMCA was significantly improved in the presence of DSP, and PrP^{res} signals were detected in samples diluted to 10⁻⁵ after one round of amplification. On the other hand, DSP was less effective in increasing signal intensity of PrP^{res} after amplifications derived using squirrel monkey, cynomolgus macaque, cow, TgBoPrP mouse and hamster brain homogenates. The detection sensitivity for cynomolgus PrP^{Sc} for these PCMA was lower than for PCMA conducted using WT mouse brain homogenate. Higher background signal in the no-seed samples was observed after amplification was conducted using macaque brain homogenate in the presence of DSP.

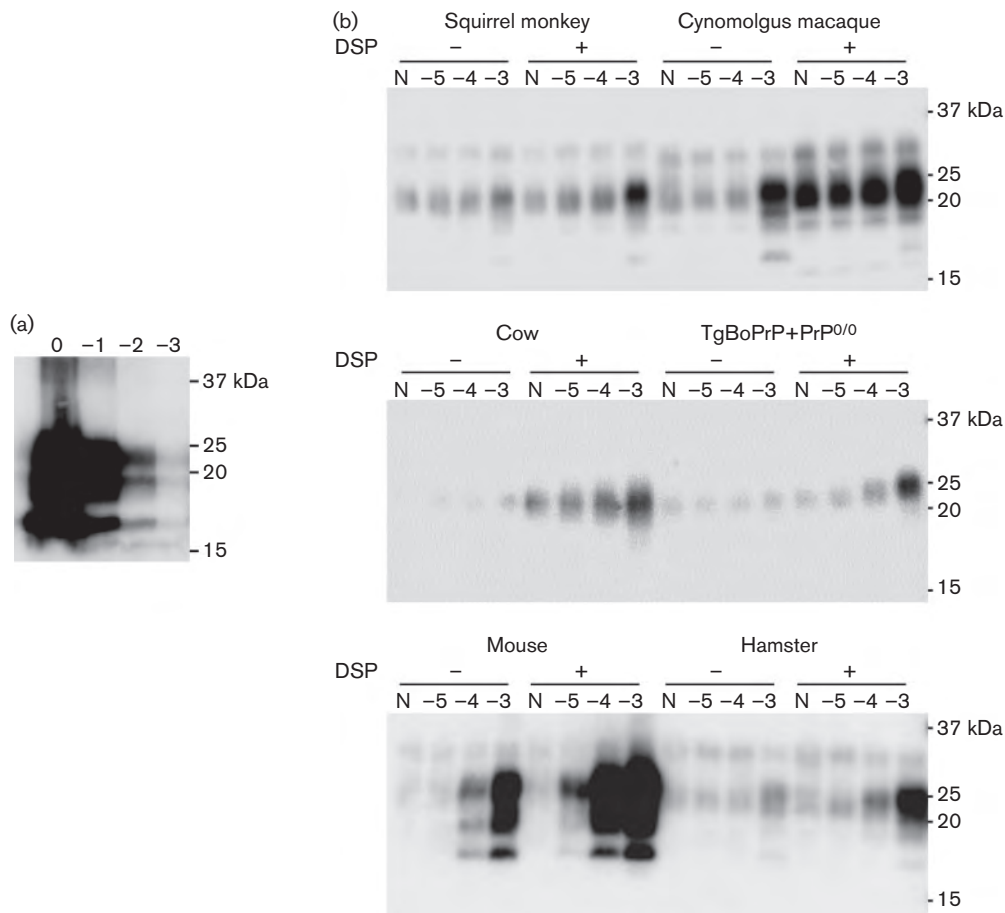


Fig. 1. Amplification of macaque PrP^{Sc} using normal brain homogenates derived from several animal species as PrP^C substrates. (a) Ten per cent brain homogenate of BSE-affected cynomolgus macaque was diluted to 10^{-1} (-1) to 10^{-3} (-3) in a normal macaque brain homogenate, an undiluted sample (0) was also included. The diluted samples were analysed by Western blot after digestion with proteinase K (PK). (b) PrP^{Sc} seed (10% brain homogenate of BSE-affected cynomolgus macaque) was diluted to 10^{-3} (-3) to 10^{-5} (-5) in normal brain homogenates obtained from the squirrel monkey, cynomolgus macaque, cow, mixture of TgBoPrP and PrP^{0/0} (TgBoPrP + PrP^{0/0}) mice, mouse and hamster. The diluted samples were amplified in the presence (+) or absence (-) of 1% (w/v) DSP. After amplification, the samples were digested with PK and analysed by Western blot. 'N' denotes unseeded control samples in which normal brain homogenate that did not receive a PrP^{Sc} seed were processed and analysed in the same manner as PrP^{Sc}-seeded samples. The molecular masses of marker proteins are indicated (kDa).

Detection sensitivity of cynomolgus macaque BSE PrP^{Sc}

PMCA using WT mouse brain homogenate containing DSP as the PrP^C substrate was used for amplification of cynomolgus macaque PrP^{Sc}. On the basis of our preliminary experiments, the optimal concentration of DSP was estimated to be 1% (w/v); therefore, we used 1% (w/v) DSP for subsequent experiments. We determined the detection limit of the interspecies PMCA technique and confirmed that PrP^{Sc} present in a 10^{-5} dilution of infected brain homogenate could be detected after one round of amplification, and both 10^{-6} and 10^{-7} dilutions were positive for PrP^{Sc} after two rounds of amplification (Fig. 2a). After three rounds of amplification, PrP^{res} signals were

detected in the samples diluted to 10^{-8} and 10^{-9} . A PrP^{res} signal was detected in the 10^{-10} dilution samples after four rounds of amplification, but almost no signal was detected in the more extreme dilutions, even after seven rounds of amplification. Thus, compared with no amplification, amplification improved the PrP^{Sc} detection sensitivity by a factor of 10^8 . No typical PrP^{res} signal was detected in samples that contained normal brain homogenate diluted 1:10 with mouse PrP^C substrate (Fig. 2b). In addition, the generation of spontaneous PrP^{res}, as has been reported for amplification in the presence of polyanions (Deleault *et al.*, 2007; Wang *et al.*, 2010), was not observed in 16 samples that contained only mouse PrP^C substrate following seven rounds of amplification (Fig. 2c).

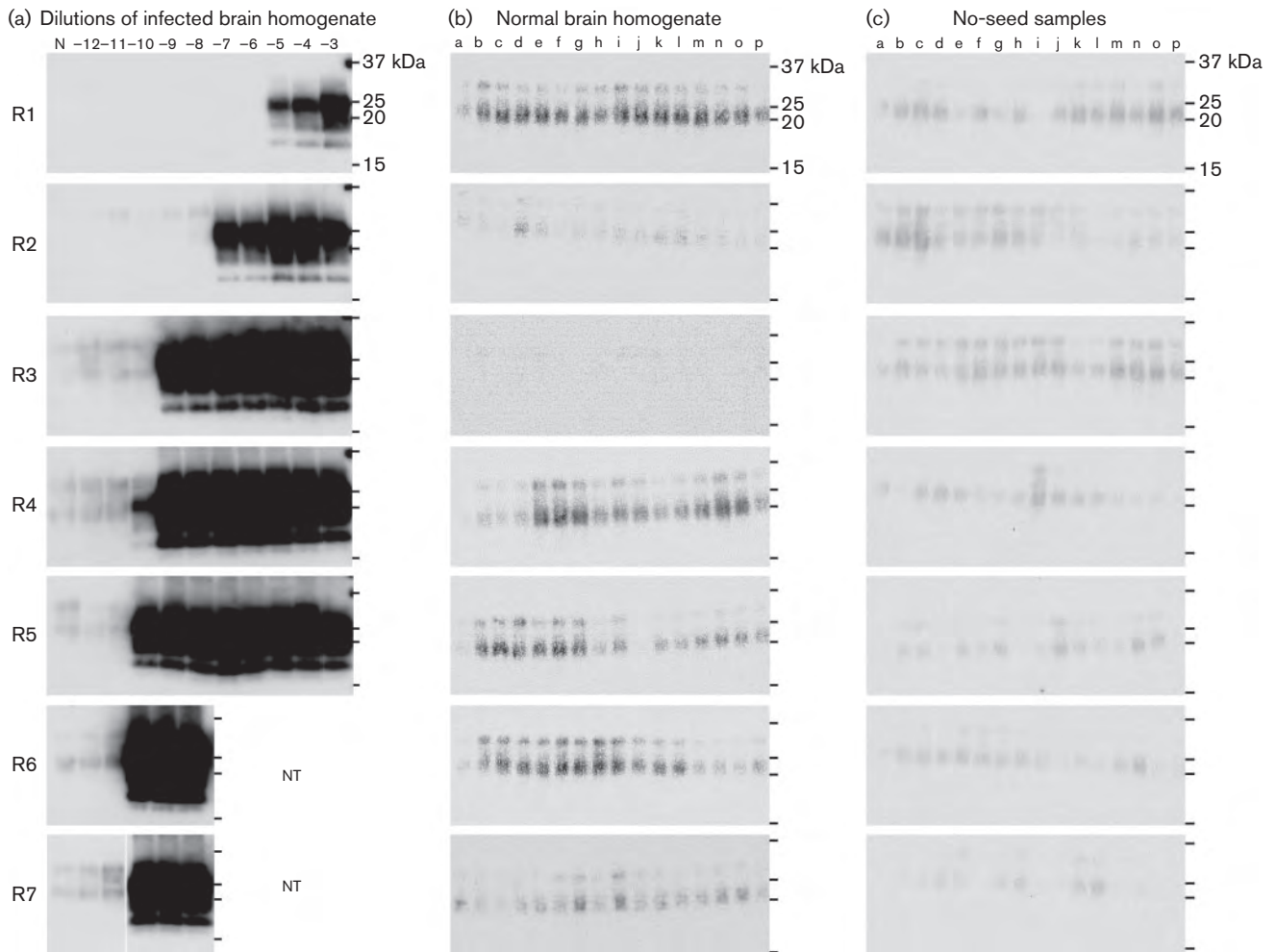


Fig. 2. Detection sensitivity for cynomolgus macaque PrP^{Sc}. (a) PrP^{Sc} seed was diluted to 10^{-3} (–3) to 10^{-12} (–12) with PrP^C substrate (10% normal mouse brain homogenate), and the samples were serially amplified in the presence of 1% (w/v) DSP. The amplified samples were analysed after each round of amplification (R1–R7) by Western blot after proteinase K (PK) digestion. (b) Normal brain homogenate was diluted to 10^{-1} with the PrP^C substrate (lanes a–p), and the samples were serially amplified in the presence of 1% (w/v) DSP. After amplification, a band with a molecular mass similar to that for PrP^{Sc} was occasionally observed, which likely corresponds to a residue of the normal isoform of prion protein resulting from incomplete PK digestion. (c) No spontaneous generation of PrP^{Sc} was observed in no-seed samples. Lanes a–p contained only PrP^C substrate and were amplified in the presence of 1% (w/v) DSP. Exclusive pipettes, a vortex mixer, and a centrifuge were used for handling unseeded samples. The molecular masses of marker proteins are indicated (kDa). NT, Not tested.

PrP^{Sc} distribution in the peripheral tissues of BSE-affected macaques

We examined PrP^{Sc} distribution in macaques that were intracerebrally administered a brain homogenate prepared from a BSE-infected cow. In BSE-infected macaques, PrP^{Sc} was detected by conventional Western blot analysis in several peripheral nervous tissues and lymph nodes (Table S1, available in the online Supplementary Material). By using serial PMCA, PrP^{Sc} was detected in all examined tissues, including: the peripheral nerves, lymph nodes, spleens, tonsils and adrenal glands (Fig. 3). Most samples were found to be positive for PrP^{Sc} after no more than two

rounds of amplification. On the other hand, PrP^{Sc} was detected after three rounds of amplification in four and two of the quadruplicate samples of the tonsil of macaque no. 10 (Fig. 3b) and spleen of macaque no. 11 (Fig. 3c), respectively. No typical PrP^{res} signal was detected in the peripheral nerves, lymph nodes, ileum and glands of an uninfected control macaque (Fig. S1).

PrP^{Sc} levels in the CSF

The amplification results for the CSF samples collected from the three macaques are illustrated in Fig. 4. No typical PrP^{res} signal was observed in samples that contained only

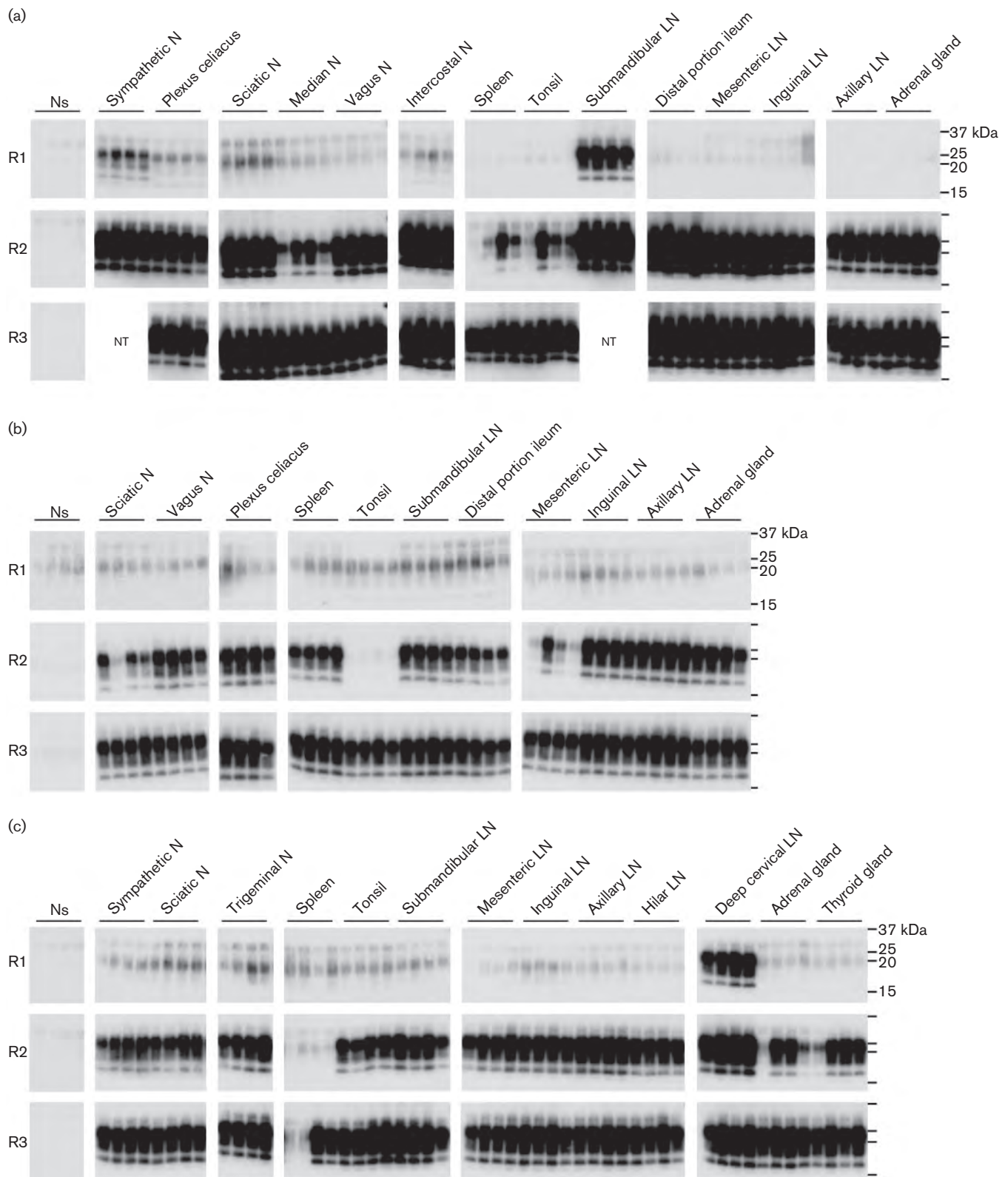


Fig. 3. Tissue distribution of PrP^{Sc} in macaques intracerebrally inoculated with BSE. Tissue distribution of PrP^{Sc} in the terminal disease stage in macaque no. 7 (a), no. 10 (b) and no. 11 (c). Quadruplicate samples of each tissue were serially amplified, and the samples were analysed by Western blot following digestion with proteinase K after each round of amplification (R1–R3). The molecular masses of marker proteins are indicated (kDa). N, Nerve; LN, lymph node; Ns, no-seed samples; NT, not tested.

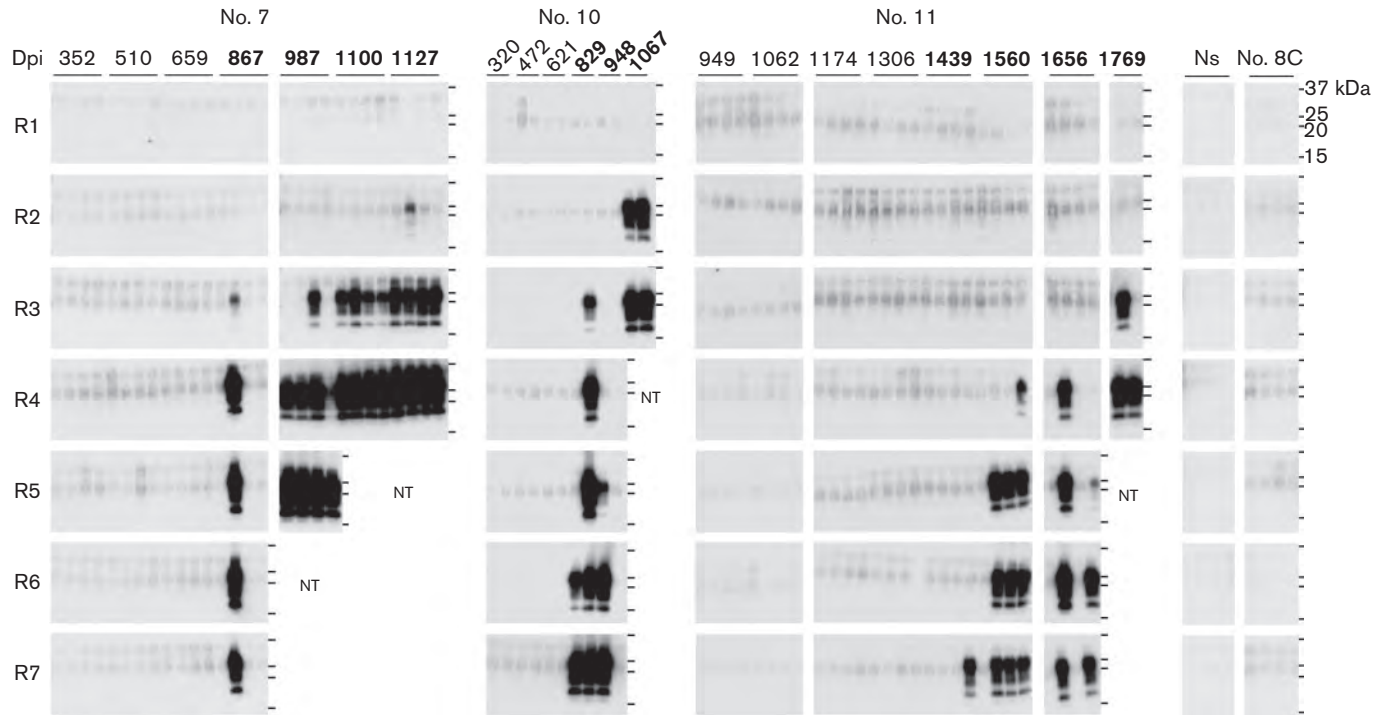


Fig. 4. The appearance of PrP^{Sc} in the cerebrospinal fluid (CSF) of BSE-infected macaques. CSF was collected at several points after intracerebral inoculation. Quadruplicate or duplicate CSF samples from BSE-infected macaque no. 7, no. 10, and no. 11 were analysed by Western blot following digestion with proteinase K after each round of amplification (R1–R7). PrP^{Sc} was also evaluated in CSF samples from an uninfected control macaque (no. 8C). Dpi, Days post-inoculation. Dpi written in boldface represents clinical stages of the disease. The molecular masses of marker proteins are indicated (kDa). Ns, No-seed samples; NT, not tested.

mouse PrP^C substrate (lanes Ns), or samples that contained normal macaque CSF diluted 1:10 with mouse PrP^C substrate (Fig. 4, no. 8C and Fig. S2). PrP^{res} signal was not detected in the samples collected 515–208 (macaque no. 7), 509–208 (macaque no. 10) and 490–133 days (macaque no. 11) before disease onset. The existence of PrP^{Sc} in the CSF samples was confirmed after the onset of clinical signs. For example, macaque no. 7 presented with early neurological clinical signs of the disease such as slight tremor, startle response and festinating gait. PrP^{res} signal was detected after four rounds of amplification in one of the quadruplicate samples collected at this time [867 days post-inoculation (p.i.)], but no other sample was positive for PrP^{Sc} even after seven rounds of amplification. Consistent with disease progression, macaque no. 7 presented with ataxia, paralysis of the extremities and rigidity; PrP^{Sc} was detected in all of the quadruplicate samples obtained at 987 days p.i. after five rounds of amplification. The macaque finally developed severe dysstasia, and after three rounds of amplification, PrP^{Sc} was detected in all of the quadruplicate samples obtained at 1100 days p.i. and at the dissection (1127 days p.i.). These observations suggested that the level of PrP^{Sc} tended to increase in the CSF as the disease progressed. Although a similar tendency was observed in other macaques, there were differences in the levels of PrP^{Sc} in the CSF. For example, duplicate CSF samples collected upon dissection (1067 days p.i.) became positive for PrP^{Sc} after two rounds of amplification in macaque no. 10, which showed the shortest latent period of 828 days. On the other hand, the disease developed after a relatively longer latent period of over 1400 days in macaque no. 11, and PrP^{res} signals were detected after four rounds of amplification in both samples collected upon dissection (1769 days p.i.).

PrP^{Sc} levels in the blood

The results of the amplification of white blood cell (WBC) samples collected at several time points after intracerebral administration are illustrated in Fig. 5. No typical PrP^{res} signal was observed in samples that contained only mouse PrP^C substrate (Fig. 5, lanes Ns), or samples that contained normal macaque WBCs (10⁴ cells) (Fig. 5, no. 8C and Fig. S2). Furthermore, we confirmed that the WBC matrix had no inhibitory effect on the amplification of PrP^{Sc} by serial PMCA (Fig. S3). In macaque no. 7, one of the quadruplicate samples collected upon dissection (1127 days p.i.) became positive for PrP^{Sc} after five rounds of amplification. Similarly, PrP^{res} signal was detected in one or both of the duplicate samples of macaque no. 11 collected at 1656 days p.i., and at dissection (1769 days p.i.). However, PrP^{Sc} was not detected in the blood of these macaques between the latent and the initial stage of disease onset. In macaque no. 10, PrP^{res} signal was not detected in the WBCs obtained during the experimental period (320–1067 days p.i.) even after seven rounds of amplification. With regard to plasma samples, no PrP^{Sc} was detected in any of the samples collected during the experimental period (data not shown).

Infectivity of the PMCA product

The PMCA product obtained after ten rounds of amplification was diluted 10-fold and inoculated intracerebrally into tga20 mice. The tga20 mice inoculated with the PMCA products derived from the brain or WBC PrP^{Sc} seeds died after an average period of 305 or 310 days, respectively (Table 1). PrP^{Sc} accumulation in the brains of mice was confirmed by Western blot analysis (data not shown). There was no significant difference between the survival periods of these PMCA product-inoculated mice (*t*-test, *P*>0.05). Control mice administered with the product containing only PrP^C substrate survived more than 478 days. These results indicated that both brain- and WBC-derived PrP^{Sc} had seeding activities following the PMCA reactions, and the amplified PrP^{Sc} maintained their infectious ability during *in vitro* xenogeneic amplification.

DISCUSSION

In the current study, we developed an ultra-efficient PMCA technique for amplifying PrP^{Sc} derived from BSE-infected cynomolgus macaques by using mouse brain homogenates with DSP as a PrP^C substrate and a polyanion additive, respectively. We first proved the existence of PrP^{Sc} in the CSF and blood of BSE-infected macaques by PMCA, and showed that cynomolgus macaque BSE PrP^{Sc}, and non-macaque PrP^C, effectively converted mouse PrP^C to a proteinase K (PK)-resistant form. It is well known that PMCA of several xenogeneic combinations of PrP^{Sc} seed and PrP^C substrate can overcome the species barrier (Kurt *et al.*, 2007, 2011; Green *et al.*, 2008; Castilla *et al.*, 2008; Yoshioka *et al.*, 2011; Murayama *et al.*, 2012; Nemecek *et al.*, 2013), despite the divergent amino acid sequence of prion proteins. Since the BSE prion was transmissible to ICR (WT) mice (Masujin *et al.*, 2008), the cynomolgus macaque PrP^{Sc} generated by the cross-species transmission of BSE prion may retain the original characteristics of BSE PrP^{Sc}, including structural compatibility with mouse PrP^C and DSP dependency in PMCA reactions.

PrP^{Sc} is detectable in the tonsil, spleen and lymph nodes in vCJD (Wadsworth *et al.*, 2001) and sCJD patients (Rubenstein & Chang, 2013). In an earlier study, PrP^{Sc} was found in the lymphoid tissues, including: the lymph nodes, spleens and tonsils of macaques intracerebrally inoculated with BSE PrP^{Sc} (Lasmézas *et al.*, 1996), as observed in vCJD-inoculated macaques (Lasmézas *et al.*, 2001). Therefore, once PrP^{Sc} accumulates in the brain, it may spread centrifugally from the brain to the peripheral tissues through the autonomic nervous system. However, in our previous study, we failed to detect PrP^{Sc} in such lymphoid tissues of the BSE-inoculated macaques by conventional Western blotting, except in the submandibular lymph nodes, deep cervical lymph nodes and inguinal lymph nodes (Ono *et al.*, 2011a; Table S1). In the current study, PMCA analysis revealed that PrP^{Sc} was distributed in all lymphoid tissues examined in the BSE-infected macaques.

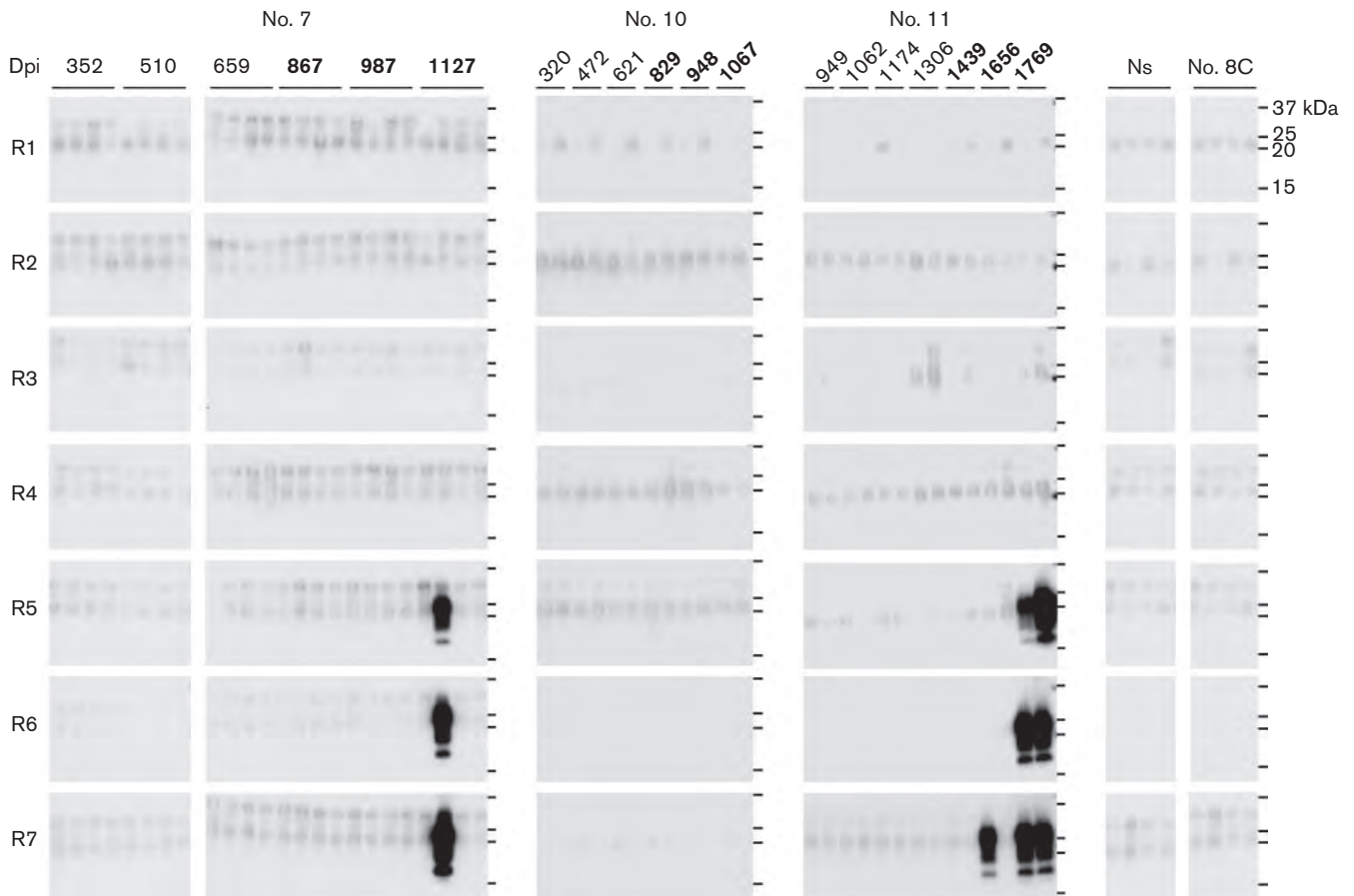


Fig. 5. Appearance of PrP^{Sc} in the WBCs of BSE-infected macaques. WBCs were collected at several points after intracerebral inoculation. Quadruplicate or duplicate WBC samples from BSE-infected macaque no. 7, no. 10 and no. 11 were analysed by Western blot following digestion with proteinase K after each round of amplification (R1–R7). PrP^{Sc} was also evaluated in WBCs from an uninfected control macaque (no. 8C). Dpi, Days post-inoculation. Dpi written in boldface represents the clinical stages of the disease. The molecular masses of marker proteins are indicated (kDa). Ns, No-seed samples.

PrP^{Sc} levels in most of the lymphoid tissues were extremely low, because PrP^{Sc} could only be detected after two or three rounds of amplification. Therefore, significant PrP^{Sc} accumulation in the peripheral non-neuronal tissues might

not have occurred in these macaques, and PrP^{Sc} levels in most lymphoid tissues might have been below the detection limit of the conventional Western blot technique used herein, even at the terminal stage of the disease.

Table 1. Mean incubation time following intracerebral inoculation in tga20 transgenic mice

Inoculum (R10 PMCA product)	Transmission rate (total death/total number)	Mean survival time \pm SD (days)
Brain seed*	100 % (6/6)	305 \pm 10
WBCs seed†	100 % (6/6)	310 \pm 23
No seed	0 % (0/4)	>478
10 % Brain homogenate from a BSE-infected cow‡	100 % (20/20)	495 \pm 43

R10, Tenth round.

*The final dilution of the infected brain homogenate (macaque no. 7) in the R10 product was 6.4×10^{-11} .

†The PMCA product from the tenth round of amplification of PrP^{Sc}-positive WBCs (macaque no. 7).

‡Classical BSE (c-BSE) prion was inoculated in tga20 mice for comparison of infectivity.

The origin of PrP^{Sc} in WBCs may be the spleen and other lymphoid organs, as suggested previously (Saá *et al.*, 2006). As in humans, PrP^C is constitutively expressed in the WBCs of cynomolgus macaques (Holada *et al.*, 2007); therefore, WBCs of cynomolgus macaques can be deemed carriers or reservoirs of PrP^{Sc}. Our finding supports the idea that prion diseases may be transmitted via infected blood in primates, as has been previously seen in scrapie-infected sheep (Houston *et al.*, 2008) and CWD-infected deer (Mathiason *et al.*, 2006). An illustration for the appearance of PrP^{Sc} in the CSF and WBCs of intracerebrally infected macaques is shown in Fig. 6. PrP^{Sc} was found in the WBCs at clinical stages of the disease in macaques no. 7 and no. 11, but PrP^{Sc} was not detected in the WBCs of macaque no. 10 throughout the experimental period. Survival time of the BSE-infected macaques ranged from 1067 days to 1769 days. During the period from the onset of clinical signs to the terminal stage of the disease, PrP^{Sc} was detected in the CSF in all three BSE-infected macaques. The highest level of PrP^{Sc} in the CSF collected upon dissection was observed in macaque no. 10.

A previous study showed that elevated levels of 14-3-3 proteins, which are widely distributed in eukaryotes and

play an important role in various signal transduction systems involved in cell proliferation and division, were observed in the CSF of a simian vCJD model (Yutzy *et al.*, 2007). The increase of PrP^{Sc} in the CSF probably reflects the leakage of PrP^{Sc} from neuronal cells after cell destruction caused by PrP^{Sc} infection. We examined 14-3-3 γ levels in the CSF of the BSE-infected macaques (Fig. S4), and found that the signal intensity of the 14-3-3 γ protein became notable after disease onset (no. 7 and no. 10), or in the latter stages of the disease (no. 11). It is worth noting that the highest levels of the 14-3-3 γ protein were observed in the CSF of macaque no. 10 collected at dissection. Therefore, the disease might have progressed most rapidly after a shorter latent period (829 days) in macaque no. 10 than in macaques no. 7 (867 days) and no. 11 (1439 days). Faster accumulation of PrP^{Sc} in the brain may cause acute brain damage and result in death before a significant number of infected WBCs begin circulating in the peripheral blood. Macaques no. 7 and 10 both belonged to a breeding colony introduced from the Philippines, and no. 11 was derived from a Malaysian lineage. Thus, the different degrees of disease progression might be related to genetic factors affecting susceptibility or resistance to prion infection.

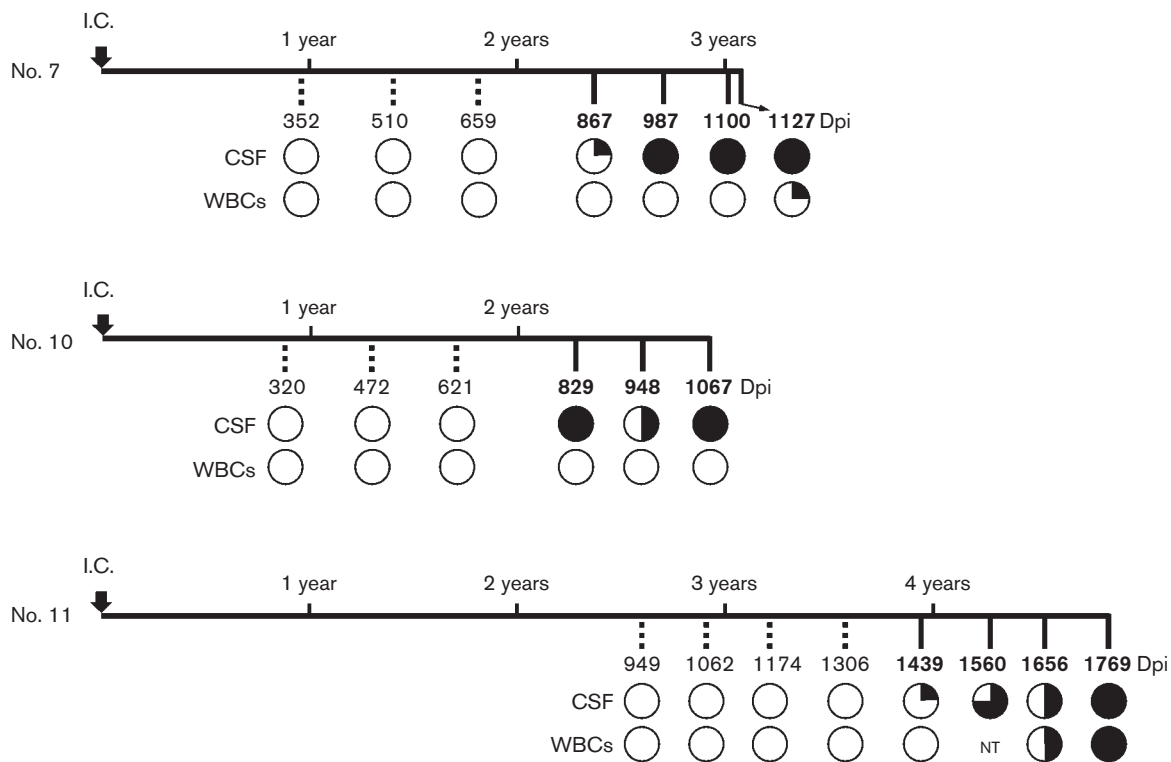


Fig. 6. Schematic illustration for the appearance of PrP^{Sc} in the CSF and WBCs of three BSE-infected macaques. After intracerebral inoculation (I. C.), the presence of PrP^{Sc} in CSF and WBCs was examined by serial PMCA during the asymptomatic (dotted line) and clinical stages (solid lines). Dpi, Days post-inoculation. Dpi written in boldface represents the clinical stages of the disease. Positive ratio of duplicate or quadruplicate samples was shown as open circle (0%), closed quadrant (25%), closed semicircle (50%), closed three quadrants (75%) and closed circle (100%). NT, Not tested.

More detailed studies are needed to clarify the above possibility.

In conclusion, we have developed a highly sensitive method that enables a detailed and precise examination of the distribution of PrP^{Sc} throughout the bodies of BSE-infected macaques. We are now conducting experiments analysing oral transmission of the BSE prion and transmission through blood transfusions from BSE-infected macaques. Using our method, PrP^{Sc} could notably be detected in bodily fluids obtained during the latent period of the disease in both primate models. Thus, the method developed in this study may be useful in furthering the understanding of tissue distribution of PrP^{Sc} in non-human primate models of CJD.

METHODS

BSE-infected macaques. This study on non-human primates was conducted according to the rules for animal care and management of the Tsukuba Primate Research Center (Honjo, 1985) and the guiding principles for animal experiments using non-human primates formulated by the Primate Society of Japan (Primate Society of Japan, 1986). The cynomolgus macaques (*Macaca fascicularis*) examined in this study originated from the Philippines (no. 7 and 10) or Malaysia (no. 11), and were bred at Tsukuba Primate Research Center of the National Institute of Biomedical Innovation. Transmission experiments were approved by the Animal Welfare and Animal Care and Use Committee (approval ID: DS18-069R1) and Animal Ethics Biosafety Committee (approval ID: BSL3-R-06.01) of the National Institute of Biomedical Innovation. The brain homogenate (200 µl of a 10% brain homogenate) derived from a classical BSE (c-BSE)-infected 83-month-old Holstein (Iwata *et al.*, 2006) was intracerebrally administered to three male macaques (no. 7, 10 and 11) that were 24–29 months in age (Ono *et al.*, 2011a). The animals were housed in biosafety level three animal rooms, and their clinical status was monitored daily. After 35–59 months, the animals were euthanized by anaesthesia overdose following evidence of progressive neurological dysfunction, after which the animals were dissected. A healthy macaque (no. 8 or 28) was used as an uninfected control in the PMCA assay of tissues and bodily fluids. All macaques examined in this study were homozygous for methionine at codon 129 (MM) and homozygous for glutamic acid at codon 219 (EE).

Sample preparation. Peripheral nervous and lymphoid tissues were collected upon dissection and stored in small aliquots at –80 °C. Samples from each tissue were homogenized at 10% (w/v) in PBS. WBCs, plasma and CSF were also collected at several time points after inoculation. The blood samples (1.5 ml) were centrifuged at 1500 g for 15 min and the plasma and buffy coat fractions were recovered. Erythrocytes contaminated in the buffy coat fraction were haemolysed in distilled water, and the samples were stored at –80 °C until analysis.

Preparation of PrP^C substrates. To avoid contamination, normal brain homogenates were prepared in a laboratory in which infected materials had never been handled. Brains of a healthy cynomolgus macaque, squirrel monkey (*Saimiri sciureus*), cow, PrP^C-overexpressing transgenic [Tg(BoPrP) 4092HOZ/Prnp^{0/0}, TgBoPrP] mouse (Scott *et al.*, 1997), PrP-knockout (PrP^{0/0}) mouse, WT mouse (ICR), and Syrian hamster were homogenized at a 20% (w/v) concentration in PBS containing a complete protease inhibitor cocktail (Roche Diagnostics). The brain homogenates were stored at –80 °C until further use. For analysis, the homogenates were mixed with an equal

volume of the elution buffer (PBS containing 2% Triton X-100, 8 mM EDTA) and incubated at 4 °C for 1 h with continuous agitation. After centrifugation at 4500 g for 5 min, the supernatant was used as the PrP^C substrate. When using brain homogenates of TgBoPrP mice, the supernatants were mixed in a 5:1 proportion of PrP^{0/0}:TgBoPrP, and this mixture was used as the PrP^C substrate.

PMCA. For the amplification of brain PrP^{Sc}, the BSE-infected brain homogenate of macaque no. 7 was diluted from 10⁻³ to 10⁻⁵ with normal brain homogenates from several animal species in an electron beam-irradiated polystyrene tube (total volume, 100 µl). Amplification was performed in the presence or absence of 1% (w/v) DSP, which has been shown to markedly improve *in vitro* amplification efficiency of bovine BSE PrP^{Sc} (Murayama *et al.*, 2010). Amplification was carried out with a fully automatic cross-ultrasonic protein activating apparatus (Elestein 070-CPR; Elekon Science Corporation), which had the capacity to generate high ultrasonic power (700 W). PMCA was performed by 40 cycles of sonication in which a 3 s pulse oscillation was repeated five times at 1 s intervals, followed by incubation at 37 °C for 1 h with agitation.

To examine the sensitivity of interspecies PMCA using the mouse PrP^C substrate for the detection of macaque BSE PrP^{Sc}, the 10% infected brain homogenate was serially diluted from 10⁻³ to 10⁻¹² with mouse PrP^C substrate containing 1% (w/v) DSP (total volume, 80 µl) in an electron beam-irradiated eight-strip polystyrene tube specially designed for PrP^{Sc} propagation (Murayama *et al.*, 2010). To obtain maximum amplification efficiency and reduce non-specific background signal in Western blot analysis, a series of amplification steps were programmed as follows: PMCA was performed with 40 cycles of sonication in which a 15 s oscillation and subsequent incubations at 31 °C for 1 h were repeated 10 times; a 15 s oscillation and subsequent incubations at 33 °C for 1 h were repeated 10 times; an intermittent oscillation (3 s pulse oscillation was repeated five times at 1 s intervals) and subsequent incubations at 35 °C for 1 h were repeated 10 times; and finally intermittent oscillations (3 s pulse oscillation was repeated five times at 1 s intervals) and subsequent incubation at 37 °C for 1 h were repeated 10 times. The amplified product obtained after the first round of amplification was diluted 1:5 with the PrP^C substrate, and a second round of amplification was performed. This process was repeated for a maximum of six times.

For amplifying PrP^{Sc} in various tissues from BSE-inoculated macaques, the mouse PrP^C substrate containing 1% (w/v) DSP was mixed with a 1/10 volume of homogenized samples or bodily fluids (total volume 80 µl) in eight-strip polystyrene tubes. The WBC pellet (approx. 10⁴ cells) was dissolved in 8 µl of the elution buffer and used as a seed. Serial PMCA was then performed using the four-step amplification programme as described above.

Western blotting. After each round of amplification, samples of 10 µl were mixed with 10 µl of PK solution (100 µg PK ml⁻¹) and incubated at 37 °C for 1 h. The digested materials were mixed with 20 µl of 2× SDS sample buffer and incubated at 100 °C for 5 min. The samples were separated by SDS-PAGE and transferred onto a PVDF membrane (Millipore). After blocking, the membrane was incubated for 1 h with HRP-conjugated T2 mAb (Hayashi *et al.*, 2004; Shimizu *et al.*, 2010) at a 1:10 000 dilution. The T2 antibody, which recognizes a discontinuous epitope in amino acid residues 132–156 in the mouse PrP sequence, also reacts with hamster and monkey PrP. After washing, the blotted membrane was developed with Immobilon Western Chemiluminescent HRP Substrate (Millipore), according to the manufacturer's instructions. Chemiluminescence signals were analysed with the Light Capture system (ATTO).

Bioassay. A 10% brain homogenate from BSE-infected macaque (no. 7) was diluted to 10⁻⁴ with WT mouse PrP^C substrate containing 1% (w/v) DSP and amplified. The 1:5 dilution of the PMCA product

and its subsequent amplification was repeated nine times. The product from the tenth round was diluted 1:10 with PBS and inoculated intracerebrally (20 µl per mouse) into tga20 mice (Fischer *et al.*, 1996) that overexpress mouse PrP^C. Infectivity of the PMCA product from the tenth round of amplification of a PrP^{Sc}-positive WBC sample from macaque no. 7 obtained at dissection 1127 days p.i. was also examined. The PMCA product from the tenth round of amplification of no-seed sample was inoculated as negative control. In addition to the PMCA products, 10% brain homogenate of a c-BSE infected cow was also inoculated into tga20 mice to compare infectivity. The bioassay experiments were approved by the Animal Care and Use Committee of the National Institute of Animal Health (approval ID: 09-44) and were conducted in accordance with the guidelines for animal transmissible spongiform encephalopathy experiments of the Ministry of Agriculture, Forestry and Fisheries of Japan.

ACKNOWLEDGEMENTS

We thank the contributions of the animal caretakers. This study was supported by a grant for BSE research from the Ministry of Health, Labour and Welfare of Japan (H20-Shokuhin-Ippan-008), and in part, by a Grant-in-Aid from the BSE and other Prion Disease Control Project of the Ministry of Agriculture, Forestry and Fisheries of Japan.

REFERENCES

- Atarashi, R., Moore, R. A., Sim, V. L., Hughson, A. G., Dorward, D. W., Onwubiko, H. A., Priola, S. A. & Caughey, B. (2007). Ultrasensitive detection of scrapie prion protein using seeded conversion of recombinant prion protein. *Nat Methods* **4**, 645–650.
- Atarashi, R., Satoh, K., Sano, K., Fuse, T., Yamaguchi, N., Ishibashi, D., Matsubara, T., Nakagaki, T., Yamanaka, H. & other authors (2011). Ultrasensitive human prion detection in cerebrospinal fluid by real-time quaking-induced conversion. *Nat Med* **17**, 175–178.
- Belay, E. D. (1999). Transmissible spongiform encephalopathies in humans. *Annu Rev Microbiol* **53**, 283–314.
- Brown, P., Rohwer, R. G., Dunstan, B. C., MacAuley, C., Gajdusek, D. C. & Drohan, W. N. (1998). The distribution of infectivity in blood components and plasma derivatives in experimental models of transmissible spongiform encephalopathy. *Transfusion* **38**, 810–816.
- Castilla, J., Gonzalez-Romero, D., Saá, P., Morales, R., De Castro, J. & Soto, C. (2008). Crossing the species barrier by PrP^{Sc} replication in vitro generates unique infectious prions. *Cell* **134**, 757–768.
- Caughey, B. W., Dong, A., Bhat, K. S., Ernst, D., Hayes, S. F. & Caughey, W. S. (1991). Secondary structure analysis of the scrapie-associated protein PrP 27–30 in water by infrared spectroscopy. *Biochemistry* **30**, 7672–7680.
- Collinge, J. (2001). Prion diseases of humans and animals: their causes and molecular basis. *Annu Rev Neurosci* **24**, 519–550.
- Comoy, E. E., Casalone, C., Lescoutra-Etcheagaray, N., Zanusso, G., Freire, S., Marcé, D., Auvré, F., Ruchoux, M. M., Ferrari, S. & other authors (2008). Atypical BSE (BASE) transmitted from asymptomatic aging cattle to a primate. *PLoS ONE* **3**, e3017.
- Deleault, N. R., Harris, B. T., Rees, J. R. & Supattapone, S. (2007). Formation of native prions from minimal components *in vitro*. *Proc Natl Acad Sci U S A* **104**, 9741–9746.
- Edgeworth, J. A., Farmer, M., Sicilia, A., Tavares, P., Beck, J., Campbell, T., Lowe, J., Mead, S., Rudge, P. & other authors (2011). Detection of prion infection in variant Creutzfeldt-Jakob disease: a blood-based assay. *Lancet* **377**, 487–493.
- Fischer, M., Rülcke, T., Raeber, A., Sailer, A., Moser, M., Oesch, B., Brandner, S., Aguzzi, A. & Weissmann, C. (1996). Prion protein (PrP) with amino-proximal deletions restoring susceptibility of PrP knockout mice to scrapie. *EMBO J* **15**, 1255–1264.
- Gajdusek, D. C., Gibbs, C. J. & Alpers, M. (1966). Experimental transmission of a Kuru-like syndrome to chimpanzees. *Nature* **209**, 794–796.
- Geissen, M., Krasemann, S., Matschke, J. & Glatzel, M. (2007). Understanding the natural variability of prion diseases. *Vaccine* **25**, 5631–5636.
- Gibbs, C. J., Jr, Gajdusek, D. C., Asher, D. M., Alpers, M. P., Beck, E., Daniel, P. M. & Matthews, W. B. (1968). Creutzfeldt-Jakob disease (spongiform encephalopathy): transmission to the chimpanzee. *Science* **161**, 388–389.
- Glatzel, M., Rogivue, C., Ghani, A., Streffer, J. R., Amsler, L. & Aguzzi, A. (2002). Incidence of Creutzfeldt-Jakob disease in Switzerland. *Lancet* **360**, 139–141.
- Gough, K. C., Baker, C. A., Rees, H. C., Terry, L. A., Spiropoulos, J., Thorne, L. & Maddison, B. C. (2012). The oral secretion of infectious scrapie prions occurs in preclinical sheep with a range of PRNP genotypes. *J Virol* **86**, 566–571.
- Green, K. M., Castilla, J., Seward, T. S., Napier, D. L., Jewell, J. E., Soto, C. & Telling, G. C. (2008). Accelerated high fidelity prion amplification within and across prion species barriers. *PLoS Pathog* **4**, e1000139.
- Haley, N. J., Mathiason, C. K., Zabel, M. D., Telling, G. C. & Hoover, E. A. (2009a). Detection of sub-clinical CWD infection in conventional test-negative deer long after oral exposure to urine and feces from CWD+ deer. *PLoS ONE* **4**, e7990.
- Haley, N. J., Seelig, D. M., Zabel, M. D., Telling, G. C. & Hoover, E. A. (2009b). Detection of CWD prions in urine and saliva of deer by transgenic mouse bioassay. *PLoS ONE* **4**, e4848.
- Haley, N. J., Mathiason, C. K., Carver, S., Zabel, M., Telling, G. C. & Hoover, E. A. (2011). Detection of chronic wasting disease prions in salivary, urinary, and intestinal tissues of deer: potential mechanisms of prion shedding and transmission. *J Virol* **85**, 6309–6318.
- Hayashi, H., Takata, M., Iwamaru, Y., Ushiki, Y., Kimura, K. M., Tagawa, Y., Shinagawa, M. & Yokoyama, T. (2004). Effect of tissue deterioration on postmortem BSE diagnosis by immunobiochemical detection of an abnormal isoform of prion protein. *J Vet Med Sci* **66**, 515–520.
- Hill, A. F., Desbruslais, M., Joiner, S., Sidle, K. C., Gowland, I., Collinge, J., Doey, L. J. & Lantos, P. (1997). The same prion strain causes vCJD and BSE. *Nature* **389**, 448–450, 526.
- Hilton, D. A., Sutak, J., Smith, M. E., Penney, M., Conyers, L., Edwards, P., McCardle, L., Ritchie, D., Head, M. W. & other authors (2004). Specificity of lymphoreticular accumulation of prion protein for variant Creutzfeldt-Jakob disease. *J Clin Pathol* **57**, 300–302.
- Holada, K., Simak, J., Brown, P. & Vostal, J. G. (2007). Divergent expression of cellular prion protein on blood cells of human and nonhuman primates. *Transfusion* **47**, 2223–2232.
- Honjo, S. (1985). The Japanese Tsukuba Primate Center for Medical Science (TPC): an outline. *J Med Primatol* **14**, 75–89.
- Houston, F., McCutcheon, S., Goldmann, W., Chong, A., Foster, J., Sisó, S., González, L., Jeffrey, M. & Hunter, N. (2008). Prion diseases are efficiently transmitted by blood transfusion in sheep. *Blood* **112**, 4739–4745.
- Ironside, J. W. (1998). Prion diseases in man. *J Pathol* **186**, 227–234.
- Ironside, J. W. (2010). Variant Creutzfeldt-Jakob disease. *Haemophilia* **16** (Suppl 5), 175–180.
- Iwata, N., Sato, Y., Higuchi, Y., Nohtomi, K., Nagata, N., Hasegawa, H., Tobiume, M., Nakamura, Y., Hagiwara, K. & other authors (2006).

- Distribution of PrP^{Sc} in cattle with bovine spongiform encephalopathy slaughtered at abattoirs in Japan. *Jpn J Infect Dis* 59, 100–107.
- Knight, R. (2010).** The risk of transmitting prion disease by blood or plasma products. *Transfus Apheresis Sci* 43, 387–391.
- Kurt, T. D., Perrott, M. R., Wilusz, C. J., Wilusz, J., Supattapone, S., Telling, G. C., Zabel, M. D. & Hoover, E. A. (2007).** Efficient *in vitro* amplification of chronic wasting disease PrP^{RES}. *J Virol* 81, 9605–9608.
- Kurt, T. D., Seelig, D. M., Schneider, J. R., Johnson, C. J., Telling, G. C., Heisey, D. M. & Hoover, E. A. (2011).** Alteration of the chronic wasting disease species barrier by *in vitro* prion amplification. *J Virol* 85, 8528–8537.
- Lasmézas, C. I., Deslys, J. P., Demaimay, R., Adjou, K. T., Lamoury, F., Dormont, D., Robain, O., Ironside, J. & Hauw, J. J. (1996).** BSE transmission to macaques. *Nature* 381, 743–744.
- Lasmézas, C. I., Fournier, J. G., Nouvel, V., Boe, H., Marcé, D., Lamoury, F., Kopp, N., Hauw, J. J., Ironside, J. & other authors (2001).** Adaptation of the bovine spongiform encephalopathy agent to primates and comparison with Creutzfeldt–Jakob disease: implications for human health. *Proc Natl Acad Sci U S A* 98, 4142–4147.
- Lasmézas, C. I., Comoy, E., Hawkins, S., Herzog, C., Mouthon, F., Konold, T., Auvré, F., Correia, E., Lescoutra-Etcheagaray, N. & other authors (2005).** Risk of oral infection with bovine spongiform encephalopathy agent in primates. *Lancet* 365, 781–783.
- Maddison, B. C., Baker, C. A., Rees, H. C., Terry, L. A., Thorne, L., Bellworthy, S. J., Whitlam, G. C. & Gough, K. C. (2009).** Prions are secreted in milk from clinically normal scrapie-exposed sheep. *J Virol* 83, 8293–8296.
- Maddison, B. C., Rees, H. C., Baker, C. A., Taema, M., Bellworthy, S. J., Thorne, L., Terry, L. A. & Gough, K. C. (2010).** Prions are secreted into the oral cavity in sheep with preclinical scrapie. *J Infect Dis* 201, 1672–1676.
- Masujin, K., Shu, Y., Yamakawa, Y., Hagiwara, K., Sata, T., Matsuura, Y., Iwamaru, Y., Imamura, M., Okada, H. & other authors (2008).** Biological and biochemical characterization of L-type-like bovine spongiform encephalopathy (BSE) detected in Japanese black beef cattle. *Prion* 2, 123–128.
- Mathiason, C. K., Powers, J. G., Dahmes, S. J., Osborn, D. A., Miller, K. V., Warren, R. J., Mason, G. L., Hays, S. A., Hayes-Klug, J. & other authors (2006).** Infectious prions in the saliva and blood of deer with chronic wasting disease. *Science* 314, 133–136.
- Mathiason, C. K., Hayes-Klug, J., Hays, S. A., Powers, J., Osborn, D. A., Dahmes, S. J., Miller, K. V., Warren, R. J., Mason, G. L. & other authors (2010).** B cells and platelets harbor prion infectivity in the blood of deer infected with chronic wasting disease. *J Virol* 84, 5097–5107.
- Murayama, Y., Yoshioka, M., Okada, H., Takata, M., Yokoyama, T. & Mohri, S. (2007).** Urinary excretion and blood level of prions in scrapie-infected hamsters. *J Gen Virol* 88, 2890–2898.
- Murayama, Y., Yoshioka, M., Masujin, K., Okada, H., Iwamaru, Y., Imamura, M., Matsuura, Y., Fukuda, S., Onoe, S. & other authors (2010).** Sulfated dextrans enhance *in vitro* amplification of bovine spongiform encephalopathy PrP^{Sc} and enable ultrasensitive detection of bovine PrP^{Sc}. *PLoS ONE* 5, e13152.
- Murayama, Y., Imamura, M., Masujin, K., Shimozaki, N., Yoshioka, M., Mohri, S. & Yokoyama, T. (2012).** Ultrasensitive detection of scrapie prion protein derived from ARQ and AHQ homozygote sheep by interspecies *in vitro* amplification. *Microbiol Immunol* 56, 541–547.
- Nemecek, J., Nag, N., Carlson, C. M., Schneider, J. R., Heisey, D. M., Johnson, C. J., Asher, D. M. & Gregori, L. (2013).** Red-backed vole brain promotes highly efficient *in vitro* amplification of abnormal prion protein from macaque and human brains infected with variant Creutzfeldt–Jakob disease agent. *PLoS ONE* 8, e78710.
- Notari, S., Moleres, F. J., Hunter, S. B., Belay, E. D., Schonberger, L. B., Cali, I., Parchi, P., Shieh, W. J., Brown, P. & other authors (2010).** Multiorgan detection and characterization of protease-resistant prion protein in a case of variant CJD examined in the United States. *PLoS ONE* 5, e8765.
- Ono, F., Terao, K., Tase, N., Hiyaoka, A., Ohyama, A., Tezuka, Y., Wada, N., Kurosawa, A., Sato, Y. & other authors (2011a).** Experimental transmission of bovine spongiform encephalopathy (BSE) to cynomolgus macaques, a non-human primate. *Jpn J Infect Dis* 64, 50–54.
- Ono, F., Tase, N., Kurosawa, A., Hiyaoka, A., Ohyama, A., Tezuka, Y., Wada, N., Sato, Y., Tobiume, M. & other authors (2011b).** Atypical L-type bovine spongiform encephalopathy (L-BSE) transmission to cynomolgus macaques, a non-human primate. *Jpn J Infect Dis* 64, 81–84.
- Orrú, C. D., Wilham, J. M., Hughson, A. G., Raymond, L. D., McNally, K. L., Bossers, A., Ligios, C. & Caughey, B. (2009).** Human variant Creutzfeldt–Jakob disease and sheep scrapie PrP^(tes) detection using seeded conversion of recombinant prion protein. *Protein Eng Des Sel* 22, 515–521.
- Pan, K. M., Baldwin, M., Nguyen, J., Gasset, M., Serban, A., Groth, D., Mehlhorn, I., Huang, Z., Fletterick, R. J. & Cohen, F. E. (1993).** Conversion of α -helices into β -sheets features in the formation of the scrapie prion proteins. *Proc Natl Acad Sci U S A* 90, 10962–10966.
- Peden, A. H., Ritchie, D. L., Head, M. W. & Ironside, J. W. (2006).** Detection and localization of PrP^{Sc} in the skeletal muscle of patients with variant, iatrogenic, and sporadic forms of Creutzfeldt–Jakob disease. *Am J Pathol* 168, 927–935.
- Peden, A. H., McGuire, L. I., Appleford, N. E., Mallinson, G., Wilham, J. M., Orrú, C. D., Caughey, B., Ironside, J. W., Knight, R. S. & other authors (2012).** Sensitive and specific detection of sporadic Creutzfeldt–Jakob disease brain prion protein using real-time quaking-induced conversion. *J Gen Virol* 93, 438–449.
- Primate Society of Japan (1986).** Guiding principles for animal experiments using nonhuman primates. *Primate Research* 2, 111–113.
- Prusiner, S. B. (1991).** Molecular biology of prion diseases. *Science* 252, 1515–1522.
- Prusiner, S. B. (1998).** Prions. *Proc Natl Acad Sci U S A* 95, 13363–13383.
- Rubenstein, R. & Chang, B. (2013).** Re-assessment of PrP^{Sc} distribution in sporadic and variant CJD. *PLoS ONE* 8, e66352.
- Saà, P., Castilla, J. & Soto, C. (2006).** Presymptomatic detection of prions in blood. *Science* 313, 92–94.
- Saborio, G. P., Permanne, B. & Soto, C. (2001).** Sensitive detection of pathological prion protein by cyclic amplification of protein misfolding. *Nature* 411, 810–813.
- Scott, M. R., Safar, J., Telling, G., Nguyen, O., Groth, D., Torchia, M., Koehler, R., Tremblay, P., Walther, D. & other authors (1997).** Identification of a prion protein epitope modulating transmission of bovine spongiform encephalopathy prions to transgenic mice. *Proc Natl Acad Sci U S A* 94, 14279–14284.
- Shimizu, Y., Kaku-Ushiki, Y., Iwamaru, Y., Muramoto, T., Kitamoto, T., Yokoyama, T., Mohri, S. & Tagawa, Y. (2010).** A novel anti-prion protein monoclonal antibody and its single-chain fragment variable derivative with ability to inhibit abnormal prion protein accumulation in cultured cells. *Microbiol Immunol* 54, 112–121.
- Tattum, M. H., Jones, S., Pal, S., Collinge, J. & Jackson, G. S. (2010).** Discrimination between prion-infected and normal blood samples by protein misfolding cyclic amplification. *Transfusion* 50, 996–1002.

- Terry, L. A., Howells, L., Hawthorn, J., Edwards, J. C., Moore, S. J., Bellworthy, S. J., Simmons, H., Lizano, S., Estey, L. & other authors (2009).** Detection of PrP^{Sc} in blood from sheep infected with the scrapie and bovine spongiform encephalopathy agents. *J Virol* **83**, 12552–12558.
- Thorne, L. & Terry, L. A. (2008).** *In vitro* amplification of PrP^{Sc} derived from the brain and blood of sheep infected with scrapie. *J Gen Virol* **89**, 3177–3184.
- Wadsworth, J. D., Joiner, S., Hill, A. F., Campbell, T. A., Desbruslais, M., Luthert, P. J. & Collinge, J. (2001).** Tissue distribution of protease resistant prion protein in variant Creutzfeldt-Jakob disease using a highly sensitive immunoblotting assay. *Lancet* **358**, 171–180.
- Wang, F., Wang, X., Yuan, C. G. & Ma, J. (2010).** Generating a prion with bacterially expressed recombinant prion protein. *Science* **327**, 1132–1135.
- Will, R. G., Ironside, J. W., Zeidler, M., Estibeiro, K., Cousens, S. N., Smith, P. G., Alperovitch, A., Poser, S., Pocchiari, M. & Hofman, A. (1996).** A new variant of Creutzfeldt-Jakob disease in the UK. *Lancet* **347**, 921–925.
- Wroe, S. J., Pal, S., Siddique, D., Hyare, H., Macfarlane, R., Joiner, S., Linehan, J. M., Brandner, S., Wadsworth, J. D. & other authors (2006).** Clinical presentation and pre-mortem diagnosis of variant Creutzfeldt-Jakob disease associated with blood transfusion: a case report. *Lancet* **368**, 2061–2067.
- Yoshioka, M., Imamura, M., Okada, H., Shimozaki, N., Murayama, Y., Yokoyama, T. & Mohri, S. (2011).** Sc237 hamster PrP^{Sc} and Sc237-derived mouse PrP^{Sc} generated by interspecies *in vitro* amplification exhibit distinct pathological and biochemical properties in tga20 transgenic mice. *Microbiol Immunol* **55**, 331–340.
- Yutzy, B., Holznagel, E., Coulibaly, C., Stuke, A., Hahmann, U., Deslys, J. P., Hunsmann, G. & Löwer, J. (2007).** Time-course studies of 14-3-3 protein isoforms in cerebrospinal fluid and brain of primates after oral or intracerebral infection with bovine spongiform encephalopathy agent. *J Gen Virol* **88**, 3469–3478.

総説

BSE の発生とその対策を振り返って

堀内基広[†]

北海道大学大学院獣医学研究科 (〒060-0818 札幌市北区北18条西9丁目)

Looking back on the occurrence of BSE and its control measures

Motohiro HORIUCHI[†]*Laboratory of Veterinary Hygiene, Graduate School of Veterinary Medicine, Hokkaido University, Kita 18, Nishi 9, Kita-ku, Sapporo 060-0818, Japan*

BSEの発生及びその後のvCJDの発生は世界を不安に陥れたが、BSEに対する管理措置が有効に機能し、2009年以降の発生数は世界全体を合計しても100例以下にまで減少した。その発生は世界的に管理下にあり、わが国でも2002年2月以降に生まれた牛でBSEは発生していない。BSEの発生は、欧州を中心に、世界的に食の安全対策が見直される契機となった。わが国でも、食品安全基本法の制定及び食品安全委員会による健康影響評価という、食の安全・安心に関して新たな枠組みが構築された。BSEの収束とともに、社会の関心も薄れているが、今一度BSEの発生と対策について整理したい。

1 プリオン病

プリオン病は人のクロイツフェルト・ヤコブ病、羊のスクレイピーに代表される致死性の神経変性疾患である。プリオン病の病原体「プリオン」の本体については、長年議論されてきたが、大腸菌で発現させた組み換えプリオンタンパク質から感染性のあるプリオンが産生可能なことから、主要構成要素はプリオンタンパク質(prion protein: PrP)であることが証明されたと考えられる。実際には、異常型プリオンタンパク質(Abnormal isoform of prion protein: PrP^{Sc})のオリゴマーあるいは凝集体に感染性が付随する。

プリオン病は、その原因により、感染性、遺伝性、特発性(原因不明)の3種に分類される。動物のプリオン病は、自然状態あるいは人為的な感染によるかは別にし

て、感染性に分類される。このうち、スクレイピーは羊間で、慢性消耗病は鹿科動物間で、自然状態で感染が成立する。

人のプリオン病は感染性、遺伝性及び特発性の3種がある。このうち、特発性に分類される孤発性CJDが80~85%を占める。牛海綿状脳症(Bovine spongiform encephalopathy: BSE)は、1980年代半ばにイギリスで出現し大流行した。BSEはイギリスで出現後、欧州、北米及びアジアへ拡散した。1996年、BSEが人に感染したことが原因と考えられる変異クロイツフェルト・ヤコブ病(vCJD)の存在が報告されてから、食生活を介して人がBSEに罹患して死に至るといった恐怖のために、BSEは大きな社会問題となった。以降、プリオン病は食品媒介性感染症、人獣共通感染症として認識されるようになった。

2 発生状況

BSEは1985年頃からイギリスで発生し、発生数は1992年にピークに達した。BSEの由来として、羊のスクレイピーが原因であるとする説と、元来まれではあるが牛に存在していた病気であったとする説があるが結論は出ていない。イギリスでは1988年7月に、反芻獣由来の肉骨粉を反芻獣に与えることを禁止する飼料規制(ruminant feed ban to ruminants)を導入した。この飼料規制導入後6年を経過した1994年以降、BSEの発生は減少に転じた。1996年にvCJDの存在が明らかと

[†] 連絡責任者: 堀内基広 (北海道大学大学院獣医学研究科教授)

〒060-0818 札幌市北区北18条西9丁目 ☎・FAX 011-706-5293

E-mail: horiuchi@vetmed.hokudai.ac.jp

[†] Correspondence to: Motohiro HORIUCHI (Laboratory of Veterinary Hygiene, Graduate School of Veterinary Medicine, Hokkaido University)

Kita 18, Nishi 9, Kita-ku, Sapporo 060-0818, Japan

TEL・FAX 011-706-5293 E-mail: horiuchi@vetmed.hokudai.ac.jp

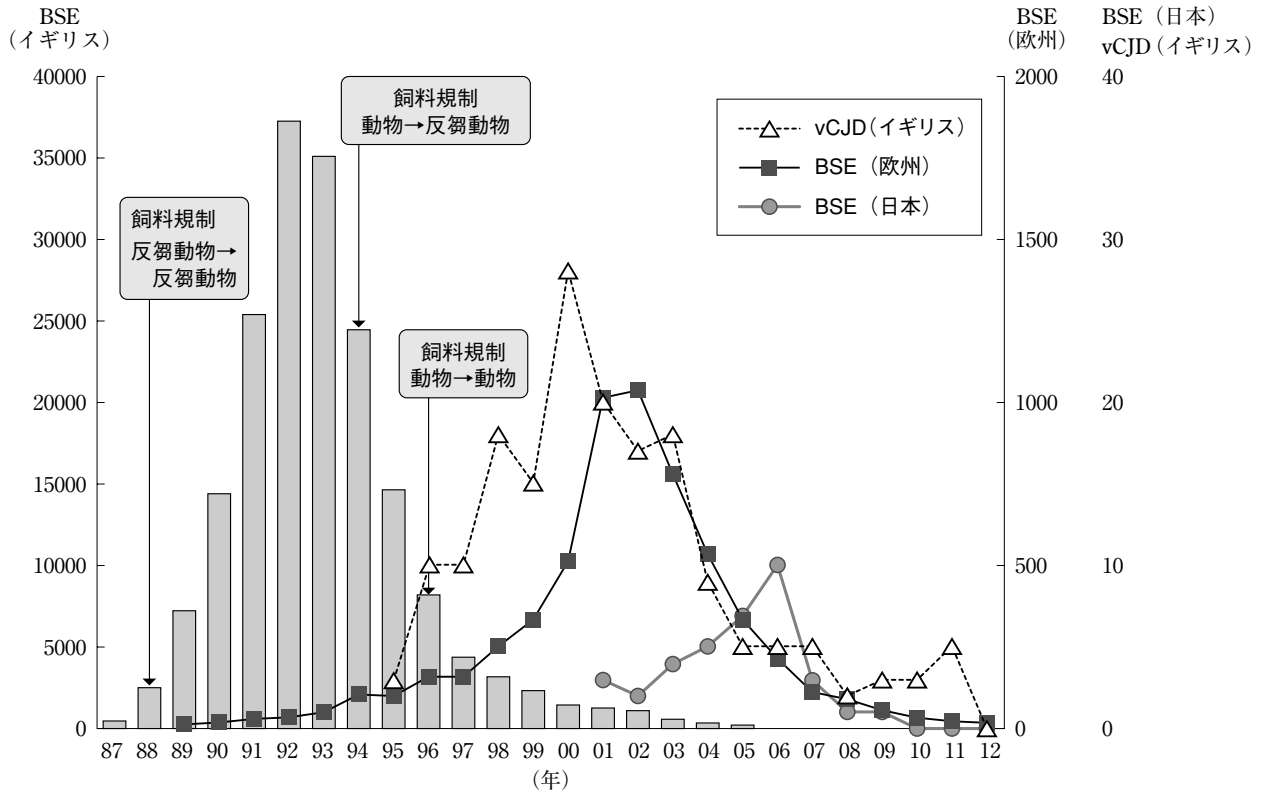


図1 イギリス、欧州及び日本におけるBSE発生数の経時変化とイギリスにおけるvCJD患者数の変化
棒グラフはイギリスにおけるBSE発生数、△はイギリスにおけるvCJD発生数、■は欧州におけるBSE発生数、●は日本におけるBSE発生数を示す。

なり、世界的に不安が増大したが、BSE管理措置は有効に機能しており、発生のピーク時（1992年）には年間37,000頭以上であった発生数が2010年には11頭までに減少した。ただし、イギリスのピーク時におけるBSEの発生数は臨床診断と病理組織学的検査による件数であり、仮に、ELISAやウエスタンブロット（WB）など、精度・感度の高い診断法を用いた場合、はるかに多数の感染牛が摘発されたと考えられる。vCJDはこれまでイギリスで177例、イギリス以外の国で51例（日本：1名）の報告があるが、イギリスでの発生は2000年をピークに減少している（図1）。

欧州諸国では2000年以降BSE牛の数が著しく増加したが、これはELISAもしくはWBにより牛の延髄門部に蓄積するPrP^{Sc}を検出する方法を導入してリスク牛及び食用に供される健康と畜牛のBSE検査を開始した結果である。後述するように、欧州諸国でもイギリスと同様の飼料規制を導入しており、2003～2004年をピークにBSEの発生数は減少している。

わが国では2001年9月に最初のBSE牛が確認され、以降計36例が確認された。BSE牛の多くは、出生後間もなく汚染飼料の給餌により感染を受ける。したがって、BSE牛の出生時期は、その当時のBSEプリオン汚染状況を反映する。わが国で摘発されたBSE牛の出生

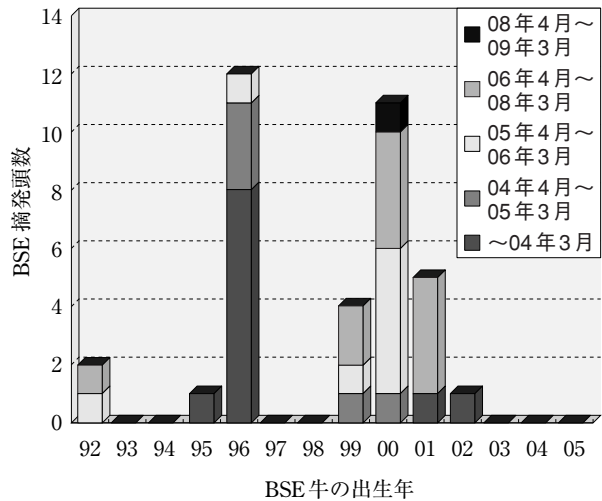


図2 日本で摘発されたBSE牛の出生年と摘発時期

時期には二つのピークがある。一つは1995～1996年生まれ、もう一方は1999～2001年生まれの子牛である（図2）。前者はBSEプリオンに汚染された飼料や油脂の輸入が原因と考えられるが、後者は、1995～1996年に輸入飼料が原因でBSEに感染した牛が国内でレンダリングされ、国内でBSEプリオン汚染肉骨粉が産生され、これにより国内で感染が拡大したと推定される。BSEは自然状態で牛から牛に水平伝播しないので、感染源

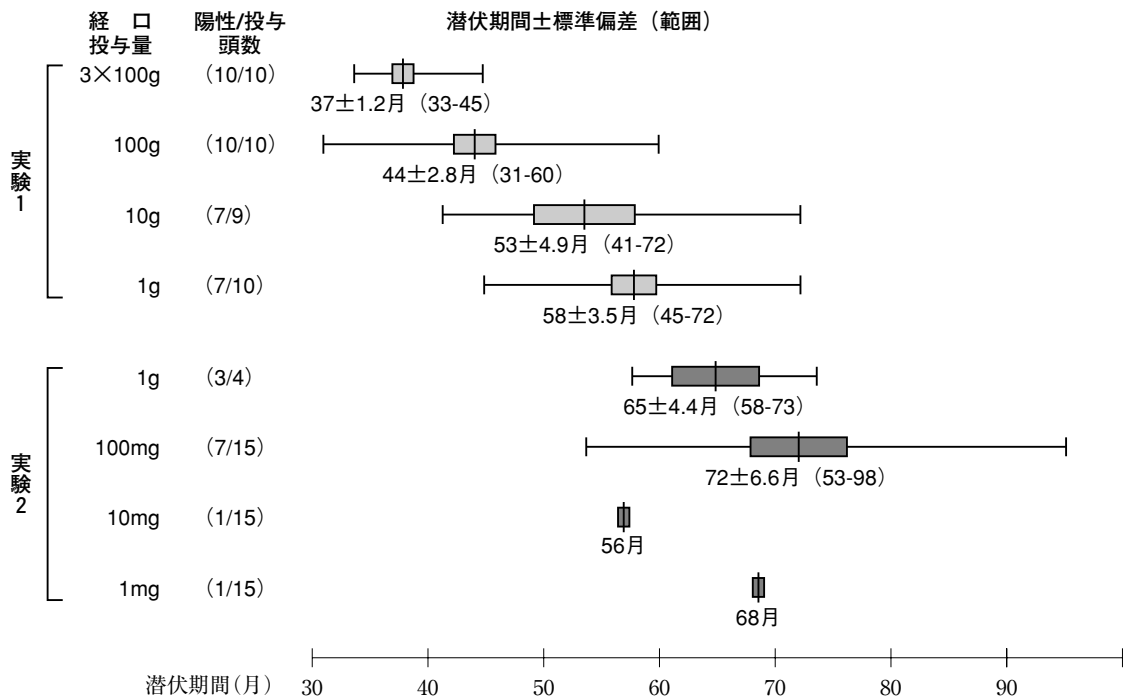


図3 BSEの牛への経口投与と実験。BSE感染牛の脳乳剤を牛に経口投与し、発症までの期間を調べた。投与量が減少するとともに、平均潜伏期が延長する。また、発症率（投与頭数に対する陽性頭数の割合）が低下する。引用文献 [2] を改変。

(BSE感染牛及びプリオン汚染飼料)と感染経路(汚染飼料の摂食)を遮断できれば、確実に制圧できる。わが国で、2002年2月以降に生まれた牛でBSEの発生がないことは、飼料規制を含む管理措置が有効に機能したことの証である。

3 BSE感染牛でのプリオンの体内分布

BSE感染牛でのプリオンの体内分布やその経時的変化を含めた感染病態の解明は、BSEに係るリスク評価を行う上での科学的知見として非常に重要である。イギリス獣医学研究所(VLA)、ドイツのFriedrich-Loeffler-Institute (FLI)及び日本の動物衛生研究所と新得畜産試験場では、牛を用いた感染試験及び野外例の解析を行っており、病態に関する知見が集積しつつある。

欧州委員会の調査によると、BSE牛由来脳乳剤を経口投与した牛の各臓器のプリオン感染性を、マウスを用いたバイオアッセイで調べた実験では、32カ月以降の脳、脊髄、背根神経節、三叉神経節、6カ月目の回腸遠位部にプリオンの感染性が確認されている。また、牛を用いたバイオアッセイでの調べで、扁桃でも低レベルながら感染性が見いだされた。スクレイピーも反芻動物のプリオン病であるが、BSE感染牛とスクレイピーの羊では、プリオンの体内分布が明らかに異なる。スクレイピー感染羊では中枢神経系以外にも、リンパ節、扁桃、粘膜下リンパ濾胞などのリンパ系組織や胎盤など非神経系の末梢組織にプリオンが容易に検出できるが、BSE病原体は神経向性が強く、BSE感染牛のリンパ系組織ではプ

リオンはまれに検出される程度としている(European Commission: Update of the opinion on TSE infectivity distribution in ruminant tissue. http://ec.europa.eu/food/fs/sc/ssc/out296_en.pdf (2002))。

羊スクレイピー、マウスやハムスターなどの実験動物におけるプリオンの経口投与から、経口ルートで侵入したプリオンは、消化管からパイエル氏板等の消化管付随リンパ濾胞の上皮に存在するM細胞から体内に取り込まれ、リンパ濾胞にある濾胞樹状細胞で増殖するとともに、末梢神経へと移行し、副交感神経系(迷走神経)を経て延髄に至る経路と、交感神経系(内臓神経)を経て脊髄胸腰部に至る経路で、中枢神経系に侵入すると考えられている。牛を用いた感染実験の結果から、経口的に取り込まれたBSE病原体は回腸遠位部に存在する集合パイエル氏板の濾胞上皮から体内に取り込まれ、同様の経路で中枢神経系に侵入することが示された[1]。

感染成立を考える上で、最小感染量の推定は重要である。VLAで実施された牛でのBSE経口投与試験では、野外発生例から推測されたように、投与量の減少とともに潜伏期間が延長し、BSE感染牛脳1mg相当でも、15頭中1頭で感染が成立した(図3)[2]。脳乳剤の経口投与と動物組織の加熱処理により産生される肉骨粉の摂取による感染効率の差異は不明であるが、最小感染量は非常に低い。

BSE感染後、中枢神経系組織でPrP^{Sc}が検出されるようになる時期、あるいは発症前どのくらいの時期からPrP^{Sc}が検出されるかという情報は、BSE検査の対象月

齢を考慮する上で重要である。BSE 経口感染牛では、BSE 感染牛脳100g 相当を投与した場合、投与後24 カ月以降、5g 相当では34 カ月以降、1g 相当では44 カ月以降で延髄でPrP^{Sc}が検出されるようになった [2, 3]。野外発生例では、潜伏期はプリオン汚染の高さ、あるいはプリオンの暴露量に逆比例するので、汚染状況や管理措置の有効性により、BSE 感染牛が延髄でPrP^{Sc}が陽性となり、発症に至るまでの時間は異なる。わが国で実施してきたBSE 検査の結果、21 カ月齢及び23 カ月齢でPrP^{Sc}陽性と判定された2例を除くと、死亡牛のBSE サーベイランスでBSEと判定された最も若い牛は48 カ月齢であり、食用に供される牛のBSE 検査で陽性と判定された最も若い牛は57 カ月齢である。これらはともに、飼料規制導入前の2000年に生まれた牛である。その後、わが国における飼料規制の遵守度を考慮すると、仮にBSEに感染した牛が発生したとしても、中枢神経系でPrP^{Sc}陽性となるまでの月齢はさらに延長すると思われる。

一方、新得畜産試験場で実施したBSEの脳内接種により牛は接種18カ月頃から臨床症状を呈するが、早い例では接種後10カ月でPrP^{Sc}が検出される。脳内接種という厳しい条件下は、発症前の8カ月前にはPrP^{Sc}が検出可能となること示す結果である [4]。

実験感染牛のプリオンの組織分布の解析から、中枢神経系でPrP^{Sc}が検出されるようになる時期と同時期あるいはそれ以降に、副腎、末梢神経等でPrP^{Sc}及び感染性が検出されるようになることから [3]、感染後期には中枢神経系に侵入したプリオンが遠心性に末梢組織に広がると考えられ、特定危険部位 (Specified risk materials : SRM) 以外の組織にもプリオンが存在する。しかし、SRM以外の組織に存在するPrP^{Sc}の量は中枢神経系と比較して1/1,000以下と少ない量である。また、消化管における病原体の分布は、経口投与量により差異はあるものの、早い例では投与後4カ月かで回腸でPrP^{Sc}が検出される [5]。

BSE 野外発生例でも、副腎、坐骨神経、顔面神経及び半膜様筋などからPrP^{Sc}あるいは感染性が検出されており、SRM以外にもBSEプリオンが分布する [6, 7]。また、回腸遠位部からPrP^{Sc}が検出され感染性もあることから、BSE 感染後早期から長期間にわたり回腸遠位部では感染性が存在する。特定危険部位に指定されている回腸遠位部よりも上部の消化管でも感染性やPrP^{Sc}が検出される場合があるが、その量は非常に少ない。

4 欧州及び北米におけるBSE対策

イギリスにおけるBSEの大流行は、斃死獣を処理して肉骨粉を生産するレンダリング工程の変更に起因する。1980～1983年にバッチ法から連続法に変わった

が、連続法ではプリオンが完全に不活化されずに肉骨粉に残存した。イギリスでは肉骨粉を代用乳に添加して子牛に与えていたためにBSEの感染が拡大した。

イギリスではBSEの存在が確認されて間もない1988年6月に、疫学的に肉骨粉がBSEの原因であることをつきとめ、反芻動物由来の肉骨粉を反芻動物に給餌することを禁止した (ruminant feed ban to ruminants)。これが功を奏して、1992～1993年をピークにBSE 摘発数は減少した (図1)。平均潜伏期が4～8年と長いため、効果が現れるまでに時間を要したのである。BSEの発生は減少傾向に転じたが、1988年のruminant feed banが導入された以降に生まれた牛でのBSEの発生 (BAB : BSE cases borne after feed ban) があったことから (4万5千頭以上がruminant feed ban 導入後に生まれた牛)、1994年には、故意あるいは過失による肉骨粉の牛への給餌を防止するため、動物由来の肉骨粉を反芻動物に使用することを禁止した (animal feed ban to ruminants)。また、1996年3月のvCJDの報告を受け、すべての家畜への動物由来の肉骨粉の使用を禁止した (complete feed ban)。1996年のcomplete feed banの導入以降に生まれた牛から160頭のBSEが摘発されている (BARB : BSE cases borne after the reinforced ban)。

イギリスでは、1989年は、特定危険部位 (当初はSBO [Specific bovine offal] と呼ばれていた) を人の食用に供することを禁止した。また、1995年には、脊髓や神経節が混入する可能性のある機械的回収肉の使用を禁止した。1996年のvCJDの発生を受けて、30カ月齢以上の牛を食用に供さずに殺処分するOver thirty months scheme (OTMS)を導入した。その後、BSE汚染状況が改善されてきたことから、2005年11月以降は、1996年以前に生まれた牛に対してのみOTMSを継続し、30カ月齢以上の健康と畜牛の検査の実施を開始した。

EU諸国では1994年、スイスでは、1990年に飼料規制 (ruminant feed ban) を導入し、2001年にはcomplete feed banを導入した。また、特定危険部位の除去も開始した。EU諸国では2000～2001年にかけて、24あるいは30カ月齢以上の食用に供される健康と畜牛のBSE検査を導入した。これにより、BSEの摘発数は急激に上昇した。24カ月齢以上のリスク牛 (死亡牛、切迫と殺牛、臨床牛) のBSEサーベイランスも実施し、これらBSE検査の実施により、欧州でのBSE発生状況及び汚染状況が正確に把握できた。EUでは飼料規制、特定危険部位の除去及びBSEサーベイランスを継続するとともに、欧州委員会 (European commission : EC) は、2005年及び2010年にTSEロードマップを公表し、BSE汚染状況の変化と管理措置の実効性を考慮して、

向こう5年間の管理措置の短・中期的及び長期的な見直し等の方向性を示してきた。ECは、2009年1月には、健康と畜牛のBSE検査の対象月齢が48カ月齢、2011年7月には72カ月齢に引き上げてもよいこととなった。また、2013年3月以降は、一部の加盟国で健康と畜牛のBSE検査を廃止してもよいとした。各国の特定危険部位の定義は表2、BSE検査対象は表3に示した。

アメリカ・カナダのBSE対策、EU諸国及びわが国とは異なる部分がある。EU諸国では一時的でもcomplete feed banを導入した。一方、アメリカ・カナダでは、1996年以降、ruminant feed banを導入したが、牛由来飼料の他種動物への使用は禁止していなかった。飼料規制はBSEの汚染を低下させ、BSEの再興を防ぐ最も重要な管理措置であるが、その遵守度の評価は難しく、最も客観的な方法は、BSEサーベイランスによるBSE発生状況の把握である。イギリスにおけるBAB及びBARBの存在や交差汚染の問題から、飼料規制の強化はBSE清浄化のために重要と考えられてきた。アメリカでは2009年10月から、カナダは2007年7月から、飼料規制が強化されたが、特定危険部位を含まない牛由来飼料は、他種動物への使用を認めている。このように、一口に飼料規制と言っても、その内容は欧州及びわが国と北米では異なる。

EU諸国及びわが国では、リスク牛のBSEサーベイランス及び食の安全・安心確保のために健康と畜牛のBSE検査と特定部位の除去が実施されてきた。一方、アメリカ・カナダ及びスイスはリスク牛のBSEサーベイランスと特定危険部位の除去を実施してきた。BSEの管理措置は国と地域により異なるため、BSEリスクの評価は一律の基準で実施することはできず、BSEの発生状況、家畜や飼料の輸入状況、家畜の飼養形態、レンダリング産物の産生様式、飼料規制の実施状況及び管理措置の実効性などから総合的にする必要があった。

5 わが国のBSE対策の変化

わが国では2001年9月にBSEの摘発を受け、BSEが食を介して人に伝播することを防止するための緊急措置として、食用に供される牛全頭を対象としたBSEスクリーニング検査（ELISAによる一次検査とWBによる確認検査）と特定危険部位の除去を柱とした対策を導入した（2001年10月開始）。この二つの対策はBSE病原体の人への感染防止を目的とした出口側の管理措置である。世界的には例がない全頭を対象とした検査は、その是非が議論されることとなったが、当時は1996年にWHOが唱えた「BSE感染牛のいかなる組織もフードチェーンにまわしてはならない」との考え方、月齢の正確な確認方法がなかったこと、汚染状況が判らなかつたこと、人に感染すると100%致死の治療法のない病気であ

ること、などを考慮すると、予防原則に基づく政治的決断は適切であったと考える。

一方、BSEの牛間での感染拡大防止とBSE汚染状況の把握のため、法的拘束力を伴う飼料規制（2001年9月開始）と死亡牛のBSEサーベイランス（2003年4月開始）を導入した。これらは、BSEの清浄化を目指すための入り口側の管理措置である。また、出生・育成履歴を明らかにするためのトレーサビリティ制度も導入した（2003年12月開始）。臨床症状によるBSEの診断は難しいことから、BSEの汚染状況の正確な把握には、PrP^{Sc}の検出による能動サーベイランスが必要である。わが国で実施してきたBSEスクリーニング検査と死亡牛のBSEサーベイランスは、2002年1月以降に生まれた牛でBSEに罹患した牛が存在せず、わが国におけるBSEの汚染度がかぎりなく低下したことが証明された。

BSEの発生状況と継続的な管理措置の実施から、わが国は2009年5月にはOIEが認定する「管理されたリスク国」となり、2013年2月には「無視できるリスク国」となった。

2001年9月のBSE発生に伴うBSE管理措置導入後、食品安全委員会では、BSE発生状況及びBSEの病態機序に関する科学的知見及び管理措置の遵守状況などを掘り所に、国内のBSE対策の見直し及び国境措置の変更に係る健康影響評価を実施してきた。厚生労働省は2005年8月に、食品安全委員会による「わが国におけるBSE対策に係る食品健康影響評価」（2005年5月）を受け、BSE検査の対象月齢を21カ月齢以上に変更した（3年間の経過期間を設けた）。しかし、変更後も、対象となる牛が10%強と少ないことと、消費者のBSEに対する根強い不安・不信などから、各自治体は全頭を対象としたBSE検査を継続した。

この時、20カ月齢以下の牛を検査対象から除外しても、「人の健康に影響を及ぼすリスクの増加は非常に小さい～無視できると」結論するに至ったのは、わが国で実施してきたBSEスクリーニングで20カ月齢以下の牛で陽性例が見つかっていないこと、イギリスがBSEに高度に汚染されていた時期では、20カ月齢でBSEと診断された症例があるもの、BSEの平均潜伏期は4～8年であること、また、BSE汚染度の低下とともにBSEと診断される最も若い牛の月齢は高くなること、実験感染牛におけるプリオンの体内分布と蓄積の程度などの科学的知見に加え、2001年9月の飼料規制導入後に生まれた牛が対象となること、SRMの除去やSRMによる枝肉の汚染防止措置などのリスク低減措置、飼料規制遵守が担保されること、などを前提とした総合的な判断であった。

2013年には、「牛海綿状脳症（BSE）対策の見直しに係る健康影響評価」（2012年10月及び2013年5月）を

BSEの発生とその対策を振り返って

表1 BSE対策

	イギリス	欧州	日本
1988年7月	反芻動物由来飼料の反芻動物への使用禁止		
1989年11月	牛（6カ月齢以上）の特定臓器（SBO）の人の食用禁止		
1990年11月		牛（6カ月齢以上）の特定危険部位の人の食用禁止	
1990年12月		肉骨粉の反芻動物への使用禁止（スイス）	
1994年6月		動物由来飼料の反芻動物への使用禁止（EU）	
1994年11月	動物由来飼料の反芻動物への使用禁止		
1996年3月	vCJDの報告 動物由来飼料の全家畜への使用禁止		反芻動物由来肉骨粉を反芻動物へ使用しないよう行政指導
1996年4月	30カ月齢以上の牛を人の食用、動物の飼料から排除するための殺処分を決定（OTMS）		
2000年6月		特定危険部位の除去	
2001年1月		食用に供される健康と畜牛のBSE検査開始（24もしくは30カ月齢以上） 動物由来飼料の全家畜への使用を暫定的に禁止	
2001年9月			BSEの発生確認 動物由来飼料の反芻動物への使用禁止
2001年10月			食用に供する牛のBSE検査開始（全頭対象） 牛の特定危険部位の除去・焼却 動物由来飼料の全家畜への使用禁止
2003年4月			死亡牛のBSEサーベイランス開始
2003年7月			食品安全委員会設立
2003年12月			アメリカからの牛肉の輸入禁止 牛のトレーサビリティ制度開始
2005年8月			食用に供する牛のBSE検査から20カ月齢以下の牛を除外
2005年11月	食用に供される健康と畜牛をEUと同等の規則を適用（1996年以降に生まれた牛）		
2005年12月			アメリカ・カナダの20カ月齢以下の牛の牛肉等の輸入再開
2009年1月		食用に供する健康と畜牛のBSE検査対象月齢を48カ月齢超に変更可能（EU15）	
2009年5月			OIEのBSEステータス：管理されたリスクに認定
2011年7月		食用に供する健康と畜牛のBSE検査対象月齢を72カ月齢超に変更可能（EU25、ブルガリア、ルーマニアを除く）	
2012年10月			BSE対策の見直しに係る食品健康影響評価
2013年2月			アメリカ、カナダ、フランスから30カ月齢以下の牛の牛肉等の輸入解禁
2013年3月	食用に供する健康と畜牛の検査を廃止	食用に供する健康と畜牛のBSE検査対象月齢を廃止してもよい（加盟国の一部）	
2013年4月			特定危険部位の変更 食用に供する牛の対象月齢を30カ月齢超に変更
2013年5月			OIEのBSEステータス：無視できるリスクに認定
2013年7月			食用に供する牛の対象月齢を48カ月齢超に変更

表2 各国における牛の特定危険部位

	日 本		アメリカ, カナダ	EU	OIE	
	～2013年2月	2013年3月～		フランス, オランダ	管理された リスク国	無視できる リスク国
頭部(頭蓋骨, 眼球を含む)	全月齢の頭部 (舌, 頬肉を除く)	30カ月齢超の頭部 (舌, 頬肉を除く)	30カ月齢超の頭部	12カ月齢超の頭部	30カ月齢超の 頭部	
扁桃	全月齢	全月齢	全月齢(アメリカ) 30カ月齢超(カナダ)	全月齢	全月齢	
脊 髄	全月齢	30カ月齢超	30カ月齢超	12カ月齢超	30カ月齢超	条件なし
脊柱(背根神 経節を含む)	全月齢	30カ月齢超	30カ月齢超	30カ月齢超	30カ月齢超	
腸	回腸遠位部 (全月齢)	回腸遠位部 (全月齢)	回腸遠位部 (全月齢)	全月例の十二指腸 から直腸までの腸 管と腸間膜	回腸遠位部 (全月齢)	



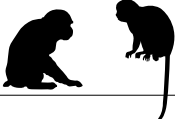

表3 各国におけるBSE検査の対象月齢と変遷

	日 本	フランス	オランダ	アメリカ・カナダ	OIE
高リスク牛のBSE サーベイランス(組 織的な能動的サー ベイランスの導入あ るいは変更時期)	24カ月齢超の死 亡牛 (2003年4月～)	24カ月齢超の高リス ク牛(2000年6月～)	24カ月齢超の高リス ク牛(2000年～) 48カ月齢超の高リス ク牛(2009年1月～)	30カ月齢超の高 リスク牛の一部 (2004年から拡 大サーベイラン ス)	30カ月齢超の高リス ク牛の一部 A型サーベイランス: 10万頭に1頭の発生率 を検出可能 B型サーベイランス: 5万頭に5万頭の1頭 の発生率を検出可能
食用に供される牛の BSE検査(スクリー ニング検査の導入あ るいは変更時期)	全月齢 (～2013年3月) 30カ月齢超 (2013年4月～) 48カ月齢超 (2013年7月～)	30カ月齢超 (2001年1月～) 24カ月齢超 (2001年7月～) 30カ月齢超 (2004年7月～) 48カ月齢超 (2009年1月～) 72カ月齢超 (2011年7月～)	30カ月齢超 (2001年～) 48カ月齢超 (2009年1月～) 72カ月齢超 (2011年7月～)	なし	なし
飼料規制後に生まれ た牛で最も直近に BSEと診断された牛 の生年月	2002年1月	2004年4月	2001年2月	2004年8月 (カナダ)	

受けて、食用に供される牛のBSE検査の対象月齢が30カ月齢以上(2013年4月施行、実際にこれを実施した自治体はない)、続いて48カ月齢以上に引き上げられた(2013年7月施行)。食品安全委員会では、2011年12月に厚生労働省からの諮問を受けて、これらの健康影響評価を開始した。わが国でBSEが確認されてから10年以上が経過したが、2002年1月以降に生まれた牛で10年間BSEの発生がなく、飼料規制が遵守されてBSE清浄化が進んだことは明らかである。加えて世界的にもBSEの発生数は激減しており、BSEリスクが低下している。また、BSE感染牛におけるプリオンの体内分布とその経時的変化に関する科学的知見も、「わが国におけるBSE対策に係る食品健康影響評価」(2005年5月)の時よりも集積している。これらを総合的に判断して、ま

ず、諮問にあった具体的な月齢として、検査対象月齢を30カ月齢以上に引き上げた場合の人への健康影響を評価し、続いて、さらなる対象月齢の引き上げについて評価し、検査対象月齢を48カ月齢以上に引き上げても、人への健康影響は無視できると判断した。検査対象月齢が48カ月齢以上に変更されたことで、対象となると畜牛は全体の15%程度となった。2013年2月には、特定危険部位も管理措置が緩和された。わが国における特定危険部位の変更の概要は表2に示した。

国境措置についても緩和が進んでいる。アメリカ・カナダでのBSEの発生を受けて禁止していた北米産の牛肉の輸入が、2005年12月に、20カ月齢以下を条件に解禁された。この管理措置の変更に係る食品健康影響評価に関しては、BSEが政争の具となったような印象を持

感染実験に使用した動物	定型BSE	非定型BSE	
		H型	L型
牛 	伝達可能 (脳内接種, 経口投与)	伝達可能 (脳内接種) 経口投与は実験結果の 報告なし	伝達可能 (脳内接種) 経口投与は実験結果の 報告なし
牛PrP発現 トランスジェニックマウス 	伝達可能 (脳内接種)	伝達可能 (脳内接種)	伝達可能 (脳内接種)
霊長類 (サル) 	伝達可能 (脳内接種, 経口投与)	感染実験結果の 報告なし	伝達可能 (脳内接種, 一部経口投与*)
ヒトPrP発現 トランスジェニックマウス 	伝達可能 (脳内接種)	伝達例の報告なし	伝達可能 (脳内接種)

*ネズミキツネザルで経口投与により伝達

図4 定型BSE, H型及びL型非定型BSEの異種動物への伝達試験

つ方も多いと思われるが、食品安全委員会では可能なかぎり科学的知見に基づく慎重な議論を行った。当時はアメリカ・カナダとともにBSEの汚染状況、飼料規制などの管理措置の遵守状況など不確実な要素が多く、アメリカ・カナダとわが国で産生される牛肉等におけるBSEリスクの科学的な同等性の評価は困難であった。しかし、アメリカ・カナダが提案する日本向け牛肉等の輸出プログラム（SRMは全月齢から除去すること、枝肉格付けあるいは生産記録に基づく月齢証明により20カ月齢以下と証明される牛であること）が遵守されることを前提として、「20カ月齢以下のアメリカ・カナダの牛に由来する牛肉等とわが国で生産される牛肉等のリスクの差は非常に小さい」と結論するに至った（2005年12月）。

また、2013年2月には、BSE発生国であった、アメリカ、カナダ及びフランス（30カ月齢以下）及びオランダ（12カ月齢以下）からの牛肉の輸入が認められた。食品安全委員会では、北米とEU諸国ではBSE管理措置の中でも飼料規制のレベル、トレーサビリティによる月齢確認体制及びサーベイランスの規模は異なるが、世界的にBSEの発生は激減してリスクが非常に低下していること、BSE感染牛におけるプリオンの体内分布などの科学的知見に加えて、SRM除去などのリスク低減措置の継続実施などを総合的に判断して、「上記4カ国からの30カ月齢以下の牛肉が輸入されても、現状とリスクの差は非常に小さく、人への健康影響は無視できる」と答申するに至った（2012年10月）。

6 非定型BSE

健康なと畜牛をも検査する能動的なBSE検査は、新たな懸念を見いだす結果ともなった。元来、世界で発生していたBSEはイギリス由来であり、同じ病原体が牛

表4 非定型BSEの発生状況

国	L型	H型	その他	型の情報がないもの	計	BSE 総計
オーストリア	2	1			3	8
デンマーク	1	0			1	16
フランス	13	13			26	1,021
ドイツ	1	1			2	419
アイルランド	0	1		2	3	1,654
イタリア	4	0		1	5	144
オランダ	2	1		1	4	88
ポーランド	8	2		1	11	74
スペイン				1	1	785
スウェーデン	0	1			1	1
スイス	0	1	2		3	467
イギリス	3	3		1	7	184,621
カナダ	1	1			2	20
アメリカ	1	2			3	3
日本	2	0			2	36
合計	38	27	2	7	74	189,357

引用文献[9, 10]及び「牛海綿状脳症(BSE)対策の見直しに係る食品健康影響評価(食品安全委員会2012年10月)」(http://www.fsc.go.jp/sonota/bse/bse_hyoka_201210.pdf)を統合

や飼料の輸出に伴い世界中に広まったと考えられていた。しかし、能動的サーベイランスは、従来のBSE（定型BSE）とは異なるタイプのBSEである非定型BSEの存在を明らかにした。最初にイタリアで発見されたが、その後、能動的サーベイランスを実施しているほとんどの国で非定型BSEが発見されるようになった（表4）。

非定型BSEにはL-BSEとH-BSEがある。これは、WBで検出されるPrP^{Sc}の分子量が、定型BSEと比較して小さい（L-BSE）、あるいは大きい（H-BSE）ことに由来する。非定型BSEは8歳以上の高齢の牛で見つかることがほとんどである。フランスでの出生コホートの

比較では、定型BSEは1996年前後生まれの牛に集中しているのに対し、非定型BSEの出生年から特定の原因を見いだすことはできない [8]。非定型BSEは高齢の牛で散発的に発見されることから、人の孤発性CJDのように特発性BSEである可能性がある。L-BSEは各種動物への伝達試験の成績も明らかになっている。牛や牛PrPを発現するTgマウスへ接種した場合、定型BSEよりも短い潜伏期で発病する。サルへの感染実験、あるいは人PrPを発現するTgマウスへ接種した場合も、定型BSEよりも短い潜伏期で発病する (図4)。したがって、L-BSEは人への感染性を有すると考えられる。仮に、非定型BSEが一定の頻度で自然発生する孤発性BSEだとすると、BSEの根絶は困難である。また、非定型BSEでも、定型BSEと同様に、蓄積量は非常に低いが末梢神経からもPrP^{sc}が検出される。しかし、高齢牛で発見される、発生頻度が1/10⁷程度と予想されるまれな疾患である。したがって、牛由来飼料の使用規制、一定の年齢以上の牛の特定部位の排除及び一定の年齢以上の牛のBSEスクリーニング/サーベイランス等の継続により、非定型BSEが新たなBSE発生の原因となる可能性及び人への感染のリスクは十分に排除できると考えられる。

7 おわりに

BSEの存在が明らかになってからもうすぐ30年が経過する。また、わが国でBSEの1例目が確認されてからは12年が経過した。当時の社会的混乱を思い起こすと、短期間で、適切な飼料規制の遵守によりBSEの発生を封じ込めたことは評価すべきである。しかし、非定型BSEの存在や、他の反芻動物へのBSE感染が起こりうる事実を考慮すると、今後も、反芻動物を対象とした飼料規制の徹底及び適切なBSEサーベイランスの維持・継続は必要である。

引用文献

- [1] Hoffmann C, Ziegler U, Buschmann A, Weber A, Kupfer L, Oelschlegel A, Hammerschmidt B, Groschup MH : Prions spread via the autonomic nervous system from the gut to the central nervous system in cattle incubating bovine spongiform encephalopathy, *J Gen Virol*, 88, 1048-1055 (2007)
- [2] Wells GA, Konold T, Arnold ME, Austin AR, Hawkins SA, Stack M, Simmons MM, Lee YH, Gavier-Widén D, Dawson M, Wilesmith JW : Bovine spongiform encephalopathy: the effect of oral exposure dose on attack rate and incubation period in cattle, *J Gen Virol*, 88, 1363-1373 (2007)
- [3] Masujin K, Matthews D, Wells GA, Mohri S, Yokoyama T : Prions in the peripheral nerves of bovine spongiform encephalopathy-affected cattle, *J Gen Virol*, 88, 1850-1858 (2007)
- [4] Fukuda S, Onoe S, Nikaido S, Fujii K, Kageyama S, Iwamaru Y, Imamura M, Masujin K, Matsuura Y, Shimizu Y, Kasai K, Yoshioka M, Murayama Y, Mohri S, Yokoyama T, Okada H : Neuroanatomical distribution of disease-associated prion protein in experimental bovine spongiform encephalopathy in cattle after intracerebral inoculation, *Jpn J Infect Dis*, 65, 37-44 (2012)
- [5] Hoffmann C, Eiden M, Kaatz M, Keller M, Ziegler U, Rogers R, Hills B, Balkema-Buschmann A, van Keulen L, Jacobs JG, Groschup MH : BSE infectivity in jejunum, ileum and ileocaecal junction of incubating cattle, *Vet Res*, 42, 21 (2011)
- [6] Buschmann A, Groschup MH : Highly bovine spongiform encephalopathy-sensitive transgenic mice confirm the essential restriction of infectivity to the nervous system in clinically diseased cattle, *J Infect Dis*, 192, 934-942 (2005)
- [7] Iwamaru Y, Okubo Y, Ikeda T, Hayashi H, Imamura M, Yokoyama T, Shinagawa M : PrP^{Sc} distribution of a natural case of bovine spongiform encephalopathy. In: Prions - Food and Drug Safety, Kitamoto T, ed, 179, Springer-Verlag, Tokyo (2005)
- [8] Biacabe AG, Morignat E, Vulin J, Calavas D, Baron TG : Atypical bovine spongiform encephalopathies, France, 2001-2007, *Emerg Infect Dis*, 14, 298-300 (2008)
- [9] Seuberlich T, Heim D, Zurbriggen A : Atypical transmissible spongiform encephalopathies in ruminants: a challenge for disease surveillance and control, *J Vet Diagn Invest*, 22, 823-842 (2010)
- [10] European Food Safety Authority : Scientific and technical assistance on the minimum sample size to test should an annual BSE statistical testing regime be authorized in healthy slaughtered cattle, *EFSA Journal*, 10, 2913 (2012)

【研究紹介】

道総研畜産試験場における非定型 BSE に関する研究

福田 茂 夫

北海道立総合研究機構畜産試験場基盤研究部生物工学グループ
 (〒081-0038 上川郡新得町新得西5線39番地1)

1. はじめに

牛海綿状脳症 (BSE : Bovine Spongiform Encephalopathy) は、羊のスクレイピー、シカの慢性消耗症 (CWD) やヒトのクロイツフェルト・ヤコブ病 (CJD) などと共に「プリオン病」と呼ばれ、中枢神経組織における空胞変性病変と異常プリオンタンパク質 (PrP^{Sc}) の蓄積を特徴とする致死性神経疾患である。また BSE は、ヒトの変異型 CJD の原因となるなど人獣共通感染症として公衆衛生上、重要な疾患である。

BSE は、1986年に英国で初めて確認され、1992年には37,280頭の発生が見られた。また英国から欧州諸国、北アメリカおよび日本に拡散した。各国が BSE 対策を

実施した結果、近年 BSE の発生頭数は年々減少しており、2013年では7頭、2014年では12頭となった (国際獣疫事務局 : OIE 公表) (図1)。わが国の BSE では、2001年9月に第1例目の BSE が報告され、大きな社会問題となった。しかしその後の飼料製造工程での混入防止策を含めた反芻家畜への動物性飼料の給与禁止、食肉処理場における特定危険部位の除去や BSE 検査の実施等の行政措置や生産者・畜産関係者の努力が功を奏し、2009年3月の36例目の患畜を最後に BSE 患畜は確認されず、終息状態となっている。また過去11年間に生まれた牛から BSE 患畜が出ていないことなどから、2013年に OIE の BSE リスクステータス「BSE のリスクを無視できる国」に承認されたところである。BSE 発生以来、継続していた食肉衛生検査での BSE 全頭検査も、リスク評価機関による評価を踏まえ、段階的に対象月齢を変更し、また死亡牛検査もこの度対象月齢が変更され、現在はともに48カ月齢超の牛が対象となっている。

当初、BSE は単一のプリオン株に起因すると考えられてきたが、定型 BSE 発生拡大に伴い各国で BSE 検査が行われた結果、2000年代に入り、これまでの「定型 BSE」と性状の異なる「非定型 BSE」が欧州、北米、南米、日本で散発的に報告されている。非定型 BSE は、ウエスタンブロット (WB) 法による BSE 検査で PrP^{Sc} の泳動パターンが定型 BSE と異なり、L 型および H 型の2つの型が報告されている。H 型は、タンパク質分解酵素プロテイナーゼ K (PK) で消化処理した後の PrP^{Sc} の分子量が、定型 BSE よりも大きく、WB のバンドの位置が高く検出され、L 型は分子量が小さく、WB のバンドの位置が低く検出される。米国で確認された非定型 BSE (H 型) 1例にプリオンタンパク質遺伝子の変異が見つかった他は、患畜の PrP にアミノ酸配列の

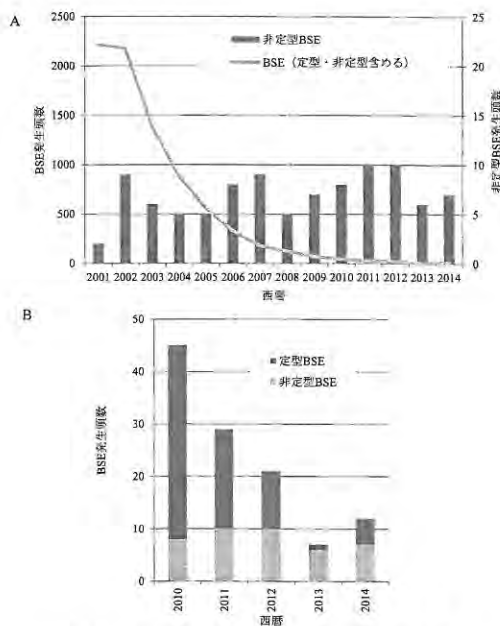


図1 世界の BSE 発生頭数の推移

- A. BSE 発生頭数 (定型・非定型を含む) と非定型 BSE 発生頭数 (2001~2014)
 B. 定型 BSE と非定型 BSE の発生頭数の推移 (2010~2014)

連絡担当者：福田 茂夫 北海道立総合研究機構畜産試験場基盤研究部生物工学グループ
 TEL : 0156-64-0618 FAX : 0156-64-3484 E-mail : fukuda-shigeo@hro.or.jp

違いは見られていない。この分子量の違いは、PK 処理に対する抵抗性部位の差によるものであり、アミノ酸配列に差がないことから立体構造の違いにより生じるものと推察されている。わが国においても、BSE 患者36例のうち2例（第8例目と第24例目）が非定型 BSE であった。非定型 BSE のほとんどは死後検査で確認されているため、臨床症状や農場段階での診断に関する情報はほとんどない。非定型 BSE の発生機序が不明であり、ヒト型 PrP 遺伝子組換えマウスや霊長類への脳内接種試験によりヒトへの感染リスクが示唆されていることから、BSE 問題の残された課題となっている。

道総研畜産試験場における定型 BSE に関する研究について、先に本誌3月号（第59巻第3号）にて紹介した。道総研畜産試験場では、さらに非定型 BSE の感染実験牛を用いた非定型 BSE の診断技術の開発と発生要因の解明について研究を行っており、本稿ではその研究成果について紹介するとともに、非定型 BSE について若干解説する。

2. 畜産試験場における非定型 BSE 研究

試験1. 非定型 BSE 感染牛の臨床症状

目的

非定型 BSE (L 型) と診断された国内24例目の BSE

患者 (BSE/JP24)^[1]の脳を接種した非定型 BSE 感染牛を作出し、非定型 BSE におけるプリオンの接種から臨床症状の発現までの期間、接種から起立不能等のため飼育困難になるまでの期間および臨床症状について定型 BSE 感染牛と比較する。

方法

BSE 非発生農場で出生したホルスタイン種雌牛14頭および黒毛和種雌牛6頭を用いた。BSE/JP24の10%脳乳剤をホルスタイン種7頭および黒毛和種3頭に、定型 BSE 感染牛の10%脳乳剤をホルスタイン種7頭および黒毛和種3頭に、それぞれ2~4カ月齢時に1ml ずつ脳内に接種した。BSE 感染牛の飼育は専用隔離牛舎(動物バイオセーフティレベル1)で行った。BSE 感染牛の観察は、BSE の臨床症状検査を実施し、すなわち頭部を低くする等の姿勢や異常行動、歩様や走行姿勢の変化、音に対する過剰反応、動くものに対する過剰反応を毎週1回観察した。

非定型 BSE 感染牛の2頭(接種後9カ月)および定型 BSE 感染牛の5頭(接種後12~22カ月)は、臨床症状を発現する前に病理解剖を行った。その他の13頭は、歩様の変化や音への過剰反応、起立困難などの BSE の臨床症状が現れた後、病理解剖した。脳および末梢組織における PrP^{Sc} の分布は、WB 法を用いて解析した。

表1. 非定型および定型 BSE 感染牛の臨床症状の経過

牛 No.	品種	初発の臨床症状	接種後の月数																解剖前の状態	
			9	10	11	12	13	14	15	16	17	18	19	20	21	22	23	24		
非定型 (L型) BSE L感染牛	A1 ¹⁾	Hol	なし	-																症状なし
	A2 ¹⁾	Hol	なし	-																症状なし
	A3 ²⁾	Hol	(起立困難)	-	-	■														起立不能
	A4	Hol	歩様の変化	-	-		+													運動失調
	A5	Hol	歩様の変化	-	-		+	+												運動失調
	A6	Hol	音に過剰反応	-	-	+	+	+												運動失調
	A7 ²⁾	Hol	(起立困難)	-	-															起立不能
	A8	JB	歩様の変化	-	-							+								運動失調
	A9	JB	音に過剰反応	-	-	+	+	+	+	+		+								運動失調
	A10	JB	音に過剰反応	-	-							+								運動失調
定型 BSE E感染牛	C1 ¹⁾	Hol	なし	-	-															症状なし
	C2 ¹⁾	Hol	なし	-	-															症状なし
	C3 ¹⁾	Hol	なし	-	-															症状なし
	C4 ¹⁾	Hol	なし	-	-															症状なし
	C5 ³⁾	Hol	起立姿勢・歩様の変化	-	-									+	+	+				姿勢異常
	C6	Hol	起立姿勢・歩様の変化	-	-									+	+	+	+	+	+	起立不能
	C7	Hol	歩様の変化	-	-										+	+	+	+	+	起立不能
	C8	JB	音に過剰反応	-	-											+				運動失調
	C9	JB	音に過剰反応	-	-												+	+		運動失調
	C10 ¹⁾	JB	なし	-	-															症状なし

*起立不能等により飼養困難となった非定型 BSE 感染牛: 8頭 (A3~A10)、定型 BSE 感染牛: 5頭 (C5~C9) について比較した。

- 1) 臨床症状が現れる前に試験殺し解剖した。
- 2) 臨床症状検査に対する反応がなく、突然起立困難となった。
- 3) 臨床症状確認後、接種後20カ月にて計画的に病理解剖した。

*品種 Hol:ホルスタイン種、JB:黒毛和種

*-:臨床症状なし、+:臨床症状あり、□:病理解剖(所見なし)、■:病理解剖(所見あり)

結果

脳内接種による非定型および定型 BSE 感染牛の臨床上の経過と病理解剖までの期間を表 1 に示した。

非定型 BSE 感染牛の初期の臨床症状として、脳内接種から 11~16カ月経過した後、歩様の異常（後肢のふらつき）が 3 頭、音への過剰反応が 3 頭に見られた。姿勢・行動の変化および動く物に対する過剰反応は見られず、また複数の臨床症状を呈した牛はいなかった。また 2 頭は、これらの臨床症状の検査項目のいずれでも異常が観察されなかったが、突然起立困難となった。定型 BSE 感染牛では、脳内接種から 18~21カ月後に、佇立姿勢や歩様の異常、音への過剰反応などの症状が見られ、複数の症状を示す牛もあった。非定型 BSE 感染牛は、定型 BSE 感染牛と比較して臨床症状が不明瞭であった。脳内接種による非定型 BSE 感染牛が飼育困難になるまでの期間は、脳内接種からおおよそ 11~16カ月後であり、定型 BSE 感染牛の 19~24カ月後よりも約 8カ月早かった。

考察

非定型 BSE 感染牛の脳内接種から臨床症状の発現までの期間および飼育困難になるまでの期間は、定型 BSE 感染牛と比較して約 8カ月短く、非定型 BSE (L 型) プリオンは、定型 BSE プリオンと比較して、牛に対する病原性が強いと考えられた。非定型 BSE 感染牛は、臨床症状の検査項目のいずれでも異常の見られない個体がいるなど、定型 BSE 感染牛と比較して臨床症状は不明瞭であった。非定型 BSE のための臨床症状の検査方法の検討が必要と考えられた。

非定型および定型 BSE 感染牛のいずれにおいても、

黒毛和種とホルスタイン種の間に臨床症状の差は見られなかった。

試験 2. 非定型 BSE 感染牛の PrP^{Sc} の体内分布

目的

非定型 BSE 感染牛の脳および末梢組織における PrP^{Sc} の蓄積時期と分布を明らかにする。

方法

試験 1 の 20 頭を用いた。非定型 BSE 感染牛のうち 2 頭（接種後 9カ月）および定型 BSE 感染牛のうち 5 頭は、臨床症状を発現する前に病理解剖を行った。病理解剖は、供試牛を鎮静および麻酔下で安楽殺し、各組織を採取した。採取した脳および末梢組織は、Hayashi ら [2] または Shimada ら [3] の方法により処理し、HRP 標識 T2マウスモノクローナル抗体を用いた WB 法により PrP^{Sc} を検出した。WB 法の結果の判定は、脳では、陽性対照であるマウススクレイピー脳 1.6mg 組織等量と比較し、発光強度が強い検体を ++、PrP^{Sc} を確認できるが発光強度がそれ以下の検体を +、PrP^{Sc} が認められなかった検体を - と判定した。また末梢組織においては、PrP^{Sc} を認めた検体を +、認められなかった検体を - と判定した。

結果

脳各部位の PrP^{Sc} の解析を行った結果、BSE 感染脳乳剤を接種したすべての牛の脳幹部から PrP^{Sc} が検出された (表 2)。非定型 BSE を接種し 9カ月後に解剖した牛では、脳幹部に加え、嗅脚、線条体および視床などの部位においても PrP^{Sc} が検出された。非定型 BSE 接種後 12カ月以降の牛では、脳のほぼ全域から PrP^{Sc} が検

表 2. 脳内接種による非定型および定型 BSE 感染牛の脳への PrP^{Sc} の蓄積

部位	牛 No. 品種 接種後 月数	非定型 BSE (L 型)										定型 BSE									
		A1	A2	A3	A4	A5	A6	A7	A8	A9	A10	C1	C2	C3	C4	C5	C6	C7	C8	C9	C10
		Hol	Hol	Hol	Hol	Hol	Hol	Hol	JB	JB	JB	Hol	Hol	Hol	Hol	Hol	Hol	Hol	JB	JB	JB
嗅脚	9	9	11	12	13	13	16	15	16	16	10	12	16	18	20	23	24	19	22	22	
前頭葉皮質	+	+	+	+	+	+	+	+	+	+	-	-	-	-	+	+	+	+	+	+	
前頭葉髄質	-	-	-	+	+	-	+	-	+	-	-	-	-	-	+	+	+	+	+	+	
線条体	+	+	-	+	+	+	+	+	+	+	-	-	+	+	+	+	+	+	+	+	
視床	+	+	+	+	+	+	+	+	+	+	-	-	-	+	+	+	+	+	+	+	
頭頂葉皮質	-	-	-	+	+	+	+	+	+	+	-	-	-	-	+	+	+	+	+	+	
頭頂葉髄質	-	-	-	+	-	-	+	-	-	-	-	-	-	-	+	+	+	+	+	+	
海馬	-	+	-	+	-	+	+	+	+	+	-	-	-	+	+	+	+	+	+	+	
小脳皮質	-	+	-	+	-	+	+	+	+	+	-	-	-	+	+	+	+	+	+	+	
小脳髄質	+	+	-	+	+	+	+	+	+	+	-	+	-	+	+	+	+	+	+	+	
中脳	+	+	+	+	+	+	+	+	+	+	+	+	+	+	+	+	+	+	+	+	
橋	+	+	+	+	+	+	+	+	+	+	+	+	+	+	+	+	+	+	+	+	
延髄門	+	+	+	+	+	+	+	+	+	+	+	+	+	+	+	+	+	+	+	+	

出された。定型 BSE を接種し10カ月後の牛では、PrP^{Sc} は脳幹部のみに検出され、接種後19カ月以降より、脳のほぼ全域から PrP^{Sc} が検出された。なお、非定型 BSE 感染牛では、WB 法により検出された PrP^{Sc} が、接種した BSE/JP24 と同じ糖鎖パターン、すなわち1糖鎖型優位を示した。

末梢組織では、接種後9、11および12カ月では頭部の末梢神経に、接種後13カ月で体幹にある星状神経節、接種後16カ月では腕神経叢など前肢の末梢神経に PrP^{Sc} が検出され、定型 BSE 感染牛と同様に、経過に伴い遠心性に PrP^{Sc} が伝播することが示唆された (表3)。また非定型 BSE 感染牛では、リンパ系組織等からは PrP^{Sc} は検出されず、定型 BSE 感染牛と同様の結果であった。

考察

非定型 BSE 感染牛では、定型 BSE 感染牛と比較して、脳において PrP^{Sc} が早期に蓄積し、早く伝播すると考えられた。試験1の結果と同様に、非定型 BSE の PrP^{Sc} は、定型 PrP^{Sc} と比較して病原性が強いと考えられた。非定型および定型 BSE 感染牛のいずれにおいても飼育困難になり病理解剖を行った時点では、PrP^{Sc} は脳のほぼ全域に分布し、分布する部位には差は見られなかった。また、脳における分布の部位には、黒毛和種とホルスタイン種に差は見られなかった。非定型 BSE 感染牛では、経過に伴い、遠心性に末梢神経組織に PrP^{Sc}

が伝播することが示唆された。また、リンパ系組織等からは PrP^{Sc} は検出されなかったことから、PrP^{Sc} が神経系組織以外へ伝播する可能性は低いと考えられた。これらのことは定型 BSE 感染牛と同様であった。Iwamaru ら^[4]は脳内接種の非定型 BSE 感染牛において、リンパ系組織、筋肉などからは PrP^{Sc} は検出されないことを報告しており、PrP^{Sc} が神経系組織以外へ伝播する可能性は低いと考えられた。非定型および定型 BSE の末梢組織への PrP^{Sc} の蓄積は、脳における PrP^{Sc} の蓄積時期の差を反映していると考えられた。

3. ま と め

BSE の発生状況について、OIE では定型と非定型を分けた報告を加盟国に求めているため、非定型 BSE の正確な発生数はまとめられていない。そこで、OIE、欧州食品安全機関 (European Food Safety Authority: EFSA) および各国の報告等から非定型 BSE の発生数を集計したところ、2015年4月末日現在までに98例が報告されている (表4)。前述のように世界各国が BSE 対策を実施した結果、定型 BSE の発生頭数は年々減少しているものの、非定型 BSE は、毎年5~10頭の範囲で報告されている。発生頭数が少ないことと各国のこれまでの BSE 検査の実施過程に違いがあることから、比較は容易にできないが、各国の非定型 BSE の発生頭数

表3. 非定型および定型 BSE 感染牛の末梢組織におけるプリオンの検出

牛 No. 接種後の月数	非定型 BSE							定型 BSE				
	A1	A2	A3	A4	A5	A6	A7	C3	C4	C5	C6	C7
	9	9	11	12	13	13	16	16	18	20	23	24
脊柱	脊髄神経節頸膨大部	-	-	-	+	+	+	+	+	-	+	+
	脊髄神経節腰膨大部	-	-	-	-	+	+	+	-	-	+	+
頭部	下垂体	-	-	+	-	-	+	+	+	-	+	+
	視神経	+	+	+	+	+	+	+	-	-	+	+
	網膜	-	-	+	+	+	+	+	+	+	+	+
	三叉神経節	-	+	+	-	+	+	+	+	+	+	+
体幹	交感神経幹	-	-	-	-	-	+	-	-	-	-	+
	星状神経節	+	-	-	-	-	+	+	-	-	+	+
	横隔神経	-	-	-	-	-	-	+	-	-	-	+
	腹腔神経節	-	-	-	-	-	-	-	-	-	-	-
四肢	腕神経叢	-	-	-	-	-	+	-	-	+	+	+
	肩甲上神経	-	-	-	-	-	+	-	-	-	-	+
	正中神経	-	-	-	-	-	-	-	-	+	+	+
	坐骨神経	-	-	-	-	-	+	-	-	-	+	-
リンパ	脾臓	-	-	-	-	-	-	-	-	-	-	-
	扁桃	-	-	-	-	-	-	-	-	-	-	-
	腸間膜リンパ節 (回盲部)	-	-	-	-	-	-	-	-	-	-	-
その他	耳下腺	-	-	-	-	-	-	-	-	-	-	-
	回腸	-	-	-	-	-	-	-	-	-	-	-
	最長腰筋	-	-	-	-	-	-	-	-	-	-	-
	腰長筋	-	-	-	-	-	-	-	-	-	-	-
	半腱様筋	-	-	-	-	-	-	-	-	-	-	-

+ : プリオン陽性、- : 陰性、空白 : 未実施

表4. 世界各国における定型および非定型 BSE 発生頭数

地域	国名	非定型 BSE				定型 BSE	牛の飼養頭数 (千頭) ¹⁾
		H 型	L 型	未分類	計		
欧州	オーストリア	1	2		3	5	1,977
	デンマーク	0	1		1	15	1,607
	フランス	16	16		32	994	19,006
	ドイツ	2	2		4	417	12,477
	アイルランド	5	0		5	1,650	6,754
	イタリア	0	5		5	139	6,252
	オランダ	1	3		4	84	3,879
	ポーランド	2	12		14	60	5,777
	ポルトガル	1	0		1	1,082	1,498
	スペイン	3	2		5	782	5,813
	スウェーデン	1	0		1	0	1,500
	イギリス	5	4		9	184,616	9,900
	ノルウェー	1	0		1	0	862
	ルーマニア	0	1		1	1	1,989
	スイス ²⁾	1	0	2	3	464	1,565
北米	アメリカ	2	1		3	0	90,769
	カナダ	1	1		2	19	12,305
南米	ブラジル	1	0	1	2	0	211,279
アジア	日本	0	2		2	34	4,172
その他の国 ³⁾		0	0		0	204	
計		43	52	3	98	190,566	

※頭数は OIE、EFSA および各国の報告等に基づき算出した。(2015年4月末日現在)

※1: 2012年(帝国書院)

※2: スイスはこの他に動物園での zebu 牛の非定型 BSE が報告されている。

※3: BSE 発生国のうち非定型 BSE の発生のない国: ベルギー、チェコ共和国、フィンランド、ギリシア、イスラエル、リヒテンシュタイン、ルクセンブルグ、スロバキア、スロベニア

と定型 BSE の発生頭数または牛の飼養頭数に強い関連性は見いだせない。また L 型と H 型の発生数の比較では、L 型 BSE の発生が多い国(イタリアやポーランド)や H 型の発生が多い国(アイルランド)があり、国ごとに異なる。また米国(カナダからの輸入牛を除く)、ブラジル、スウェーデン、ノルウェーのように、これまで定型 BSE の発生が見られず、非定型 BSE が報告される国もある。スイスでは、L 型と H 型のいずれとも異なる 2 例が報告されている。アジアにおいては、我が国の 8 例目(23カ月齢、BSE/JP08)^[5]と 24 例目(168カ月齢、BSE/JP24)の 2 例の BSE 患者がそれぞれ非定型 BSE (L 型)と報告されている。

BSE/JP08は、生後23カ月齢でと殺された去勢牛で、採取された脳を牛 PrP 遺伝子組換えマウスに脳内接種しても感染が成立しない程 PrP^{Sc} の蓄積が極微量であった^[6]。BSE/JP24は、カナダ、ドイツおよびフランスで発生した L 型 BSE と比較し、PK で消化した PrP^{Sc} の分子量や糖鎖パターンがほぼ同様である。また、それぞれの L 型 BSE プリオンを牛 PrP 遺伝子組換えマウスに脳内接種により継代したところ、3 回目の継代では約145日に集束するなど、BSE/JP24は、欧州の L 型 BSE と

同様の性質を持つことが明らかとなっている^[7]。H 型 BSE の国内発生はこれまでにないが、カナダで発生した H 型 BSE プリオンの脳内接種による牛への感染試験によれば、接種から終末までの期間が 560 ± 47 日と定型 BSE よりも短く、L 型 BSE よりも長い^[8,9]。

定型 BSE は 3~8 歳の牛に多く発見されたが、非定型 BSE は国内 8 例目など一部を除いてほとんど 8 歳以上の高齢牛で見つかっている。しかし脳内接種による非定型 BSE 感染牛では、L 型および H 型共に、PrP^{Sc} の蓄積が早く、臨床症状の発現や飼育困難になるまでの時期も定型 BSE 感染牛と比較して早かった。また非定型 BSE プリオンの牛への経口投与試験については、これまでに経口投与牛の中枢神経組織への PrP^{Sc} の蓄積を確認した報告はない。非定型 BSE の感染・発症機序は未だ明らかではないが、1) 定型 BSE と同様に肉骨粉等のプリオンが混入した飼料を摂取することにより感染する、2) 飼料摂取とは関係なく孤発性に発生する、などが考えられる。1) の場合、飼料の摂取から中枢神経系への移行に定型 BSE 以上の時間を要するものの脳での増幅・蓄積は早いことが考えられる。また 2) の場合では、加齢による細胞レベルの蛋白質代謝異常に起因する

ことなどが考えられる。

以上のように、非定型 BSE には不明な点が未だ多くあり、孤発性であることが示唆されている。定型 BSE の発生数や OIE の BSE リスクステータスなどを問わず、極めて稀であるものの発生することが懸念される。非定型 BSE の発生リスクのある高齢牛は必ず BSE 検査が行われることや特定危険部位は全て除去されることから、ヒトへの感染リスクは排除され、畜産物の安全は確保されている。しかしながら、今後、科学的知見に基づいた非定型 BSE のリスク評価と効率的なリスク管理を行うため、非定型 BSE の発生要因や PrP^{Sc} の蓄積機序を明らかにすることは重要であり、ヒトの孤発性 CJD や羊のスクレイピー、シカの CWD を含め、プリオン病の感染・発症機序解明にさらに知見の集積が必要である。

現在、道総研畜産試験場では、脳内接種による非定型 BSE 感染牛を用いた試験を継続しており、これまでに、歩様と行動量の変化から、非定型 BSE 感染牛の臨床症状を把握できる可能性を示した。また、非定型 BSE の感染初期における PrP^{Sc} の経時的な蓄積量の変化を調査する試験を実施中である。さらに、ヒトや牛で加齢に伴い脳内の酵素活性が低下することで不溶性タンパク質が増加すると報告されることから、高齢牛の脳内不溶性タンパク質と非定型 BSE の関連性を調査する試験を実施している。これらの研究成果により、今後の BSE のリスク評価と効果的な BSE リスク管理措置の策定に必要なデータを提供することを目指している。

引用文献

- [1] Hagiwara K, Yamakawa Y, Sato Y, Nakamura Y, Tobiume M, Shinagawa M, Sata T : Accumulation of mono-glycosylated form-rich, plaque-forming PrP^{Sc} in the second atypical bovine spongiform encephalopathy case in Japan, *Jpn J Infect Dis*, 60, 305-308 (2007)
- [2] Hayashi H, Takata M, Iwamaru Y, Ushiki Y, Kimura KM, Tagawa Y, Shinagawa M, Yokoyama T : Effect of tissue deterioration on postmortem BSE diagnosis by immunobiochemical detection of an abnormal isoform of prion protein, *J Vet Med Sci*, 66, 515-520 (2004).
- [3] Shimada K, Hayashi HK, Ookubo Y, Iwamaru Y, Imamura M, Takata M, Schmerr MJ, Shinagawa M, Yokoyama T : Rapid PrP(Sc) detection in lymphoid tissue and application to scrapie surveillance of fallen stock in Japan : variable PrP(Sc) accumulation in palatal tonsil in natural scrapie, *Microbiol Immunol*, 49, 801-804 (2005)
- [4] Iwamaru Y, Imamura M, Matsuura Y, Masujin K, Shimizu Y, Shu Y, Kurachi M, Kasai K, Murayama Y, Fukuda S, Onoe S, Hagiwara K, Yamakawa Y, Sata T, Mohri S, Okada H, Yokoyama T : Accumulation of L-type bovine prions in peripheral nerve tissues, *Emerg Infect Dis*, 16, 1151-1154 (2010)
- [5] Yamakawa Y, Hagiwara K, Nohtomi K, Nakamura Y, Nishijima M, Higuchi Y, Sato Y, Sata T : Atypical proteinase K-resistant prion protein (PrPres) observed in an apparently healthy 23-month-old Holstein/Friesian steer, *Jpn J Infect Dis*, 56, 221-222 (2003).
- [6] Yokoyama T, Masujin K, Yamakawa Y, Sata T, Murayama Y, Shu Y, Okada H, Mohri S, Shinagawa M : Experimental transmission of two young and one suspended bovine spongiform encephalopathy (BSE) cases to bovinized transgenic mice, *Jpn J Infect Dis*, 60, 317-320 (2007).
- [7] Masujin K, Miwa R, Okada H, Mohri S, Yokoyama T : Comparative analysis of Japanese and foreign L-type BSE prions, *Prion*, 6, 89-93 (2012)
- [8] Okada H, Masujin K, Iwamaru Y, Imamura M, Matsuura Y, Mohri S, Czub S, Yokoyama T : Experimental transmission of h-type bovine spongiform encephalopathy to bovinized transgenic mice. *Vet Pathol*, 48, 942-947 (2011)
- [9] Fukuda S, Iwamaru Y, Imamura M, Masujin K, Shimizu Y, Matsuura Y, Shu Y, Kurachi M, Kasai K, Murayama Y, Onoe S, Hagiwara K, Sata T, Mohri S, Yokoyama T, Okada H : Intraspecies transmission of L-type-like Bovine Spongiform Encephalopathy detected in Japan, *Microbiol Immunol*, 53, 704-707 (2009)



L-Arginine ethylester enhances *in vitro* amplification of PrP^{Sc} in macaques with atypical L-type bovine spongiform encephalopathy and enables presymptomatic detection of PrP^{Sc} in the bodily fluids



Y. Murayama ^{a, *}, F. Ono ^b, N. Shimosaki ^a, H. Shibata ^c

^a Influenza Prion Disease Research Center, National Institute of Animal Health, Tsukuba, Ibaraki, Japan

^b Chiba Institute of Science Faculty of Risk and Crisis Management, Choshi, Chiba, Japan

^c Tsukuba Primate Research Center, National Institutes of Biomedical Innovation, Health and Nutrition, Tsukuba, Ibaraki, Japan

ARTICLE INFO

Article history:

Received 13 January 2016

Accepted 17 January 2016

Available online 21 January 2016

Keywords:

Atypical bovine spongiform encephalopathy

Protein misfolding cyclic amplification

Arginine ethylester

Bodily fluid

Nonhuman primate

ABSTRACT

Protease-resistant, misfolded isoforms (PrP^{Sc}) of a normal cellular prion protein (PrP^C) in the bodily fluids, including blood, urine, and saliva, are expected to be useful diagnostic markers of prion diseases, and nonhuman primate models are suited for performing valid diagnostic tests for human Creutzfeldt-Jakob disease (CJD). We developed an effective amplification method for PrP^{Sc} derived from macaques infected with the atypical L-type bovine spongiform encephalopathy (L-BSE) prion by using mouse brain homogenate as a substrate in the presence of polyanions and L-arginine ethylester. This method was highly sensitive and detected PrP^{Sc} in infected brain homogenate diluted up to 10¹⁰ by sequential amplification. This method in combination with PrP^{Sc} precipitation by sodium phosphotungstic acid is capable of amplifying very small amounts of PrP^{Sc} contained in the cerebrospinal fluid (CSF), saliva, urine, and plasma of macaques that have been intracerebrally inoculated with the L-BSE prion. Furthermore, PrP^{Sc} was detectable in the saliva or urine samples as well as CSF samples obtained at the preclinical phases of the disease. Thus, our novel method may be useful for furthering the understanding of bodily fluid leakage of PrP^{Sc} in nonhuman primate models.

© 2016 Elsevier Inc. All rights reserved.

1. Introduction

Prion diseases are characterized by the pronounced accumulation of the misfolded isoforms (PrP^{Sc}) of a normal cellular protein (PrP^C) in the central nervous system [1,2]. PrP^{Sc} exhibit several peculiar pathophysiological characteristics: They are rich in beta-sheet structures [3,4], resistant to protease digestion and various inactivating treatments [5], and considered to be the infectious agents of fatal neurodegenerative diseases in both humans and animals [6].

Abbreviations: PrP^{Sc}, Pathogenic form of prion protein; PrP^C, cellular prion protein; CJD, Creutzfeldt–Jakob disease; BSE, Bovine spongiform encephalopathy; CSF, cerebrospinal fluid; PMCA, protein misfolding cyclic amplification; LAE, L-arginine ethylester; NaPTA, sodium phosphotungstic acid; Poly-A, polyadenylic acid potassium salt; PPS, sodium polyphosphate; PK, proteinase K; WB, western blotting.

* Corresponding author. Influenza/Prion Disease Research Center, National Institute of Animal Health, 3-1-5 Kannondai, Tsukuba, Ibaraki 305-0856, Japan.

E-mail address: ymura@affrc.go.jp (Y. Murayama).

Bovine spongiform encephalopathy (BSE) is an emerging prion disease that first appeared in the United Kingdom [7]. Since variant Creutzfeldt-Jakob disease (vCJD), a human neurodegenerative disease, is suspected to be attributable to infectious agents associated with BSE [8–10], infected cattle should be identified and eradicated as part of preventive health management. Several etiological studies of BSE prion-infected cattle have identified BSE prion types distinct from that of the classical BSE (C-BSE) in many countries, although these are rare. These atypical BSEs have been classified as H- or L-types according to the molecular weight of the non-glycosylated band derived from the protease-resistant PrP^{Sc} core [11]. These new types of BSE prions are transmissible to transgenic mice expressing human prion protein [12,13] and to nonhuman primates [14], and infected animals develop the diseases after a shorter incubation period than that observed for animals with C-BSE. In addition, L-BSE prion was transmissible to nonhuman primates by oral administration [15]. Therefore, identification of L-BSE-affected animals is attracting considerable attention of for not only animal hygiene management, but also from the human public health perspective.

Nonhuman primate models are well suited for validating diagnostics for human prion diseases, because C-BSE in macaques resembled vCJD in humans in many aspects, including the pathological features of the brain tissue, biochemical characteristics of the PrP^{Sc} glycoform profile, and PrP^{Sc} distribution in the peripheral tissues [16]. In order to effectively prevent the spread of prion diseases, it is necessary to detect PrP^{Sc} as soon after infection as possible. It is now possible to amplify PrP^{Sc} *in vitro* using the protein misfolding cyclic amplification (PMCA) technique [17]. PMCA has been applied to the detection of bovine C-BSE PrP^{Sc} in cattle [18] and macaques [19]. In our previous study, we demonstrated the PrP^{Sc} was detectable in the bodily fluids such as cerebrospinal fluid (CSF) and blood as well as in various tissues of C-BSE prion-infected macaques. However, the PMCA method developed for macaque C-BSE PrP^{Sc} was not effective for amplification of macaque λ -BSE PrP^{Sc}.

In this study, we developed a highly efficient PMCA method suitable for amplification of cynomolgus macaque λ -BSE PrP^{Sc}. We further investigated PrP^{Sc} levels in the bodily fluids during the period from the latent to terminal stages of the disease.

2. Materials and methods

2.1. λ -BSE prion-infected macaques

The study on nonhuman primates was conducted according to the Rules for Animal Care and Management of the Tsukuba Primate Research Center [20] and the Guiding Principles for Animal Experiments Using Nonhuman Primates formulated by the Primate Society of Japan [21]. The cynomolgus macaques (*Macaca fascicularis*) used in this study originated from Malaysia, and were bred at the Tsukuba Primate Research Center of the National Institutes of Biomedical Innovation, Health and Nutrition. Transmission experiments were approved by the Animal Welfare and Animal Care and Use Committee (approval ID: DS23-41) and Animal Ethics Biosafety Committee (approval ID: BSL3-R-10.04, BSL3-R-11.09, and BSL3-R-12.07) of the National Institutes of Biomedical Innovation, Health and Nutrition. The brain homogenate (200 μ l of a 10% brain homogenate) derived from an λ -BSE prion-infected macaque (#15) [22] was intracerebrally administered to two male macaques (#22 and #23) that were 1.4 years of age. These macaques were homozygous for codon 129 methionine/methionine (M/M) and 219 glutamic acid/glutamic acid (E/E). The second passage macaques were housed in biosafety level three animal rooms, and their clinical status was monitored daily. After 23–24 months, the animals were euthanized by anesthesia overdose following evidence of progressive neurologic dysfunction such as tremor and paralysis. Two healthy macaques were used as uninfected controls in the PMCA assay of bodily fluids.

2.2. Preparation of bodily fluid samples

The CSF, saliva, urine, and blood samples were collected from two macaques under anesthesia at intervals of approximately 3–7.5 months after inoculation. The bodily fluids, except saliva, were also collected 14–15 days before inoculation. The heparinized blood samples were centrifuged at 1500 g for 15 min, and the plasma fraction was recovered. These bodily fluids were stored in small aliquots at -80°C . Before use in PMCA analysis, each sample was concentrated by precipitation with sodium phosphotungstic acid (NaPTA) [23]. Briefly, the samples were thawed and then centrifuged at 600 g for 1 min to remove large aggregates and cell debris, and the supernatants were used for precipitation. The supernatants (1000 μ l from urine and plasma samples; 300–600 μ l from CSF samples, and 400–1000 μ l from saliva samples) were mixed with 4% NaPTA–170 mM MgCl₂–10 mM Tris (hydroxymethyl)

aminomethane (pH7.5) in a 15:1 ratio. The mixtures were incubated at 37°C for 18 h with continuous agitation. The samples were then centrifuged at 20000 g for 30 min at 25°C . The supernatants were completely removed, and the precipitates were stored at -80°C until analysis.

2.3. Preparation of PrP^C substrates

In our previous study, we found that cynomolgus macaque C-BSE PrP^{Sc} effectively converted mouse PrP^C to a proteinase K (PK)-resistant form [19]. Therefore, we used mouse brain homogenates as PrP^C substrate in the present study. To avoid contamination, normal brain homogenates were prepared in a laboratory in which infected materials had never been handled. Briefly, brains of wild-type mice (ICR) were homogenized in the presence of a complete protease inhibitor cocktail (Roche Diagnostics, Mannheim, Germany) at a 10% (w/v) concentration in PBS containing 1% Triton X-100 and 4 mM EDTA. The homogenates were then centrifuged at 4500 g for 5 min, and the supernatant was used as the PrP^C substrate as previously described [19]. Heparin sodium salt (Santa Cruz Biotechnology, Texas), polyadenylic acid potassium salt (Poly-A, Sigma–Aldrich, Missouri), and sodium polyphosphate (PPS, Sigma–Aldrich) were dissolved in PBS and added to the PrP^C substrate at final concentrations of 100 $\mu\text{g}/\text{ml}$, 100 $\mu\text{g}/\text{ml}$, and 0.05%, respectively. Optimal concentration of each polyanion was determined in our preliminary experiments.

For efficient amplification of λ -BSE PrP^{Sc}, λ -arginine ethylester dihydrochloride (LAE, Sigma–Aldrich) was used as an additive to promote PMCA reaction. LAE was dissolved in distilled water at 2 M, and pH was adjusted to 7.0 by adding 1 N sodium hydroxide aqueous solution. To estimate the optimal concentration of LAE, the solution (final concentrations of 0–100 mM LAE) was added to the PrP^C substrate containing the polyanion cocktail.

2.4. PMCA and western blotting

For the amplification of brain PrP^{Sc}, the λ -BSE prion-infected brain homogenate of macaque #14 [22] was serially diluted from 10^{-3} to 10^{-11} with the mouse PrP^C substrate in an electron beam-irradiated 8-strip polystyrene tube (total volume, 80 μ l) [18]. Amplification was carried out with an Elestein 070-CPR (Elekon Science Corporation, Chiba, Japan). Serial PMCA was performed in quadruplicate using the four-step amplification program with 40 cycles of sonication in which a 15-s oscillation and subsequent incubations at 31°C for 1 h were repeated 10 times; 15-s oscillation and subsequent incubations at 33°C for 1 h were repeated 10 times; an intermittent oscillation (3-s pulse oscillation was repeated five times at 0.1-s intervals) and subsequent incubations at 35°C for 1 h were repeated 10 times; and intermittent oscillations (3-s pulse oscillation was repeated five times at 0.1-s intervals) and subsequent incubation at 37°C for 1 h were repeated 10 times. The amplified product obtained after the first round of amplification was diluted 1:5 with the PrP^C substrate, and a second round of amplification was performed. This process was repeated for a maximum of seven times. After each round of amplification, the amplified products were digested with proteinase K (PK, 100 $\mu\text{g}/\text{ml}$) and incubated at 37°C for 1 h. The digested materials were separated by SDS-PAGE and analyzed by western blotting (WB) as previously described [24].

For amplifying PrP^{Sc} in bodily fluids from λ -BSE prion-inoculated macaques, the frozen precipitates were dissolved in 20 μ l of PBS and used as a seed. The concentration rates were 50 in the urine and plasma samples, 15–30 in the CSF samples, and 20–50 in the saliva samples. The mouse PrP^C substrate containing polyanion cocktail (100 $\mu\text{g}/\text{ml}$ heparin, 100 $\mu\text{g}/\text{ml}$ poly-A and 0.05% PPS) and

12.5 mM of LAE was mixed with a 1/10 volume (8 μ l) of concentrated bodily fluids in 8-strip polystyrene tubes (total volume 80 μ l). Serial PMCA was then performed in duplicate using the amplification protocol described above.

3. Results

3.1. Effect of *L*-arginine ethylester on amplification of *L*-BSE PrP^{Sc}

We examined the amplification efficiency of PMCA, using the mouse PrP^C substrate and brain homogenate of *L*-BSE prion-infected macaque as the PrP^{Sc} seed. In contrast to the amplification of C-BSE PrP^{Sc}, efficient amplification was not achieved even in the presence of polyanions such as Poly-A [25], sulfated dextran [18], heparin [26], and PPS. PPS was found to be an effective agent for amplification of macaque C-BSE PrP^{Sc} in our screening of polyanions (unpublished work). The possible additive effects by the combined use of these polyanions were also examined, but various combinations of polyanions were not quite effective for amplification of *L*-BSE PrP^{Sc}. For example, in the presence of polyanion cocktail containing heparin, Poly-A and PPS, only weak PrP^{Sc} signal was detected in the brain homogenate diluted to 10⁻³ even after two rounds of amplification (Fig. 1).

Other factors affecting PMCA reaction, such as ultrasonic condition and chelating agent dependency, were also evaluated, but none of the changes examined led to a significant improvement in amplification efficiency. We further investigated the validity of protein denaturants and stabilizing agents, because the amplification deficiency of *L*-BSE PrP^{Sc} may be due to folded structures that were not suitable for *in vitro* amplification by sonication. Among these reagents, we found that LAE, an arginine derivative known as a powerful inhibitor for protein aggregation [27], is the most effective reagent for amplification of *L*-BSE PrP^{Sc}. Although LAE alone did not work well enough to induce amplification of *L*-BSE PrP^{Sc} (data not shown), it strongly promoted the amplification of *L*-BSE PrP^{Sc} in the range of 12.5–25 mM in the presence of the polyanion cocktail (Fig. 1). In other words, amplification of PrP^{Sc} was

achieved in samples diluted up to 10⁻⁵ after one round of amplification, and the PrP^{Sc} signals were significantly intensified at the next round of amplification. However, LAE had little or no effect on amplification at higher molarity (50–100 mM).

3.2. Detection sensitivity of *L*-BSE PrP^{Sc}

On the basis of our preliminary experiments, the optimal concentration of LAE was estimated to be 12.5 mM; therefore, we used 12.5 mM LAE for subsequent experiments. In addition, we confirmed that the most effective amplification was achieved by the combined use of three polyanions, heparin (100 μ g/ml), Poly-A (100 μ g/ml), and PPS (0.05%), in the presence of 12.5 mM LAE. To determine the detection limit of our novel PMCA technique, 10% brain homogenates of an experimentally infected macaque #14 was serially diluted with the mouse PrP^C substrate containing the polyanion cocktail and LAE and amplified. PrP^{Sc} signal was detected in all the quadruplicate samples diluted up to 10⁻⁹ after five rounds of amplification (Fig. 2). Moreover, PrP^{Sc} signal was detected in one of the quadruplicate samples diluted to 10⁻¹⁰ after six or seven rounds of amplification. However, no typical PrP^{Sc} signal was detected in the more extreme dilution, even after eight rounds of amplification. The generation of spontaneous PrP^{Sc} was not observed in the quadruplicate samples that contained only the PrP^C substrate following eight rounds of amplification.

3.3. PrP^{Sc} levels in bodily fluids

Neurological clinical signs of the disease, such as tremors and paralysis, appeared in the macaques after latent periods of 486 (#22) and 407 (#23) days. The incubation periods were shorter than those of the primary passaged macaques [22], but the neurological symptoms slowly progressed in these secondary passage macaques.

The presence or absence of PrP^{Sc} in the bodily fluids is summarized in Fig. 3 on the basis of the detection results obtained after eight rounds of amplification (Fig. 4A). There were differences in the levels of PrP^{Sc} in these bodily fluids, and PrP^{Sc} signals were detectable after three–eight rounds of amplification. The complete sets of amplification results are given in the supplementary figures (Fig. S1 for #22, Fig. S2 for #23). After the onset of clinical signs, the presence of PrP^{Sc} in the CSF, saliva, and urine samples was confirmed in both macaques. Furthermore, PrP^{Sc} was also detectable in the CSF samples collected 94–91 days before disease onset. The significant finding is that salivary PrP^{Sc} were detected in the sample collected 150 days before disease onset in macaque #22. Although the time of positive conversion for salivary PrP^{Sc} in this macaque was not clear, PrP^{Sc} was continuously detected in one of the duplicate samples until the dissection. In addition, urinary PrP^{Sc} was detected in the sample obtained 92 days before disease onset in macaque #23. With regard to plasma samples, one of the duplicate samples collected 111 days after disease onset became positive for PrP^{Sc} after four rounds of amplification in macaque #23. However, no PrP^{Sc} was detected in any of the plasma samples collected during the experimental period in macaque #22. No typical PrP^{Sc} signal was observed in samples that contained only the PrP^C substrate (Ns) or samples that contained concentrated bodily fluids from normal macaques (N1 and N2, Fig. 4B and Fig. S3).

4. Discussion

In this study, we developed an ultra-efficient PMCA technique for amplifying PrP^{Sc} derived from *L*-BSE prion-infected cynomolgus macaques by using mouse brain homogenates with polyanions and

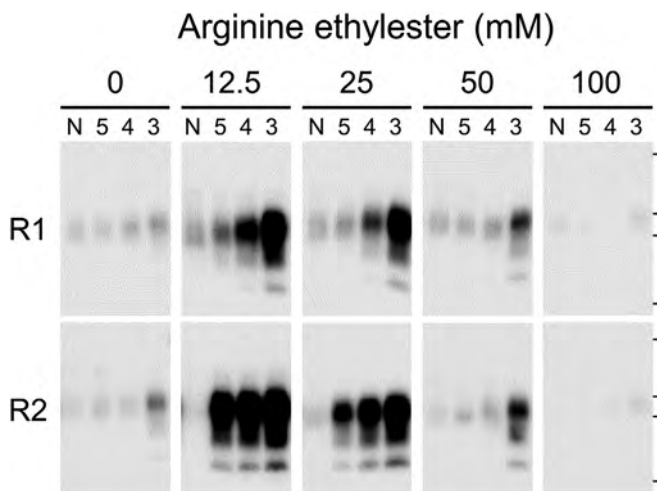


Fig. 1. Amplification of macaque *L*-BSE PrP^{Sc} using normal mouse brain homogenates. The PrP^{Sc} seed (10% brain homogenate of *L*-BSE-affected cynomolgus macaque #14) was diluted to 10⁻³ (3) to 10⁻⁵ (5) in normal mouse brain homogenates containing 100 μ g/ml heparin, 100 μ g/ml Poly-A and 0.05% PPS. The diluted samples were amplified in the presence (12.5–100 mM) or absence (0) of LAE. The amplified samples were analyzed after each round of amplification (R1–R2) by WB after PK digestion. “N” designates unseeded control samples, which were treated similarly, but containing only the PrP^C substrate. Horizontal lines indicate the positions of molecular weight markers corresponding to 37, 25, 20, and 15 kDa.

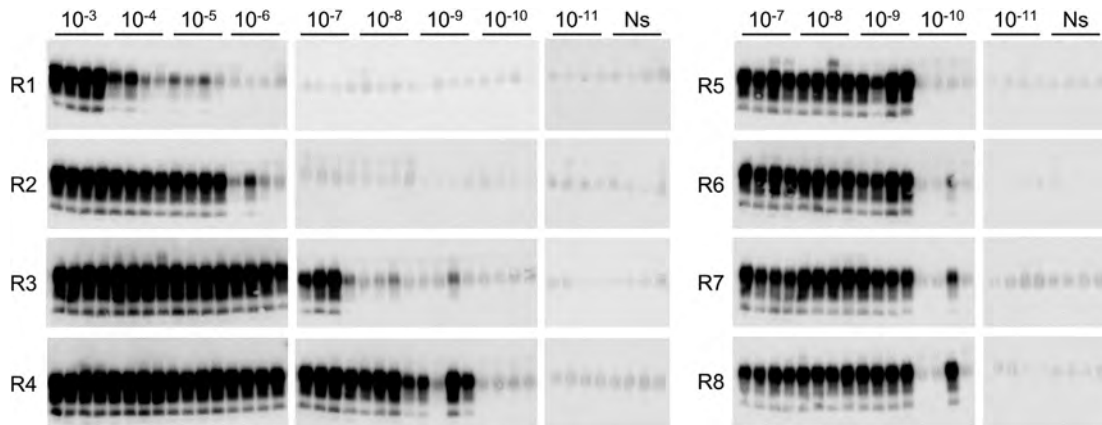


Fig. 2. Detection sensitivity for cynomolgus macaque 1-BSE PrP^{Sc}. The PrP^{Sc} seed was diluted to 10⁻³–10⁻¹¹ with the PrP^C substrate (10% normal mouse brain homogenate), and the quadruplicate samples were serially amplified in the presence of the polyanion cocktail and 12.5 mM LAE. The amplified samples were analyzed after each round of amplification (R1–R8) by WB after PK digestion. The samples diluted to 10⁻³–10⁻⁶ were not amplified after five rounds of amplification because sufficient amount of PrP^{Sc} was produced in all the quadruplicate samples. “Ns” designates unseeded control samples, which were treated similarly, but containing only the PrP^C substrate.

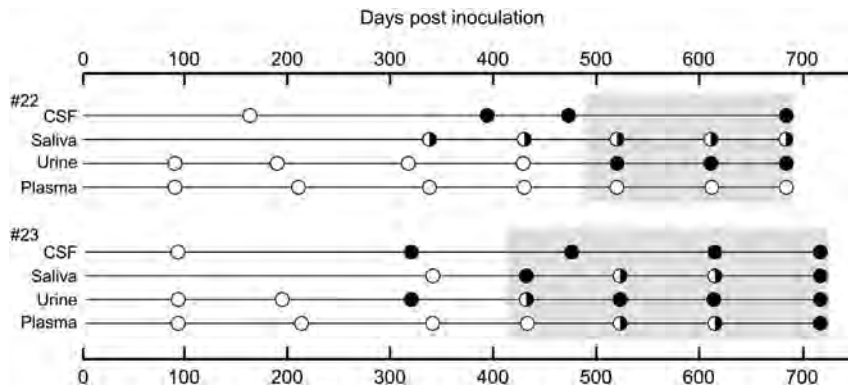


Fig. 3. Schematic illustration for the appearance of PrP^{Sc} in the bodily fluids of two 1-BSE prion-infected macaques. After intracerebral inoculation, the presence of PrP^{Sc} in CSF, saliva, urine and plasma samples was examined by serial PMCA during the asymptomatic (circles with white back ground) and clinical stages (circles with gray back ground). Positive ratio of duplicate samples after eight rounds of amplification was shown as open circle (0%), closed semicircle (50%) and closed circle (100%).

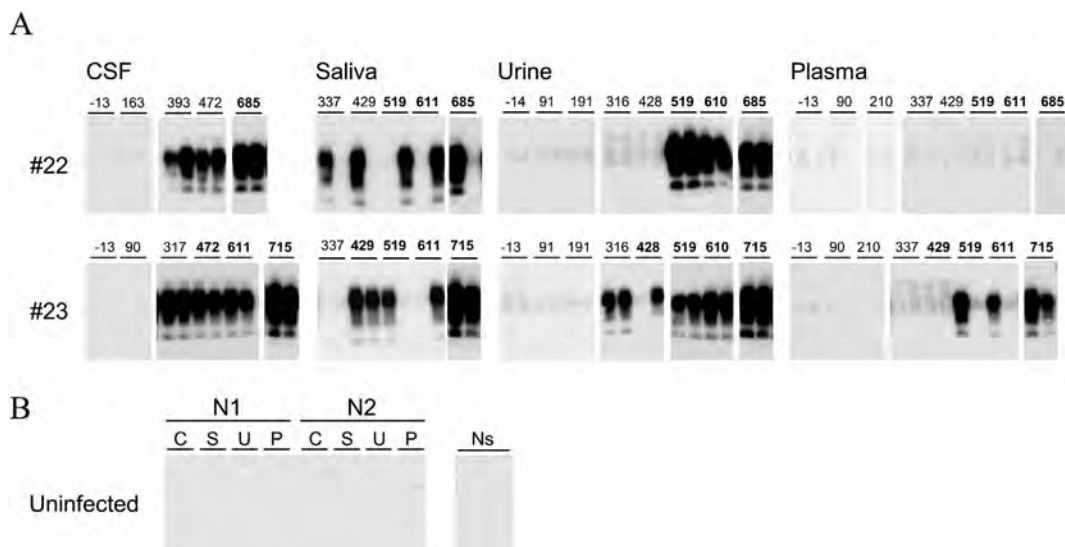


Fig. 4. Detection of PrP^{Sc} in the bodily fluids of 1-BSE prion-infected macaques. CSF, saliva, urine, and plasma samples were collected at several points after intracerebral inoculation. (A) Duplicate samples from two 1-BSE prion-infected macaques (#22 and #23) were analyzed by WB following digestion with PK. The results of final round (R8) of amplification are shown. The complete set of results of each round of amplification (R1–R8) is given in [Supplementary figures](#). (B) PrP^{Sc} was also evaluated in bodily fluids (C, CSF; S, saliva; U, urine; P, plasma) from uninfected control macaques (N1 and N2). Numerals on the blots represent days post inoculation (dpi), and dpi written in boldface represent the clinical stage of the disease. Negative values represent days before inoculation. Ns: No seed samples.

LAE as a PrP^C substrate. We first proved the presence of PrP^{Sc} in the bodily fluids, including CSF, saliva, urine, and plasma, of the L-BSE-infected macaques by PMCA and then showed that the L-BSE PrP^{Sc} was detectable in saliva and urine samples during the pre-clinical phase of the disease after intracerebral inoculation.

To establish an efficient method to amplify PrP^{Sc} derived from animals with L-BSE, we examined the effects of various additives on the PMCA reaction: protein denaturants or stabilizers such as guanidine, urea, polyamines (spermine and spermidine), high-molecular weight compounds (dextran and polyethylene glycol), trehalose, and L-arginine and its derivatives. Among these additives, LAE was the most effective in enhancing the *in vitro* amplification of macaque L-BSE PrP^{Sc} in the presence of polyanions such as heparin, Poly-A, and PPS. L-arginine was not effective enough whereas an L-arginine methylester compound significantly, but less effectively than LAE, induced amplification of L-BSE PrP^{Sc} in combination with the polyanion cocktail (unpublished work). Therefore, the introduced hydrophobic end on the carboxyl group may play an important role in the amplification of L-BSE PrP^{Sc}.

The functional mechanism of LAE is thought to be different from that of polyanions, which may act as cofactors required to facilitate the propagation of PrP^{Sc} by stabilizing interactions between PrP^{Sc} and PrP^C [18]. L-Arginine enhances the solubility of aggregated molecules, thereby increasing refolding by decreasing aggregation [28,29]. Furthermore, LAE prevented heat-induced aggregation of lysosome more effectively than arginine [27]. The known effect of LAE and the finding that LAE enhanced PrP^{Sc} formation are seemingly contradictory with each other. Hydrophobic side chains of prion protein, which gather inside of a normal PrP^C molecule, become exposed outside of PrP^{Sc} by structural conversion, leading to clustering to form PrP^{Sc} aggregates. LAE may bind preferentially to these misfolded molecules by the hydrophobic ethyl group, and may accelerate the rate of structural conversion by acting as a regulatory factor that prevents excessive aggregation of existing PrP^{Sc} molecules. Further study is necessary to clarify the precise mechanism of LAE in the amplification of L-BSE PrP^{Sc}.

The PMCA technique has been used to identify PrP^{Sc} in a variety of bodily fluids in prion-infected animals and humans [30]. In particular, several reports have described the successful detection of PrP^{Sc} in blood or urine of humans with vCJD [31–33]. In addition to urine, the present study revealed the existence of PrP^{Sc} in the saliva of primates. Salivary or urinary PrP^{Sc} were detected in the samples collected before disease onset in the macaques. Although a limited number of macaques were analyzed in this study, the findings indicate that a non-invasive test for early diagnosis may be developed using this nonhuman primate model. We are now conducting experiments analyzing oral transmission of the L-BSE prion from L-BSE prion-infected cattle. The method developed in this study may be useful in furthering the understanding of leakage of PrP^{Sc} into bodily fluids in nonhuman primate models.

Author contributions

F.O., and H.S conceived and designed the experiments. Y.M., F.O., N.S., and H.S. performed the experiments. Y.M. wrote the manuscript.

Competing financial interests

The authors declare no competing financial interests.

Acknowledgments

We would like to thank Dr. Kenichi Hagiwara of the National Institute of Infectious Diseases for giving us BSE prion-infected

animal materials. We also thank the contributions of the animal caretakers. This study was supported by a grant for BSE research from the Ministry of Health, Labor and Welfare of Japan (H23-Shokuhin-Ippan-005).

Transparency document

Transparency document related to this article can be found online at <http://dx.doi.org/10.1016/j.bbrc.2016.01.105>.

Appendix A. Supplementary data

Supplementary data related to this article can be found at <http://dx.doi.org/10.1016/j.bbrc.2016.01.105>.

References

- [1] S.B. Prusiner, Molecular biology of prion disease, *Science* 252 (1991) 1515–1522.
- [2] S.B. Prusiner, Prions, *Proc. Natl. Acad. Sci. U. S. A.* 95 (1998) 13363–13383.
- [3] B.W. Caughey, A. Dong, K.S. Bhat, et al., Secondary structure analysis of the scrapie-associated protein PrP 27–30 in water by infrared spectroscopy, *Biochemistry* 30 (1991) 7672–7680.
- [4] K.M. Pan, M. Baldwin, J. Nguyen, et al., Conversion of α -helices into β -sheets features in the formation of the scrapie prion proteins, *Proc. Natl. Acad. Sci. U. S. A.* 90 (1993) 10962–10966.
- [5] A. Sakudo, Y. Ano, T. Onodera, et al., Fundamentals of prions and their inactivation (review), *Int. J. Mol. Med.* 27 (2011) 483–489.
- [6] J. Collinge, Prion diseases of humans and animals: their causes and molecular basis, *Annu. Rev. Neurosci.* 24 (2001) 519–550.
- [7] G.A. Wells, A.C. Scott, C.T. Johnson, et al., A novel progressive spongiform encephalopathy in cattle, *Vet. Rec.* 121 (1987) 419–420.
- [8] R.G. Will, J.W. Ironside, M. Zeidler, et al., A new variant of Creutzfeldt-Jakob disease in the UK, *Lancet* 347 (1996) 921–925.
- [9] A.F. Hill, M. Desbruslais, S. Joiner, et al., The same prion strain causes vCJD and BSE, *Nature* 389 (1997) 448–450.
- [10] J.W. Ironside, Variant Creutzfeldt-Jakob disease, *Haemophilia* 16 (2010) S5175–S5180.
- [11] T. Yokoyama, Bovine spongiform encephalopathy and scrapie, in: A. Skudo, T. Onodera (Eds.), *Prions: Current Progress in Advanced Research*, Caister Academic Press, UK, 2013, pp. 93–110.
- [12] V. Béringue, L. Herzog, F. Reine, et al., Transmission of atypical bovine prions to mice transgenic for human prion protein, *Emerg. Infect. Dis.* 14 (2008) 1898–1901.
- [13] Q. Kong, M. Zheng, C. Casalone, et al., Evaluation of the human transmission risk of an atypical bovine spongiform encephalopathy prion strain, *J. Virol.* 82 (2008) 3697–3701.
- [14] E.E. Comoy, C. Casalone, N. Lescoutra-Etcheagaray, et al., Atypical BSE (BASE) transmitted from asymptomatic aging cattle to a primate, *PLoS One* 3 (2008) e3017.
- [15] N. Mestre-Francés, S. Nicot, S. Rouland, et al., Oral transmission of L-type bovine spongiform encephalopathy in primate model, *Emerg. Infect. Dis.* 18 (2012) 142–145.
- [16] S. Krasemann, B. Sikorska, P.P. Liberski, et al., Non-human primates in prion research, *Folia Neuropathol.* 50 (2012) 57–67.
- [17] M.A. Barria, D. Gonzalez-Romero, C. Soto, Cyclic amplification of prion protein misfolding, *Methods Mol. Biol.* 849 (2012) 199–212.
- [18] Y. Murayama, M. Yoshioka, K. Masujin, et al., Sulfated dextrans enhance *in vitro* amplification of bovine spongiform encephalopathy PrP^{Sc} and enable ultrasensitive detection of bovine PrP^{Sc}, *PLoS One* 5 (2010) e13152.
- [19] Y. Murayama, K. Masujin, M. Imamura, et al., Ultrasensitive detection of PrP^{Sc} in the cerebrospinal fluid and blood of macaques infected with bovine spongiform encephalopathy prion, *J. Gen. Virol.* 95 (2014) 2576–2588.
- [20] S. Honjo, The Japan Tsukuba Primate Center for Medical Science: an outline, *J. Med. Primatol.* 14 (1985) 75–89.
- [21] Primate Society of Japan, Guiding principles for animal experiments using nonhuman primates, *Primate Res.* 2 (1986) 111–113.
- [22] F. Ono, N. Tase, A. Kurosawa, et al., Atypical L-type bovine spongiform encephalopathy (L-BSE) transmission to cynomolgus macaques, a non-human primate, *Jpn. J. Infect. Dis.* 64 (2011) 81–84.
- [23] J. Safar, H. Wille, V. Itri, et al., Eight prion strains have PrP^{Sc} molecules with different conformations, *Nat. Med.* 4 (1998) 1157–1165.
- [24] Y. Murayama, M. Yoshioka, H. Okada, et al., Urinary excretion and blood level of prions in scrapie-infected hamsters, *J. Gen. Virol.* 88 (2007) 2890–2898.
- [25] N.R. Deleault, J.C. Geoghegan, K. Nishina, et al., Protease-resistant prion protein amplification reconstituted with partially purified substrates and synthetic polyanions, *J. Biol. Chem.* 280 (2005) 26873–26879.
- [26] T. Yokoyama, A. Takeuchi, M. Yamamoto, et al., Heparin enhances the cell-protein misfolding cyclic amplification efficiency of variant Creutzfeldt-Jakob disease, *Neurosci. Lett.* 498 (2011) 119–123.

- [27] K. Shiraki, M. Kudou, S. Nishikori, et al., Arginine ethylester prevents thermal inactivation and aggregation of lysozyme, *Eur. J. Biochem.* 271 (2004) 3242–3247.
- [28] J. Buchner, R. Rudolph, Renaturation, purification and characterization of recombinant Fab-fragments produced in *Escherichia coli*, *Biotechnology* 9 (1991) 157–162.
- [29] K. Tsumoto, M. Umetsu, I. Kumagai, et al., Role of arginine in protein refolding, solubilization, and purification, *Biotechnol. Prog.* 20 (2004) 1301–1308.
- [30] P. Saá, L. Cervenakova, Protein misfolding cyclic amplification (PMCA): current status and future directions, *Virus Res.* 207 (2015) 47–61.
- [31] C. Lacroux, E. Comoy, M. Moudjou, et al., Preclinical detection of variant CJD and BSE prions in blood, *PLoS Pathog.* 10 (2014) e1004202.
- [32] F. Moda, P. Gambetti, S. Notari, et al., Prions in the urine of patients with variant Creutzfeldt-Jakob disease, *N. Engl. J. Med.* 371 (2014) 530–539.
- [33] M. Oshita, T. Yokoyama, Y. Takei, et al., Efficient propagation of variant Creutzfeldt-Jakob disease prion protein using the cell-protein misfolding cyclic amplification technique with samples containing plasma and heparin, *Transfusion* 56 (2016) 223–230, <http://dx.doi.org/10.1111/trf.13279>.

SCIENTIFIC REPORTS



OPEN

A direct assessment of human prion adhered to steel wire using real-time quaking-induced conversion

Received: 05 January 2016

Accepted: 08 April 2016

Published: 26 April 2016

Tsuyoshi Mori^{1, #}, Ryuichiro Atarashi^{1, #}, Kana Furukawa¹, Hanae Takatsuki¹, Katsuya Satoh², Kazunori Sano³, Takehiro Nakagaki¹, Daisuke Ishibashi¹, Kazuko Ichimiya⁴, Masahisa Hamada⁴, Takehisa Nakayama⁴ & Noriyuki Nishida¹

Accidental transmission of prions during neurosurgery has been reported as a consequence of re-using contaminated surgical instruments. Several decontamination methods have been studied using the 263K-hamster prion; however, no studies have directly evaluated human prions. A newly developed *in vitro* amplification system, designated real-time quaking-induced conversion (RT-QuIC), has allowed the activity of abnormal prion proteins to be assessed within a few days. RT-QuIC using human recombinant prion protein (PrP) showed high sensitivity for prions as the detection limit of our assay was estimated as 0.12 fg of active prions. We applied this method to detect human prion activity on stainless steel wire. When we put wires contaminated with human Creutzfeldt–Jakob disease brain tissue directly into the test tube, typical PrP-amyloid formation was observed within 48 hours, and we could detect the activity of prions at 50% seeding dose on the wire from $10^{2.8}$ to $10^{5.8}$ SD₅₀. Using this method, we also confirmed that the seeding activities on the wire were removed following treatment with NaOH. As seeding activity closely correlated with the infectivity of prions using the bioassay, this wire-QuIC assay will be useful for the direct evaluation of decontamination methods for human prions.

Prion diseases, also known as transmissible spongiform encephalopathies (TSEs), such as bovine spongiform encephalopathy in cattle, scrapie in sheep and Creutzfeldt–Jakob disease (CJD) in humans, are fatal neurodegenerative disorders. At present, there is no effective therapy available for the diseases¹. A host encoded normal prion protein, PrP^C, is required for susceptibility to prion infection^{3–5}, and a hallmark of prion diseases is the accumulation of misfolded forms of PrP, PrP^{Sc}. This amyloidogenic abnormally folded protein can be infectious. In human prion diseases, most cases (80%) are categorised as sporadic and approximately 15% of cases are a genetic form carrying a mutation in the prion protein gene *PRNP*. Less than 1% are caused by accidental transmission⁶. The possible iatrogenic transmission of such diseases was originally pointed out by Gajdusek in 1970s when the transmissibility of Kuru and CJD was evidenced⁷. In Japan, more than 140 cases of iatrogenic CJD have been identified following dura mater grafting from 1985 until now⁸. Accidental iatrogenic transmission of sporadic CJD (sCJD) has only occurred during neurosurgical procedures⁹. Until now, no cases of iatrogenic transmission following general surgery of nervous tissue or through endoscopic procedures have been reported⁹. Furthermore, experimental transmission studies using non-human primates demonstrated that bodily secretions are not infectious and that potential prion contamination of endoscopic instruments is not sufficient to cause human-to-human transmission¹⁰. In the case of CJD, infectivity is limited to the central nervous system; however, more recently many peripheral tissues from patients with variant CJD have been shown to be infectious, and PrP^{Sc} has also been detected in lymphoid organs such as the thymus, tonsils and spleen¹¹. Moreover, PrP^{Sc} has been detected in muscle, but no evidence of iatrogenic transmission was reported, suggesting a risk of iatrogenic transmission via contaminated surgical instruments¹².

¹Department of Molecular Microbiology and Immunology, Nagasaki University Graduate School of Biomedical Sciences, 1-12-4 Sakamoto, Nagasaki 852-8523, Japan. ²Department of Locomotive Rehabilitation Science, Nagasaki University Graduate School of Biomedical Sciences, 1-7-1 Sakamoto, Nagasaki 852-8523, Japan. ³Department of Physiology and Pharmacology, Faculty of Pharmaceutical Sciences, Fukuoka University, 8-19-1 Nanakuma, Jonan-ku, Fukuoka 814-0180, Japan. ⁴Krypton Co., Ltd., Dai 12 Daitetsu Bldg. 7F., 4-3-12 Yotsuya, Shinjuku-ku, Tokyo 160-0004, Japan. [#]Present address: Department of Infectious Diseases, Faculty of Medicine, University of Miyazaki, 5200 Kihara, Kiyotake, Miyazaki 889-1692, Japan. Correspondence and requests for materials should be addressed to T.M. (email: morit@nagasaki-u.ac.jp)

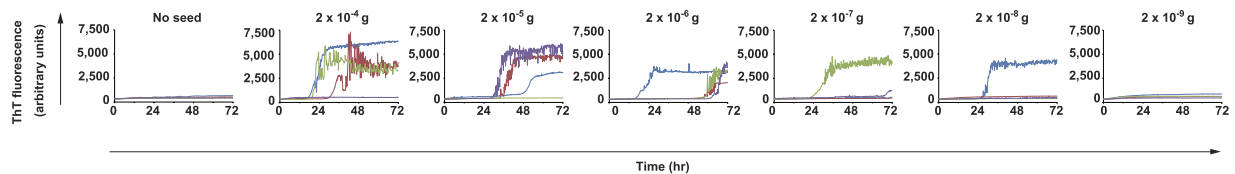


Figure 1. Stainless steel-wire with small amounts of prion seed attached can be detected by RT-QuIC reaction (wire-QuIC). The limiting dilution of 263K-BH was used for wire-QuIC reaction. Fibril formations of recombinant PrP were visualised by measurement of ThT fluorescence.

Infectious agents are highly resistant to routine decontamination methods¹³. High concentrations of sodium hydroxide, sodium hypochlorite or prolonged steam sterilisation are recommended methods for prion disinfection; however, most methods damage the surgical instruments^{14–17}. Therefore, the development of new disinfection methods is needed for the safe handling and reprocessing of surgical instruments. To estimate the effectiveness of the methods, the evaluation of prion activity is of key importance.

Because of the lack of nucleic acid components, approaches for TSE rely upon methods of immunodetection including immunohistochemistry and enzyme-linked immunosorbent assay using antibodies against PrP^{18–21}. Another evaluation method is Western blotting for protease-resistant PrP²². However, the detection range of Western blotting is narrow and not suitable to evaluate the decontamination of prion seeds. For evaluation of prion decontamination, the prion contaminated stainless steel wire test has often been used and infectivity assessed using a bioassay^{23–26}. However, bioassays are needed for at least 1 year to quantify the infectivity, even if transgenic mice expressing PrP are used²⁷. Recently, various *in vitro* PrP^{Sc} formation methods were developed. We have shown that a new *in vitro* amplification technology called real-time quaking-induced conversion (RT-QuIC) is highly sensitive for human prion and useful for detecting small amounts of PrP^{Sc} in cerebrospinal fluid. For the RT-QuIC reaction, intermittent shaking enhances the conversion of soluble recombinant PrP into amyloid fibrils only in the presence of PrP^{Sc}^{28–30}.

Here, we show that a new modified method named wire-QuIC can be applied for the direct evaluation of prion activity. Prion seeds 263K and sCJDs could firmly bind to stainless steel wire and gave rise to QuIC-positive reactions. Moreover, we demonstrated that treatment of wire with 1 mol/L NaOH solution was suitable for decontamination of prions. These results indicate that wire-QuIC can be useful to evaluate the decontamination of human prions on medical devices such as surgical instruments.

Results

To determine whether stainless steel wire is viable and does not affect amyloid formation, we conducted RT-QuIC using prion-seed-contaminated wire (wire-QuIC) instead of liquid brain homogenates (BH). To compare the efficiency of wire-QuIC, the classical RT-QuIC reaction with liquid BH was performed in parallel. As shown in Supplementary Fig. S1, the RT-QuIC reaction can detect prion seeding activities in more than 10^{-8} g of BH. Importantly, the QuIC signal could also detect prion seeds attached to the wire (Fig. 1). Wire-QuIC could detect prion seeds in more than 2×10^{-8} g of 263K-BH.

To determine whether the wire-QuIC reaction was useful to evaluate the decontamination rate of prion from instruments such as medical equipment by washing procedures, wires with attached 263K-BH were treated with two prion-inactivation procedures (1 mol/L of NaOH solution for 2 h and 3% (w/v) sodium dodecyl sulfate (SDS) solution at 100 °C for 10 min). The positive signal of 263K-prion-seeds was lost after treatment with 1 mol/L of NaOH solution (Fig. 2b). In contrast, no significant deletion of signal was obtained from wire-QuIC-reaction incubated with SDS solution (Fig. 2c). The same results were obtained using the classical method of RT-QuIC with liquid BHs (Supplementary Fig. S1). Although NaOH treatment removed the positive signal of RT-QuIC, there was no significant change following incubation with SDS solution.

To determine whether wire-QuIC reaction can also detect human prion, we used wire-QuIC reaction with sCJD patient BH. The positive signal of sCJD-prion-seeds was detected in more than 10^{-11} g of brain using the classical method of RT-QuIC with liquid BHs (Fig. 3a). The relative concentration of prion-seeding activity, which is the number of seeding doses giving 50% positive replicate reactions (SD_{50}) per unit of tissue, as determined by end-point dilution RT-QuIC was $10^{10.5} SD_{50}/g$ brain (Fig. 3b)²⁸. In accord with the results of 263K-BHs (Fig. 1), wire-QuIC reaction with sCJD-BH could detect prion seeding activities (Fig. 3c). However, the wire-QuIC reaction had a lower sensitivity than the RT-QuIC reaction, and could detect more than $10^{2.8} SD_{50}$. Importantly, there was no signal in wire-QuIC with a wire that attached high concentrations ($10^{6.8} SD_{50}$) of sCJD-BH (Fig. 3c).

For decontamination rate experiments, where sCJD-BH was treated with NaOH or SDS solution, the residuals of prion-seeds were tested by RT-QuIC and wire-QuIC. In accord with results of 263K-BHs, in the RT-QuIC reaction, sCJD prion seeds were inactivated after NaOH treatment (Fig. 4b), but partial inactivation was obtained from treatments with SDS solution (Fig. 4c). The same results were obtained in wire-QuIC experiments (Fig. 5). Importantly, wires contaminated with high concentrations of sCJD-BH ($10^{6.8} SD_{50}$) were QuIC-positive when treated with SDS (Fig. 5c). This phenomenon may be because excessive dirt came off or detergents stabilised the prion-seed structure. These results suggest that the wire-QuIC reaction is useful for evaluating human sCJD prion-seed decontamination.

We developed a new washing procedure for rigid endoscopes for which electrolysis water and sonication are used. To test the decontaminating efficiency of human prion, wires that attached 10-fold diluted sCJD-BH were

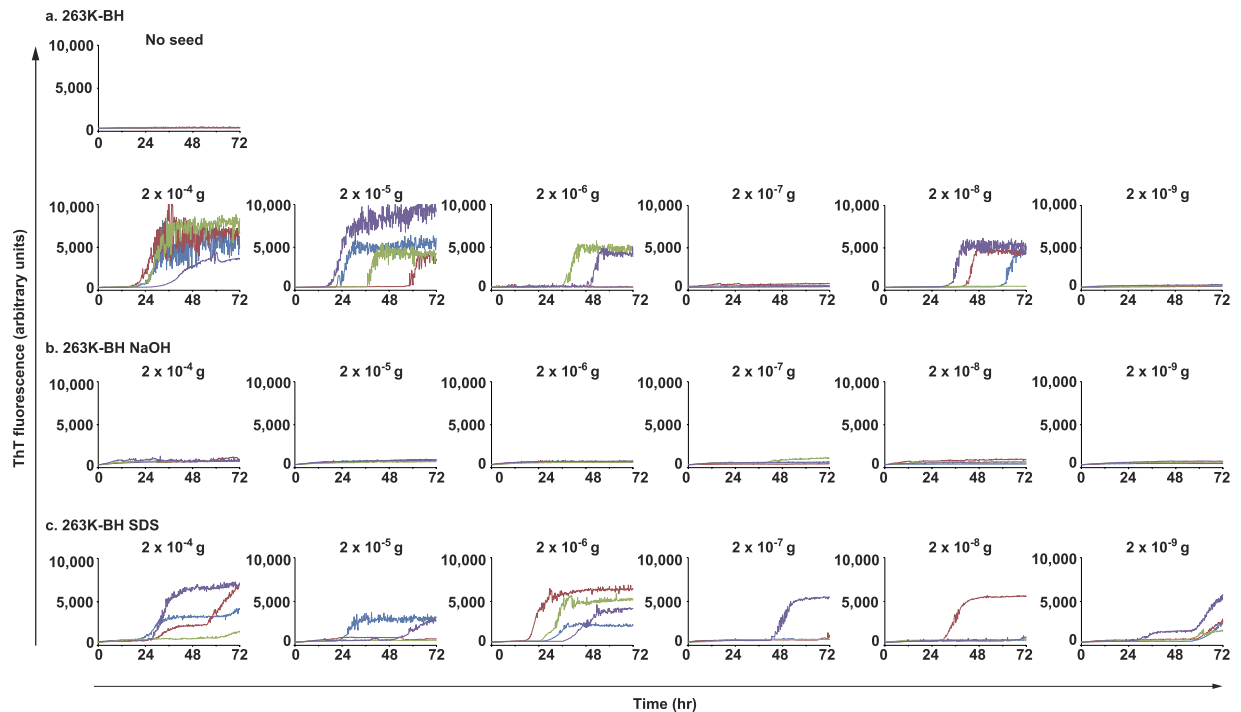


Figure 2. Wire-QuIC reaction can be useful to evaluate the decontamination rate of 263K hamster prions. Decontamination of prion 263K treated with NaOH or SDS was evaluated by wire-QuIC reaction. Dilutions of 263K-BH (10-fold) were attached to wires, and then were treated with 1 mol/L of NaOH for 2 h (b) or 3% (w/v) SDS at 100 °C for 10 min (c). Wire-QuIC reactions were performed to measure the residual prion seeds to evaluate the decontamination rates of prion.

washed as described in “Materials and Methods” in 1.5 mL tubes, and then evaluated using the wire-QuIC reaction. No positive signal was detected with the wire-QuIC reaction (Fig. 6).

Discussion

A basic problem to prevent iatrogenic transmission of prion diseases is the lack of a convenient system to detect infectious prion on surgical instruments. In this study, we modified RT-QuIC to evaluate the residual prion seeds on wires (wire-QuIC). Although normal RT-QuIC is more suitable for and more sensitive in detect prion in cerebrospinal fluid or the brain, the wire-QuIC can detect dried prion seeds attached to wire. Both 263K-prion (Fig. 1) and sCJD prion (Fig. 3) on wire was amplified *in vitro*. This finding is in agreement with other studies showing that stainless steel wire can bind prion seeds firmly, and that surface-bound prions can transmit scrapie to recipient mice^{23,24}. Notably, there was no signal in QuIC with high concentrations of sCJD-BH attached to the wire (Fig. 3c), and no seeding activity was observed at 2×10^{-7} g brain dilution, while it was present at 2×10^{-8} g (Fig. 2a). These paradoxical results may reflect the fact that the QuIC reaction is extremely sensitive and may be influenced by unknown inhibitory factors such as blood, salts or lipids.

Previous transmission studies have evaluated the prion decontamination process of wire^{25,26,31–34}. Among the inactivating methods for prion, we selected two commonly used inactivation methods, treatment with NaOH (1 mol/L NaOH for 2 h) or SDS solution (3% (w/v) SDS at 100 °C for 10 min), to see whether the wire-QuIC can be used for quantitative evaluation. Similar to bioassay studies^{25,26}, the positive signals of wire-QuIC with prion seeds disappeared after treatment with NaOH. However, SDS treatment had no significant effect. A previous study reported that a mouse adapted human prion strain, Fukuoka-1, could be completely inactivated by boiling with 3% (w/v) SDS for at least 3 min³⁵. Three reasons may explain this controversial result. (1) Seeding activity is not equal to infectivity. According to a previous report using 263K scrapie, the LD₅₀ of the hamster brain was approximately 10–50-fold lower than the SD₅₀²⁸. (2) One hundred degrees Celsius is not enough for SDS inactivation, and “boiling” is an important factor. We cannot exclude this possibility without direct evaluation of these two conditions. (3) Each prion strain has a different sensitivity against SDS. We used hamster 263K or human sCJD for evaluation instead of the mouse-adapted Fukuoka-1 strain. Lemmer *et al.* also indicated that 5% (w/v) SDS treatment at 90 °C could not inactivate 263K-prion²⁶. Other groups also showed that rodent adapted prions have a different sensitivity to SDS compared with naturally developed original prions³⁶.

We also tested a new washing procedure designed for endoscopes using wire-QuIC. This new procedure washes the objects with electrolysed water in combination with sonication to remove organic substances and to inactivate microorganisms and viruses (unpublished). As shown in Fig. 6, this washing procedure can decontaminate prion pathogens completely from wire. High concentrations of sodium hydroxide, sodium hypochlorite or prolonged steam sterilisation are known to be effective against prion. However, some instruments, such as flexible endoscopes, cannot withstand the heat and high concentrations of disinfectants, resulting in the discarding of

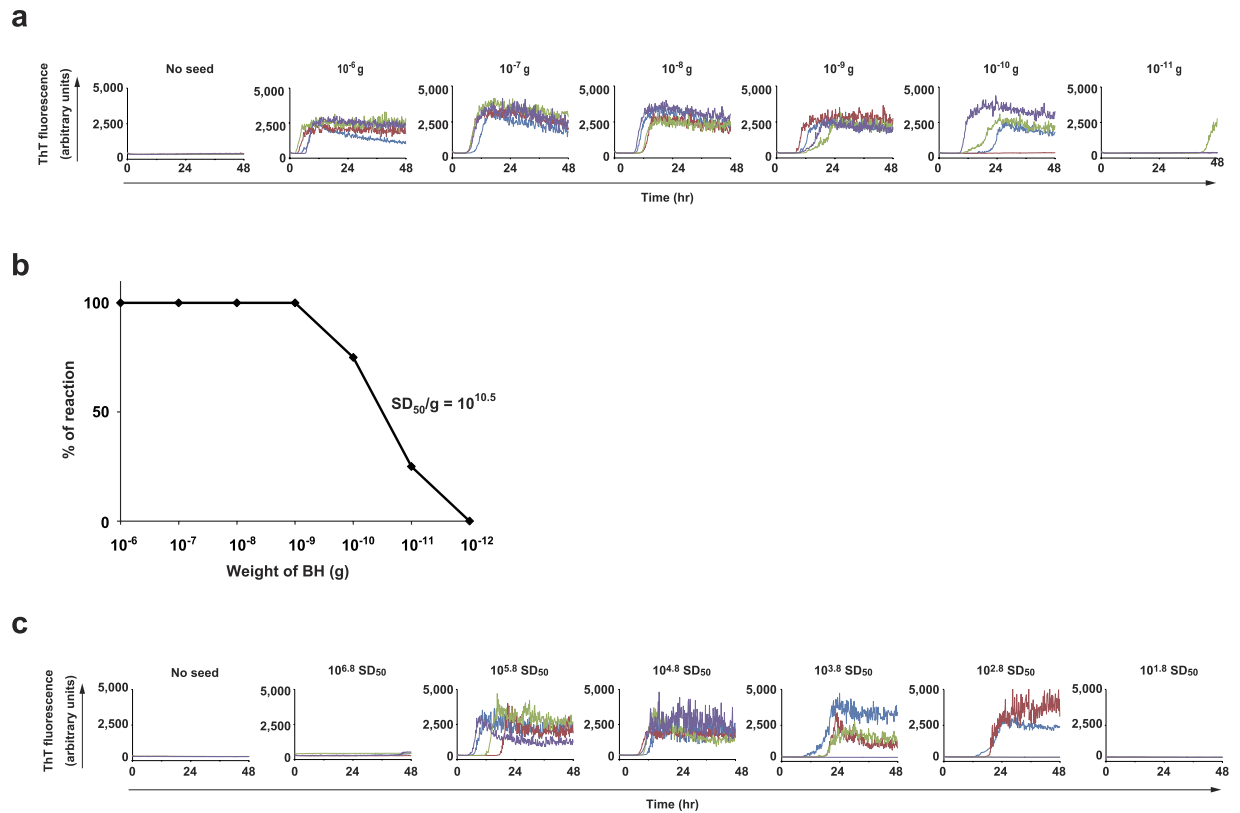


Figure 3. Wire-QuIC reaction can detect human prion seeds from contaminated stainless steel wires. (a) Limiting dilution of sCJD-BH was used for RT-QuIC reaction. Fibril formations of recombinant PrP were visualised by measurement of ThT fluorescence. (b) Curve of seeding dose activities. Seeding dose 50% (SD₅₀) per gram was $10^{10.5}$. (c) Limiting dilution of sCJD-BH was used for wire-QuIC reaction.

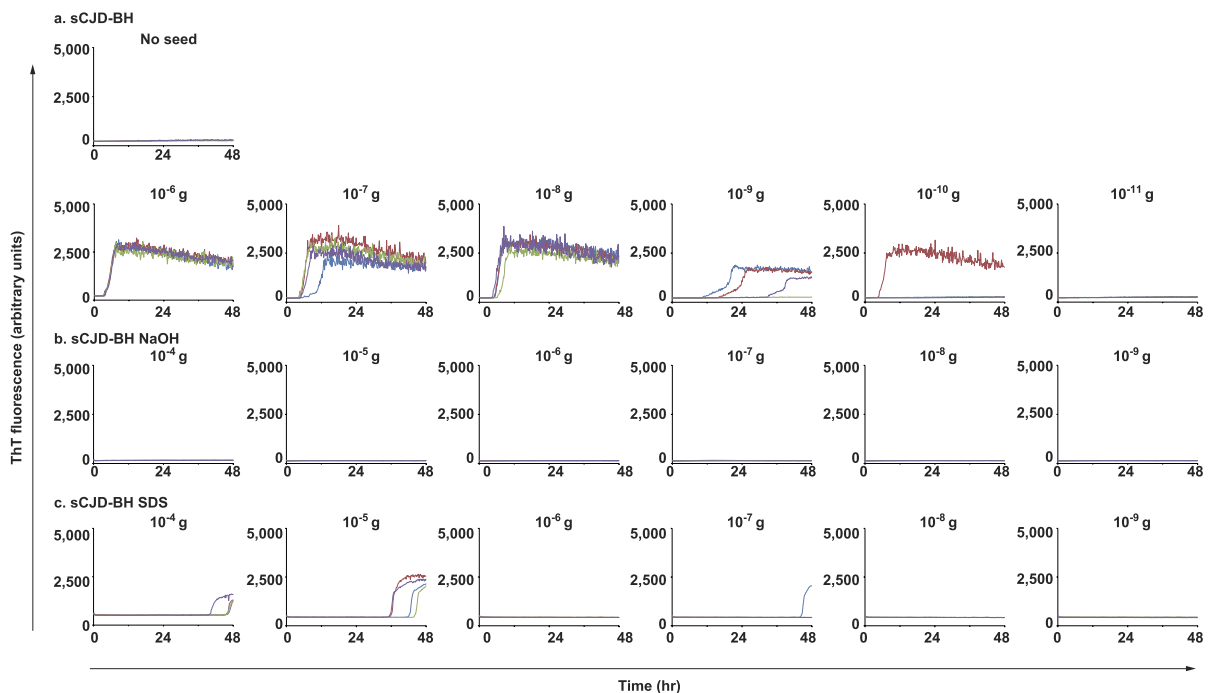


Figure 4. Inactivation of human prion seeds treated with NaOH or SDS solution, as evaluated by RT-QuIC reactions. Dilutions of sCJD-BH (10-fold) were treated with 1 mol/L NaOH solution for 2 h (b) or 3% (w/v) SDS solution at 100 °C for 10 min (c). RT-QuIC reactions were performed to measure the residual prion-seeding activities.

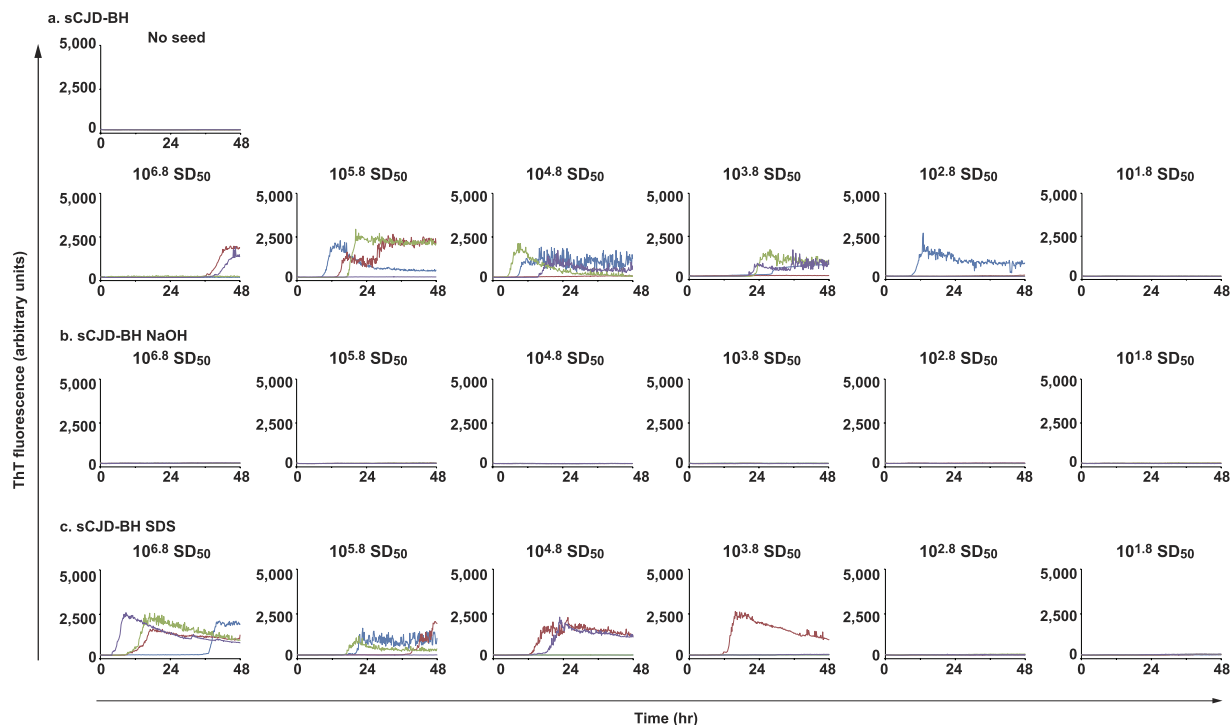


Figure 5. Wire-QuIC reaction can be useful to evaluate the decontamination rate of human prions. Decontamination of human sCJD prion with NaOH or SDS were evaluated by wire-QuIC reactions. Dilutions of sCJD-BH (10-fold) were attached to wires and then were treated with 1 mol/L of NaOH solution for 2 h (b) or 3% (w/v) SDS solution at 100 °C for 10 min (c). Wire-QuIC reactions were performed to measure the residual prion seeds to evaluate the decontamination rates of prion.

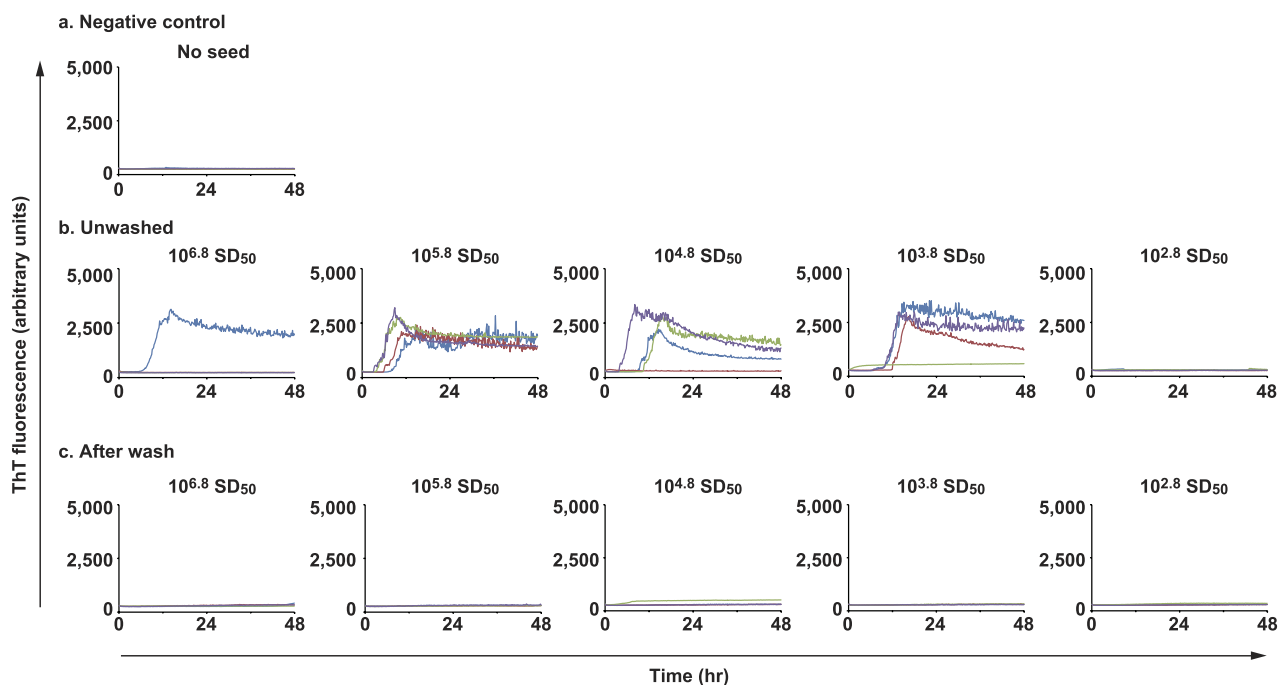


Figure 6. Evaluation of cleaning using the new washing procedure by wire-QuIC reaction. Dilutions of sCJD-BH (10-fold) were attached to wires and then washed using the new procedure described in “Materials and Methods.” Wire-QuIC reactions were performed to measure residual prion seeds.

instruments after use in patients with CJD¹⁷. Therefore, this new washing procedure will reduce the risk of accidental transmission of prion. However, experiments need to be substantiated by transmission experimental data because the negative RT-QuIC reaction does not necessarily exclude the presence of infectivity on the instrument.

Taken together, the present study indicates that wire-QuIC is a useful method to evaluate washing procedures for prion contamination; however, further studies are needed in order to determine the quantitative relationship between QuIC positivity and infectivity of human prions.

Methods

Recombinant prion protein. Recombinant prion protein (recPrP) from Syrian hamster (recShaPrP23-231) or human (recHuPrP23-231) construct were expressed in *Escherichia coli* strain BL21 (DE3) (Stratagene, La Jolla, CA, USA) and purified as previously described²⁹. Concentrations of recPrPs were determined by measuring the absorbance at 280 nm. After purification, aliquots of proteins were stored at -80°C in distilled water.

Preparation of brain tissue. For hamster prion (263K), brain tissues from Syrian golden hamsters infected with scrapie strain 263K were collected following euthanasia at the clinical stage of disease. Animal care and experimental procedures were performed in accordance with the Regulations and Guidelines for Animal Experimentation of Nagasaki University, reviewed by the Institutional Animal Care and Use Committee of Nagasaki University and approved by the president of Nagasaki University (ID: 1107040937). For human prion, brain tissue from a human prion disease (sCJD) patient was obtained for use in this study. Written informed consent to participate in the study was given by the patient's family. The protocol for investigation was approved by the Ethics Committee of Nagasaki University Hospital (ID: 10042823), and the study was registered with the University Hospital Medical Information Network (ID: UMIN00003301). The methods were carried out in accordance with the approved guidelines. BH in phosphate-buffered saline (PBS) were prepared (10% w/v) using a multi-bead shaker (Yasui Kikai, Osaka, Japan). After centrifugation at 2,000 g for 2 min, supernatants were collected and stored at -80°C . Dilutions of BH were carried out in PBS immediately prior to the reactions. For Wire-QuIC reaction, stainless steel wires (SUS304, RKC Instrument Inc., Kanagawa, Japan; diameter 0.2 mm) were cut into 5-mm-long pieces. In order to contaminate wires with BH *in vitro*, wires were incubated with several concentrations of BH and air-dried at room temperature for 1 day in a Petri dish.

Real-time quaking-induced conversion reaction (RT-QuIC). RT-QuIC was performed as previously described³⁰. Briefly, 95 μL of reaction buffer (50 mM PIPES pH 7.0, 500 mM NaCl, 1 mM EDTA and 10 μM Thioflavin T (ThT) including 80 $\mu\text{g}/\text{mL}$ of recHamPrP23-231 for 263K-BH, or 100 $\mu\text{g}/\text{mL}$ of recHuPrP23-231 for sCJD-BH) were loaded into wells of a 96-well optical-bottom black plate (Thermo Fisher Scientific 265301, MA, USA). Diluted BH (5 μL) was used for seeding. For the wire-QuIC reaction, air-dried wire was used. Ninety-six-well plates were covered with sealing tape (Greiner bio-one 676060, Frickenhausen, Germany) and incubated at 37°C in a plate reader (Infinite F200 PRO fluorescence plate reader; Tecan, Zurich, Switzerland) with intermittent shaking, consisting of shaking (432 rpm orbital) for 30 sec and no shaking for 30 sec, with a 2-min pause to measure the fluorescence. ThT fluorescence measurements were taken every 10 min at 440 nm excitation and 485 nm emission wavelengths. Four replicates of each diluted sample were measured. Each curve represents a single well.

Calculation of seeding dose. Seeding dose 50% (SD_{50}), analogous to a bioassay's lethal dose 50% (LD_{50}), were calculated using the amount of BHs which cause RT-QuIC positive signal of 50% of the wells³⁷.

Decontaminations. Air-dried wires with attached BH were incubated for decontamination in 1 mol/L of NaOH solution for 2 h or 3% (w/v) Sodium dodecyl sulfate (SDS) solution at 100°C for 10 min. Subsequently, wires were rinsed three times in distilled water for 1 min, and were air-dried again.

The new washing procedure for rigid endoscopes, for which electrolysis water and sonication were used, in collaboration with Krypton Co., Ltd. and Kyowakiden Industry Co., Ltd. in the project of "Program to support development of medical equipment and devices to solve unmet medical needs 2012, 2013" and "Development of Medical Device through Collaboration between Medicine and Industry 2014" under the Ministry of Economy, Trade and Industry (METI), Japan, was performed. To prevent diffusion of the pathogen, the same washing process was performed in 1.5 mL tubes. Electrolysed alkaline and acidic water were prepared in the electrolysis apparatus. The apparatus consists of anode and cathode plates, made of titanium and coated with platinum, that are separated by an electrolytic diaphragm (Y-9201T, Yuasa Membrane Systems Co. Ltd., Tokyo, Japan). The electrolysed water were collected in 500 mL bottles and used for the experiment. Our new washing procedure consisted of five processes to perform disinfection. Wires that attached BH were kept separately from each other in 1.5 mL tube, and were then pre-washed in tap water. Wires were then treated with electrolysed alkaline water while being sonicated at 45 kHz. Subsequently, wires were rinsed in water with sonication, and treated with electrolysed acidic water, followed by rinsing in tap water. Alkaline treatment and acidic water processing were performed sequentially for 3 min each.

References

- Rutala, W. A. & Weber, D. J. Creutzfeldt-Jakob disease: recommendations for disinfection and sterilization. *Clin Infect Dis* **32**, 1348–1356, doi: 10.1086/319997 (2001).
- Chesebro, B. Introduction to the transmissible spongiform encephalopathies or prion diseases. *Br Med Bull* **66**, 1–20 (2003).
- Brandner, S. *et al.* Normal host prion protein (PrP^C) is required for scrapie spread within the central nervous system. *Proc Natl Acad Sci USA* **93**, 13148–13151 (1996).
- Bueller, H. *et al.* Mice devoid of PrP are resistant to scrapie. *Cell* **73**, 1339–1347 (1993).
- Sakaguchi, S. *et al.* Accumulation of proteinase K-resistant prion protein (PrP) is restricted by the expression level of normal PrP in mice inoculated with a mouse-adapted strain of the Creutzfeldt-Jakob disease agent. *J Virol* **69**, 7586–7592 (1995).

6. Brown, P., Brandel, J. P., Preece, M. & Sato, T. Iatrogenic Creutzfeldt-Jakob disease: the waning of an era. *Neurology* **67**, 389–393, doi: 10.1212/01.wnl.0000231528.65069.3f (2006).
7. Gajdusek, D. C. & Gibbs, C. J., Jr. Transmission of two subacute spongiform encephalopathies of man (Kuru and Creutzfeldt-Jakob disease) to new world monkeys. *Nature* **230**, 588–591 (1971).
8. Hamaguchi, T. *et al.* Insight into the frequent occurrence of dura mater graft-associated Creutzfeldt-Jakob disease in Japan. *J Neurol Neurosurg Psychiatry* **84**, 1171–1175, doi: 10.1136/jnnp-2012-304850 (2013).
9. Brown, P. & Farrell, M. A practical approach to avoiding iatrogenic Creutzfeldt-Jakob disease (CJD) from invasive instruments. *Infect Control Hosp Epidemiol* **36**, 844–848, doi: 10.1017/ice.2015.53 (2015).
10. Brown, P. *et al.* Human spongiform encephalopathy: the National Institutes of Health series of 300 cases of experimentally transmitted disease. *Ann Neurol* **35**, 513–529, doi: 10.1002/ana.410350504 (1994).
11. Wadsworth, J. D. *et al.* Tissue distribution of protease resistant prion protein in variant Creutzfeldt-Jakob disease using a highly sensitive immunoblotting assay. *Lancet* **358**, 171–180 (2001).
12. Peden, A. H., Ritchie, D. L., Head, M. W. & Ironside, J. W. Detection and localization of PrP^{Sc} in the skeletal muscle of patients with variant, iatrogenic, and sporadic forms of Creutzfeldt-Jakob disease. *Am J Pathol* **168**, 927–935, doi: 10.2353/ajpath.2006.050788 (2006).
13. Rutala, W. A. & Weber, D. J. & Society for Healthcare Epidemiology of, A. Guideline for disinfection and sterilization of prion-contaminated medical instruments. *Infect Control Hosp Epidemiol* **31**, 107–117, doi: 10.1086/650197 (2010).
14. Ernst, D. R. & Race, R. E. Comparative analysis of scrapie agent inactivation methods. *J Virol Methods* **41**, 193–201 (1993).
15. Steelman, V. M. Creutzfeldt-Jakob disease: recommendations for infection control. *Am J Infect Control* **22**, 312–318 (1994).
16. Steelman, V. M. Prion diseases—an evidence-based protocol for infection control. *AORN J* **69**, 946–954, 956–967 passim; quiz 968–976 (1999).
17. Antloga, K., Meszaros, J., Malchesky, P. S. & McDonnell, G. E. Prion disease and medical devices. *ASAIO J* **46**, S69–72 (2000).
18. Prusiner, S. B., Scott, M. R., DeArmond, S. J. & Cohen, F. E. Prion protein biology. *Cell* **93**, 337–348 (1998).
19. Schaller, O. *et al.* Validation of a western immunoblotting procedure for bovine PrP(Sc) detection and its use as a rapid surveillance method for the diagnosis of bovine spongiform encephalopathy (BSE). *Acta Neuropathol* **98**, 437–443 (1999).
20. Nicholson, E. M., Kunkle, R. A., Hamir, A. N., Lebepe-Mazur, S. & Orcutt, D. Detection of the disease-associated isoform of the prion protein in formalin-fixed tissues by Western blot. *J Vet Diagn Invest* **19**, 548–552 (2007).
21. Nicholson, E. M., Greenlee, J. J. & Hamir, A. N. PrP^{Sc} detection in formalin-fixed paraffin-embedded tissue by ELISA. *BMC Res Notes* **4**, 432, doi: 10.1186/1756-0500-4-432 (2011).
22. Lemmer, K., Mielke, M., Pauli, G. & Beekes, M. Decontamination of surgical instruments from prion proteins: *in vitro* studies on the detachment, destabilization and degradation of PrP^{Sc} bound to steel surfaces. *J Gen Virol* **85**, 3805–3816, doi: 10.1099/vir.0.80346-0 (2004).
23. Zobeley, E., Flechsig, E., Cozzio, A., Enari, M. & Weissmann, C. Infectivity of scrapie prions bound to a stainless steel surface. *Mol Med* **5**, 240–243 (1999).
24. Flechsig, E. *et al.* Transmission of scrapie by steel-surface-bound prions. *Mol Med* **7**, 679–684 (2001).
25. Fichet, G. *et al.* Novel methods for disinfection of prion-contaminated medical devices. *Lancet* **364**, 521–526, doi: 10.1016/S0140-6736(04)16810-4 (2004).
26. Lemmer, K. *et al.* Decontamination of surgical instruments from prions. II. *In vivo* findings with a model system for testing the removal of scrapie infectivity from steel surfaces. *J Gen Virol* **89**, 348–358, doi: 10.1099/vir.0.83396-0 (2008).
27. Fischer, M. *et al.* Prion protein (PrP) with amino-proximal deletions restoring susceptibility of PrP knockout mice to scrapie. *EMBO J* **15**, 1255–1264 (1996).
28. Willham, J. M. *et al.* Rapid end-point quantitation of prion seeding activity with sensitivity comparable to bioassays. *PLoS Pathog* **6**, e1001217, doi: 10.1371/journal.ppat.1001217 (2010).
29. Atarashi, R. *et al.* Ultrasensitive detection of scrapie prion protein using seeded conversion of recombinant prion protein. *Nat Methods* **4**, 645–650, doi: 10.1038/nmeth1066 (2007).
30. Atarashi, R. *et al.* Ultrasensitive human prion detection in cerebrospinal fluid by real-time quaking-induced conversion. *Nat Med* **17**, 175–178, doi: 10.1038/nm.2294 (2011).
31. Lehmann, S. *et al.* New hospital disinfection processes for both conventional and prion infectious agents compatible with thermosensitive medical equipment. *J Hosp Infect* **72**, 342–350, doi: 10.1016/j.jhin.2009.03.024 (2009).
32. Yan, Z. X., Stitz, L., Heeg, P., Pfaff, E. & Roth, K. Infectivity of prion protein bound to stainless steel wires: a model for testing decontamination procedures for transmissible spongiform encephalopathies. *Infect Control Hosp Epidemiol* **25**, 280–283, doi: 10.1086/502392 (2004).
33. Fichet, G. *et al.* Investigations of a prion infectivity assay to evaluate methods of decontamination. *J Microbiol Methods* **70**, 511–518, doi: 10.1016/j.mimet.2007.06.005 (2007).
34. Vadrot, C. & Darbord, J. C. Quantitative evaluation of prion inactivation comparing steam sterilization and chemical sterilants: proposed method for test standardization. *J Hosp Infect* **64**, 143–148, doi: 10.1016/j.jhin.2006.06.007 (2006).
35. Tateishi, J., Tashima, T. & Kitamoto, T. Practical methods for chemical inactivation of Creutzfeldt-Jakob disease pathogen. *Microbiol Immunol* **35**, 163–166 (1991).
36. Giles, K. *et al.* Resistance of bovine spongiform encephalopathy (BSE) prions to inactivation. *PLoS Pathog* **4**, e1000206, doi: 10.1371/journal.ppat.1000206 (2008).
37. Karber, G. 50% End point calculation. *Archiv fur Experimentelle Pathologie und Pharmakologie* **162**, 480–483 (1931).

Acknowledgements

We thank Dr. Yuhzo Fujita from the Teraoka Seikei Geka Hospital and Dr. Hidehiro Mizusawa, Director of the National Center Hospital of Neurology and Psychiatry for expert advice. This work was supported by a grant-in-aid for the “Program to Support Development of Medical Equipment and Devices to Solve Unmet Medical Needs 2012, 2013” and “Development of Medical Devices through Collaboration between Medicine and Industry 2014” under the Ministry of Economy, Trade and Industry, Japan (24–084). Furthermore, this research was partially supported by a grant-in-aid of the Research Committee of Prion Disease and Slow Virus Infection, from the Ministry of Health, Labour and Welfare of Japan; a grant-in-aid of the Research Committee of Molecular Pathogenesis and Therapies for Prion Disease and Slow Virus Infection, the Practical Research Project for Rare and Intractable Disease from Japan Agency for Medical Research and Development, AMED; a grant from Takeda Science Foundation; a grant from the Japan Intractable Disease Research Foundation; a grant-in-aid from the Tokyo Biochemical Research Foundation; a grant provided by the Ichiro Kanehara Foundation, and a grant provided by Yokoyama Foundation for Clinical Pharmacology (No. YRY1502). These funders had no role in study design, data collection and analysis, decision to publish, or preparation of the manuscript.

Author Contributions

T.M., R.A. and N.N. designed the study and wrote the main manuscript text. T.M., K.F., H.T. and K. Sano performed the experiments. T.M., R.A. and K. Satoh analysed the data. R.A., K. Satoh, K.I., M.H. and T. Nakayama contributed reagents/materials/analysis tools. T.M., R.A., K. Satoh, T. Nakagaki, D.I. and N.N. discussed the data.

Additional Information

Supplementary information accompanies this paper at <http://www.nature.com/srep>

Competing financial interests: The authors declare no competing financial interests.

How to cite this article: Mori, T. *et al.* A direct assessment of human prion adhered to steel wire using real-time quaking-induced conversion. *Sci. Rep.* **6**, 24993; doi: 10.1038/srep24993 (2016).



This work is licensed under a Creative Commons Attribution 4.0 International License. The images or other third party material in this article are included in the article's Creative Commons license, unless indicated otherwise in the credit line; if the material is not included under the Creative Commons license, users will need to obtain permission from the license holder to reproduce the material. To view a copy of this license, visit <http://creativecommons.org/licenses/by/4.0/>

Comparison of abnormal isoform of prion protein in prion-infected cell lines and primary-cultured neurons by PrP^{Sc}-specific immunostaining

Misaki Tanaka,¹ Ai Fujiwara,¹ Akio Suzuki,¹ Takeshi Yamasaki,¹ Rie Hasebe,¹ Kentaro Masujin^{2,3} and Motohiro Horiuchi¹

Correspondence

Motohiro Horiuchi
horiuchi@vetmed.hokudai.ac.jp

¹Laboratory of Veterinary Hygiene, Graduate School of Veterinary Medicine, Hokkaido University, Kita 18, Nishi 9, Kita-ku, Sapporo 060-0818, Japan

²National Agriculture Food Research Organization (NARO), 3-1-5 Kannondai, Tsukuba, Ibaraki, 305-0856, Japan

³Laboratory of Persistent Viral Diseases, Rocky Mountain Laboratories, National Institute for Allergy and Infectious Diseases, National Institutes of Health, Hamilton, MT, USA

We established abnormal isoform of prion protein (PrP^{Sc})-specific double immunostaining using mAb 132, which recognizes aa 119–127 of the PrP molecule, and novel PrP^{Sc}-specific mAb 8D5, which recognizes the N-terminal region of the PrP molecule. Using the PrP^{Sc}-specific double immunostaining, we analysed PrP^{Sc} in immortalized neuronal cell lines and primary cerebral-neuronal cultures infected with prions. The PrP^{Sc}-specific double immunostaining showed the existence of PrP^{Sc} positive for both mAbs 132 and 8D5, as well as those positive only for either mAb 132 or mAb 8D5. This indicated that double immunostaining detects a greater number of PrP^{Sc} species than single immunostaining. Double immunostaining revealed cell-type-dependent differences in PrP^{Sc} staining patterns. In the 22 L prion strain-infected Neuro2a (N2a)-3 cells, a subclone of N2a neuroblastoma cell line, or GT1-7, a subclone of the GT1 hypothalamic neuronal cell line, granular PrP^{Sc} stains were observed at the perinuclear regions and cytoplasm, whereas unique string-like PrP^{Sc} stains were predominantly observed on the surface of the 22 L strain-infected primary cerebral neurons. Only 14 % of PrP^{Sc} in the 22 L strain-infected N2a-3 cells were positive for mAb 8D5, indicating that most of the PrP^{Sc} in N2a-3 lack the N-terminal portion. In contrast, nearly half PrP^{Sc} detected in the 22 L strain-infected primary cerebral neurons were positive for mAb 8D5, suggesting the abundance of full-length PrP^{Sc} that possesses the N-terminal portion of PrP. Further analysis of prion-infected primary neurons using PrP^{Sc}-specific immunostaining will reveal the neuron-specific mechanism for prion propagation.

Received 29 December 2015

Accepted 25 May 2016

INTRODUCTION

Transmissible spongiform encephalopathies, also known as prion diseases, are fatal neurodegenerative disorders in humans and animals that are caused by infectious agents called prions. The pathological hallmarks of prion diseases include microglial activation, astrogliosis, and accumulation of the abnormal isoform of prion protein (PrP^{Sc}) in the central nervous system. PrP^{Sc} is generated from a host-encoded cellular isoform of prion protein (PrP^C) by post-translational modifications such as conformational transformation (Prusiner, 1998). The generation of PrP^{Sc} is believed to be strongly associated with prion propagation and

neurodegeneration in prion diseases (Mallucci *et al.*, 2003). Therefore, the clarification of the cellular mechanism of PrP^{Sc} formation would be useful.

Cell biological studies using immortalized neuronal cell lines such as Neuro2a (N2a) neuroblastoma and GT1 hypothalamic neuronal cells have greatly contributed to the elucidation of the cellular mechanism underlying prion propagation. Earlier studies suggested that PrP^{Sc} is generated from mature PrP^C expressed on the cell surface and that the PrP^{Sc} generation occurs at cellular compartments on the endocytotic pathway, including the cholesterol-rich membrane microdomains called lipid rafts (Borchelt *et al.*, 1992; Caughey & Raymond, 1991; Naslavsky *et al.*, 1997; Vey *et al.*, 1996). Further cell biological studies within the following decade indicated the involvement of endocytic recycling compartments and endocytic recycling pathway in

Two supplementary figures are available with the online Supplementary Material.

PrP^{Sc} formation (Béranger *et al.*, 2002; Marijanovic *et al.*, 2009; Pimpinelli *et al.*, 2005; Veith *et al.*, 2009; Yamasaki *et al.*, 2012). We recently reported that after the inoculation of prions, newly generated PrP^{Sc} appeared on the cell surface, early endosomes, and late endosomes of N2a cells (Yamasaki *et al.*, 2014a). These cell biological studies suggest the intracellular vesicular compartments to be the major sites for PrP^{Sc} formation, whereas it was reported that PrP^{Sc} formation occurs on the cell surface within a minute (Goold *et al.*, 2011). On the other hand, ultrastructural studies using the brains of prion-infected mice showed that PrP^{Sc} was frequently detected on the plasma membranes of neuropils, and occasionally in the intracellular vesicles (Godsave *et al.*, 2008, 2013; Jeffrey *et al.*, 1992, 1994). Further immuno-electron microscopic studies using anti-PrP, recognizing the N-terminal region of PrP, suggested that neuronal plasma membranes such as membrane invaginations and sites of cell-to-cell contact are primary sites for PrP^{Sc} formation (Godsave *et al.*, 2013). To resolve the partly contradictory results regarding the site of PrP^{Sc} formation between cell culture and ultrastructural studies, primary-cultured neurons are considered to be a good *ex vivo* model. There are only a few reports on prion propagation in primary-cultured neurons derived from the cerebellum, striatum, and cerebral cortex of mouse brains (Cronier *et al.*, 2004; Dron *et al.*, 2010; Hannaoui *et al.*, 2013). However, little information is available on the localization of PrP^{Sc} in primary neurons infected with prions.

Taraboulos and colleagues reported that treatment of fixed cells with guanidinium salts prior to incubation with anti-PrP antibodies significantly increases the PrP^{Sc} signals in immunocytochemical staining (Taraboulos *et al.*, 1990). This method is being used for PrP^{Sc}-specific detection by immunofluorescence assay (IFA). However, careful adjustment of the threshold level by manipulation of the detector gain or the exposure time is required for the discrimination of PrP^{Sc} signals from PrP^C. A rising concern is that such manipulations may limit the detailed analysis of PrP^{Sc}. We recently reported that mAb 132, recognizing the epitope comprising mouse PrP aa 119–127, distinguishes PrP^{Sc} from PrP^C in prion-infected cells and tissues with a minimum manipulation of threshold setting (Sakai *et al.*, 2013; Yamasaki *et al.*, 2012). Although the pretreatment with guanidinium salts is still prerequisite, the advantage in threshold setting made it possible to disclose the detailed intracellular localization of PrP^{Sc} in cells persistently infected with prions (Yamasaki *et al.*, 2012, 2014a, 2014b). The use of mAb 132 improved the specificity of PrP^{Sc} detection; however, PrP^{Sc} comprises a heterologous PrP^{Sc} population in the size and rigidity of aggregates. Therefore, whether mAb 132 can detect all of PrP^{Sc} species in cells remains obscure.

Recently, Masujin and his colleagues reported a new PrP^{Sc}-specific antibody, mAb 8D5, which recognizes the N-terminal region comprising mouse PrP aa 31–39 (Masujin *et al.*, 2013). This mAb is expected to react with full-length PrP^{Sc} but not with the N-terminally truncated form of

PrP^{Sc} that is generated by endogenous enzymes after PrP^{Sc} formation in the cells (Caughey *et al.*, 1991; Taraboulos *et al.*, 1992). The mAb 8D5 specifically immunoprecipitated PrP^{Sc} from brain homogenates of prion-infected animals, similar to other PrP^{Sc}-specific antibodies reported to date (Curin Serbec *et al.*, 2004; Horiuchi *et al.*, 2009; Korth *et al.*, 1997; Paramithiotis *et al.*, 2003; Ushiki-Kaku *et al.*, 2010). Of relevance is that the mAb 8D5 detected PrP^{Sc} in non-denatured histoblot and in the cryosections of scrapie-infected mouse brains. This feature appeared to be useful for the immunocytochemical detection of PrP^{Sc}; thus, we attempted to use mAb 8D5 in combination with mAb 132 for PrP^{Sc}-specific detection.

In the current study, we prepared primary neuronal cultures from mouse cerebra with enrichment of neuronal population by antimetabolic treatment and confirmed the prion propagation in the neurons. Then we compared PrP^{Sc} in immortalized cell lines and in primary neuronal cultures using PrP^{Sc}-specific double immunostaining.

RESULTS

Detection of PrP^{Sc} in prion-infected immortalized cells by PrP^{Sc}-specific staining with mAbs 132 and 8D5

First we examined whether mAb 8D5 reacts with PrP^{Sc} in prion-infected cells with or without pretreatment of cells with guanidine isothiocyanate (GdnSCN) (Fig. 1a). As expected, mAb 132 detected PrP^{Sc} in ScN2a-3-22L cells, which were a subclone of Neuro2a mouse neuroblastoma cell line (N2a-3), persistently infected with the 22L prion strain after pretreatment of cells with 5 M GdnSCN. Although fluorescence intensities were weaker than those by mAb 132, PrP^{Sc} signals were detected by mAb 8D5 in ScN2a-3-22L cells with or without GdnSCN pretreatment. Under the same conditions of fluorescent-image acquisition, mAb 8D5 did not show any specific fluorescent signals in prion-uninfected cells, demonstrating the PrP^{Sc}-specific detection.

To confirm the optimum condition of GdnSCN pretreatment for PrP^{Sc}-specific double immunostaining with mAbs 132 and 8D5, influence of the pretreatment on the PrP^{Sc} detection was analysed using GT1 hypothalamic neuronal cell line (GT1-7) persistently infected with the 22L prion strain (ScGT1-7-22L) (Fig. S1, available in the online Supplementary Material). The GdnSCN pretreatment did not enhance or degrade the reactivity of mAb 8D5 to PrP^{Sc} in ScGT1-7-22L cells so much. In contrast, the reactivity of mAb 132 was drastically enhanced after the 5 min GdnSCN pretreatment. However, a longer GdnSCN pretreatment did not affect the reactivity of mAb 132. This result demonstrated that the 10 min pretreatment of cells with 5 M GdnSCN was optimal for the PrP^{Sc}-specific double immunostaining with mAbs 132 and 8D5, and thus, in the following experiments, 10 min GdnSCN pretreatment was performed unless otherwise specified.

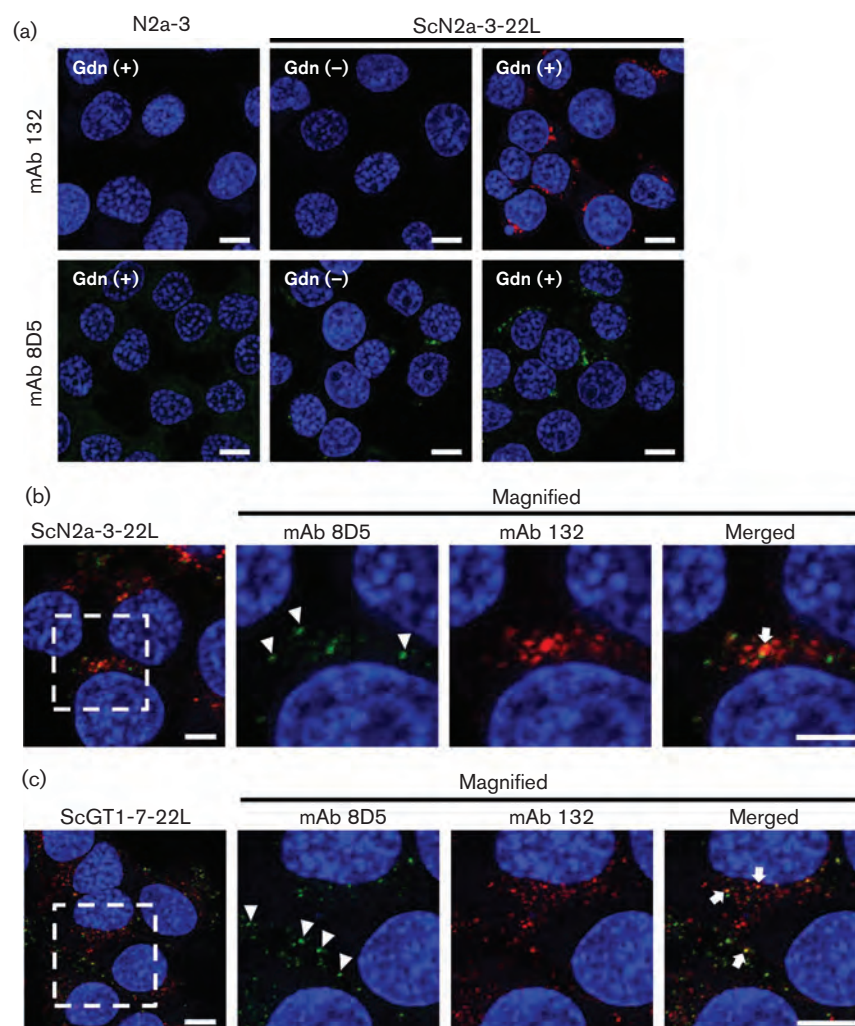


Fig. 1. PrP^{Sc}-specific staining in immortalized cell lines persistently infected with 22L prion strain. (a) Detection of PrP^{Sc} in ScN2a-3-22L with [Gdn(+)] or without GdnSCN pretreatment [Gdn(-)]. Alexa Fluor 647-conjugated mAb 132 (red) and Alexa Fluor 488-conjugated mAb 8D5 (green) were used for direct detection of PrP^{Sc}. Nuclei were counterstained with 4',6-diamidino-2-phenylindole (DAPI) (blue). (b, c) Double staining of PrP^{Sc} using mAbs 132 and 8D5. PrP^{Sc} in GdnSCN-pretreated ScN2a-3-22L cells (b) and ScGT1-7-22L cells (c) was simultaneously detected by Alexa Fluor-labelled mAbs 132 (red) and 8D5 (green). Magnified images of the boxed areas in the leftmost panels are shown in the three panels on the right. Arrowheads show representative granular stains with mAb 8D5 near the edges of cells. Arrows indicate representative overlapping stains with mAbs 132 and 8D5. Scale bars: (a and c) 10 μ m, (b) 5 μ m.

Fig. 1(b) shows double immunofluorescent staining of PrP^{Sc} in ScN2a-3-22L cells using mAbs 132 and 8D5. In ScN2a-3-22L cells, mAb 132 detected bright granular PrP^{Sc} signals at perinuclear regions as previously described (Yamasaki *et al.*, 2012). In contrast, mAb 8D5 showed relatively faint granular PrP^{Sc} signals in ScN2a-3-22L cells (Fig. 1b, arrowheads). Although some granular PrP^{Sc} signals detected by mAb 132 merged with those by mAb 8D5 (Fig. 1b, arrow), the majority of granular PrP^{Sc} stains by mAb 132 did not appear to be colocalized with those by mAb 8D5. The results of the detailed colocalization analysis are described later (see Fig. 6).

The same double immunofluorescent staining was carried out on ScGT1-7-22L cells. MAb 132 showed perinuclear granular stains of PrP^{Sc}; however, the granular signals appeared to be scattered to the cytoplasm compared with ScN2a-3-22L cells (Fig. 1c). MAb 8D5 appeared to detect a greater number of PrP^{Sc} granules in ScGT1-7-22L cells than in ScN2a-3-22L cells. PrP^{Sc} granular stains detected by mAb 8D5 were scattered to the cytoplasm and some granules with intense fluorescence were observed at the peripheral region of the cytoplasm, possibly proximate to the plasma membranes (Fig. 1c, arrowheads). PrP^{Sc} detected by mAbs 132

and 8D5 was partly but not extensively merged (Fig. 1c, arrows).

Neuron-enriched primary cultures from mouse cerebra

Cells isolated from the cerebra of mouse embryos were abundant in neurons and contained a few glial cells [Fig. 2b, e.g. 7 days *in vitro* (div), cytosine arabinoside (Ara-C) (-)]. However, in the absence of Ara-C, glial fibrillary acidic protein (GFAP)-positive astrocytes readily increased by 14 div (Fig. 2b). Ara-C treatment at 0.25 μ M from 4 to 7 div and following treatment at 0.125 μ M from 7 to 11 div successfully suppressed the appearance of GFAP-positive astrocytes up to 28 div; only a few astrocytes were found in Ara-C-treated cultures until 28 div. The result of GFAP expression in immunoblot analysis also demonstrated the successful reduction of astrocytes (Fig. 2c). A neuron-specific protein, β -III tubulin, was detected from primary neuronal cultures in the presence or absence of Ara-C by immunoblot analysis (Fig. 2c). Lower levels of GFAP but higher levels of β -III tubulin in Ara-C-treated primary neuronal cultures at each time point also indicated that the Ara-C treatment by the indicated schedule securely resulted in the enrichment of neurons in the primary neuronal cultures. We

designate this culture 'primary cerebral neurons' (CNs) in the description below.

PrP^{Sc} generation in cerebral neurons

The CNs at 7 div were exposed to microsomes as described in the Methods. At 4 days after the exposure, the medium was replaced with fresh, Ara-C-free Neuronal Medium to remove inocula (Fig. 2a). The CNs at 0, 7, 14, 21, 28 and 35 days post infection (dpi) were subjected to immunoblot analysis for proteinase K (PK)-resistant PrP^{Sc} (PrP-res) detection (Fig. 3a). PrP-res was detected in cells exposed to three different prion strains from at least 7 dpi. In CNs infected with 22L or Chandler strain, PrP-res levels increased up to 21 dpi, demonstrating prion propagation. In Obihiro strain-infected CNs, the PrP-res level was lower than CNs infected with the other two prion strains. No PrP-res was detected in mock-infected CNs. Fig. 3(b) shows PrP^{Sc}-specific immunostaining using mAb 132. PrP^{Sc} signals were observed around cell bodies and neurites in prion-infected CNs from 7 dpi but not in mock-infected CNs. The PrP^{Sc} stains per cell appeared to gradually increase up to 21 dpi, and most CNs were positive for PrP^{Sc} at 14 dpi (data not shown). The granular PrP^{Sc} stains at perinuclear regions, as observed in ScN2a-3-22L cells and N2a-3 cells persistently infected with the Chandler prion strain (ScN2a-3-Ch), were scarcely

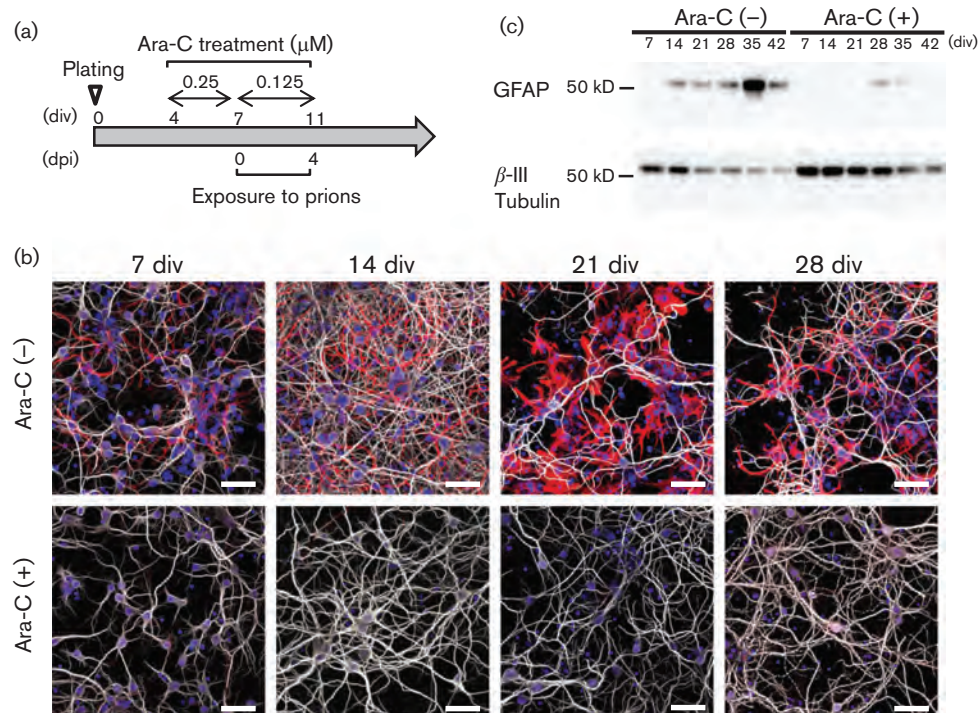


Fig. 2. Purity of primary neuronal culture from mouse cerebra. (a) The scheme for the Ara-C treatment. Cells were treated with 0.25 and 0.125 μ M Ara-C from 4 to 6 and 7 to 10 div, respectively, and Ara-C was completely removed at 11 div, corresponding to 4 days post infection (dpi). (b) Visualization of neurons and activated astrocytes in primary neuronal cultures. Mock-infected cultures at 7, 14, 21, and 28 div were stained with MAP2 (grey), GFAP (red), and DAPI (blue). Scale bars: 50 μ m. (c) Kinetics of the expression of GFAP and β -III tubulin.

observed in prion-infected CNs. However, string-like stains around the edges of cell bodies and neurites were evident during the later stage of infection (Fig. 3b, arrows).

PrP^{Sc}-specific double immunostaining of prion-infected cerebral neurons using mAbs 132 and 8D5

To characterize the string-like PrP^{Sc} stains in prion-infected CNs that were detected by mAb 132 (Fig. 3b), PrP^{Sc}-specific double immunostaining was performed with mAbs 132 and 8D5. In 22L- or Chandler strain-infected CNs (at 14 dpi), string-like PrP^{Sc} stains (Fig. 4, closed arrows) were detected by both mAbs 132 and 8D5, and they were partly merged (Fig. 4, arrowheads). In addition to string-like PrP^{Sc} stains, granular PrP^{Sc} stains, single-positive for mAb 132, were observed at neurites, but hardly at somas (Fig. 4, open arrows). The string-like PrP^{Sc} stains were evident but less obvious in Obihiro strain-infected CNs compared with 22L- or Chandler strain-infected CNs.

Since PrP^{Sc} stains in prion-infected CNs appeared at the plasma membranes or extracellular space, living CNs were incubated with Alexa Fluor 488-conjugated mAb 8D5 and subjected to microscopic examination to confirm whether the string-like PrP^{Sc} is present on the cell surface (Fig. 5). The CNs infected with 22L, Chandler or Obihiro strains at 14 dpi were incubated with mAb 8D5 and were directly subjected to microscopic observation without fixation, permeabilization or denaturation. String- and granular-like stains of PrP^{Sc} similar to those in fixed cells (Fig. 4) were observed in CNs infected with prions, demonstrating the presence of PrP^{Sc} on the cell surface (Fig. 5). The result also indicated that a certain population of PrP^{Sc} on the surface of CNs possesses the N-terminal region that is recognized with mAb 8D5. PrP^{Sc} stains were also clearly detected on the surface of ScGT1-7-22L cells but not obvious on the surface of ScN2a3-22L cells (Fig. S2).

Colocalization of PrP^{Sc} detected by mAbs 132 and 8D5 in immortalized cells and cerebral neurons

PrP^{Sc}-specific double staining revealed differences in immunoreactivity of PrP^{Sc} between immortalized cell lines and CNs; PrP^{Sc} positive for mAb 8D5 was more apparent in CNs infected with the 22L strain than in ScN2a-3-22L cells. To assess the differences in detail, quantitative analysis of PrP^{Sc} populations was performed based on the reactivity with mAbs 132 and 8D5 (Fig. 6). In ScN2a-3-22L cells, only 6.6% of the total PrP^{Sc} signals were positive for both mAbs (Fig. 6b). In contrast, the proportion of double-positive PrP^{Sc} appeared to be higher in ScGT1-7-22L cells and prion-infected CNs than in ScN2a-3-22L cells: 18.9% in ScGT1-7-22L cells and 13.5–24.9% in CNs infected with three different prion strains. In ScN2a-3-22L cells, 92.3% of PrP^{Sc} were positive for mAb 132 (Fig. 6c, red and yellow

bars), whereas only 14.3% were positive for mAb 8D5 (Fig. 6c, green and yellow bars). The proportion of PrP^{Sc} population detected by mAb 132 in CNs infected with the 22L prion strain (78.9%) was significantly lower than that in ScN2a-3-22L cells (Fig. 6c, $P < 0.05$). Conversely, nearly half of PrP^{Sc} was positive for mAb 8D5 in CNs infected with 22L prion strain (46.0%), which was significantly higher than that in ScN2a-3-22L cells (Fig. 6c, $P < 0.01$). Although no difference was observed in the proportion of mAb 132-positive PrP^{Sc} between ScN2a-3-22L and ScGT1-7-22L cells (88.8%) or between ScGT1-7-22L and CNs infected with the 22L prion strain, the proportion of mAb 8D5-positive PrP^{Sc} in ScGT1-7-22L cells (30.2%) was significantly higher than in ScN2a-3-22L cells, but lower than in CNs infected with 22L prion strain (Fig. 6c, $P < 0.05$).

Biochemical properties of PrP molecules in cells

PrP^{Sc}-specific immunofluorescence staining revealed differences in staining pattern of PrP^{Sc} among cell types, particularly between ScN2a-3-22L cells and ScGT1-7-22L cells or CNs infected with the 22L strain. To address the differences, we performed immunoblotting to detect total PrP (both PK-sensitive and PK-resistant PrP) without PK treatment (Fig. 7a). The level of the full length PrP was apparently lower in ScN2a-3-22L cells than in N2a-3 cells. In contrast, GT1-7 and ScGT1-7-22L cells, and CNs and CNs infected with the 22L strain had comparable amounts of full length PrP. These results suggest that ScN2a-3-22L cells have a higher N-terminal-processing activity and that the cells produce N-terminal-truncated PrP^{Sc} that lacks the epitope for mAb 8D5. This idea is consistent with the results of PrP^{Sc}-specific immunofluorescence staining: PrP^{Sc} stains positive for mAb 132 were more evident than those positive for mAb 8D5 in ScN2a3-22L cells (Fig. 1a). By contrast, mAb 8D5 seemed to detect PrP^{Sc} efficiently in ScGT1-7-22L cells (Fig. 1d) and CNs infected with the 22L strain (Figs 4 and 5).

To analyse PrP^{Sc} recognized by mAb 8D5, PrP^{Sc} was immunoprecipitated from GT1-7 cells with mAb 8D5 and then subjected to immunoblotting with mAb 110, which recognizes the epitope in the octapeptide repeat region (Fig. 7b). PrP bands were detected only in the precipitates from ScGT1-7-22L cells, demonstrating the PrP^{Sc}-specificity of immunoprecipitation. The mAb 110 detected broad bands around 36 and 30 kDa, as well as bands at lower than 25 kDa. The 36 kDa broad band corresponds to full-length PrP^{Sc}, indicating the existence of full-length PrP^{Sc} on the cell surface. Regarding broad bands around 30 kDa and bands with approximately 25 kDa, it is difficult to conclude whether these bands represent mono- or non-glycosylated full-length PrP^{Sc} or di- or mono-glycosylated N-terminal-truncated PrP^{Sc} that were co-precipitated with full-length PrP^{Sc} during the immunoprecipitation. However, no immunoreactive bands were observed below 15 kDa, even around the running front (data not shown). This suggests that the PrP molecule, possessing the extreme

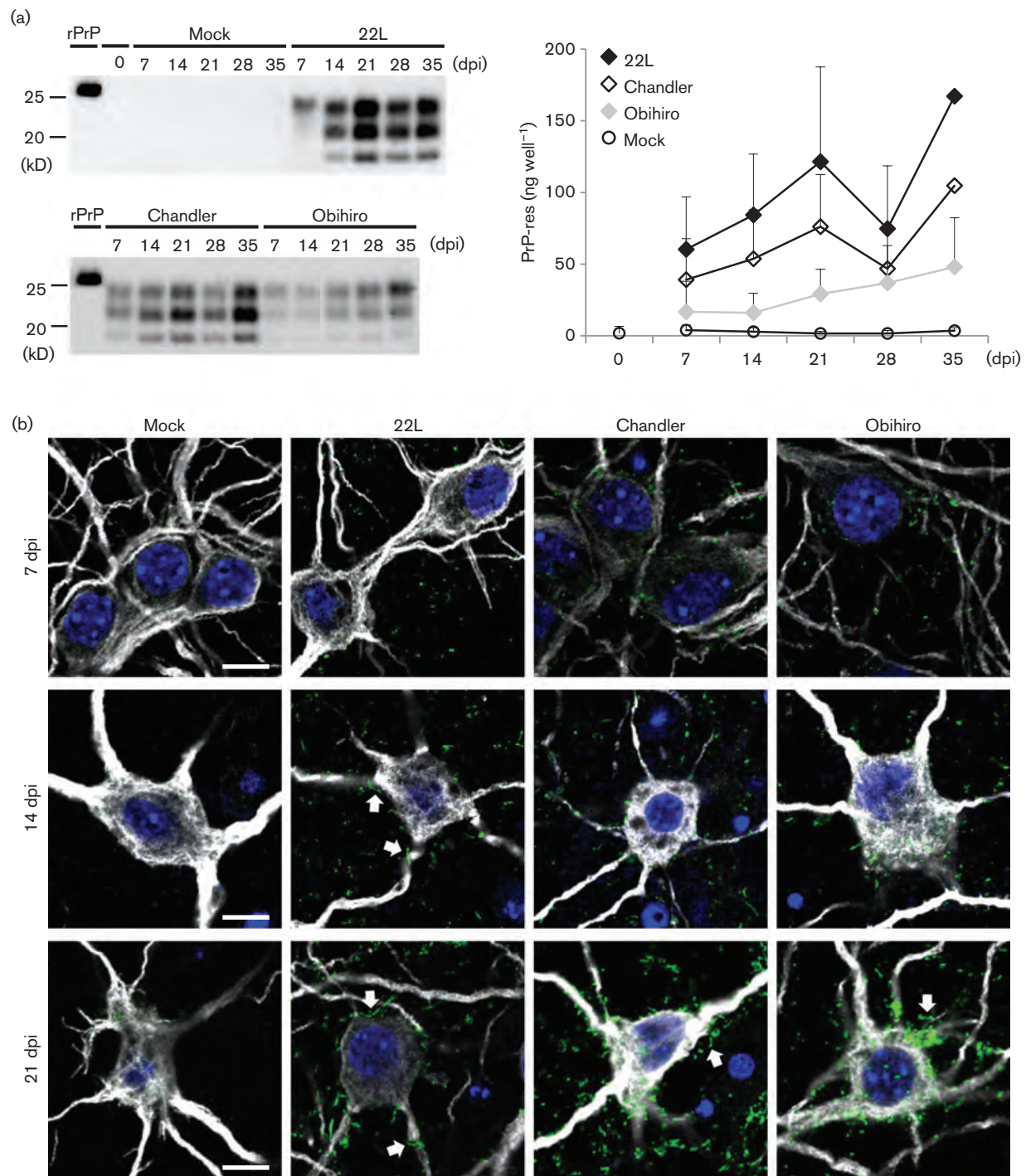


Fig. 3. Generation of PrP^{Sc} in CNs. (a) Kinetics of PrP-res generation in CNs. PK-treated cell lysates were subjected to SDS-PAGE followed by immunoblot analysis using anti-PrP antibody mAb 31C6. Purified recombinant PrP (rPrP) (5 ng lane⁻¹) was used as a standard for the quantification. The sample at 0 dpi was harvested before the exposure to prions. Figures on the left show representative immunoblot images of PrP-res. The graph on the right in (a) shows quantitative results (means and standard deviations of triplicate experiments, except 22L or Chandler strain-infected CNs at 35 dpi, which are shown as a single datum). Values indicate the total amount of PrP-res in each well. (b) PrP^{Sc} in CNs. PrP^{Sc} in prion-infected CNs was detected by PrP^{Sc}-specific immunostaining using mAb 132 (green) at 7, 14 and 21 dpi. Arrows indicate string-like PrP^{Sc} stains. Neuronal cell bodies and dendrites were identified by the staining of MAP2 (grey), and nuclei were counter-stained with DAPI (blue). Scale bars: 10 μ m.

N-terminus but lacking the C-terminal core region, will be negligible even if it exists.

DISCUSSION

The mAb 8D5 recognizes the epitope composed of the extreme N-terminus of PrP (aa 31–39) (Masujin *et al.*, 2013). It is well known that the N-terminus of PrP is partly digested by cellular events (Caughey *et al.*, 1991; Chen *et al.*, 1995). mAb 132 recognizes the epitope composed of aa 119–127 of PrP that remains in the C-terminal core fragment of PrP^{Sc}, possibly analogous to the C2 fragment (Chen *et al.*, 1995). Thus, PrP^{Sc}-specific double staining using the mAbs is expected to provide more precise information on intracellular localization of PrP^{Sc}. Indeed, PrP^{Sc} stains with mAb 132 were not always merged with those by mAb 8D5, indicating that the double staining detected greater numbers of PrP^{Sc} molecules than single staining (Figs 1, 4 and 6). The mAb 132-positive but mAb 8D5-negative PrP^{Sc} signals may represent the N-terminally

truncated PrP^{Sc} molecules. Unexpectedly, however, certain PrP^{Sc} was mAb 8D5-positive but mAb 132-negative in the double staining. The reactivity implies the existence of PrP^{Sc} composed only of the N-terminal portion of the PrP molecule; however, this is unlikely. The N-terminal portion of PrP^{Sc} is easily digested by PK treatment, indicating that the N-terminal portion locates the accessible surface of PrP^{Sc} oligomers/aggregates. Thus, anti-PrP antibodies may be able to more readily access the N-terminal portion than the C-terminal portion of PrP^{Sc}. The antibody molecule is nearly fivefold larger than a single PrP molecule; therefore, once mAb 8D5 binds to PrP^{Sc}, it may disturb the binding of mAb 132 to the epitope even on the neighbouring PrP molecule of PrP^{Sc} oligomers by steric hindrance. Indeed, ScN2a-3-22L cells were stained with Alexa Fluor 488-labelled mAb 132 and Alexa Fluor 647-labelled mAb 132 simultaneously; $65.7 \pm 2.3\%$ of Alexa 488-labelled PrP^{Sc} stains were also stained with Alexa Fluor-647. These factors will affect the interpretation of the results; nevertheless, PrP^{Sc}-specific multiple staining using two or more

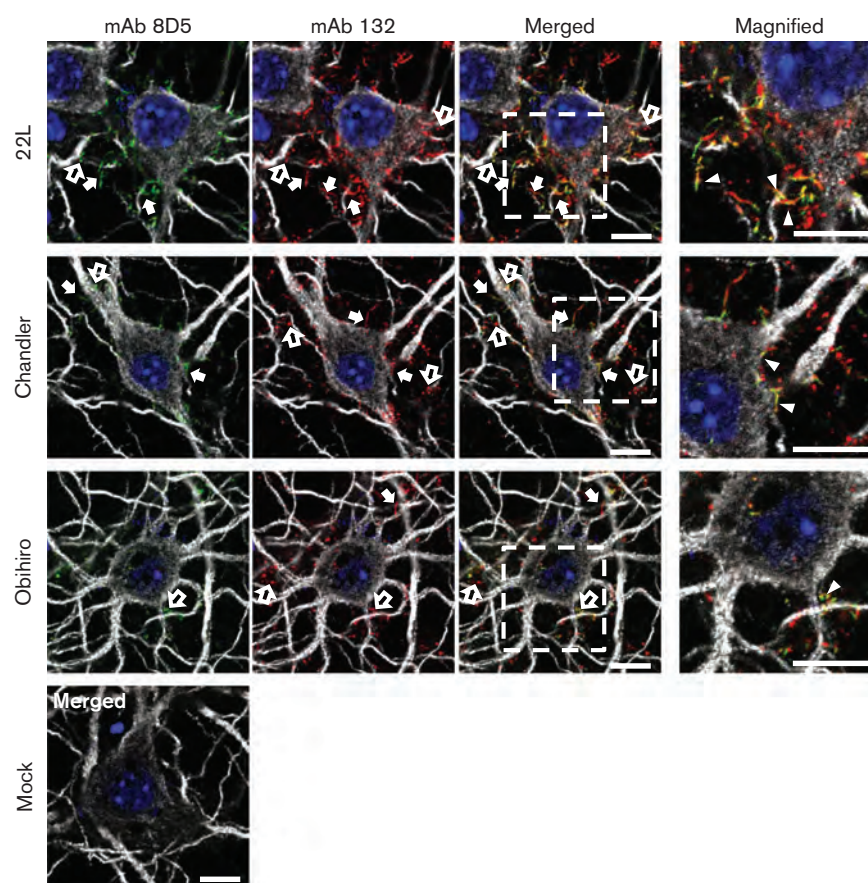


Fig. 4. PrP^{Sc}-specific double staining of prion-infected CNs. CNs infected with 22L, Chandler or Obihiro prion strain were fixed and pretreated with GdnSCN and stained simultaneously with Alexa Fluor 647-conjugated mAb 132 (red) and Alexa Fluor 488-conjugated mAb 8D5 (green) at 14 dpi. Neurons were visualized with anti-MAP2 antibody (grey) and nuclei were stained with DAPI (blue). Boxed areas in merged images are enlarged in the corresponding rightmost columns. Closed arrows indicate string-like stains of PrP^{Sc} by mAbs 132 and 8D5, and open arrows indicate granular stains of PrP^{Sc}. Arrowheads show representative overlapping stains with mAbs 132 and 8D5. Scale bars: 10 μ m.

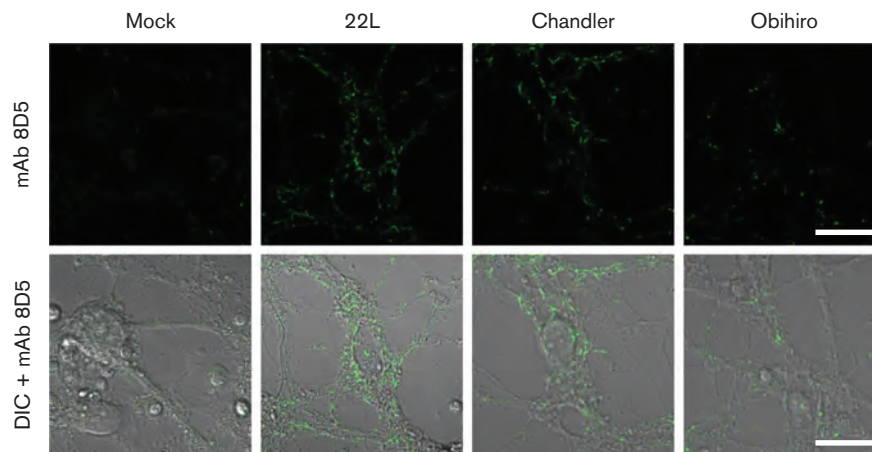


Fig. 5. Detection of PrP^{Sc} on the cell surface of living CNs by mAb 8D5. CNs at 14 dpi were incubated with Alexa Fluor 488-conjugated mAb 8D5 at 37 °C for 1 h without fixation, permeabilization or denaturation. Upper panels show the signals detected by mAb 8D5 (green), and lower panels show the merged images with a differential interference contrast image (DIC). Scale bars: 20 μ m.

antibodies, as shown here, is one of the effective approaches for precise understanding of intracellular localization of PrP^{Sc} and the mechanism for prion propagation.

Although PrP^{Sc} has been reported as detected on the cell surface of prion-infected immortalized neuronal cells (Goold *et al.*, 2011; Rouvinski *et al.*, 2014; Yamasaki *et al.*, 2012), cell biological studies using immortalized cell lines strongly suggested that the PrP^{Sc} formation takes place at cellular compartments along with the endocytic recycling pathway such as the endocytic recycling compartments, or those along with the endo-lysosomal pathway such as multivesicular bodies (Beranger *et al.*, 2002; Borchelt *et al.*, 1992; Marijanovic *et al.*, 2009; Pimpinelli *et al.*, 2005; Veith *et al.*, 2009; Yamasaki *et al.*, 2012, 2014a). In contrast, ultrastructural analyses using brains of prion-infected mice and hamsters identified PrP^{Sc} frequently at the plasma membranes and less frequently at synapses and compartments of the endo-lysosomal system (Arnold *et al.*, 1995; Fournier *et al.*, 2000; Godsavage *et al.*, 2008). Recently, Godsavage and colleagues reported that in RML strain-infected mouse brains, the majority of PrP^{Sc} clusters were detected at the plasma membranes, including membrane invaginations and the site of cell-to-cell contact, whereas in the other subcellular regions such as synapses and intracellular vesicles, PrP^{Sc} clusters were detected only occasionally by immuno-electron microscopic examination using an antibody that recognizes the N-terminal region of PrP (Godsavage *et al.*, 2013). The authors believed that PrP^{Sc} detected by the anti-PrP N-terminus mAb Saf32 included nascent full-length PrP^{Sc}, as the N-terminal region tends to be processed after generation of PrP^{Sc} (Caughey *et al.*, 1991; Taraboulos *et al.*, 1992). Considered collectively, ultrastructural studies suggest the plasma membranes as

the primary site for PrP^{Sc} formation. In the current study, we found that morphology and cellular localization of PrP^{Sc} differ in immortalized cell lines and CNs: in N2a-3 and GT1-7 cells infected with 22L prion strain (Fig. 1b, c), PrP^{Sc} was mainly detected as granule-like stains at the perinuclear regions, as previously reported (Schätzl *et al.*, 1997; Yamasaki *et al.*, 2012), whereas in CNs infected with the 22L or Chandler strain, PrP^{Sc} was detected as unique string-like stains, possibly on the cell surface; however, a few were detected in the cytoplasm (Figs 4 and 5). Rouvinski and colleagues recently reported that in addition to granule-like PrP^{Sc} stains in the cytoplasm, string-like PrP^{Sc} stains were detected on the surface of 22L or RML prion strain-infected GT1 cells. The string-like PrP^{Sc} was detected by anti-PrP antibodies recognizing the N-terminal part of PrP and was demonstrated as glycosylphosphatidylinositol-anchored PrP^{Sc} amyloids (Rouvinski *et al.*, 2014). However, compared with the results by Rouvinski and colleagues, string-like PrP^{Sc} stains were predominantly observed on the surface of CNs; however, a few intracellular granule-like PrP^{Sc} stains were observed in the CNs (Fig. 4). Taken together, the differences in PrP^{Sc} stains suggest that the mechanism of PrP^{Sc} formation in immortalized cell lines may not be exactly the same as that in CNs. Interestingly, Rouvinski and colleagues also detected string-like PrP^{Sc} stains in brains of scrapie-infected mice (Rouvinski *et al.*, 2014). Furthermore, filamentous depositions of PrP^{Sc} were frequently observed in the white matter of patients with inherited prion diseases (Reiniger *et al.*, 2013) and in the neuropils of the 22L prion strain-infected cerebellar slices (Wolf *et al.*, 2015). In addition, it was reported that PrP^{Sc} accumulates predominantly as unprocessed forms in brain tissues and in the primary-cultured cerebellar-granule neurons (Dron *et al.*, 2010).

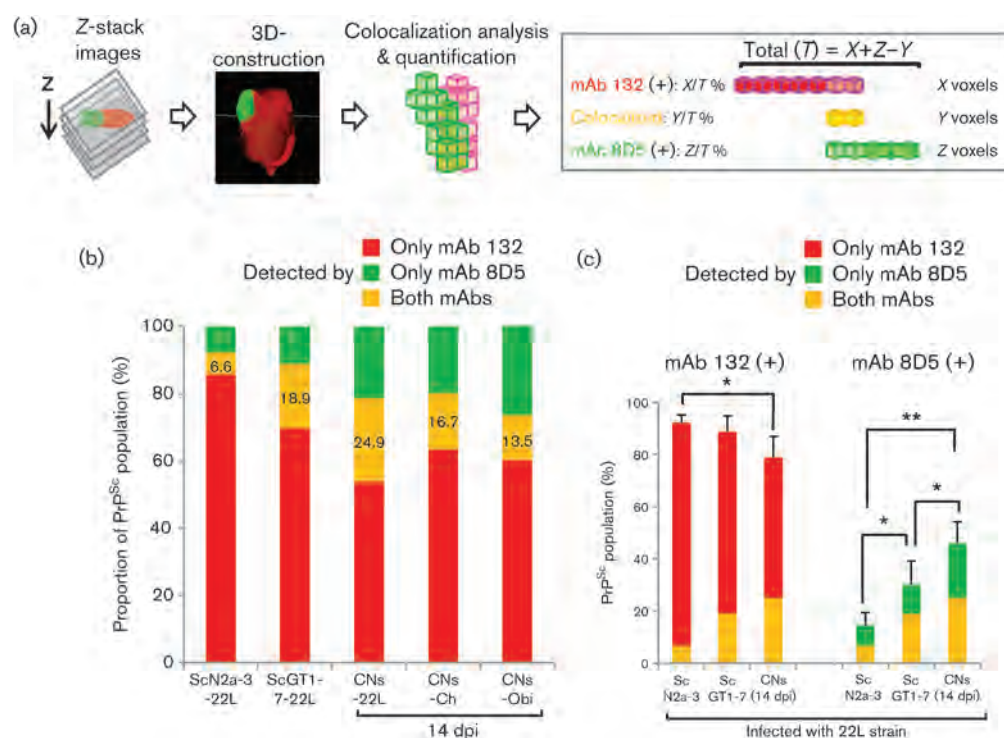


Fig. 6. Colocalization analysis of PrP^{Sc} in cells. (a) A scheme for the colocalization analysis. First, 3D-fluorescence images were constructed from Z-stack images, then fluorescence-positive 3D regions, 'surface', were created by IMARIS software. Next, PrP^{Sc}-positive surfaces were broken down into voxels, the minimum unit of 3D images, for subsequent quantification. Voxels positive for mAb 132, mAb 8D5, or both mAbs were counted, and the proportion to the total voxels positive for PrP^{Sc} detected in cells was calculated by dividing the voxel number of each population by that of total PrP^{Sc}. (b) Proportions of PrP^{Sc} populations with different immunoreactivity. Each bar shows the percentage of PrP^{Sc} detected by only mAb 132 (red) or 8D5 (green) or both mAbs (yellow) in cells. The numbers in yellow bars indicate the percentage of PrP^{Sc} positive for both mAbs. Cell types used for this analysis are shown at the bottom: ScN2a-22L and ScGT1-7-22L cells as immortalized cell lines; CNs infected with 22L (CN-22L), Chandler (CN-Ch) or Obihiro (CN-Obi) strain (at 14 dpi). (c) Proportions of PrP^{Sc} detected by mAb 132 or mAb 8D5 in three cell types. The proportions of mAb 132-positive or mAb 8D5-positive PrP^{Sc} to total PrP^{Sc} in the corresponding cells were picked out from (b). Graphs represent the means and standard deviations of nine wells from three independent experiments for N2a-3 and GT1-7 cells, and those of six wells from two independent experiments for CNs. Z-stack images were acquired from three to four view fields per well, which contained ten cells for N2a-3, seven cells for GT1-7, or four cells for CNs. Statistical analysis was done by one-way ANOVA, and *post hoc* comparisons were carried out using Tukey–Kramer multiple comparisons test. **P*<0.05; ***P*<0.01.

Since PrP^{Sc} detected by mAb 8D5 is expected to be a full-length PrP^{Sc}, therefore the morphological and locational, as well as biochemical, similarities of PrP^{Sc} stains in prion-infected CNs and brains of patients or animals affected by prion diseases suggest that the mechanism of PrP^{Sc} formation in CNs is, at least to some extent, similar to that in neurons in the central nervous system.

In the previous reports using prion-infected primary cultured neurons, antimetotics were used throughout the culture period to suppress the growth of astrocytes (Carimalo *et al.*, 2005; Cronier *et al.*, 2007; Hannaoui *et al.*, 2013), and some of them confirmed the neuronal predominance with astrocytes at 4–5 % of the cellular composition at an early stage (Cronier *et al.*, 2004). However, antimetotics will be harmful to neurons depending on concentrations and the

period of treatment. In the current study, we showed that temporary treatment of Ara-C successfully reduced astrocyte proliferation and enabled us to keep CNs up to 4 weeks after prion inoculation (Fig. 2). The CNs supported prion propagation with various prion strains including Obihiro strain, which is not propagated well in N2a-3 and GT1-7 cells (Uryu *et al.*, 2007). Difference in PrP^{Sc} stains in CNs infected with Obihiro strain (Fig. 4) may be partly due to a biochemical difference of PrP^{Sc} among prion strains. Furthermore, PrP^{Sc}-specific double staining using mAbs 132 and 8D5 suggested that CNs share the same mechanism for prion propagation with neurons in the central nervous system. The presence of PrP^{Sc} at neurites in the CNs is of interest because neurodegeneration in prion diseases is reported to be initiated at axonal terminals (Gray *et al.*, 2009),

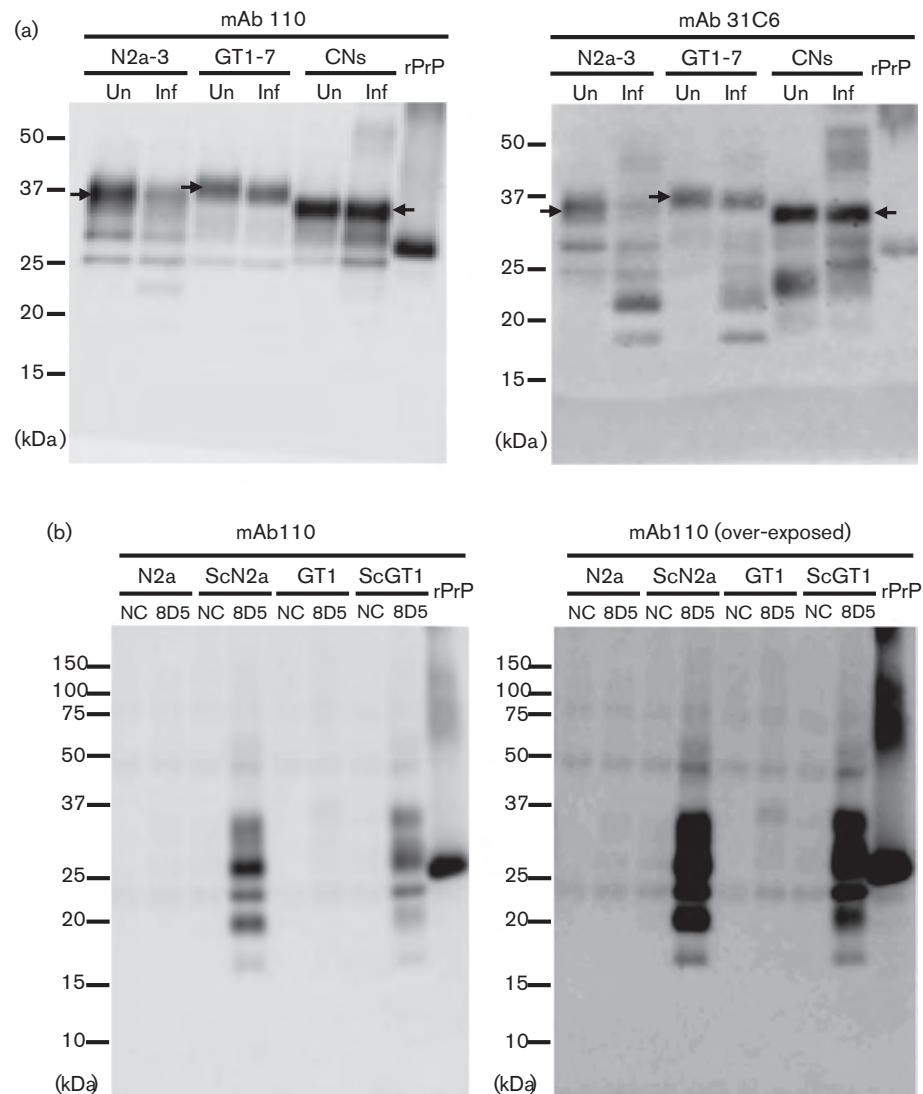


Fig. 7. Biochemical properties of PrP molecules in cells. (a) Total PrP molecules in cells. PK-untreated cell lysates from N2a-3, GT1-7 and primary cerebral neurons (CNs, at 21 dpi) were subjected to immunoblotting using mAbs 110 and 31C6. Lysate equivalent to 3 μ g total protein was loaded onto each lane. Arrows indicate full length PrP. Un, uninfected; Inf, infected with 22L prion strain; rPrP, recombinant PrP as a marker. (b) Immunoprecipitation of PrP^{Sc} with mAb 8D5. Immunoprecipitates from GT1-7 (GT1) or ScGT1-17-22L (ScGT1) cells with mAb 8D5 or negative control mAb (NC) were subjected to immunoblotting using mAb 110, which recognizes the epitope in the octapeptide repeat at aa 59–65 and 83–89.

dendrites (Fuhrmann *et al.*, 2007) or synapses (Jeffrey *et al.*, 2000), rather than at the soma of neurons. Thus, neuron-enriched primary cultures used in the current study will be an invaluable *ex vivo* model for analysing the mechanism of neurodegeneration caused by prion infection.

METHODS

Antibodies. mAbs 31C6, 132 and 8D5, which recognize epitopes consisting of mouse PrP aa 143–149, 119–127 (Kim *et al.*, 2004) and 31–39 (Masujin *et al.*, 2013), respectively, were used. MAb 110, which recognizes the epitope consisting of seven amino acids, PHGGGWG, at

aa59–65 and 83–89 in the octapeptide repeat of PrP, was also used (Kim *et al.*, 2004). For direct immunofluorescent staining of PrP^{Sc}, mAbs 132 and 8D5 were conjugated with Alexa Fluor 647 and 488, respectively, using Alexa Fluor carboxylic acid succinimidyl ester mixed isomers (Life Technologies). The following antibodies were also used for IFA or immunoblot analysis: anti-microtubule-associated protein 2 (MAP2) chicken polyclonal antibodies (pAbs) (ab5392; Abcam), anti-GFAP rabbit pAbs (0334; Dako), and anti- β -III tubulin rabbit pAbs (ab18207; Abcam). MAb P2-284 against feline panleukopenia virus was used as an isotype control antibody (Horiuchi *et al.*, 1997).

Cell lines. Subclones of the Neuro2a mouse neuroblastoma cell line, N2a-3 (Uryu *et al.*, 2007), and the GT1 hypothalamic neuronal cell line, GT1-7 (Schatzl *et al.*, 1997) were used. ScN2a-3-22L (Nakamitsu *et al.*,

2010), ScN2a-3-Ch (Uryu *et al.*, 2007) and GT1-7 persistently infected with the 22L prion strain (ScGT1-7-22L) (Yamasaki *et al.*, 2012) were used as prion-infected cells. Those cells were cultured as described previously (Uryu *et al.*, 2007; Yamasaki *et al.*, 2012) and used at passage history between 5 and 30.

Primary neuronal cell culture. Chamber covers of 8-well configurations (Matsunami), 96-well μ -plates (ibidi), and 24-well plastic culture plates were coated with 20 μ g poly-L-lysine (Sigma) ml^{-1} in PBS and settled overnight at room temperature (RT). After washing twice with sterilized de-ionized water, Neurobasal Medium (Life Technologies) containing 1 \times B-27 Supplement (Life Technologies) and 6 mM Glutamax (Life Technologies) (hereafter neuronal medium) was added into each well and the plates were kept at 37 °C in 5% CO₂ atmosphere until use.

Primary neuronal cell cultures were prepared from ICR mouse embryos of embryonic day 14 (pregnant mice were purchased from Japan Clea). The experimental procedures were approved by the Institutional Animal Care and Use Committee at Hokkaido University (no. 13–0141). The diencephalon, mesencephalon, medulla oblongata, and cerebellum were removed from embryonic brains, and the olfactory bulb, hippocampi and meninges were resected under a stereo microscope. The remaining tissues including cerebral cortices were digested using the Neural Tissue Dissociation Kit (P) (Miltenyi Biotec) according to the manufacturer's instructions, but modified by enzymatic reactions being performed on ice. Tissues were dispersed by gentle pipetting, and filtered through a cell strainer with 100 μ m nylon mesh (Corning). The cells were collected by centrifugation at 300 g for 5 min at 4 °C. All procedures described above were performed using ice-cold Hank's Balanced Salt Solution (Sigma) containing 100 μ M HEPES (Life Technologies) and 10 μ M sodium pyruvate (Life Technologies). Cells were resuspended in the neuronal medium and were plated at a density of 1.0×10^5 cells on poly-L-lysine pre-coated glass or plastic plates cm^{-2} . Half of the culture medium was replaced with fresh neuronal medium every week. To inhibit astrocyte proliferation, Ara-C (Sigma) was added at a final concentration of 0.25 μ M to cultures at 4 div. The Ara-C concentration was reduced by half accompanying the prion infection at 7 div, and cultures were maintained in Ara-C-free neuronal medium after 11 div (see Fig. 2a).

Inocula-containing prions were prepared from brains of mice infected with the 22L, Chandler or Obihiro prion strains (all are mouse-adapted scrapie prions) at the terminal stage of the disease, and brains of age-matched, uninfected ICR mice were used as the control. The brains were homogenized in sterile PBS at a concentration of 10% w/v. The homogenates were sonicated for 3.5 min and centrifuged at 3000 g for 10 min at 4 °C. The resulting supernatant was centrifuged at 100 000 g for 60 min at 4 °C, and the pellet containing microsomes was suspended in sterile PBS. The amount of PrP-res in the material was quantified by immunoblot analysis using purified PrP-res as a standard (Yamasaki *et al.*, 2014a). Primary neuronal cell cultures at 7 div were exposed to inocula equivalent to 5 ng of PrP-res per 1.0×10^5 cells by replacement of half of the medium in each well. The medium was completely replaced by fresh neuronal medium at 4 dpi, which corresponds to 11 div (see Fig. 2a).

Immunoblot analysis. Neurons cultured on 24-well plastic plates were washed with PBS and treated with 200 μ l of lysis buffer (0.5% Triton X-100, 0.5% sodium deoxycholate, 150 mM NaCl, 5 mM EDTA, and 10 mM Tris-HCl [pH 7.5]) for 30 min at 4 °C. The cells were then lysed by one cycle of freeze–thaw and subsequent pipetting. The lysate was clarified by centrifugation at 2000 g for 5 min at 4 °C. Protein concentration of the lysates was measured using a DC protein assay kit (Bio-Rad) and adjusted to 0.3 mg ml^{-1} . For detection of PrP-res, PK was added to the lysates at a final concentration of 4% of the amount of total protein and incubated at 37 °C for 20 min. PK digestion was

terminated by the addition of Pefabloc (Roche) to 1 mM, and the lysates were then treated with 50 μ g DNase I ml^{-1} at room temperature for 15 min. Precipitation of PrP-res by phosphotungstic acid (PTA) followed by SDS-PAGE, Western transfer, and chemiluminescence detection were carried out as described elsewhere (Shindoh *et al.*, 2009; Uryu *et al.*, 2007). For detection of GFAP and β -III tubulin, the procedures from PK digestion to PTA precipitation were omitted, and 2 μ g of total protein was loaded onto each lane.

Immunoprecipitation. GT1-7 cells grown on 10 cm dish to approximately 80% confluence were used. After washing cells gently with cold PBS, cells were incubated with 15 μ g of mAb at 4 °C for 1 h. After washing the cells three times, cells were collected by cell scraper and lysed with PBS containing 1% Zwittergent 3–14 (Calbiochem) and 1 \times cOmplete Protease Inhibitor Cocktail (Roche). The cell lysates were clarified by centrifugation at 500 g for 10 min, the resulting supernatants (50 μ g protein equivalent) were mixed with Dynabeads Protein G (Miltenyi) that were blocked with 1% I-BLOCK (Applied Biosystems) and 20% N-101 (NOF Corporation) and pre-incubated with anti-mouse IgG Fc-specific goat IgG. Mixtures were incubated at 4 °C for 90 min with constant rotation and then the beads were washed five times with PBS containing 1% Tween 20 using a magnetic separator. Immunoprecipitates were eluted with the SDS sample buffer by boiling for 10 min and subjected to immunoblotting. Blots were probed with mAb 110 labelled with HRP (Horiuchi *et al.*, 2009).

Immunofluorescence assay. Primary neurons grown on 8-well chamber covers or 96-well μ -plates, and N2a-3 or GT1-7 cells grown on 8-well Lab-Tek II chambered coverglass (Nunc) were fixed with PBS, containing 4% paraformaldehyde and 4% sucrose at room temperature for 10 min. Subsequently, procedures for IFA were carried out as described previously (Yamasaki *et al.*, 2014a, b). In some cases, mAbs conjugated with Alexa Fluor fluorescent dye were used for the direct immunostaining of PrP^{Sc}.

For the detection of PrP^{Sc} on the cell surface, cells were gently rinsed with prewarmed sterile PBS and incubated with neuronal medium containing 1 μ g Alexa Fluor 488-conjugated mAb 8D5 ml^{-1} at 37 °C for 1 h. The cells were gently rinsed and covered with PBS for the microscopic examination.

Colocalization analysis. 3D fluorescent images were constructed from the Z-stack images and surfaces. The 3D bodies that were positive for each antibody were identified by Imaris software version 7.6.1. (Bitplane). The minimum unit of the surfaces, termed voxel(s), that was positive for each antibody was counted for colocalization statistics.

ACKNOWLEDGEMENTS

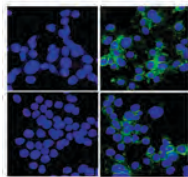
This work was supported by a Grant-in-Aid for Science Research (A) (grant no. 15H02475), a grant from the Program for Leading Graduate Schools (F01), and the Japan Initiative for Global Research Network on Infectious Diseases (J-GRID), from the Ministry of Education, Culture, Sports, Science and Technology, Japan. This work was also supported by grants for TSE research (H26-Shokuhin-Ippan-004) and Research on Measures for Intractable Diseases from the Ministry of Health, Labour and Welfare of Japan. We thank Zensho Co. Ltd., for the BSL3 facility. This work was also supported in part by the Intramural Research Program of NIAID.

REFERENCES

Arnold, J. E., Tipler, C., Laszlo, L., Hope, J., Landon, M. & Mayer, R. J. (1995). The abnormal isoform of the prion protein accumulates in late-

- endosome-like organelles in scrapie-infected mouse brain. *J Pathol* 176, 403–411.
- Béranger, F., Mangé, A., Goud, B. & Lehmann, S. (2002).** Stimulation of PrP(C) retrograde transport toward the endoplasmic reticulum increases accumulation of PrP(Sc) in prion-infected cells. *J Biol Chem* 277, 38972–38977.
- Borchelt, D. R., Taraboulos, A. & Prusiner, S. B. (1992).** Evidence for synthesis of scrapie prion proteins in the endocytic pathway. *J Biol Chem* 267, 16188–16199.
- Carimalo, J., Cronier, S., Petit, G., Peyrin, J. M., Boukhtouche, F., Arbez, N., Lemaigre-Dubreuil, Y., Brugg, B. & Miquel, M. C. (2005).** Activation of the JNK–c-Jun pathway during the early phase of neuronal apoptosis induced by PrP106–126 and prion infection. *Eur J Neurosci* 21, 2311–2319.
- Caughey, B. & Raymond, G. J. (1991).** The scrapie-associated form of PrP is made from a cell surface precursor that is both protease- and phospholipase-sensitive. *J Biol Chem* 266, 18217–18223.
- Caughey, B., Raymond, G. J., Ernst, D. & Race, R. E. (1991).** N-terminal truncation of the scrapie-associated form of PrP by lysosomal protease(s): implications regarding the site of conversion of PrP to the protease-resistant state. *J Virol* 65, 6597–6603.
- Chen, S. G., Teplow, D. B., Parchi, P., Teller, J. K., Gambetti, P. & Autilio-Gambetti, L. (1995).** Truncated forms of the human prion protein in normal brain and in prion diseases. *J Biol Chem* 270, 19173–19180.
- Cronier, S., Laude, H. & Peyrin, J. M. (2004).** Prions can infect primary cultured neurons and astrocytes and promote neuronal cell death. *Proc Natl Acad Sci U S A* 101, 12271–12276.
- Cronier, S., Beringue, V., Bellon, A., Peyrin, J. M. & Laude, H. (2007).** Prion strain- and species-dependent effects of antiprion molecules in primary neuronal cultures. *J Virol* 81, 13794–13800.
- Curin Serbec, V., Bresjanac, M., Popovic, M., Pretnar Hartman, K., Galvani, V., Ruprecht, R., Cernilec, M., Vranac, T., Hafner, I. & other authors (2004).** Monoclonal antibody against a peptide of human prion protein discriminates between Creutzfeldt-Jacob's disease-affected and normal brain tissue. *J Biol Chem* 279, 3694–3698.
- Dron, M., Moudjou, M., Chapuis, J., Salamat, M. K., Bernard, J., Cronier, S., Langevin, C. & Laude, H. (2010).** Endogenous proteolytic cleavage of disease-associated prion protein to produce C2 fragments is strongly cell- and tissue-dependent. *J Biol Chem* 285, 10252–10264.
- Fournier, J. G., Escaig-Haye, F. & Grigoriev, V. (2000).** Ultrastructural localization of prion proteins: physiological and pathological implications. *Microsc Res Tech* 50, 76–88.
- Fuhrmann, M., Mitteregger, G., Kretzschmar, H. & Herms, J. (2007).** Dendritic pathology in prion disease starts at the synaptic spine. *J Neurosci* 27, 6224–6233.
- Godsave, S. F., Wille, H., Kujala, P., Latawiec, D., DeArmond, S. J., Serban, A., Prusiner, S. B. & Peters, P. J. (2008).** Cryo-immunogold electron microscopy for prions: toward identification of a conversion site. *J Neurosci* 28, 12489–12499.
- Godsave, S. F., Wille, H., Pierson, J., Prusiner, S. B. & Peters, P. J. (2013).** Plasma membrane invaginations containing clusters of full-length PrP^{Sc} are an early form of prion-associated neuropathology in vivo. *Neurobiol Aging* 34, 1621–1631.
- Goold, R., Rabbanian, S., Sutton, L., Andre, R., Arora, P., Moonga, J., Clarke, A. R., Schiavo, G., Jat, P. & other authors (2011).** Rapid cell-surface prion protein conversion revealed using a novel cell system. *Nat Commun* 2, 281.
- Gray, B. C., Siskova, Z., Perry, V. H. & O'Connor, V. (2009).** Selective presynaptic degeneration in the synaptopathy associated with ME7-induced hippocampal pathology. *Neurobiol Dis* 35, 63–74.
- Hannaoui, S., Maatouk, L., Privat, N., Levavasseur, E., Faucheux, B. A. & Haïk, S. (2013).** Prion propagation and toxicity occur *in vitro* with two-phase kinetics specific to strain and neuronal type. *J Virol* 87, 2535–2548.
- Horiuchi, M., Mochizuki, M., Ishiguro, N., Nagasawa, H. & Shinagawa, M. (1997).** Epitope mapping of a monoclonal antibody specific to feline panleukopenia virus and mink enteritis virus. *J Vet Med Sci* 59, 133–136.
- Horiuchi, M., Karino, A., Furuoka, H., Ishiguro, N., Kimura, K. & Shinagawa, M. (2009).** Generation of monoclonal antibody that distinguishes PrP^{Sc} from PrP^C and neutralizes prion infectivity. *Virology* 394, 200–207.
- Jeffrey, M., Goodsir, C. M., Bruce, M. E., McBride, P. A., Scott, J. R. & Halliday, W. G. (1992).** Infection specific prion protein (PrP) accumulates on neuronal plasmalemma in scrapie infected mice. *Neurosci Lett* 147, 106–109.
- Jeffrey, M., Goodsir, C. M., Bruce, M., McBride, P. A., Scott, J. R. & Halliday, W. G. (1994).** Correlative light and electron microscopy studies of PrP localisation in 87V scrapie. *Brain Res* 656, 329–343.
- Jeffrey, M., Halliday, W. G., Bell, J., Johnston, A. R., MacLeod, N. K., Ingham, C., Sayers, A. R., Brown, D. A. & Fraser, J. R. (2000).** Synapse loss associated with abnormal PrP precedes neuronal degeneration in the scrapie-infected murine hippocampus. *Neuropathol Appl Neurobiol* 26, 41–54.
- Kim, C. L., Umetani, A., Matsui, T., Ishiguro, N., Shinagawa, M. & Horiuchi, M. (2004).** Antigenic characterization of an abnormal isoform of prion protein using a new diverse panel of monoclonal antibodies. *Virology* 320, 40–51.
- Korth, C., Stierli, B., Streit, P., Moser, M., Schaller, O., Fischer, R., Schulz-Schaeffer, W., Kretzschmar, H., Raeber, A. & other authors (1997).** Prion (PrP^{Sc})-specific epitope defined by a monoclonal antibody. *Nature* 390, 74–77.
- Mallucci, G., Dickinson, A., Linehan, J., Klöhn, P. C., Brandner, S. & Collinge, J. (2003).** Depleting neuronal PrP in prion infection prevents disease and reverses spongiosis. *Science* 302, 871–874.
- Marijanovic, Z., Caputo, A., Campana, V. & Zurzolo, C. (2009).** Identification of an intracellular site of prion conversion. *PLoS Pathog* 5, e1000426.
- Masujin, K., Kaku-Ushiki, Y., Miwa, R., Okada, H., Shimizu, Y., Kasai, K., Matsuura, Y. & Yokoyama, T. (2013).** The N-terminal sequence of prion protein consists an epitope specific to the abnormal isoform of prion protein (PrP(Sc)). *PLoS One* 8, e58013.
- Nakamitsu, S., Kurokawa, A., Yamasaki, T., Uryu, M., Hasebe, R. & Horiuchi, M. (2010).** Cell density-dependent increase in the level of protease-resistant prion protein in prion-infected Neuro2a mouse neuroblastoma cells. *J Gen Virol* 91, 563–569.
- Naslavsky, N., Stein, R., Yanai, A., Friedlander, G. & Taraboulos, A. (1997).** Characterization of detergent-insoluble complexes containing the cellular prion protein and its scrapie isoform. *J Biol Chem* 272, 6324–6331.
- Paramithiotis, E., Pinard, M., Lawton, T., LaBoissiere, S., Leathers, V. L., Zou, W. Q., Estey, L. A., Lamontagne, J., Lehto, M. T. & other authors (2003).** A prion protein epitope selective for the pathologically misfolded conformation. *Nat Med* 9, 893–899.
- Pimpinelli, F., Lehmann, S. & Maridonneau-Parini, I. (2005).** The scrapie prion protein is present in flotillin-1-positive vesicles in central- but not peripheral-derived neuronal cell lines. *Eur J Neurosci* 21, 2063–2072.
- Prusiner, S. B. (1998).** Prions. *Proc Natl Acad Sci U S A* 95, 13363–13383.
- Reiniger, L., Mirabile, I., Lukic, A., Wadsworth, J. D., Linehan, J. M., Groves, M., Lowe, J., Druyeh, R., Rudge, P. & other authors (2013).** Filamentous white matter prion protein deposition is a distinctive feature of multiple inherited prion diseases. *Acta Neuropathol Commun* 1, 8.
- Rouvinski, A., Karniely, S., Kounin, M., Moussa, S., Goldberg, M. D., Warburg, G., Lyakhovetsky, R., Papy-Garcia, D., Kutzsche, J. & other**

- authors (2014).** Live imaging of prions reveals nascent PrP^{Sc} in cell-surface, raft-associated amyloid strings and webs. *J Cell Biol* **204**, 423–441.
- Sakai, K., Hasebe, R., Takahashi, Y., Song, C. H., Suzuki, A., Yamasaki, T. & Horiuchi, M. (2013).** Absence of CD14 delays progression of prion diseases accompanied by increased microglial activation. *J Virol* **87**, 13433–13445.
- Schätzl, H. M., Laszlo, L., Holtzman, D. M., Tatzelt, J., DeArmond, S. J., Weiner, R. I., Mobley, W. C. & Prusiner, S. B. (1997).** A hypothalamic neuronal cell line persistently infected with scrapie prions exhibits apoptosis. *J Virol* **71**, 8821–8831.
- Shindoh, R., Kim, C. L., Song, C. H., Hasebe, R. & Horiuchi, M. (2009).** The region approximately between amino acids 81 and 137 of proteinase K-resistant PrP^{Sc} is critical for the infectivity of the Chandler prion strain. *J Virol* **83**, 3852–3860.
- Taraboulos, A., Serban, D. & Prusiner, S. B. (1990).** Scrapie prion proteins accumulate in the cytoplasm of persistently infected cultured cells. *J Cell Biol* **110**, 2117–2132.
- Taraboulos, A., Raeber, A. J., Borchelt, D. R., Serban, D. & Prusiner, S. B. (1992).** Synthesis and trafficking of prion proteins in cultured cells. *Mol Biol Cell* **3**, 851–863.
- Uryu, M., Karino, A., Kamihara, Y. & Horiuchi, M. (2007).** Characterization of prion susceptibility in Neuro2a mouse neuroblastoma cell subclones. *Microbiol Immunol* **51**, 661–669.
- Ushiki-Kaku, Y., Endo, R., Iwamaru, Y., Shimizu, Y., Imamura, M., Masujin, K., Yamamoto, T., Hattori, S., Itohara, S. & other authors (2010).** Tracing conformational transition of abnormal prion proteins during interspecies transmission by using novel antibodies. *J Biol Chem* **285**, 11931–11936.
- Veith, N. M., Plattner, H., Stuermer, C. A., Schulz-Schaeffer, W. J. & Bürkle, A. (2009).** Immunolocalisation of PrP^{Sc} in scrapie-infected N2a mouse neuroblastoma cells by light and electron microscopy. *Eur J Cell Biol* **88**, 45–63.
- Vey, M., Pilkuhn, S., Wille, H., Nixon, R., DeArmond, S. J., Smart, E. J., Anderson, R. G., Taraboulos, A. & Prusiner, S. B. (1996).** Subcellular colocalization of the cellular and scrapie prion proteins in caveolae-like membranous domains. *Proc Natl Acad Sci U S A* **93**, 14945–14949.
- Wolf, H., Hossinger, A., Fehlinger, A., Büttner, S., Sim, V., McKenzie, D. & Vorberg, I. M. (2015).** Deposition pattern and subcellular distribution of disease-associated prion protein in cerebellar organotypic slice cultures infected with scrapie. *Front Neurosci* **9**, 410.
- Yamasaki, T., Suzuki, A., Shimizu, T., Watarai, M., Hasebe, R. & Horiuchi, M. (2012).** Characterization of intracellular localization of PrP^{Sc} in prion-infected cells using a mAb that recognizes the region consisting of aa 119–127 of mouse PrP. *J Gen Virol* **93**, 668–680.
- Yamasaki, T., Baron, G. S., Suzuki, A., Hasebe, R. & Horiuchi, M. (2014a).** Characterization of intracellular dynamics of inoculated PrP-res and newly generated PrP^{Sc} during early stage prion infection in Neuro2a cells. *Virology* **450–451**, 324–335.
- Yamasaki, T., Suzuki, A., Hasebe, R. & Horiuchi, M. (2014b).** Comparison of the anti-prion mechanism of four different anti-prion compounds, anti-PrP monoclonal antibody 44B1, pentosan polysulfate, chlorpromazine, and U18666A, in prion-infected mouse neuroblastoma cells. *PLoS One* **9**, e106516.



Establishment of a simple cell-based ELISA for the direct detection of abnormal isoform of prion protein from prion-infected cells without cell lysis and proteinase K treatment

Zhifu Shan, Takeshi Yamasaki, Akio Suzuki, Rie Hasebe & Motohiro Horiuchi

To cite this article: Zhifu Shan, Takeshi Yamasaki, Akio Suzuki, Rie Hasebe & Motohiro Horiuchi (2016) Establishment of a simple cell-based ELISA for the direct detection of abnormal isoform of prion protein from prion-infected cells without cell lysis and proteinase K treatment, Prion, 10:4, 305-318, DOI: [10.1080/19336896.2016.1189053](https://doi.org/10.1080/19336896.2016.1189053)

To link to this article: <http://dx.doi.org/10.1080/19336896.2016.1189053>



Published online: 26 Aug 2016.



Submit your article to this journal [↗](#)



Article views: 7



View related articles [↗](#)



View Crossmark data [↗](#)

Establishment of a simple cell-based ELISA for the direct detection of abnormal isoform of prion protein from prion-infected cells without cell lysis and proteinase K treatment

Zhifu Shan, Takeshi Yamasaki, Akio Suzuki, Rie Hasebe, and Motohiro Horiuchi

Laboratory of Veterinary Hygiene, Graduate School of Veterinary Medicine, Hokkaido University, Sapporo, Japan

ABSTRACT. Prion-infected cells have been used for analyzing the effect of compounds on the formation of abnormal isoform of prion protein (PrP^{Sc}). PrP^{Sc} is usually detected using anti-prion protein (PrP) antibodies after the removal of the cellular isoform of prion protein (PrP^C) by proteinase K (PK) treatment. However, it is expected that the PK-sensitive PrP^{Sc} (PrP^{Sc}-sen), which possesses higher infectivity and conversion activity than the PK-resistant PrP^{Sc} (PrP^{Sc}-res), is also digested through PK treatment. To overcome this problem, we established a novel cell-based ELISA in which PrP^{Sc} can be directly detected from cells persistently infected with prions using anti-PrP monoclonal antibody (mAb) 132 that recognizes epitope consisting of mouse PrP amino acids 119–127. The novel cell-based ELISA could distinguish prion-infected cells from prion-uninfected cells without cell lysis and PK treatment. MAb 132 could detect both PrP^{Sc}-sen and PrP^{Sc}-res even if all PrP^{Sc} molecules were not detected. The analytical dynamic range for PrP^{Sc} detection was approximately 1 log. The coefficient of variation and signal-to-background ratio were 7%–11% and 2.5–3.3, respectively, demonstrating the reproducibility of this assay. The addition of a cytotoxicity assay immediately before PrP^{Sc} detection did not affect the following PrP^{Sc} detection. Thus, all the procedures including cell culture, cytotoxicity assay, and PrP^{Sc} detection were completed in the same plate. The simplicity and non-requirement for cell lysis or PK treatment are advantages for the high throughput screening of anti-prion compounds.

KEYWORDS. cell-based ELISA, monoclonal antibody, prion, PK-treatment, screening

INTRODUCTION

Prion diseases are a group of neurodegenerative disorders that include scrapie in sheep and goats, bovine spongiform encephalopathy in cattle, chronic wasting disease in deer, and

Creutzfeldt-Jakob disease (CJD) in human. The preclinical period of the diseases is extremely long; however, after the clinical onset, the diseases are subacutely progressive and inevitably fatal. The diseases are characterized by neuronal vacuolation, astrocytosis, microglial

Correspondence to: Motohiro Horiuchi, DVM, PhD, Laboratory of Veterinary Hygiene, Graduate School of Veterinary Medicine, Hokkaido University, Kita 18, Nishi 9, Kita-ku, Sapporo 060-0818, Japan. Email: horiuchi@vetmed.hokudai.ac.jp

Received January 13, 2016; Revised May 5, 2016; Accepted May 6, 2016.

Color versions of one or more of the figures in the article can be found online at www.tandfonline.com/kprn.

activation and accumulation of an abnormal isoform of prion protein (PrP^{Sc}) in the central nervous system (CNS).¹ PrP^{Sc} is the only known proteinaceous component of prions, the causative agents of the diseases, and the infectivity of prions is thought to be associated with PrP^{Sc} oligomers.^{2,3} PrP^{Sc} is generated from a host-encoded cellular isoform of prion protein (PrP^C) by post-translational modifications including conformational transformation. Once PrP^{Sc} appears, PrP^{Sc} is gradually generated and accumulates in CNS. The conversion of PrP^C to PrP^{Sc} in neurons is believed to cause neurodegeneration,^{4,5} therefore, the inhibition of PrP^{Sc} formation is one of the therapeutic targets for prion diseases.

Screening of chemical libraries is one of the ways to identify therapeutic compounds for prion diseases. Cells persistently infected with prions provide a good platform for screening compound libraries to identify inhibitors of PrP^{Sc} formation and for analyzing the cell biology underlying prion propagation.⁶⁻¹¹ For example, Kocisko et al.¹² screened 2,000 FDA-approved drugs using prion-infected cells and obtained 17 potent inhibitors. Ghaemmaghani et al.¹³ screened more than 10,000 compounds and identified 4 lead chemical scaffolds for PrP^{Sc} formation inhibitors on the basis of structure-activity relationships among 121 compounds that inhibit PrP^{Sc} formation in cells.

As the deletion of PrP gene prevented clinical onset of the disease¹⁴ and the reduction of the PrP^C level by small interference RNA prolonged the survival of prion-infected mice,¹⁵ reduction of the PrP^C level is also a target for the inhibition of PrP^{Sc} formation. Karapetyan et al.¹⁶ screened 1,280 drugs approved for use in human from the US Drug Collection for their ability to decrease PrP^C expression in cells, and they identified Astemizole as a candidate for the treatment and prophylaxis of prion diseases. Silber et al. also screened large chemical libraries to find compounds that lower PrP^C expression in T98G human glioblastoma and IMR 32 human neuroblastoma cells using a cell-based ELISA.¹⁷ Alternatively, stabilization of PrP^C, which inhibits the conformational transition of PrP^C into PrP^{Sc}, is also a target for the inhibition of PrP^{Sc} formation. In silico screening of

compounds that are capable of binding to PrP^C using docking simulation has identified a new class of compounds that inhibit PrP^{Sc} formation in prion-infected cells.¹⁸⁻²⁰

Although screening for compounds that bind PrP^C or affect PrP^C expression is two of the ways to identify potential therapeutic compounds, the advantage of the use of prion-infected cells is that compounds that inhibit PrP^{Sc} formation through interaction with PrP^C, PrP^{Sc}, or other cellular factors will be screened. However, one technical limitation of using prion-infected cells is the requirement for proteinase K (PK) treatment to remove PrP^C from the cell lysates. It is well known that PrP^{Sc} comprises PK-sensitive PrP^{Sc} (PrP^{Sc}-sen) and PK-resistant PrP^{Sc} (PrP^{Sc}-res)^{21,22} and that PrP^{Sc}-sen is reported to possess higher infectivity and conversion activity than PrP^{Sc}-res.² PK treatment is expected to digest PrP^{Sc}-sen; so when PK-treatment is used, the effect of compounds on PrP^{Sc} formation may be underestimated.

Recently, we reported that the anti-PrP monoclonal antibody (mAb) 132, which recognizes amino acids 119–127 of PrP, is useful for PrP^{Sc} detection in cells and frozen tissue sections of animals infected with prions.^{23,24} Although fixation and treatment of cells or tissue sections with guanidinium salts are prerequisite, this method does not require PK treatment for the discrimination of PrP^{Sc} from PrP^C. To take advantage of this, we established a cell-based ELISA in which PrP^{Sc} is directly detected in cells without preparation of a cell lysate and PK treatment. The cell-based ELISA established in this study provides a simple and practical method for the primary screening of anti-prion compounds.

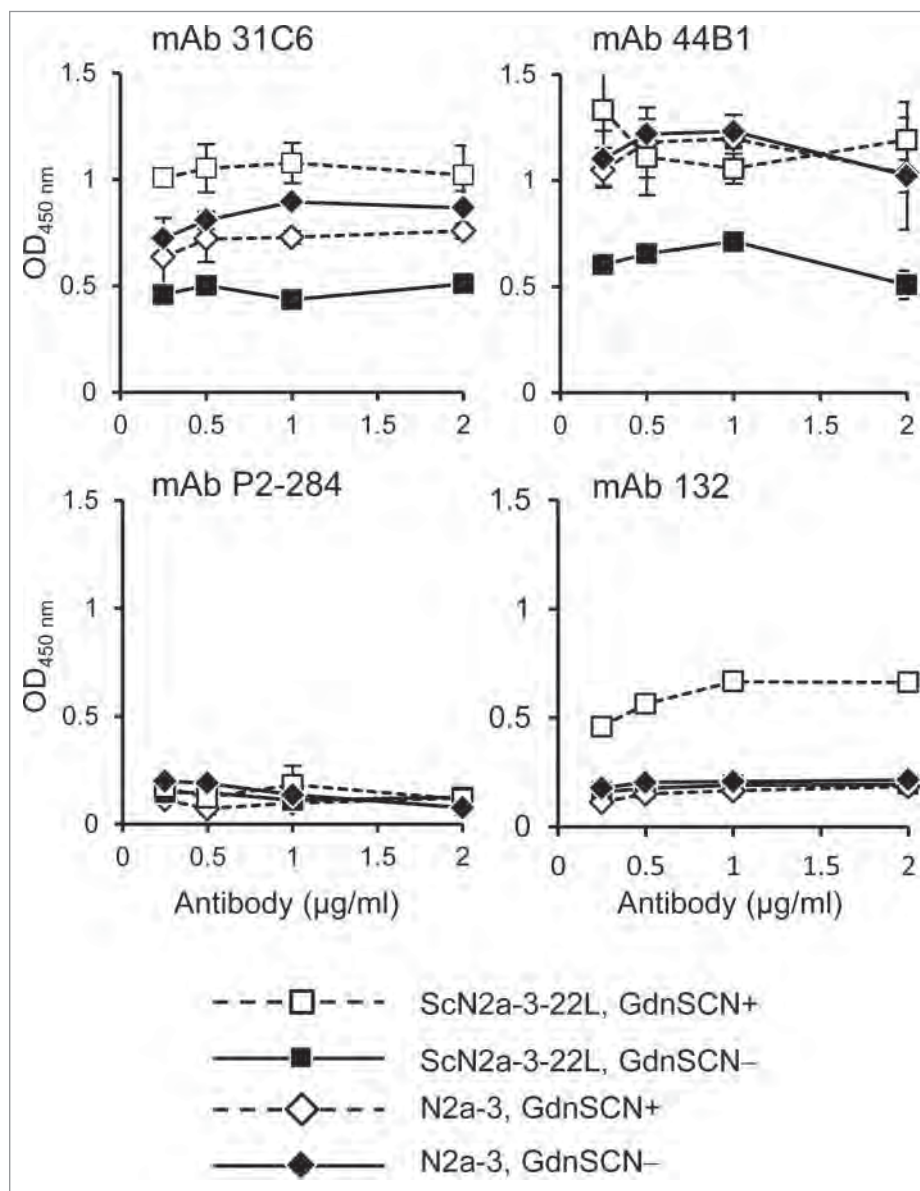
RESULTS

MAb 132 Discriminates Prion-Infected Cells from Uninfected Cells in a Cell-Based ELISA

First we examined whether anti-PrP mAbs 31C6, 44B1, and 132 could discriminate prion-infected cells from prion-uninfected cells by direct staining of cells. Cells grown in 96-well

plates were fixed with paraformaldehyde (PFA) and treated briefly with guanidine thiocyanate (GdnSCN) to denature PrP^{Sc}, and subsequently subjected to immunostaining. The mAbs 31C6 and 44B1 gave higher signals from ScN2a-3-22L cells, a subclone of Neuro2a mouse neuroblastoma (N2a-3) cells persistently infected with the 22L prion strain, than from prion-uninfected N2a-3 cells when these cells were pretreated with GdnSCN (Fig. 1). However, compared with the negative control mAb, these mAbs also showed positive signals from

FIGURE 1. MAb 132 discriminates prion-infected cells from uninfected cells in cell-based ELISA. Prion-infected cells (ScN2a-3-22L) and uninfected cells (N2a-3) were cultured in 96-well plates for 72 h. Cells were then fixed with PFA, permeabilized with Trion X-100, and treated with (GdnSCN+) or without (GdnSCN-) 5 M GdnSCN. After blocking, the cells were subjected to immunostaining with various anti-PrP antibodies at the indicated concentrations. MAb P2-284 was used as a negative control.



prion-uninfected N2a-3 cells, indicating that these mAbs are not suitable for the specific detection of PrP^{Sc} in prion-infected cells. In contrast, mAb 132 showed a positive reaction only when prion-infected cells were pretreated with GdnSCN. Absorbances obtained by mAb 132 staining from uninfected cells or GdnSCN-untreated prion-infected cells remained at levels comparable with the corresponding signals obtained using the negative control antibody. Thus, among the antibodies tested, only mAb 132 could distinguish prion-infected cells from uninfected cells in a cell-based ELISA.

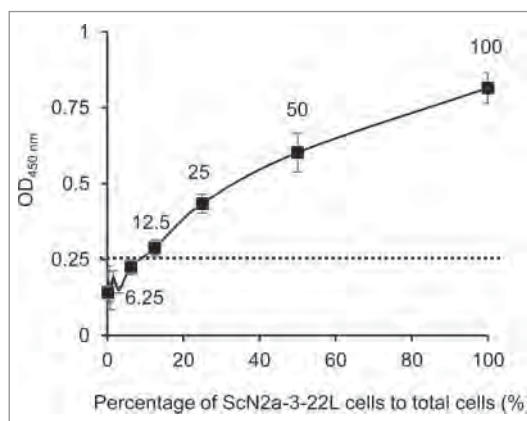
Performance of Cell-Based ELISA Using mAb 132

Next we examined the dynamic range of the cell-based ELISA. ScN2a-3-22L cells were 2-fold serially diluted with N2a-3 cells, and a total of 10,000 cells per well were seeded in a 96-well plate. The reaction became positive when 12.5% of cells in the well were prion-infected cells, and the signal was still in the linear range when all the cells were prion-infected cells (Fig. 2). These results indicate that the cell-based ELISA has approximately a 1 log dynamic range. Although it was expected that some uninfected cells became infected during the 72-h incubation, the spread of infection did not influence the interpretation because the linear increase of OD₄₅₀ was observed in parallel with the ratio of infected and uninfected cells.

To examine whether mAb 132 is applicable to other prion strains or other cells, we used N2a-3 cells infected with the Chandler prion strain (ScN2a-3-Ch) and GT1-7 mouse immortalized hypothalamic neurons infected with the 22L prion strain (ScGT1-7-22L). The mAb 132 showed positive reaction to ScN2a-3-Ch and to ScGT1-7-22L cells (Fig. 3). These results suggested that the cell-based ELISA is applicable to different prion strains and cell types.

To evaluate the performance of the cell-based ELISA, basic indices of the PrP^{Sc} detection were analyzed (Table 1). The coefficient of variation (CV), which is the standard index for measuring variability, and is ideally < 10% when measuring intra-assay variability, was

FIGURE 2. Dynamic range of PrP^{Sc} detection in cell-based ELISA. ScN2a-3-22L cell suspension (1.0×10^5 cells/ml) was 2-fold serially diluted with a N2a-3 cell suspension of the same concentration. Cell suspensions (10,000 cells/100 μ l/well) were added to wells and incubated for 72 h. After the incubation, the cells were subjected to PrP^{Sc} detection with mAb 132. The cutoff value (dotted line) was determined as the mean plus $3 \times$ SD of the N2a-3 signal. Numbers with plots indicate percentages of ScN2a-3-22L cells to total cells in well.

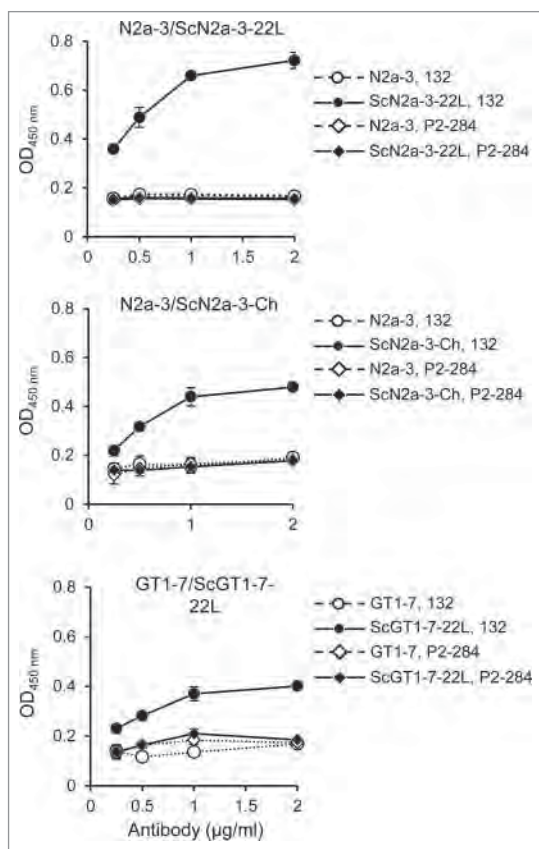


approximately 10%. The signal-to-background ratio (S/B), which is the standard index for acceptable breadth for determining negative and positive responses, and which is ideally > 2, was 2.6–3.6. The signal-to-noise ratio (S/N), which is index for signal intensity level to background fluctuations, and which should desirably be > 10, was 14.7–27.3. These indices demonstrate the reproducibility of the cell-based ELISA.

Utility of Cell-Based ELISA in Combination with Cytotoxicity Assay

If the cytotoxicity of test compounds could be assessed before PrP^{Sc} detection, all the procedures of the cell-based ELISA, from the cell culture, assessment of cytotoxicity, to the immunological detection of PrP^{Sc}, could be completed with in the same plate. Thus, we examined if the cytotoxicity assay (WST assay) affects the following PrP^{Sc} detection. Cells

FIGURE 3. Detection of PrP^{Sc} of other prion strains and from other cell types. N2a-3 cells persistently infected with the 22L (ScN2a-3-22L), and the Chandler prion strain (ScN2a-3-Ch), and GT1-7 cells infected with the 22L prion strain (ScGT1-7-22L), were cultured in 96-well plates. After 72 h incubation, the cells were subjected to PrP^{Sc} detection with mAb 132 (open and closed circles). MAb P2-284 (open and closed diamonds) was used as a negative control mAb.



were treated with U18666A²⁵ or Pentosan polysulfate (PPS),²⁶ which are known as inhibitors for PrP^{Sc} formation, for 48 h and the WST assay was performed immediately before PrP^{Sc} detection. When ScN2a-3-22L cells were treated with U18666A, cell viability gradually decreased and obvious cytotoxicity was observed at U18666A concentrations > 5 μ M. PrP^{Sc} detection using mAb 132 also decreased with increasing U18666A concentration and became lower than cutoff value at U18666A

TABLE 1. Reliability of novel cell-based ELISA.

	N2a-3	ScN2a-3-22L
OD ₄₅₀ (Average \pm SD)	0.145 \pm 0.026	0.635 \pm 0.081
CV (%) ^a	9%–11%	7%–11%
S/B ^b	2.54–3.35	
S/N ^c	14.72–27.33	

^aCoefficient of variation = SD/average \times 100

^bSignal-to-background ratio = $AV_{ScN2a-3-22L}/AV_{N2a-3}$

^cSignal-to-noise ratio = $(AV_{ScN2a-3-22L} - AV_{N2a-3})/SD_{N2a-3}$

concentrations > 5 μ M (Fig. 4A). However, no remarkable differences in levels of PrP^{Sc} detection were observed with (ScN2a-3-22L, WST+) or without (ScN2a-3-22L, WST-) the WST assay (Fig. 4A, see < 5 μ M U18666A). This result indicates the WST assay has little effect on the subsequent PrP^{Sc} detection. In contrast to U18666A, PPS treatment showed no cytotoxicity even at the highest concentration tested, while PPS drastically decreased PrP^{Sc} levels to below the cutoff value at low concentrations (Fig. 4B). These results demonstrate that the effect of test compounds on PrP^{Sc} formation and their cytotoxicity can be assessed in the same plate. In Figure 4B, low dose PPS treatment appeared to enhance cell viability; however those were among experimental variations and we confirmed that the low dose PPS treatment did not influence the viability of N2a-3 and ScN2a-3-22L cells (data not shown).

To confirm the accuracy of PrP^{Sc} detection after U18666A or PPS treatment in the cell-based ELISA, we analyzed PrP^{Sc} in PPS- or U18666A-treated cells by immunofluorescence assay (IFA) (Fig. 4C) and PrP^{Sc}-res by immunoblot analysis (Fig. 4D). In IFA, PrP^{Sc} signals were decreased but were still detected after treatment with 5 μ M U18666A and further weakened at 20 μ M U18666A (Fig. 4C). The expressions of PrP^C in N2a-3 and ScN2a-3-22L cells were confirmed by mAb 31C6 without pretreatment of cells with GdnSCN (Fig. 4D). The result of the immunoblot analysis of U18666A-treated cells was consistent with that of the IFA (Fig. 4E). In contrast, treatment of cells with 5 μ g/ml PPS decreased PrP^{Sc} signals to levels comparable with those seen in cells

treated with 20 $\mu\text{g/ml}$ PPS. The gradual decrease in PrP^{Sc} levels with the increase of U18666A but drastic decrease in PrP^{Sc} levels at PPS concentrations < 5 $\mu\text{g/ml}$ of PPS, is consistent with those obtained with the cell-based ELISA, demonstrating the utility of the cell-based ELISA for screening anti-prion compounds.

Detection of PrP^{Sc}-sen and PrP^{Sc}-res by mAb 132

Since the cell-based ELISA established here does not require PK treatment for PrP^{Sc} detection, it is possible that both PrP^{Sc}-res and PrP^{Sc}-sen could be detected using mAb 132, even if not all the PrP species are detected. To assess this possibility, lysates from N2a-3 and ScN2a-3-22L cells were blotted onto polyvinylidene difluoride (PVDF) membranes, and after PK treatment and subsequent GdnSCN exposure (or in the reverse order), the membranes were probed with mAb 132.

No PrP was detected from the lysates of N2a-3 or ScN2a-3-22L cells lacking both PK and GdnSCN treatment (Fig. 5A, I). PrP was

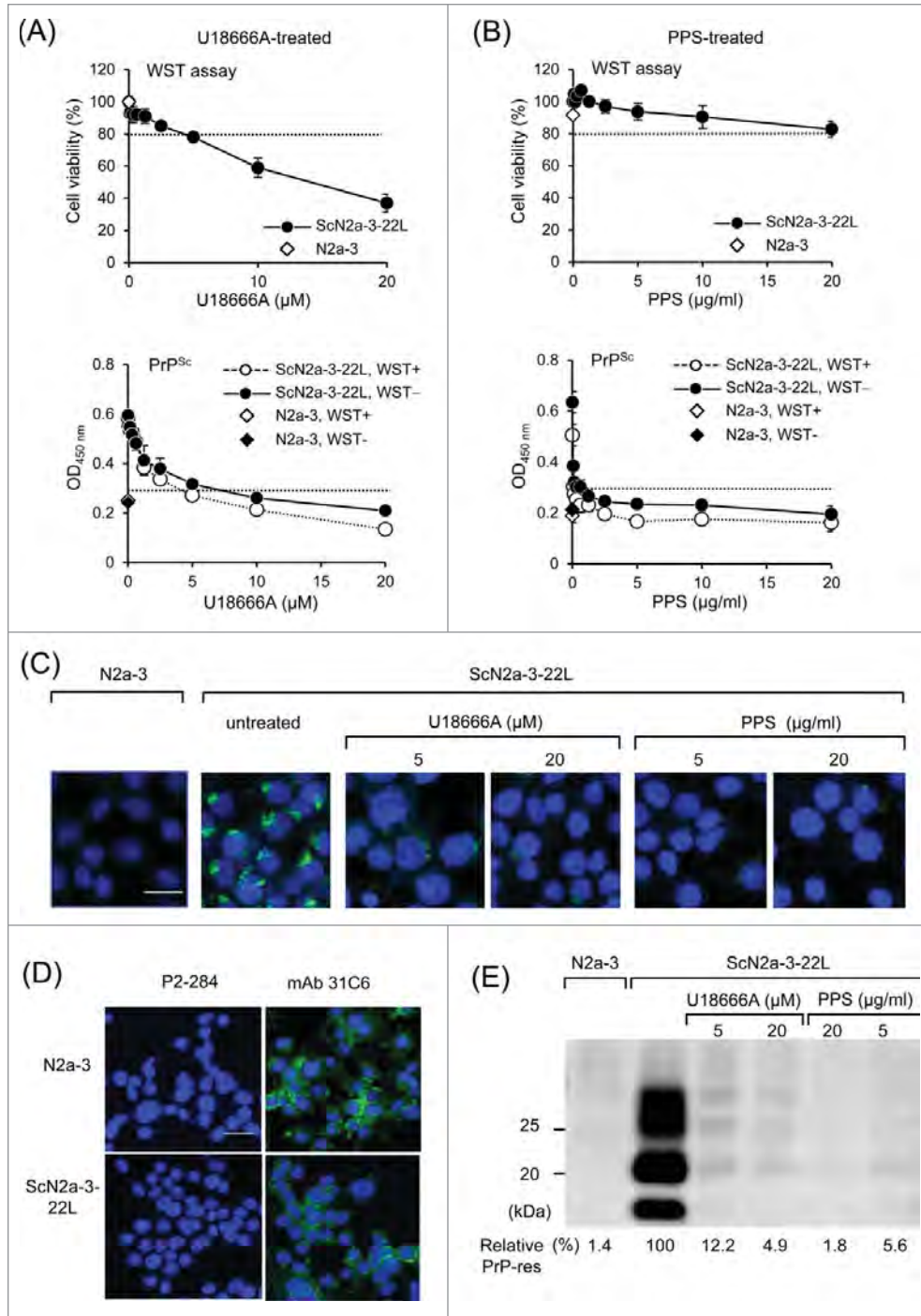
detected in the lysate of ScN2a-3-22L cells when the membrane was not treated with PK but treated with GdnSCN (Fig. 5A, II). These signals represent PrP^{Sc} because no PrP was detected from the lysate of N2a-3 cells under the same condition. However, the intensity of PrP^{Sc} signals decreased to approximately 40% of those seen in Figure 5A II when the PVDF membrane was first treated with PK and then with GdnSCN (Fig. 5A, III, and 5B). The PrP^{Sc} signals detected under these conditions were considered to be those from PrP^{Sc}-res and the decrease in the PrP^{Sc} signal accounted for the digestion of PrP^{Sc}-sen by PK. When the PVDF membrane was treated with GdnSCN but not PK (Fig. 5A, IV), PrP^{Sc} levels were as high as those obtained in Figure 5A II, suggesting that the signal accounted for the sum of PrP^{Sc}-sen and PrP^{Sc}-res. When the membrane was first treated with GdnSCN and then treated with PK, no PrP signals were obtained, since PrP^{Sc} denatured by GdnSCN was digested with PK (Fig. 5A, V). The presence of PrP^C in the lysate of N2a-3 was confirmed with mAb 31C6 (Fig. 5C).

To further examine whether mAb 132 detects PrP^{Sc}-sen, ScN2a-3-22L cells were

FIGURE 4. Utility of cell-based ELISA in combination with cytotoxicity assay. (A and B) Influence of the cytotoxicity assay on subsequent PrP^{Sc} detection. ScN2a-3-22L cells were cultured in 96-well plates for 24 h and then incubated with U18666A (A) or PPS (B) for 48 h at the indicated concentrations. Immediately before fixation, cell viability was measured with the WST assay using CCK-8. After removal of the CCK-8 reagent, cells were subjected to PrP^{Sc} detection in the same plate. Regarding PrP^{Sc} detection, PrP^{Sc} signals detected after the WST assay (WST+, open diamonds and circles) or without WST assay (WST-, closed diamonds and circles) are shown. The dashed lines in WST assay indicate survival rate at 80%. The PrP^{Sc} signal detected from N2a-3 cells was used to calculate cutoff values (mean plus 3 \times SD) for PrP^{Sc} detection (dashed lines). (C) IFA for PrP^{Sc} detection. ScN2a-3-22L cells were cultured in a chambered coverglass for 24 h and then treated or with U18666A or PPS for 48 h at the indicated concentrations. ScN2a-3-22L and N2a-3 cells untreated with these compounds were used as positive and negative controls for PrP^{Sc}, respectively. The cells were subjected to PrP^{Sc}-specific staining with mAb 132 (green), and cell nuclei were counterstained with 4', 6-diamidino-2-phenylindole (DAPI) (blue). (D) Expression of PrP^C in N2a-3 and ScN2a-3-22L cells. Cells were stained with mAb 31C6 (green) without pretreatment of GdnSCN for the detection of PrP^C. Nuclei were counterstained with DAPI (blue). P2-284: negative control mAb. Scale bar: 20 μm . (E) Immunoblot analysis. ScN2a-3-22L cells were cultured in 24-well plates for 24 h and subsequently treated with U18666A or PPS for 48 h at the indicated concentrations. Cells were then subjected to immunoblot analysis for the detection of PrP^{Sc}-res. N2a-3 cells untreated with these compounds were used as negative controls for PrP^{Sc}-res. PrP^{Sc}-res levels relative to untreated ScN2a-3-22L cells are shown at the bottom. Scale bar: 20 μm .

treated with low concentrations of PK and then subjected to PrP^{Sc}-specific immunostaining. The fluorescent intensities of PrP^{Sc} signals in PK-treated ScN2a-3-22L cells decreased to less than a half of those in PK-untreated ScN2a-3-

22L cells, even at the lowest PK concentration tested (Fig. 6, 0.31 $\mu\text{g/ml}$). The decrease in fluorescence intensities of PrP^{Sc} signals by PK treatment supported the idea that mAb 132 detected both PrP^{Sc}-sen and PrP^{Sc}-res.



DISCUSSION

We have reported that mAb 132, which recognizes an epitope consisting of mouse PrP aa 119–127, can specifically detect PrP^{Sc} from prion-infected cells or tissues without the removal of PrP^C by PK treatment.^{23,24} This feature of mAb 132 facilitated the establishment of a novel cell-based ELISA in which PrP^{Sc} levels in prion-infected cells are assessed without the removal of PrP^C. As anticipated, mAb 132 was the only anti-PrP mAbs tested that could distinguish prion-infected cells from uninfected cells (Fig. 1). Signals obtained from uninfected cells and GdnSCN-untreated prion-infected cells probed with mAb 132 were comparable with signals obtained using a negative control mAb, providing a suitable S/B ratio (Table 1). MAb 132 reacted poorly with PrP^C on the cell surface,²⁷ but reacted with PrP^{Sc}, PrP^C and recombinant

PrP in immunoblot analysis.²⁸ Thus, mAb 132 appears to recognize a linear epitope that becomes antibody-accessible after denaturation of the PrP molecule. However, mAb 132 did not show a positive reaction to uninfected cells, even after GdnSCN treatment. We do not have any clear explanation for this phenomenon, one possibility is that once the region containing the mAb 132 epitope on PrP^C was exposed by GdnSCN treatment, the region may refold into antibody-inaccessible form after the removal of GdnSCN. Surface plasmon resonance analysis revealed that the binding of monovalent mAb132 (e.g., recombinant Fab) was significantly weaker than bivalent mAb 132 (e.g., recombinant IgG), indicating that the bivalent binding is required for the efficient binding to the epitope (A.S. & M.H., manuscript in preparation). Reaction of mAb 132 to PrP^C expressed in the cells will be a monovalent binding, whereas that to PrP^{Sc} will

FIGURE 5. Detection of PrP^{Sc}-sen and PrP^{Sc}-res by mAb 132 in a dot-blot analysis. (A) Dot-blot analysis. Lysates from N2a-3 or ScN2a-3-22L cells were transferred onto PDVF membranes using a dot-blotter (quadruplicates). The membranes were treated with PK (10 μ g/ml; PK+) (III) or not (PK-) (I and II) for 1 h at RT and subsequently with (Gdn+) (II and III) or without (Gdn-) 3 M GdnSCN (II) for 30 min at RT, or in the reverse order (IV and V). Then, the membranes were stained with mAb 132, and chemiluminescence signals were detected and quantified with a LAS 3000 chemiluminescence image analyzer. The PrP levels (%) relative to the PrP level in II, detected using mAb 132, are shown in (B). *, $p < 0.05$, Student's t -test). (C) Confirmation of PrP^C in dot-blot analysis. Lysates from N2a-3 (Mock) or ScN2a-3-22L (22L) cells were blotted onto PDVF membranes (quadruplicates). The membranes were treated with PK (10 μ g/ml) or not (0 μ g/ml) for 1 h at RT. After the termination of PK digestion, the membranes were treated with DNase I and then with 3 M GdnSCN for 30 min at RT as described in Materials and Methods. Finally membranes were stained with mAbs 132 and 31C6 for chemiluminescence detection.

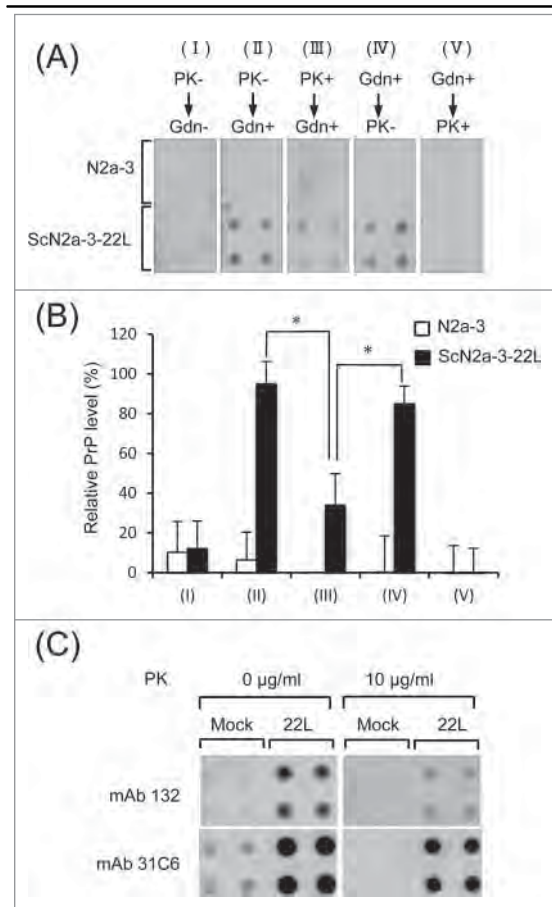
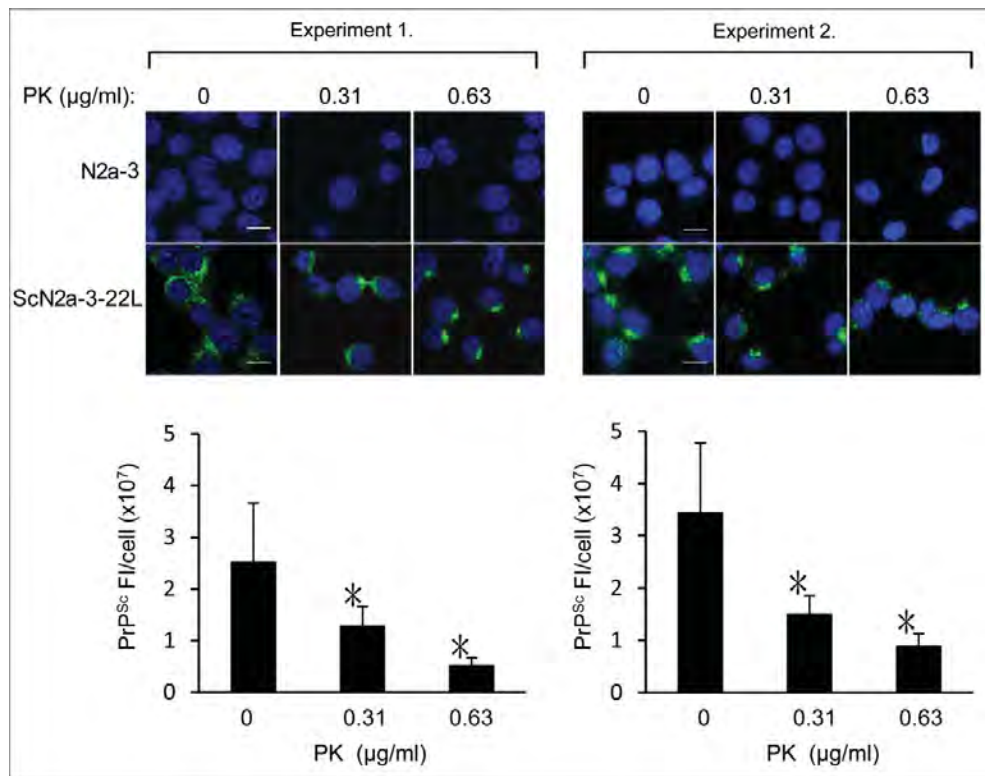


FIGURE 6. Possible detection of PrP^{Sc}-sen and PrP^{Sc}-res using mAb 132 in IFA. N2a-3 and ScN2a-3-22L cells and were cultured in a chambered coverglass for 24 h. Cells were fixed with 4% paraformaldehyde in PBS for 10 min and then treated with 0.1% Triton X-100 and 0.1 M glycine in PBS. Subsequently, cells were treated with PK at the indicated concentrations at 4°C for 30 min. Cells were then treated with 5 M GdnSCN for 10 min at RT and subjected to PrP^{Sc}-specific immunofluorescence staining. Representative fluorescence images of two independent experiments are shown at the top. Graphs show the corresponding quantification result of PrP^{Sc} fluorescence intensities (FI) per ScN2a-3-22L cell. Fluorescence intensities from perinuclear regions of N2a-3 were subtracted as background. Experiment 1: mean fluorescence intensities and standard deviations of 16 cells from 5 microscopic fields (3–4 cells/field). Experiment 2: mean fluorescence intensities and standard deviations of 16–24 cells from 4 to 5 microscopic fields (3–5 cells/field). *, $p < 0.001$, Welch's t -test). Scale bars: 10 μ m.



occur as bivalent binding because PrP^{Sc} exists as oligomer/aggregate of PrP molecules. Thus the binding kinetics of mAb 132 may partly explain the inefficient binding of mAb 132 to PrP^C: monovalent binding is not enough to stain PrP^C efficiently in IFA. However, further studies are still required for the elucidation of the mechanism of PrP^{Sc}-specific staining by mAb 132.

Conformation-dependent immunoassay (CDI) has demonstrated the existence of PrP^{Sc}-sen and PrP^{Sc}-res in the brains of prion-affected humans and animals.²⁹ The proportion of PrP^{Sc}-sen is

believed to be high; for example, CDI revealed that PrP^{Sc}-sen constituted approximately 50–90% and 90% of PrP^{Sc} in the brains of hamsters infected with hamster-adapted prion strains and CJD patients, respectively.^{29,30} Also immunoelectron microscopic analysis of mice infected with the RML let to an estimate that > 85% of the PrP^{Sc} in the brain was PK sensitive.³¹ The PK-sensitive fraction of PrP^{Sc} is reported to possess higher infectivity and higher conversion activity per PrP molecule than the PK-resistant fraction.² Taken together, these results suggest that PrP^{Sc}-

sen may be the more substantial entity of prions. Thus, evaluation of the effect of compounds on PrP^{Sc}-sen may be important for screening anti-prion compounds. Screening methods of anti-prion compounds using prion-infected cells reported to date included PK treatment for the removal of PrP^C.^{12,13,32,33} However, effect of compounds on PrP^{Sc}-sen cannot be assessed or may be underestimated if PK treatment is included during the analysis.

mAb 132 discriminated PrP^{Sc} from PrP^C without PK treatment, suggesting that mAb could detect both PrP^{Sc}-sen and PrP^{Sc}-res;^{23,24,34} however, this had not yet been directly demonstrated. In a dot-blot analysis performed using cell lysates prepared with non-ionic detergent, the PrP^{Sc} level detected after PK digestion and subsequent GdnSCN treatment was much lower than that detected after GdnSCN treatment alone (Fig. 5). Consistent with the result of dot-blot analysis, the fluorescence intensities of PrP^{Sc} decreased after treatment of the cells with even low concentrations of PK (Fig. 6). Quantification of the result of dot-blot analysis and the IFA implies that > 50% of PrP^{Sc} in N2a-3 cells infected with the 22L strain are sensitive to PK, which is similar to the proportion of PK-sensitive PrP^{Sc} in the brains of prion-affected humans and animals.^{29,30,35} Taken together, these results demonstrate that mAb 132 detects not only PrP^{Sc}-res, but at least a certain fraction of PrP^{Sc}-sen if not all.

The absolute sensitivity for the detection of PrP^{Sc} in the cell-based ELISA is not expected to be high because of the lack of procedures for PrP^{Sc} concentration such as phosphotungstic acid precipitation.^{13,36} However, a 1 log dynamic range for direct PrP^{Sc} detection in prion-infected cells is enough to evaluate the anti-prion effect exerted by a 50% effective dose as a primary screening method. The remarkable advantage of the cell-based ELISA is its simplicity: all the procedures, from cell culture to PrP^{Sc} detection, can be completed in the same plate without making cell lysates or PK treatment. Probing both PrP^{Sc}-res and PrP^{Sc}-sen is another technical improvement, which is difficult to achieve using procedures that include PK treatment. It is believed that

human cells or human PrP^C-expressing cells infected with human prions are a better platform for screening for potential therapeutic reagents than prion-infected cells of other species. The epitope for mAb 132 is well conserved from mammals to chickens,^{37,38} so mAb 132 will be applicable to the detection of PrP^{Sc} from human prion-infected cells using a protocol similar to the one developed in this study.

MATERIALS AND METHODS

Antibodies and Regents

The anti-PrP mAbs 132, 31C6, and 44B1, which recognize amino acids 119–127, 143–149, and discontinuous epitopes of mouse PrP, respectively, were used.²⁸ Anti-feline parvovirus subgroup mAb P2-284 was used as a negative control antibody.³⁹ ECLTM anti-mouse IgG, horseradish peroxidase (HRP)-linked F(ab')₂ fragment from sheep was purchased from GE Healthcare. The Alexa Fluor 488 F(ab')₂ fragment of goat anti-mouse IgG (H+L) was purchased from Life Technologies. PPS was purchased from Dainippon Sumitomo Pharma and U18666A was purchased from Sigma-Aldrich.

Cell Culture

N2a-3 cells, a subclone of the N2a mouse neuroblastoma cell line⁴⁰ and N2a-3 cells persistently infected with the 22L prion strain (ScN2a-3-22L)⁴¹ or the Chandler prion strain (ScN2a-3-Ch)⁴⁰ were used. GT1-7 mouse immortalized hypothalamic neurons⁴² that are persistently infected with the 22L prion strain (ScGT1-7-22L)²³ were also used.

Cell-Based ELISA

N2a-3 and ScN2a-3-22L cells were seeded into 96-well plates (Thermo Scientific) at a density of 1×10^4 cells/100 μ l/well and cultured for 24 h. Cells were then freshly fed with the medium with or without anti-prion

compounds and incubated for 48 h. After the removal of medium, cells were fixed with 50 μ l/well of 4% PFA in phosphate-buffered saline (PBS) for 10 min at room temperature (RT). After the removal of PFA, 100 μ l of 0.1% Triton X-100 and 0.1 M glycine in PBS was added to each well to permeabilize the cell membrane and quench residual PFA. The plates were then incubated for 10 min at RT. After the removal of glycine and Triton X-100, the cells were treated with 50 μ l of 5 M GdnSCN for 10 min at RT. Cells were then washed once with PBS and blocked with 5% skim milk in PBS for 30 min at RT. Immunostaining was carried out using anti-PrP mAb 132 (1 μ g/ml) as the primary antibody for at least 6 h at 4°C and diluted (1:5,000) HRP-conjugated anti-mouse IgG as the secondary antibody for 1 h at RT. Finally, antigen-antibody complexes were detected with the colorimetric HRP substrate 3,3',5,5' tetramethylbenzidine (Sigma). After incubation for 15 min at RT, the reaction was stopped by adding sulfuric acid to 0.25 M and optical density at 450 nm was measured using a microplate reader (Infinite M200 Pro, Tecan). In some cases, the cytotoxicity assay described below was carried out immediately before fixation of the cells.

Cytotoxicity Assay

After removal of the medium, the cells were washed with Opti-MEM without phenol red (Gibco) and subjected to the WST cytotoxicity assay using Cell Counting Kit 8 (CCK-8; DojinDo). CCK-8 reagent was diluted 1:100 with Opti-MEM (Thermo) and added to each well (100 μ l/well). After incubation at 37°C for 1 h, the absorbance at 450 nm was measured using a microplate reader.

Immunoblot Analysis

SDS-PAGE and immunoblotting for PrP^{Sc} detection were carried out as described elsewhere.^{40,41}

Dot-Blotting

N2a-3 and ScN2a-3-22L cells were cultured for 72 h in 6-well plates. Cells were lysed with 200 μ l/well of lysis buffer (0.5% Triton X-100, 0.5% sodium deoxycholate, 150 mM NaCl, 5 mM EDTA, and 10 mM Tris-HCl [pH 7.5]) and the protein concentration of the lysate was measured using a DC protein assay kit (Bio-Rad). Cell lysates equivalent to 40 μ g of total protein were transferred onto a PVDF membrane using a dot-blotter (Bio-Rad). The PVDF membrane was treated with PK (10 μ g/ml), or not, for 1 h at RT, and then PK digestion was terminated by the addition of Pefabloc (Roche) to 1 mM for 15 min at 4°C. The membrane was then treated with 50 μ g/ml DNase I for 15 min and subsequently with 3 M GdnSCN for 30 min at RT. For the detection of PrP, the membrane was incubated with mAb 132 (1 μ g/ml) in 1% skim milk-PBS containing 0.1% Tween 20 (PBST) at 4°C overnight. After washing the membrane with PBST, HRP-conjugated anti-mouse IgG was used as the secondary antibody for 1 h at RT. ECL Western Blotting Detection Reagents (GE Healthcare) and a LAS-3000 chemiluminescence image analyzer (Fujifilm) were used to visualize the immune-reactive proteins.

IFA

PrP^{Sc}-specific immunofluorescence staining using mAb 132 and quantitative analysis of the signals were performed as described previously.^{23,34}

Calculation of CV, S/B, and S/N

Forty-eight wells were seeded with N2a-3 cells and another 48 wells were seeded with ScN2a-3-22L at the density of 1×10^4 cells/100 μ l/well. After 72 h incubation, the PrP signals were detected as described in the section entitled "Cell-based ELISA." Twenty-well sections were assigned for staining with mAb 132 or mAb P2-284 (negative control mAb), and the remaining 8 wells were assigned as blank

wells. Four independent experiments were carried out to calculate CV, S/B, and S/N.

ABBREVIATIONS

aa	amino acid(s)
CDI	Conformation-dependent immunoassay
CJD	Creutzfeld-Jakob disease
CNS	central nervous system
CV	coefficient of variation
DAPI	4',6-diamidino-2-phenylindole
ELISA	enzyme-linked immunosorbent assay
FDA	Food and Drug Administration
FI	fluorescence intensities
GdnSCN	guanidine thiocyanate
IFA	immunofluorescence assay
HRP	horseradish peroxidase
mAb	monoclonal antibody
N2a	Neuro2a
PBS	phosphate buffered saline
PBST	PBS containing 0.1% Tween 20
PFA	paraformaldehyde
PK	proteinase K
PPS	Pentosan polysulfate
PrP ^C	cellular isoform of prion protein
PrP ^{Sc}	abnormal isoform of prion protein
PrP ^{Sc} -res	PK-resistant PrP ^{Sc}
PrP ^{Sc} -sen	PK-sensitive PrP ^{Sc}
PVDF	polyvinylidene difluoride
RML	Rocky mountain laboratories
RT	room temperature
S/B	signal-to-background ratio
ScGT1-7-22L	GT1-7 mouse immortalized hypothalamic neurons infected with the 22L strain
ScN2a-3-22L	N2a-3 cells persistently infected with the 22L prion strain
ScN2a-3-Ch	N2a-3 cells persistently infected with the Chandler prion strain
S/N	signal-to-noise ratio
WST	2-(4-iodophenyl)-3-(4-nitrophenyl)-5-(2,4-disulfophenyl)-2H-tetrazolium, monosodium salt

DISCLOSURE OF POTENTIAL CONFLICTS OF INTEREST

The authors have no conflict of interest to declare. The authors also declare no competing financial interests.

FUNDING

This work was supported by a Grant-in-Aid for Science Research (A) (grant no. 15H02475), a grant from the Program for Leading Graduate Schools (F01), from the Ministry of Education, Culture, Sports, Science, and Technology, Japan. This work was also supported by grants for TSE research (H26-Shokuhin-Ippan-004) and Research on Measures for Intractable Diseases from the Ministry of Health, Labour and Welfare of Japan. This work was also supported by the Global Institution for Collaborative Research and Education (GI-CoRE). We thank Zensho Co., Ltd, for the BSL3 facility.

REFERENCES

- [1] Aguzzi A, Baumann F, Bremer J. The prion's elusive reason for being. *Annu Rev Neurosci* 2008; 31:439-77; PMID:18558863; <http://dx.doi.org/10.1146/annurev.neuro.31.060407.125620>
- [2] Silveira JR, Raymond GJ, Hughson AG, Race RE, Sim VL, Hayes SF, Caughey B. The most infectious prion protein particles. *Nature* 2005; 437:257-61; PMID:16148934; <http://dx.doi.org/10.1038/nature03989>
- [3] Wang F, Wang X, Yuan CG, Ma J. Generating a prion with bacterially expressed recombinant prion protein. *Science* 2010; 327:1132-5; PMID:20110469; <http://dx.doi.org/10.1126/science.1183748>
- [4] Mallucci G, Dickinson A, Linehan J, Klohn PC, Brandner S, Collinge J. Depleting neuronal PrP in prion infection prevents disease and reverses spongiosis. *Science* 2003; 302:871-4; PMID:14593181; <http://dx.doi.org/10.1126/science.1090187>
- [5] Chesebro B, Trifilo M, Race R, Meade-White K, Teng C, LaCasse R, Raymond L, Favara C, Baron G, Priola S, et al. Anchorless prion protein results in infectious amyloid disease without clinical scrapie. *Science* 2005; 308:1435-9; PMID:15933194; <http://dx.doi.org/10.1126/science.1110837>
- [6] Marijanovic Z, Caputo A, Campana V, Zurzolo C. Identification of an intracellular site of prion

- conversion. *PLoS Pathog* 2009; 5:e1000426; PMID:19424437; <http://dx.doi.org/10.1371/journal.ppat.1000426>
- [7] Veith NM, Plattner H, Stuermer CA, Schulz-Schaeffer WJ, Burkle A. Immunolocalisation of PrP^{Sc} in scrapie-infected N2a mouse neuroblastoma cells by light and electron microscopy. *Eur J Cell Biol* 2009; 88:45-63; PMID:18834644; <http://dx.doi.org/10.1016/j.ejcb.2008.08.001>
- [8] Caughey B, Raymond GJ. The scrapie-associated form of PrP is made from a cell surface precursor that is both protease- and phospholipase-sensitive. *J Biol Chem* 1991; 266:18217-23; PMID:1680859
- [9] Taraboulos A, Raeber AJ, Borchelt DR, Serban D, Prusiner SB. Synthesis and trafficking of prion proteins in cultured cells. *Mol Biol Cell* 1992; 3:851-63; PMID:1356522; <http://dx.doi.org/10.1091/mbc.3.8.851>
- [10] Goold R, Rabbani S, Sutton L, Andre R, Arora P, Moonga J, Clarke AR, Schiavo G, Jat P, Collinge J, et al. Rapid cell-surface prion protein conversion revealed using a novel cell system. *Nat Commun* 2011; 2:281; PMID:21505437; <http://dx.doi.org/10.1038/ncomms1282>
- [11] Yamasaki T, Baron GS, Suzuki A, Hasebe R, Horiuchi M. Characterization of intracellular dynamics of inoculated PrP-res and newly generated PrP(Sc) during early stage prion infection in Neuro2a cells. *Virology* 2014; 450-451:324-35; PMID:24503096; <http://dx.doi.org/10.1016/j.virol.2013.11.007>
- [12] Kocisko DA, Baron GS, Rubenstein R, Chen J, Kuzon S, Caughey B. New inhibitors of scrapie-associated prion protein formation in a library of 2000 drugs and natural products. *J Virol* 2003; 77:10288-94; PMID:12970413; <http://dx.doi.org/10.1128/JVI.77.19.10288-10294.2003>
- [13] Ghaemmaghami S, May BC, Renslo AR, Prusiner SB. Discovery of 2-aminothiazoles as potent anti-prion compounds. *J Virol* 2010; 84:3408-12; PMID:20032192; <http://dx.doi.org/10.1128/JVI.02145-09>
- [14] Bueler H, Aguzzi A, Sailer A, Greiner RA, Autenried P, Aguet M, Weissmann C. Mice devoid of PrP are resistant to scrapie. *Cell* 1993; 73:1339-47; PMID:8100741; [http://dx.doi.org/10.1016/0092-8674\(93\)90360-3](http://dx.doi.org/10.1016/0092-8674(93)90360-3)
- [15] White MD, Farmer M, Mirabile I, Brandner S, Collinge J, Mallucci GR. Single treatment with RNAi against prion protein rescues early neuronal dysfunction and prolongs survival in mice with prion disease. *Proc Natl Acad Sci U S A* 2008; 105:10238-43; PMID:18632556; <http://dx.doi.org/10.1073/pnas.0802759105>
- [16] Karapetyan YE, Sferrazza GF, Zhou M, Ottenberg G, Spicer T, Chase P, Fallahi M, Hodder P, Weissmann C, Lasmezas CI. Unique drug screening approach for prion diseases identifies tacrolimus and astemizole as anti-prion agents. *Proc Natl Acad Sci U S A* 2013; 110:7044-9; PMID:23576755; <http://dx.doi.org/10.1073/pnas.1303510110>
- [17] Silber BM, Gever JR, Rao S, Li Z, Renslo AR, Widjaja K, Wong C, Giles K, Freyman Y, Elepano M, et al. Novel compounds lowering the cellular isoform of the human prion protein in cultured human cells. *Bioorg Med Chem* 2014; 22:1960-72; PMID:24530226; <http://dx.doi.org/10.1016/j.bmc.2014.01.001>
- [18] Kuwata K, Nishida N, Matsumoto T, Kamatari YO, Hosokawa-Muto J, Kodama K, Nakamura HK, Kimura K, Kawasaki M, Takakura Y, et al. Hot spots in prion protein for pathogenic conversion. *Proc Natl Acad Sci U S A* 2007; 104:11921-6; PMID:17616582; <http://dx.doi.org/10.1073/pnas.0702671104>
- [19] Hosokawa-Muto J, Kamatari YO, Nakamura HK, Kuwata K. Variety of anti-prion compounds discovered through an in silico screen based on cellular-form prion protein structure: Correlation between anti-prion activity and binding affinity. *Antimicrob Agents Chemother* 2009; 53:765-71; PMID:19015328; <http://dx.doi.org/10.1128/AAC.01112-08>
- [20] Ferreira NC, Marques IA, Conceicao WA, Macedo B, Machado CS, Mascarello A, Chiaradia-Delatorre LD, Yunes RA, Nunes RJ, Hughson AG, et al. Anti-prion activity of a panel of aromatic chemical compounds: in vitro and in silico approaches. *PLoS One* 2014; 9:e84531; PMID:24400098; <http://dx.doi.org/10.1371/journal.pone.0084531>
- [21] Tzaban S, Friedlander G, Schonberger O, Horonchik L, Yedidia Y, Shaked G, Gabizon R, Taraboulos A. Protease-sensitive scrapie prion protein in aggregates of heterogeneous sizes. *Biochemistry* 2002; 41:12868-75; PMID:12379130; <http://dx.doi.org/10.1021/bi025958g>
- [22] Pastrana MA, Sajani G, Onisko B, Castilla J, Morales R, Soto C, Requena JR. Isolation and characterization of a proteinase K-sensitive PrP^{Sc} fraction. *Biochemistry* 2006; 45:15710-7; PMID:17176093; <http://dx.doi.org/10.1021/bi0615442>
- [23] Yamasaki T, Suzuki A, Shimizu T, Watarai M, Hasebe R, Horiuchi M. Characterization of intracellular localization of PrP(Sc) in prion-infected cells using a mAb that recognizes the region consisting of aa 119-127 of mouse PrP. *J Gen Virol* 2012; 93:668-80; PMID:22090211; <http://dx.doi.org/10.1099/vir.0.037101-0>
- [24] Sakai K, Hasebe R, Takahashi Y, Song CH, Suzuki A, Yamasaki T, Horiuchi M. Absence of CD14 delays progression of prion diseases accompanied by increased microglial activation. *J Virol* 2013; 87:13433-45; PMID:24089559; <http://dx.doi.org/10.1128/JVI.02072-13>
- [25] Klingenstein R, Lober S, Kujala P, Godsav S, Leliveld SR, Gmeiner P, Peters PJ, Korth C. Tricyclic antidepressants, quinacrine and a novel, synthetic chimera thereof clear prions by destabilizing

- detergent-resistant membrane compartments. *J Neurochem* 2006; 98:748-59; PMID:16749906; <http://dx.doi.org/10.1111/j.1471-4159.2006.03889.x>
- [26] Caughey B, Raymond GJ. Sulfated polyanion inhibition of scrapie-associated PrP accumulation in cultured cells. *J Virol* 1993; 67:643-50; PMID:7678300
- [27] Kim CL, Karino A, Ishiguro N, Shinagawa M, Sato M, Horiuchi M. Cell-surface retention of PrPC by anti-PrP antibody prevents protease-resistant PrP formation. *J Gen Virol* 2004; 85:3473-82; PMID:15483265; <http://dx.doi.org/10.1099/vir.0.80113-0>
- [28] Kim CL, Umetani A, Matsui T, Ishiguro N, Shinagawa M, Horiuchi M. Antigenic characterization of an abnormal isoform of prion protein using a new diverse panel of monoclonal antibodies. *Virology* 2004; 320:40-51; PMID:15003861; <http://dx.doi.org/10.1016/j.virol.2003.10.026>
- [29] Safar J, Wille H, Itri V, Groth D, Serban H, Torchia M, Cohen FE, Prusiner SB. Eight prion strains have PrP(Sc) molecules with different conformations. *Nat Med* 1998; 4:1157-65; PMID:9771749; <http://dx.doi.org/10.1038/2654>
- [30] Safar JG, Geschwind MD, Deering C, Didorenko S, Sattavat M, Sanchez H, Serban A, Vey M, Baron H, Giles K, et al. Diagnosis of human prion disease. *Proc Natl Acad Sci U S A* 2005; 102:3501-6; PMID:15741275; <http://dx.doi.org/10.1073/pnas.0409651102>
- [31] Godsave SF, Wille H, Kujala P, Latawiec D, DeArmond SJ, Serban A, Prusiner SB, Peters PJ. Cryo-immunogold electron microscopy for prions: toward identification of a conversion site. *J Neurosci* 2008; 28:12489-99; PMID:19020041; <http://dx.doi.org/10.1523/JNEUROSCI.4474-08.2008>
- [32] Heal W, Thompson MJ, Mutter R, Cope H, Louth JC, Chen B. Library synthesis and screening: 2,4-diphenylthiazoles and 2,4-diphenyloxazoles as potential novel prion disease therapeutics. *J Med Chem* 2007; 50:1347-53; PMID:17305326; <http://dx.doi.org/10.1021/jm0612719>
- [33] Leidel F, Eiden M, Geissen M, Kretschmar HA, Giese A, Hirschberger T, Tavan P, Schatzl HM, Groschup MH. Diphenylpyrazole-derived compounds increase survival time of mice after prion infection. *Antimicrob Agents Chemother* 2011; 55:4774-81; PMID:21746938; <http://dx.doi.org/10.1128/AAC.00151-11>
- [34] Yamasaki T, Suzuki A, Hasebe R, Horiuchi M. Comparison of the anti-prion mechanism of four different anti-prion compounds, anti-PrP monoclonal antibody 44B1, pentosan polysulfate, chlorpromazine, and U18666A, in prion-infected mouse neuroblastoma cells. *PLoS One* 2014; 9:e106516; PMID:25181483; <http://dx.doi.org/10.1371/journal.pone.0106516>
- [35] Cronier S, Gros N, Tattum MH, Jackson GS, Clarke AR, Collinge J, Wadsworth JD. Detection and characterization of proteinase K-sensitive disease-related prion protein with thermolysin. *Biochem J* 2008; 416:297-305; PMID:18684106; <http://dx.doi.org/10.1042/BJ20081235>
- [36] Wadsworth JD, Joiner S, Hill AF, Campbell TA, Desbruslais M, Luthert PJ, Collinge J. Tissue distribution of protease resistant prion protein in variant Creutzfeldt-Jakob disease using a highly sensitive immunoblotting assay. *Lancet* 2001; 358:171-80; PMID:11476832; [http://dx.doi.org/10.1016/S0140-6736\(01\)05403-4](http://dx.doi.org/10.1016/S0140-6736(01)05403-4)
- [37] Ishiguro N, Inoshima Y, Sassa Y, Takahashi T. Molecular characterization of chicken prion proteins by C-terminal-specific monoclonal antibodies. *Vet Immunol Immunopathol* 2009; 128:402-6; PMID:19118905; <http://dx.doi.org/10.1016/j.vetimm.2008.11.025>
- [38] Wopfner F, Weidenhofer G, Schneider R, von Brunn A, Gilch S, Schwarz TF, Werner T, Schatzl HM. Analysis of 27 mammalian and 9 avian PrPs reveals high conservation of flexible regions of the prion protein. *J Mol Biol* 1999; 289:1163-78; PMID:10373359; <http://dx.doi.org/10.1006/jmbi.1999.2831>
- [39] Horiuchi M, Mochizuki M, Ishiguro N, Nagasawa H, Shinagawa M. Epitope mapping of a monoclonal antibody specific to feline panleukopenia virus and mink enteritis virus. *J Vet Med Sci* 1997; 59:133-6; PMID:9070987; <http://dx.doi.org/10.1292/jvms.59.133>
- [40] Uryu M, Karino A, Kamihara Y, Horiuchi M. Characterization of prion susceptibility in Neuro2a mouse neuroblastoma cell subclones. *Microbiol Immunol* 2007; 51:661-9; PMID:17641468; <http://dx.doi.org/10.1111/j.1348-0421.2007.tb03954.x>
- [41] Nakamitsu S, Kurokawa A, Yamasaki T, Uryu M, Hasebe R, Horiuchi M. Cell density-dependent increase in the level of protease-resistant prion protein in prion-infected Neuro2a mouse neuroblastoma cells. *J Gen Virol* 2010; 91:563-9; PMID:19812263; <http://dx.doi.org/10.1099/vir.0.016287-0>
- [42] Schatzl HM, Laszlo L, Holtzman DM, Tatzelt J, DeArmond SJ, Weiner RI, Mobley WC, Prusiner SB. A hypothalamic neuronal cell line persistently infected with scrapie prions exhibits apoptosis. *J Virol* 1997; 71:8821-31; PMID:9343242